ALADIN-HIRLAM Newsletter

No. 16, February 8th, 2021

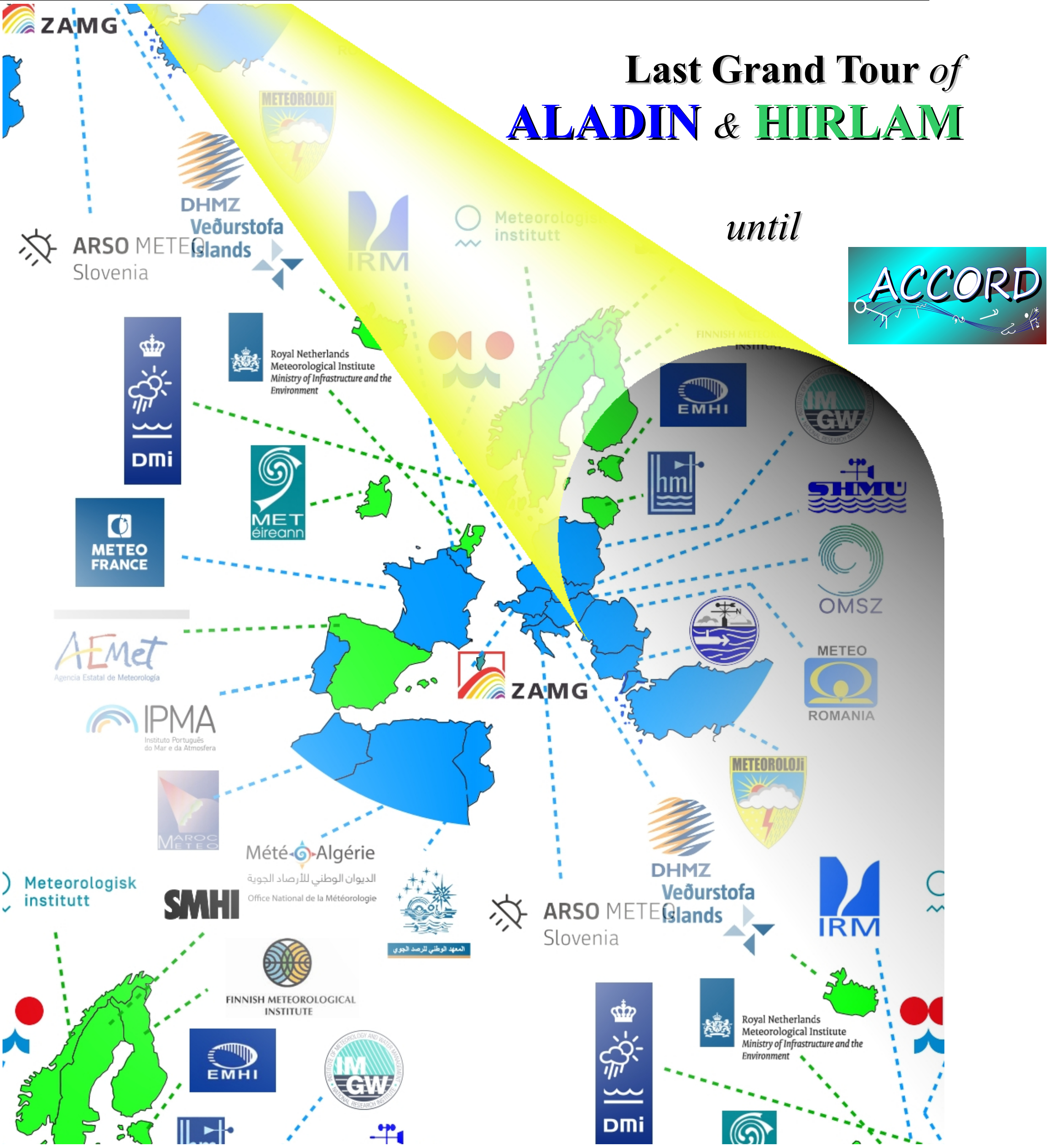

ALADIN Programme, c/o P. Termonia, IRM, Avenue Circulaire 3, 1180 Bruxelles, Belgium
HIRLAM-C Programme, c/o J. Onvlee, KNMI, P.O. Box 201, 3730 AE De Bilt, The Netherlands

CONTENT

Last Tour of ALADIN & HIRLAM

Welcome to the combined 16th edition Newsletter of the ALADIN and HIRLAM consortia. This is the last Newsletter of its kind as the collaboration between the consortia reached its peak at the end of 2020 with their merge into a single consortium ACCORD.

We first propose to have a Tour of ALADIN and HIRLAM activities (national and project reports) in 2020 that ends with a look back at 30 year working together in ALADIN, and in a close and more formalised collaboration with HIRLAM during the last 3 years.

Furthermore, AEMET colleagues, Inger-Lise Frogner and Jeanette Onvlee share with us some memories of Antonio Garcia-Moya after his shocking passing in December.

We also introduce a special issue of the (French) journal "La Météorologie" that is dedicated to Jean-François Geleyn, after the symposium held in February last year to pay a tribute to the scientific career of Jean-François.

We announce two new Doctors from Casablanca. Congratulations !

Last but not least, a summary list of upcoming events, planned for 2021, is available.

We hope you enjoy reading this last ALADIN-HIRLAM Newsletter. Once again, thanks all authors for their contributions and rendez-vous for the future ACCORD Newsletters.

Patricia and Frank

Further consortia information needed?
Please visit the ALADIN and HIRLAM websites or contact us.

Events announced for 2021 (and later on)

The Newsletters presents a static overview (twice a year) with upcoming meetings for the (near) future time frame. For actual updates (year round) please check the ALADIN / HIRLAM websites and the LACE website … and the (under development) ACCORD website.

1 Meetings of ACCORD governance bodies in 2021

Below are listed the meeting planned in the framework of the ACCORD new consortium:

- 1st ACCORD Assembly, 8 March 2021, video-conference
- ACCORD Assembly : Autumn 2021 (date and place t.b.d.)
- ACCORD STAC: Autumn
- ACCORD PAC: on request by the Assembly
- ACCORD LTM: kick-off meeting on 14 January 2021, 1st meeting during the ASW week
- ACCORD Management Group: after the ASW week

To know more about the ACCORD governance, please consult the ACCORD MoU. A synthesis is proposed in the organizational chart below.

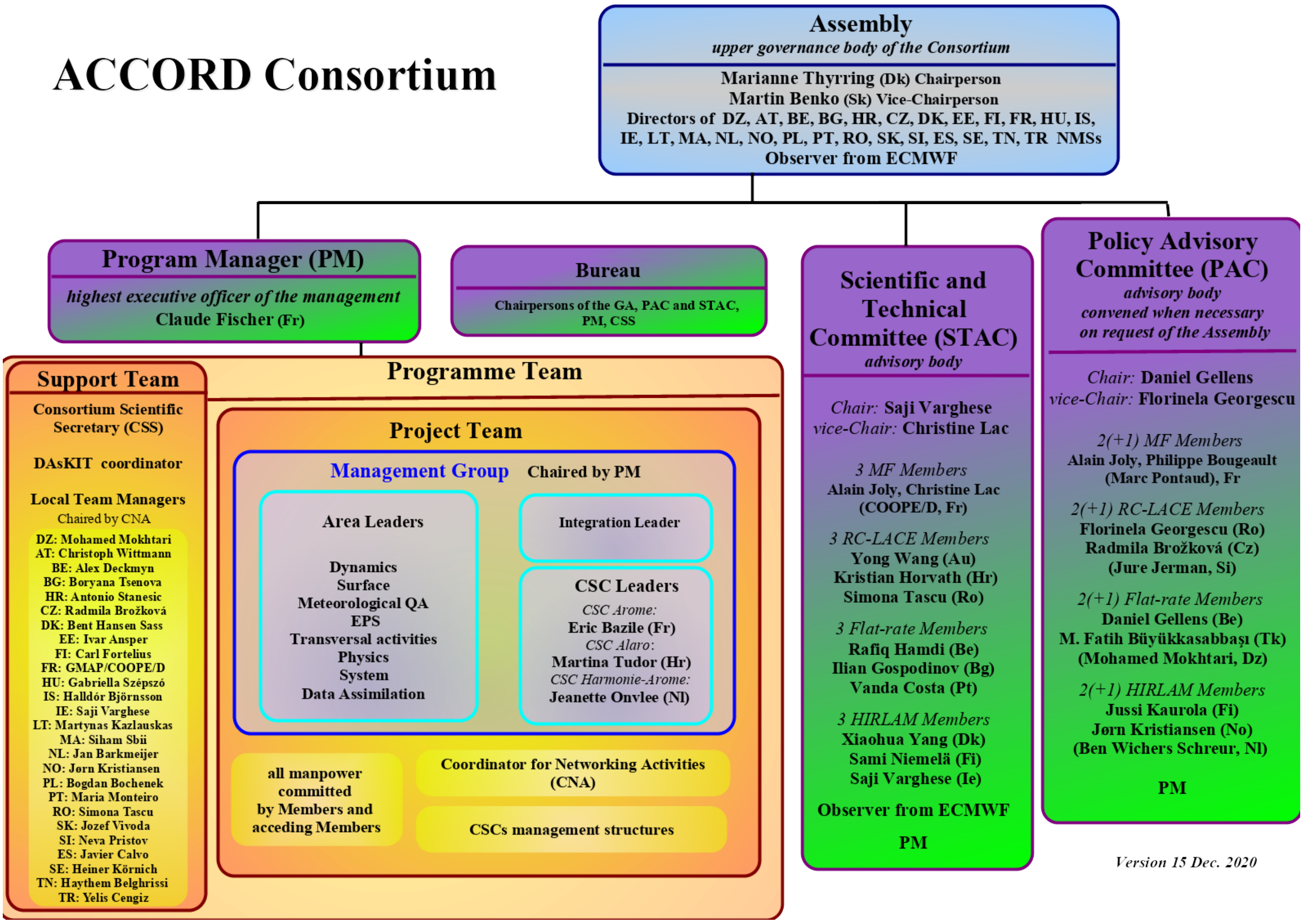

2 Working Weeks / Days

Following topics through working weeks/days will be addressed (due to the uncertainties around the covid-19 situation, only indication of planning for the first part of 2021 is indicated):

- Surface working week: 8-12 February 2021, virtual meeting
- Hirlam System working week with additional invitation to broad community [Gross families working week]: Spring 2021 (virtual meetings?)
- EPS stochastic physics meeting, 2-3 March 2021, organisation by DWD
- ACCORD All Staff Workshop, 12-16 April April 2021, and LTM meeting, virtual meetings
- Several DA video meeting (series of subtopics): Spring
- Working week DA: Spring.
- EPS, working day, virtual in May and EPS working week in September if travel is allowed and possible
- Code training days Assimilation, autumn, t.b.c.
- ALARO WD, autumn
- Joint LACE Data Assimilation & DAsKIT Working Days: autumn

3 Regular group video meetings

Regular group video meetings (via google hangouts) are organized for several topics (from both ALADIN and HIRLAM). Outcomes are noted as very valuable. If you like more details how to organize please contact Roger Randriamiampianina, Daniel Santos Munoz or Patrick Samuelsson.

Maria Monteiro (ALADIN DA coordinator) has established regular specific regular video-conferences with DAsKIT countries (ALADIN DA starter countries).

4 About the past joint events

During the last semester of 2020:

- the (virtual-)LTM met on 5 October 2020 ;
- the HAC and PAC met by virtual meeting in 19-20 October 2020
- the last joint ALADIN Assembly and HIRLAM Council met by virtual meeting on 26 November 2020, and was followed by the ACCORD kick-off Assembly.

The minutes of these meetings have been validated and are on-line (use the links below):

- joint ALADIN Workshops & HIRLAM All Staff Meetings,
- minutes of the HMG/CSSI meetings,
- minutes of HAC/PAC meetings,
- minutes and presentations : joint ALADIN General Assemblies and HIRLAM Councils / Kick-off Assembly of the ALH Consortium

Testing AROME 3DVar and ALADIN 3DVar with cy43t2 using different observations over ALGERIA

M. Ait Meziane, G. Chemrouk

1 Introduction

This short paper is dedicated to describe a set of 3DVar experiences on both AROME and ALADIN configurations, based on Cy43t2, and using different types of observations. In the following, we will highlight all data assimilation and data processing related activities of Météo Algérie as part of DAsKit program during the past few years:

In 2017:

In the beginning, We computed the background matrix error covariance for ALADIN using NMC method locally. After that, during our internship at Météo France, we computed the background matrix error covariances for AROME Algeria configuration using AEARP method. We built a first 3DVar assimilation setup for ALADIN and AROME using SYNOP data.

In 2018 :

We realised a pre-operational 3DVar based on cy40t1 for ALADIN and AROME configurations with 2 productions networks: 00h and 12h

We tested BATOR (cy40t1) with AMDAR after back-phased the cy40t1 (M. Monteiro, F. Guillaum, A. Trajakova).

Then, we installed MANDALAY tool to read ODB.

In 2019:

We tested upper-air observation TEMP and AMDAR with ALADIN 3DVar.

We tested also canari-oimain surface for AROME.

We realised a pre-operational 3DVar cycle based on cy40t1 for ALADIN and AROME configurations with 04 productions networks: 00h,06h,12h and 18h.

In 2020:

We installed a new version of code ARPEGE/IFS cy43t2 and we updated our both ALADIN 3DVar and AROME 3DVar chain.

We assimilated different observation types : SYNOP, TEMP,AMDAR and ASCAT.

2 Experience

We performed an experience of 3DVar assimilation with ALADIN and AROME configurations during two periods :

1st period : June 2020 (from 14th to 29th), production network R12.

2nd period : July 2020 (from 1st to 15th), production network R12.

This experiment was performed based on cy43t2, using the following observations type: SYNOP, TEMP and AMDAR

2-1 Configurations :

Table 1 : configuration ALADIN cy43t2

Resolution	8km, 450*450 grid point
Number of levels	70
Time step integration	514 s
Coupling model	ARPEGE
Coupling frequency	Every 3 hours
Forcast range	72h at 00h, 12h
Type of initialisation	First ARPEGE couplig file

Table 2 : configuration AROME cy43t2

Resolution	3 km, 500*500 grid point
Number of levels	41
Time step	60 s
Couling model	ALADIN
Coupling frequency	Every 01 hour.
Forcast range	48h at 00h, 12h
Type of initialisation	First ALADIN coupling file.

Results and discussion :

We've realized a comparison between ALADIN-ADAPT (no DA) and ALADIN-3DVar, AROME-ADAPT (no DA) and AROME-3DVar, by using synop data.

Activated observations in E002 :

Figure 1 shows the number of observations : SYNOP, AMDAR and TEMP activated in the configuration E002 during the first 15 days of our experience

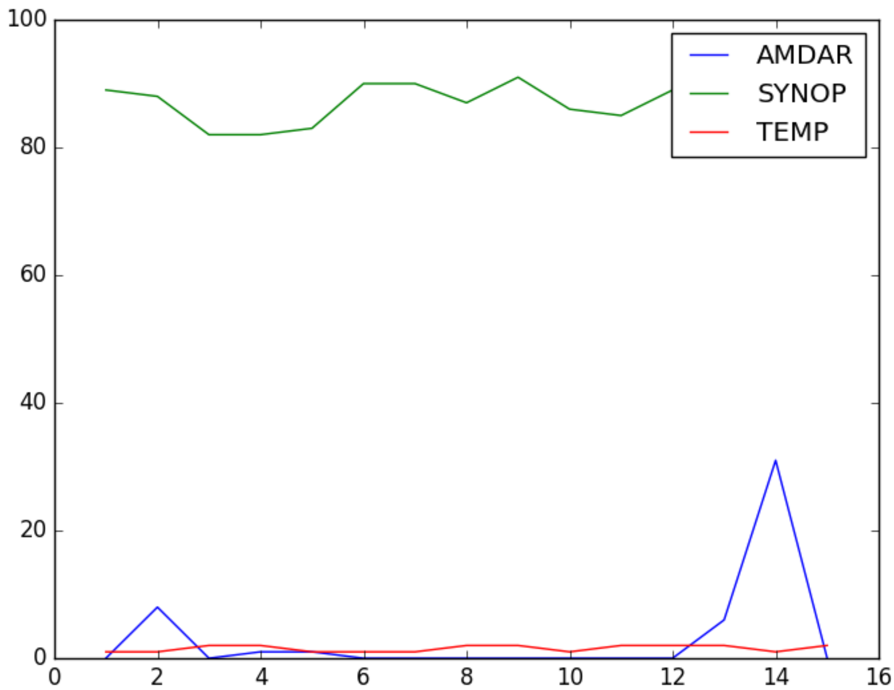

Figure 1: Number of observations activated in screening for ALADIN Algeria

In the following, we show bias calculated for these parameters : t2m, clsh, clsuv and mslp.

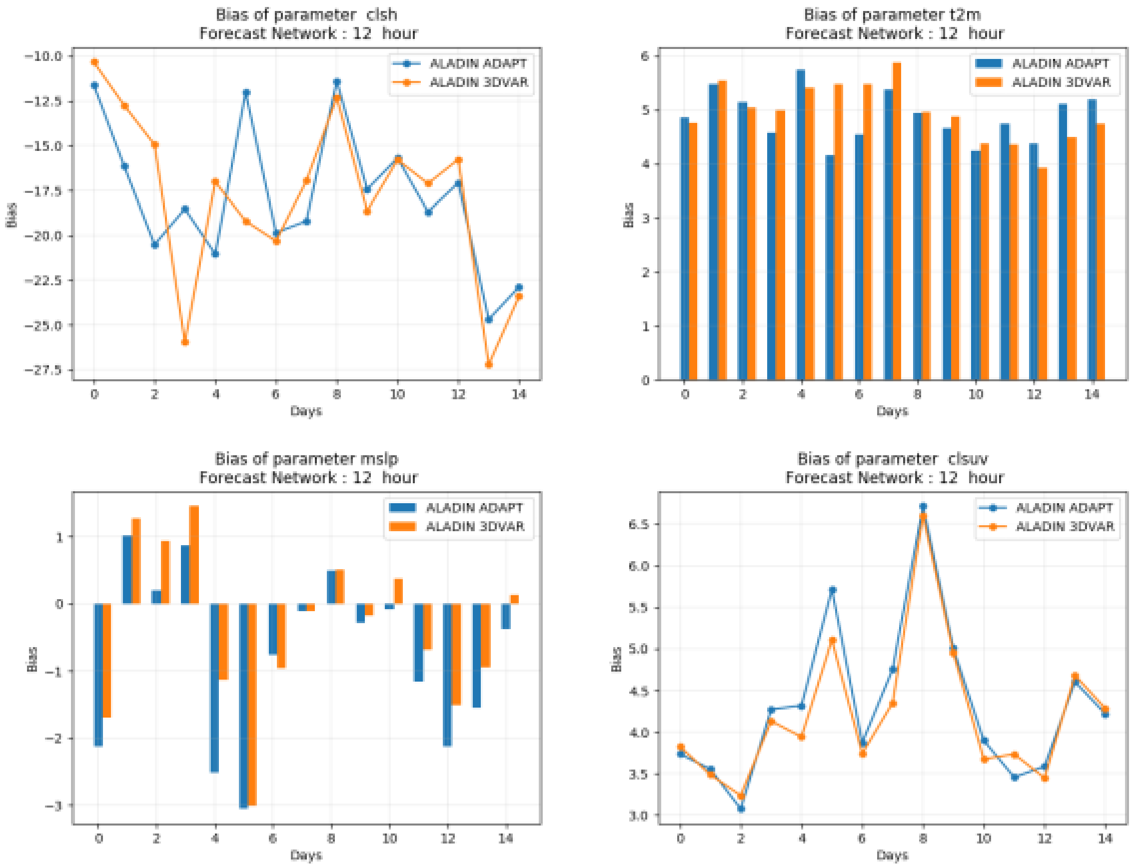

Figure 2: Comparison between ALADIN-3DVar (orange) and ALADIN ADAPT (Blue)

Table 3: Score of ALADIN-3DVar/ALADIN-ADAPT

14-06-2020 to 29 -06-2020 : 01-07-2020 to 15-07-2020 :

model Parameter	ALADIN-3DVAR	ALADIN-ADAPT	model parameter	ALADIN-3DVAR	ALADIN-ADAPT
Clsh	07	08	**Clsh**	08	07
t2m	07	08	**t2m**	04	11
clsuv	10	05	**clsuv**	09	06
mslp	08,5	06.5	**mslp**	11	04
Total	32.5	27.5	**Total**	32	28

Figure 2 shows the biases of clshumidity, temperature at 2 meters, mslp and wind speed.

The bias of clshumidity in ALADIN-3DVar ranges from -27.0 % to -10.0 %, and from -25.0 to -11.0 for ALADIN-ADAPT. The difference of these biases ranges from 0.0% to 8.0%.

The bias of t2m in ALADIN-3DVar ranges from 0.0^0 C to 5.8^0 C , and from 0.0^0 C to 5.7^0 C for ALADIN-ADAPT. The difference of these biases ranges from 0.0^0 C to1.3^0 C.

The bias of mslp in ALADIN-3DVar ranges from -3.0 HPa to 1.5 HPa, and from -3.1 HPa to 0.9 HPa for ALADIN-ADAPT. The difference of these ranges variates from 0.0 HPa to 1.2 HPa.

The bias of clsuv in ALADIN-3DVar ranges from 3.3 m/s to 6.5 m/s, and from 3.0 m/s to 6.6 m/s for ALADIN-ADAPT. The difference of these biases ranges from 0.0 m/s to 0.6 m/s.

Table 3 shows the scores of gains between ALADIN-3DVar and ALADIN-ADAPT during the two periods for the different parameters: clsh,t2m,clsuv and mslp.

- Scores for clsh are equal between the two configurations during the whole period: 15-15
- The score for t2m is higher for ALADIN-ADAPT : 19-11
- The score for clsuv is higher for ALADIN-3DVar : 19-11
- The score for mslp is higher for ALADIN-3DVar : 18.5-11.5

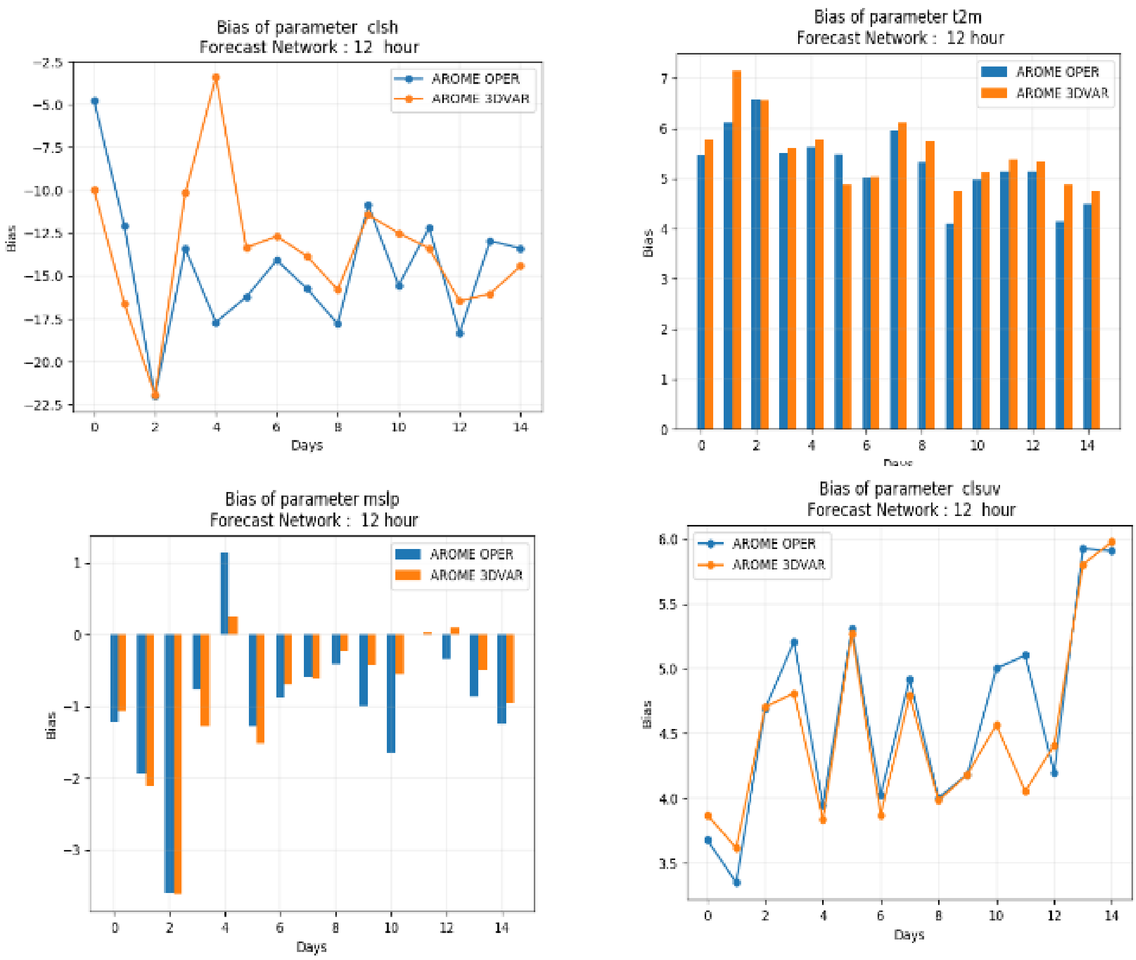

Figure 3: AROME-3DVar and AROME ADAPT

Table 4: Score of AROME-3DVar/AROME-ADAPT

14 -06-2020 to 29 -06-2020 : 01-07-2020 to 15 -07-2020 :

model Parameter	AROME-3DVAR	AROME-ADAPT	model parameter	AROME-3DVAR	AROME-ADAPT
Clsh	09.5	05.5	**Clsh**	09	06
t2m	04.5	10.5	**t2m**	02	13
clsuv	09.5	05.5	**clsuv**	09.5	05.5
Mslp	09.5	05.5	**mslp**	09	06
Total	33	27	**Total**	29.5	30.5

Figure 3 shows biases of clshumidity, temperature at 2 meters, mslp and wind speed of AROME-3DVAR and AROME-ADAPT (no DA).

The bias of clshumidity in AROME-3DVar ranges from -6.5 % to -21.0 %, and from -6.5 to -19.0 for AROME-OPER. The difference of these biases ranges from 0.0% to 3.0%.

The bias of t2m in AROME-3DVar ranges from 0.0^{0}C to 7.1^{0}C , and from 0.0^{0} C to 6.5^{0} C for AROME-OPER. The difference of these biases ranges from 0.0^{0}C to1.0^{0} C.

The bias of mslp in AROME-3DVar ranges from 0.9 HPa to -2.7 HPa, and from -3.1 HPa to 0.9 HPa for AROME-OPER. The difference of these biases ranges from 0.0 HPa to 0.5 HPa.

The bias of clsuv in AROME-3DVar ranges from 3.1 m/s to 6.9 m/s, and from 2.9 m/s to 6.9 m/s for AROME-OPER. The difference of these biases ranges from 0.0 m/s to 1.5 m/s.

Table 4 shows the scores of gains between AROME-3DVar and AROME-ADAPT (no DA) during the two periods for the different paramaters: clsh,t2m,clsuv and mslp.

- The score for clsh is higher for AROME-3DVar :18.5-11.5
- The score for t2m is higher for AROME-ADAPT : 23.5-6.5
- The score for clsuv is higher for AROME-3DVar : 19-11
- The score for mslp is higher for AROME-3DVar : 18.5-11.5

Conclusion :

For clsh, mslp and clsuv parameters, the results obtained in case of data assimilations configurations (AROME-3DVar and ALADIN-3DVar) showed clearly a significant improvement of the scores comparing to the dynamic adaptation configurations (no DA). However, a degradation of t2m scores has been noticed for data assimilations configurations.

3-References

1- Courtier, P. et al., 1994, Quarterly Journal of the Royal Meteorological Society, 120,1367-1387
2- ParrishD.F.,Derber er J.C. , The National Meteorological Center's spectral statistical interpolation analysis system. Mon. Wea. Rev.12017471763 (1992). Original reference for the NMC method.

Highlights of the NWP activities at the Croatian Meteorological and Hydrological Service

Antonio Stanešić, Endi Keresturi, Mario Hrastinski, Alica Bajić, Iva Dominović, Kristian Horvath, Kristina Kozić, Ines Muić, Suzana Panežić, Iris Odak Plenković, Ana Šljivić, Martina Tudor

1 Introduction

The main event that marked 2020 was Zagreb earthquake that severely damaged the headquarters of Croatian Meteorological and Hydrological Service (DHMZ) and forced us to quickly set up backup of NWP operations at offsite facility. In new working conditions, influenced by this and ongoing pandemic, work on optimisation and upgrade of the operational system was continued. At the beginning of 2020., the new dynamical adaptation of wind based on 4km-configuration was validated and put in operations, enabling us to switch off 8-km model configuration and continue work on new export cycle (cy43). Optimisation of postprocessing suite was continued and several new developments were made.

2 Highlighted activities

Zagreb earthquake and backup of operational suite

On March 22, 2020, shortly after 06 AM, Croatia was hit by an earthquake having magnate of $5.5M_L$, with epicentre 7 km north of the Zagreb city centre. The earthquake severely damaged DHMZ headquarters that were declared as unsafe for return of employees (Figure 1).

Figure 1: Photos of damage on DHMZ headquarters.

Since HPC and other important servers were also placed at DHMZ headquarters, it was decided that backup of NWP operational system should be established at ECMWF High-Performance Computing Facility (HPCF). As we have number of users, the first step was to set up a list of most important ones with the aim to provide a backup solution to them and then to gradually include others. Next, we started to make a plan for moving ALADIN operational configurations at ECMWF HPCF.

At that time at DHMZ we had several operational configurations: ALADIN-HR8 (dx=8km, 37 lev), ALADIN-HR4 (dx=4km, 73 lev) and ALADIN-HRDA (dynamical adaptation of wind at 2 km). The data assimilation system provided initial conditions for ALADIN-HR8 and ALADIN-HR4, while ECMWF's forecast in lagged mode was used for LBCs. Also, different model cycles were used for those configurations.

We set up the plan to implement all configurations with cy43 that we already started to test at ECMWF HPCF. In coordination with ECMWF, a new channel for LBC distribution was promptly established. So, the same products distributed regularly to DHMZ were also sent directly to ECMWF's HPCF to feed into the ALADIN model. For initial conditions, setting up a data assimilation system at ECMWF's HPCF seemed too demanding in such a short time. Thus, the solution was to use the initial conditions obtained from an unperturbed member of the A-LAEF (RC-LACE ensemble system), which was already running at ECMWF HPCF. As a substitute for dynamical adaptation of wind, the idea was to set up a full model run at 2 km. After this, the hard work on porting different model configurations and post-processing started with the help of ECMWF user documentation and guidance (as we had little experience with ECMWF HPCF system). After a week we had test runs for all planned configurations. Days after the model was configured and had started to run, parallelised post-processing using conda environments and a python/bash framework was set up. As all servers that we use to display products to the end users are also located in the DHMZ headquarters, we searched for some feasible alternative and solution was to use the European Weather Cloud (EWC). At the EWC we have set up virtual machine and installed all needed components (Apache, PHP…) to display our products.

End users were informed about the availability of products based on the operational backup at HPCF, which were ready to use in case of a major failure of DHMZ's local IT infrastructure and during occasional delays with local operations. DHMZ received a lot of appreciation for the work done from its critical end users, who felt safe knowing that they would not have any issues with their weather-related decision-making.

Operational suite optimization and upgrade

A lot of effort was put into optimization of operational forecast suite over the 2019 and 2020. For many years several operational ALADIN model configurations were provided to our forecasters and customers: ALADIN-HR8 (dx=8 km, 37 lev, ALARO-0, cy32), ALADIN-HR4 (dx=4km, 73 lev, ALARO-0, cy35) and ALADIN-HRDA (dynamical adaptation of wind at dx=2km coupled to ALADIN-HR8, cy29; Žagar and Rakovec 1999., Ivatek-Šahdan and Tudor 2004). Also, once per day dx=2km full model run coupled to ALADIN-HR8 (ALADIN-HR2; ALARO-0, cy36) with forecast up to 48 hours is executed. For ALADIN-HR8 and ALADIN-HR4 two assimilation systems (cy32 and cy35) were set up and maintained. Also, except different configurations, various ALADIN cycles were used. Postprocessing system was a combination of different programming languages and applications: fortran, GrADS, perl, shell… To simplify and optimize this system, we decided to switch off ALADIN-HR8 configuration. This further required to couple ALADIN_HRDA and ALADIN-HR2 to ALADIN-HR4 and eventually to move all components to cycle 43 of the ALADIN model. To optimize postprocessing suite decision was made to use python-based tools as much as possible.

The new version of the ALADIN-HRDA, coupled to the ALADIN-HR4 configuration, was set up. It covers the same area as its predecessor, but the number of vertical levels is increased to 32 (from 15). Furthermore, the orography is updated utilizing the data from the GMTED2010 database. To tune the wind gusts with the new setup (HRDA42) and to assess the quality of the wind forecast model, the results were compared with measurements in statistical sense and as time series for cases of the interest. Model gusts were tuned by modifying the FACRAF coefficient in the range 8-15 for several severe bora events. The value of FACRAF=10 proved as optimal for majority of locations.

The new HRDA configuration with the above-mentioned value of FACRAF coefficient, 32 vertical levels and coupled to ALADIN-HR4 was tested during the period of 6 months (01.10.2018. – 31.3.2019.). The results were compared with the old configuration (coupled to ALADIN-HR8 -

HRDA82). Statistical verification indicates that HRDA42 has overall smaller RMSE for 10m mean wind (Figure 2) and that better results are mainly due to the smaller RMSE for inland stations. A bit worser results were obtained for the Southern Adriatic, while at Northern Adriatic they are mostly improved (Figure 2.; right panel).

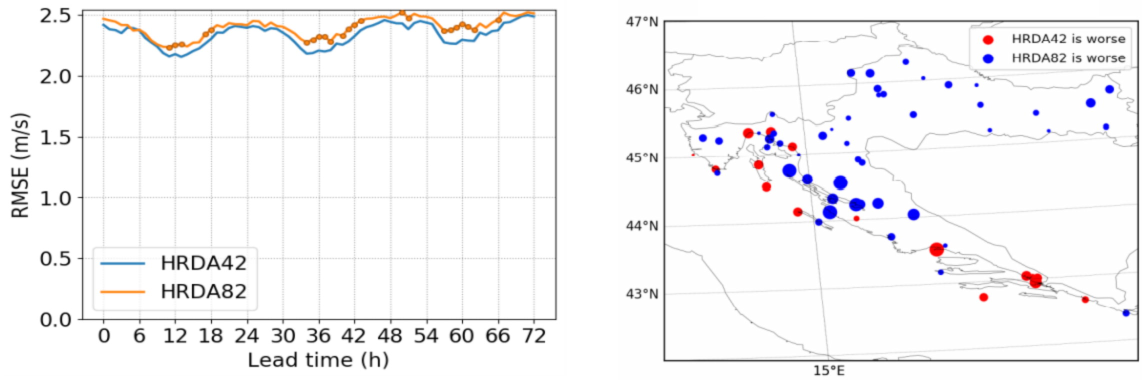

Figure 2: Root mean square error (RMSE) of 10m mean wind calculated for period 01.10.2018.-31.03.2019. Left: RMSE calculated over Croatian automatic stations vs. forecast lead time. With circle are denoted differences that are statistically significant with 95% confidence level. Right: RMSE calculated over o 72h forecast for DHMZ meteorological stations.

Even better results were obtained for wind gusts (Figure 3), where clearly smaller RMSE was obtained for almost all lead times compared to HRDA82. Those better results are occurred for most of the stations, except the ones on the far south of the Croatian coast.

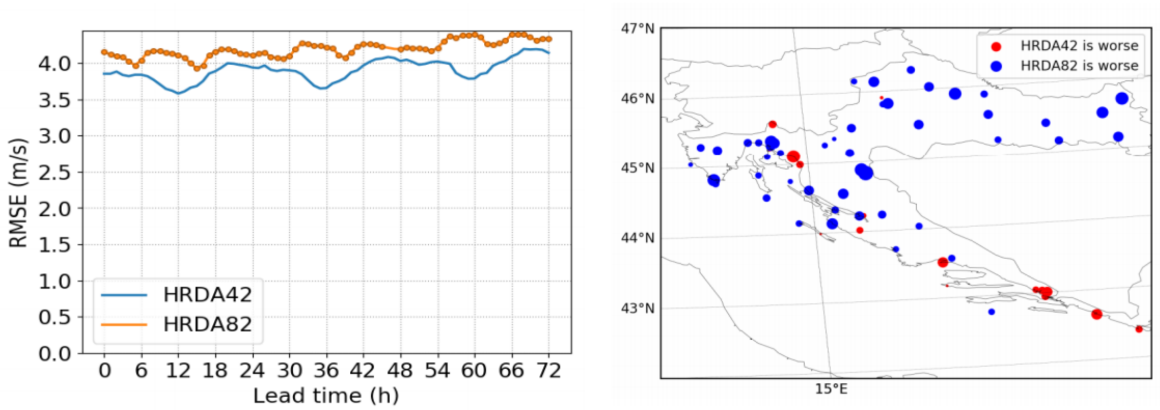

Figure 3: Root mean square error (RMSE) of 10m wind gusts calculated for period 01.10.2018.-31.03.2019. Left: RMSE calculated over Croatian automatic stations vs. forecast lead time. With circle are denoted differences that are statistically significant with 95% confidence level. Right: RMSE calculated over o 72h forecast for DHMZ meteorological stations.

The categorical verification scores Extremal Dependency Index (EDI) and Equitable Threat Score (ETS) were also calculated, and results are shown on Figure 4 and Figure 5. Results indicate that mean wind speed is better for the highest wind speed category, while for wind gusts improvement is also visible for smaller wind speeds. Like earlier, the main contribution to better results comes from inland stations, while the improvement for coastal stations is visible only for wind gusts.

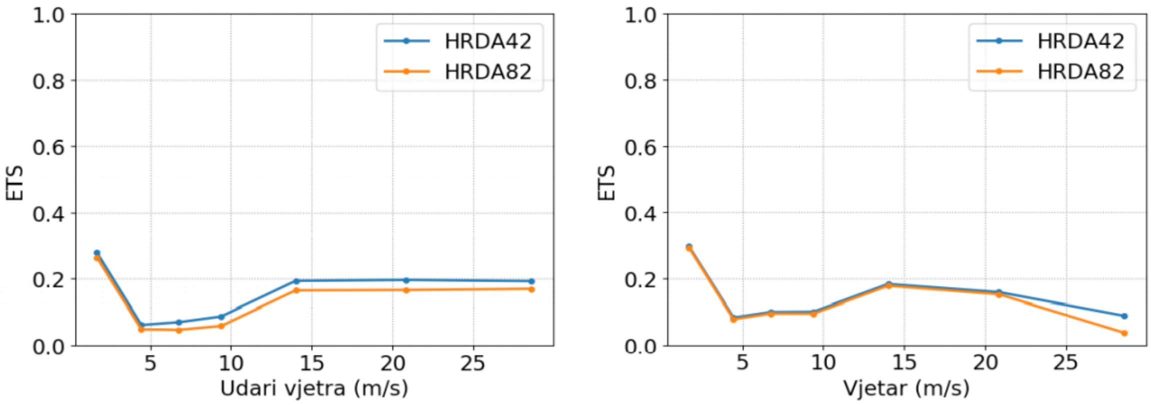

Figure 4: Equitable Threat Score (ETS) of old (HRDA82) and new (HRDA42) dynamical adaptation of wind configuration for wind gusts (left) and for mean wind speed (right) and for period 1.10.2018.-31.3.2019. calculated by comparison with DHMZ meteorological stations.

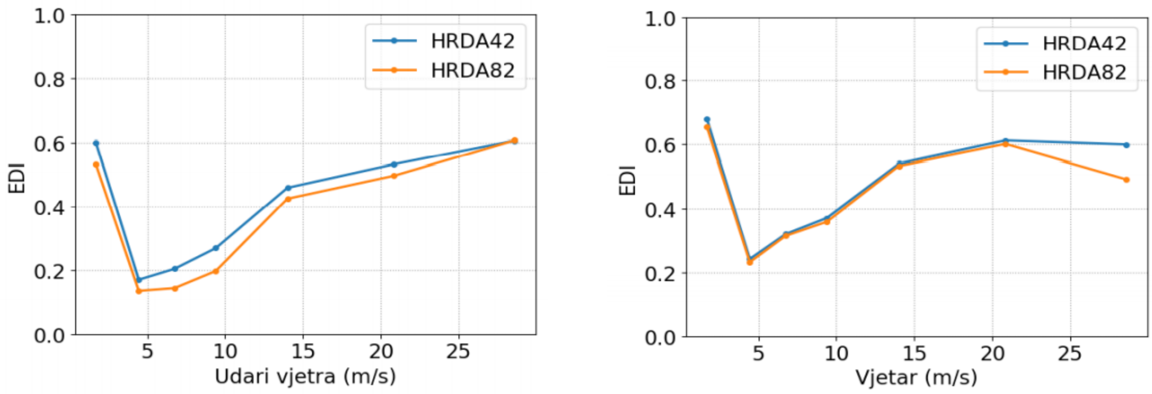

Figure 5 Equitable Threat Score (ETS) of old (HRDA82) and new (HRDA42) dynamical adaptation of wind configuration for wind gusts (left) and for mean wind speed (right) and for period 1.10.2018.-31.3.2019. calculated by comparison with DHMZ meteorological stations

After coupling the new setup of dynamical adaptation to ALADIN-HR4, the ALADIN-HR8 was finally switched off 01.07.2020., and the work on e-suite based on cy43 was started. Full e-suite system (data assimilation and integration) started with parallel run from 01.10.2010. and evaluation is ongoing.

Postprocessing upgrade

Postprocessing of the ALADIN forecast was updated with switch from several programming languages to mainly one: python. The new procedures for plotting 2D ALADIN fields, vertical cross sections, meteograms and number of ASCII products were developed and put to operations. Except for procedures for displaying ALADIN forecast some method that give additional value to the raw forecast were also developed and they are briefly described in the following text.

Model grid size is not the same as the model resolution (e.g., Grasso, 2000). The second is sometimes referred to as the model effective resolution and is generally, at least, 5 times lower than the first (e.g., Skamarock, 2004; Horvath *et al*., 2011). Therefore, all point predictions within that area (i.e., neighbourhood) should be considered equally likely and the output of the model should be viewed as the spatial and (or) temporal function of that neighbourhood. Adding this to the fact that small scale errors saturate in a few hours, we realize that one cannot expect that a convection-permitting model forecast exactly matches the observations on the grid scale (Theis *et al.*, 2005; Mittermaier, 2014). Furthermore, the double-penalty effect (e.g., Mass *et al.*, 2002) makes this problem even worse.

In order to alleviate beforementioned difficulties, neighbourhood methods were developed (Theis et al., 2005; Ebert, 2008, among others). The concept of the neighbourhood is illustrated in Figure 6. Left-hand side of the Figure shows (x, y)-plane of the model grid. Shaded area denotes a 5 × 5 neighbourhood of the point ($x0$, $y0$) (shown in red), while Δx and Δy denote the model grid size in x and y direction, respectively. On the right-hand side, extension of the neighbourhood to time dimension is shown, i.e., (x, t)-plane and Δt denotes the time step between successive model output times. Total number of grid points inside a neighbourhood (Nb) is obtained by choosing a neighbourhood length scale r which can be either a number of grid boxes or physical distance and can be applied using square or circular neighbourhood geometry. For example, left-hand side of Figure 7 shows a square $r \times r$ neighbourhood where Nb (= $r2$) = 25 grid points and r = 5 grid points. In addition, Nb can also be extended to a time dimension (right-hand side of the Figure 7). One can now create a new deterministic forecast as a function of the neighbourhood or take the whole neighbourhood and treat it as a probabilistic forecast instead (i.e., neighbourhood ensemble).

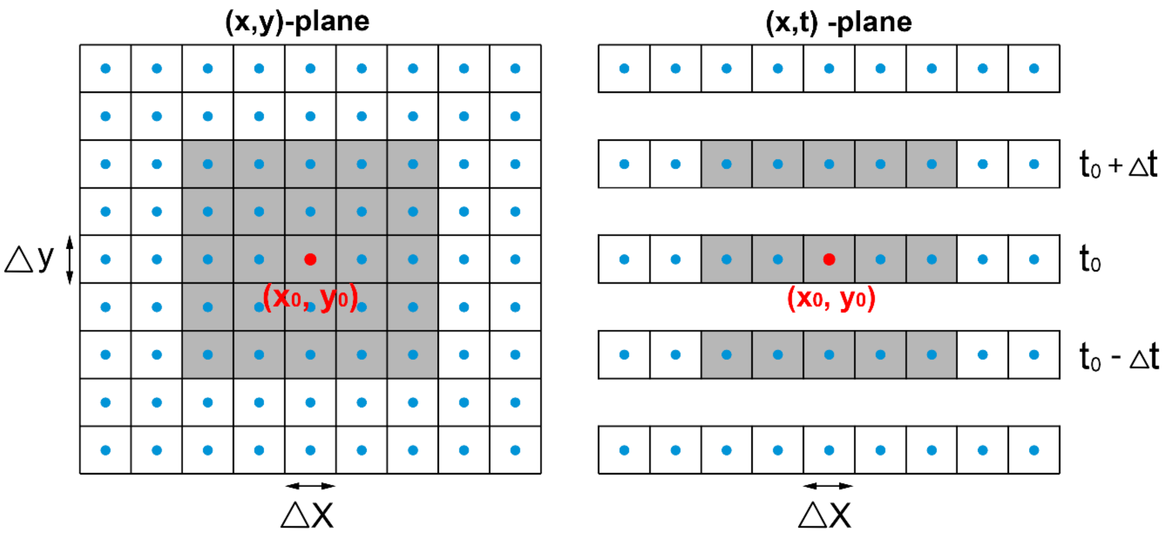

Figure 6: A square spatio-temporal neighbourhood of a given grid point (red) at location (x0, y0) and forecast lead time t0. The spatial neighbourhood in the (x, y)-plane is shown on the left. The spatio-temporal neighbourhood in the (x, t)-plane is shown on the right. Δx and Δy denote he size of a grid box and Δt denotes the time step between successive model output times. Shaded grid boxes belong to the neighbourhood.

Different values for r were tested (and thus for Nb), as previous studies reported that no universally optimal value for neighbourhood size exists, but depend on variable and threshold (e.g., Mittermaier, 2014). As a metric to determine the value of r, we have used the RMSE of the neighbourhood ensemble mean but we did not want to go to much above model's effective resolution (i.e, we want to keep local characteristic of the point if interest). In addition, attention must be paid to the orography and land-sea boundary around the point of interest. For example, temperature and humidity can vary greatly between land and sea points. The same is true for the points with greatly different altitude. We do not want to include mountainous model point from Medvednica to the neighbourhood of Zagreb when forecasting 2 m temperature. For those reasons, filtering of the model points based on altitude (AT) and land-sea (L-S) mask was performed. Table 1 shows chosen values of r, AT and L-S for the used variables.

Table 1. Chosen values for neighbourhood length scale (r), altitude tolerance (AT) and land-sea (L-S) filtering.

Variable	r [grid points]	AT [m]	L-S filtering
MSLP	7	100	False
T2M	7	100	True
RH2M	7	100	True
W10M	5	200	True
RR1H	7	300	False

Several operational products were developed. Figure 7 shows precipitation in meteograms extended by box-plot from the neighbourhood ensemble. Here, a time dimension is also included as described under the Figure. Figure 8 shows box-plots and plumes of 2 m temperature forecast. Verification of this type of product has shown that neighbourhood ensemble mean has about 10 % (15 %) lower RMSE for wind speed (gusts). For precipitation, ensemble median has about 20 % lower MAE. Figure 9 shows a 2-D neighbourhood product – forecasted probability of precipitation above a given threshold. Probability is calculated within a neighbourhood of a given point and the result is assigned to that point. This is done for all the points inside the domain.

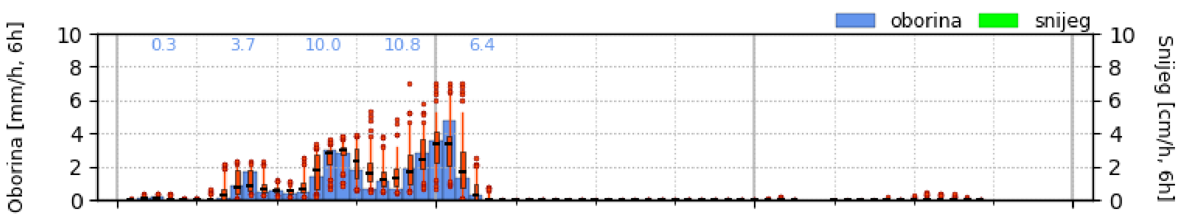

Figure 7: Standard deterministic precipitation histogram. Box-plots representing neighbourhood ensemble are shown in red. Black horizontal bars represent ensemble median. Here, neighbourhood is extended to the time dimension. In the first 36 h, ±Δt is used, and after that ±2Δt is used.

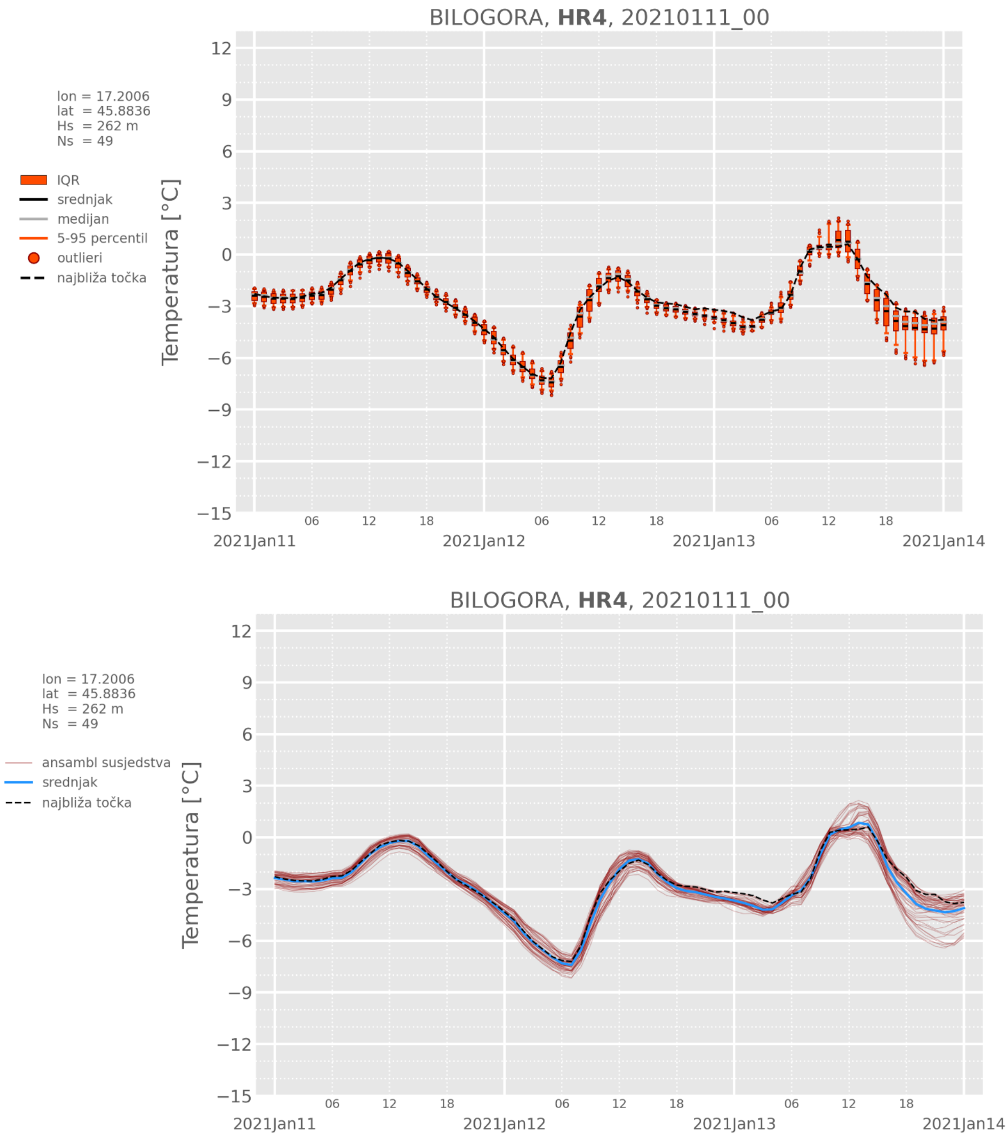

Figure 8: ALADIN-HR4 2 m temperature forecast with lead time. Dashed black line denotes standard nearest point deterministic forecast. Upper plot shows neighbourhood ensemble as box-plots with mean (solid black) and median (solid grey). Lower plots show neighbourhood ensemble as plumes (solid red) and mean (solid blue) lines.

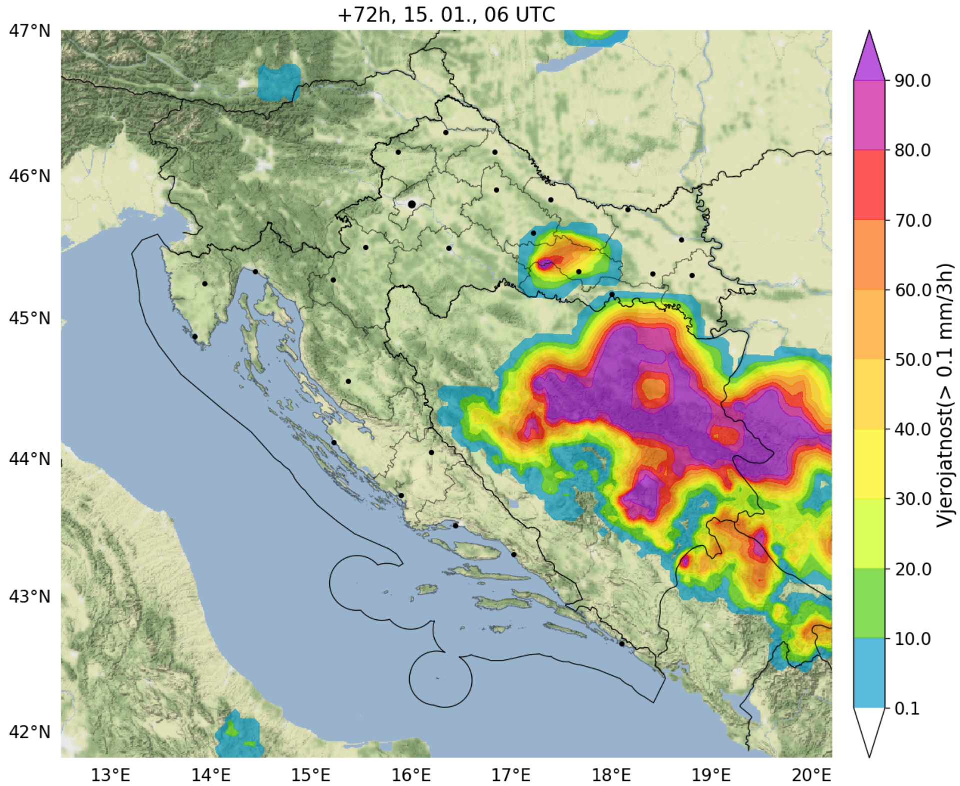

Figure 9: ALADIN-HR4 precipitation probability forecast (above 0.1 mm/3h) derived from the neighbourhood ensemble.

We have done some tests with the neighbourhood postprocessing of deterministic precipitation forecast plotted in meteograms on DHMZ official web pages. There, for a specific location, precipitation is plotted as a value from the closest model grid point. But, if we choose, for example, a 55th or 60th percentile from the neighbourhood instead, a forecast can be significantly improved (not shown). We are considering replacing the old procedure with the neighbourhood approach. Lastly, initial tests show promising results when a convection-permitting EPS is combined with the neighbourhood approach and should be studied further.

3 References

Ivatek-Šahdan, S., and M. Tudor, 2004: Use of high-resolution dynamical adaptation in operational suite and research impact studies. Meteor. Z., 13, 99-108.

Ebert, E., 2008: Fuzzy verification of high-resolution gridded forecasts: a review and proposed framework. Meteorol. Appl., 15, 51–64.

Grasso, L. D., 2000: The differentiation between grid spacing and resolution and their application to numerical modeling. Bull. Amer. Meteol. Soc., 81, 579–580.

Horvath, K., Bajić, A. and Ivatek-Šahdan, S., 2011: Dynamical downscaling of wind speed in complex terrain prone to bora-type flows. JAMC, 50, 1676–1691.

Mass, C. F., Ovens, D., Westrick, K. and Colle, B. A., 2002: Does increasing horizontal resolution produce more skillful forecasts? Bull. Amer. Meteor. Soc., 83, 407–430.

Mittermaier, M., 2014: A Strategy for verifying near-convection-resolving model forecasts at observing sites. Wea. Forecasting, 29, 185–204.

Skamarock, W. C., 2004: Evaluating mesoscale NWP models using kinetic energy spectra. Mon. Wea. Rev., 132, 3019–3032.

Theis, S. E., Hense, A. and Damrath, U., 2005: Probabilistic precipitation forecasts from a deterministic model: A pragmatic approach. Meteor. Appl., 12, 257–268.

Žagar, M., and J. Rakovec, 1999: Small-scale surface wind prediction using dynamic adaptation. Tellus, 51A, 489-504

HARMONIE-AROME 4D-Var

Jan Barkmeijer[1], Magnus Lindskog[2], Nils Gustafsson[2], Jelena Bojarova[2]
Roohollah Azad[3], Isabel Monteiro[4], Pau Escribà[5], Eoin Whelan[6], Martin Ridal[2],
Jana Sánchez-Arriola[5] Ole Vignes[3] Roel Stappers[3] Roger Randriamampianina[3]

[1] Royal Netherlands Meteorological Institute, De Bilt, The Netherlands
[2] Swedish Meteorological and Hydrological Institute, Norrköping, Sweden
[3] Norwegian Meteorlogical Institute, Oslo, Norway
[4] Portuguese Institute for Sea and Atmosphere, Lisbon, Portugal
[5] Spanish Meteorological Agency, Barcelona and Santander, Spain
[6] The Irish Meteorological Service, Dublin, Ireland

Abstract

The status of CY43 HARMONIE-AROME 4D-Var is presented. Central to the HARMONIE-AROME 4D-Var implementation is the multi-incremental approach and the current setup comprises two outer loops at six and three times the main forecast grid resolution of 2.5 km. This setup is flexible though, as is the length of the observation window. Results will be given for 4D-Var in comparison to 3D-Var for three domains, centered around Scandinavia, the Iberian Peninsula and the Netherlands. The starting point here is that both 3D-Var and 4D-Var are using identical observations types. Generally speaking it can be concluded that 4D-Var forecasts are superior. The paper also gives an extensive list of opportunities from which particularly HARMONIE-AROME 4D-Var can benefit. For example, increasing the observation set, improving the treatment of observations during the observation window and new algorithmic avenues.

1 Introduction

1.1 General

The development of HARMONIE-AROME 4D-Var has been a long running data assimilation project of the HIRLAM consortium. After its first working version back in 2008 (CY38h1.2) the 4D-Var suite has matured over the years and has now reached a level that it can be considered for operational use.

At the core of the HARMONIE-AROME 4D-Var implementation is the use of the multi-incremental variational approach (Courtier *et al.*, 1994). Hereby the nonlinearities of the forecast model and the observation operators are better handled through a sequence of iterative re-linearizations (Trémolet, 2004). By solving a series (i=1,...,N) of minimizations, each minimization producing an analysis increment δx_i, the final increment δx is obtained through setting $\delta x = \sum_{i=1}^{N} \delta x_i$. For the i-th minimization or i-th loop, the corresponding cost function $\mathrm{J_i}$ reads as

$$\begin{aligned} J_i &= J_i^b + J_i^o \\ &= \frac{1}{2}((\delta\mathbf{x_i} - (\mathbf{x_b} - \mathbf{x_i})^{\mathrm{T}}\mathbf{B^{-1}}(\delta\mathbf{x_i} - (\mathbf{x_b} - \mathbf{x_i})) \qquad (1) \\ &+ \frac{1}{2}\sum_{k=0}^{K}(\mathbf{H_k^i M_k^i}\delta\mathbf{x^i} - \mathbf{d_k^i})^{\mathrm{T}}\mathbf{R_k^{-1}}(\mathbf{H_k^i M_k^i}\delta\mathbf{x^i} - \mathbf{d_k^i}) \end{aligned}$$

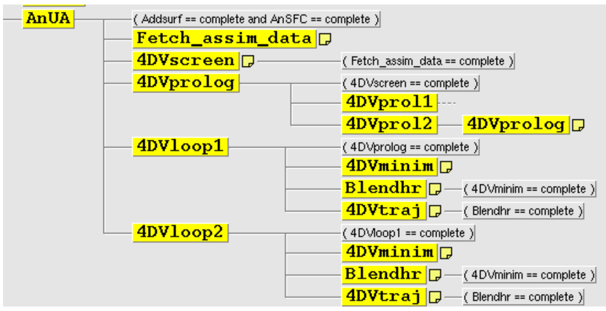

Figure 1: Illustration of the HARMONIE-AROME 4D-Var graphical workflow and the underlying script system, using two outer loops.

where x^b is the model background state valid at time t_0, $\mathbf{B}$ is the background error covariance matrix and the subscript k denotes time $t_k = t_0 + k\Delta t$ within the assimilation window, $d_k^i = y_k - \mathcal{H}(\mathcal{M}_k(x^i))$ are the innovations (observation minus background) where y_k denotes the observation vector at time t_k, $\mathcal{M}_k(.)$ denotes integration of the nonlinear model from time t_0 to time t_k and $\mathcal{H}(.)$ is the nonlinear observation operator, $\mathbf{M}_k^i$ and $\mathbf{H}_k^i$ denote the corresponding tangent linear (TL) model and TL observation operator respectively, linearized around the nonlinear trajectory $\mathcal{M}_k(x_i)$. In the first loop the model background state, x^b, is typically used as the first-guess $x^1 = x^b$ for the minimization. Eq. 1 is then minimized to yield δx^i, with $i = 1$. Following this, the first-guess state is updated with $x^{i+1} = x^i + \delta x^i$ ready to be used in the next loop.

In recent years HARMONIE-AROME 4D-Var has undergone several enhancements such as the possibility to assimilate an increased number of observation types (see Section 1.2), the use of spectral specific humidity and the use of a 3-hour observation window instead of 2-hour. The need for spectral specific humidity turned out to be essential in ensuring the tangent and adjoint models pass the so-called adjoint test ([TL$x, y$]=[x,ADy] for arbitrary model field perturbations x and y and with [.] the inner product used for deriving the adjoint model AD), a prerequisite for a well-defined minimization problem. Recently the 2-hour observation window version has been adapted to a 3-hour observations window. This in conjunction with the already 3-hourly cycling frequency ensures all observations from satellite overpasses are available for assimilation. The current HARMONIE-AROME 4D-Var further comprises two loops at 6 and 3 times the main forecast grid resolution of 2.5 km. This flexible setup allows for a minimization that is computationally affordable and with 10 and 15 iterations respectively most of the reduction in the gradient norm and cost function can be achieved (see Section 2.1). During the minimization use is made of the linear physics package developed for the ARPEGE and ALADIN models. It is comprised of linearized versions of some key physical processes. See Section 2.2 for a comparison between linear and nonlinear model evolution of increments in HARMONIE-AROME. Finally it is worth noting that a carefully designed scripting system together with the ecFlow graphical workflow package enables users to work with HARMONIE-AROME 4D-Var in a controlled manner, which is illustrated in Fig. 1 for a two outer loops set-up. At the end of each 4DVminim task the high resolution first-guess is modified by the computed low resolution analysis increment. After complementing with some extra model fields, using the Blendhr task, the trajectory run, 4DVtraj, propagates the analysis from the beginning of the observation window forward in time to produce the initial state for the high resolution forecast and updates the minimisation statistics in the ODB.

1.2 Observation usage

HARMONIE-AROME 4D-Var has been prepared to handle conventional (*in-situ* measurement) observation types (Table 1) as well as non-conventional types of observations (Table 2), including remote-sensing measurements. In the case of a 2-hour observation window for producing a forecast model initial state at hour HH observations from $HH - 60$ min to $HH + 59$ min are used. This will be changed to using observations from $HH - 60$ min to $HH + 60$ min, which is more appropriate. In the case of a 3-hour observation window for producing a forecast model initial state at hour HH observations from $HH - 120$ min to $HH + 59$ min are used. Observations are sorted into seven and ten time-slots (for the 2-hour and 3-hour setup repsectively), sub-dividing the observation window in 10 min intervals at the beginning and the end and 20 min otherwise.

With respect to conventional observation usage z refers to geopotential height at mean sea level, $t2m$ temperature at the height of two metres, $rh2m$ relative humidity at the height of two metres, $u10$, $v10$ wind-components at 10 m, u, v wind-components, t temperature and q specific humidity. By default hourly SYNOP observations are used. There is also an option to apply a temporal thinning to use only the SYNOP observations valid at main analysis time. The reason for applying this temporal thinning is to avoid serially correlated observation errors that are presently not accounted for. These serially correlated observation errors can be caused by systematic observation errors at a particular station. In future HARMONIE-AROME 4D-Var versions a procedure for handling of these correlations (Järvinen *et al.*, 1999) will be considered.

Table 1: Usage of conventional types of *in-situ* measurements in 4D-Var.

Observation type	Variable
SYNOP	z
SHIP	z, u10, v10
DRIBU	z, u, v
AMDAR	u, v, t
PILOT	u, v
TEMP	u, v, t, q

For non-conventional observation usage as ztd refers to zenith total delay and std to slant total delay. RADAR observations are used with a temporal resolution of 1 h. The reason for not using RADAR observations with an even higher temporal resolution is again to avoid spurious effects of serially correlated observation errors not accounted for. Pre-processed RADAR observations of rh are derived by applying a 1-D Bayesian approach following strategies described by Caumont *et al.* (2010) and Wattrelot *et al.* (2014) using an observation handling in accordance with Ridal and Dahlbom (2017). It should be mentioned that SEVIRI radiances were assimilated in an earlier HARMONIE-AROME version (CY40) using hourly SEVIRI radiances in GRIB format. No problems are foreseen to introduce assimilation of these SEVIRI radiances also into the in the current (CY43) HARMONIE-AROME 4D-Var version. Observation types not yet tested in HARMONIE-AROME 4D-Var that are prepared for in HARMONIE-AROME 3D-Var are Global Navigation Satellite System (GNSS) Radio Occultations (RO) and Atmospheric Motion Vectors (AMV), radiances from the ATMS radiances and AMDAR humidity observations. No problems are foreseen with introduction of these remaining observation types into HARMONIE-AROME 4D-Var.

As in HARMONIE-AROME 3D-Var a Variational Bias Correction (VARBC) based on ideas of Dee (2005) is applied to handle systematic errors for satellite radiances and Ground-Based (G-B) GNSS ztds. Randriamampianina *et al.* (2011) studied VARBC configurations in the context of limited-area radiance assimilation. Following G-B GNSS ztd HARMONIE-AROME 3D-Var handling (Sánchez Arriola *et al.*, 2016; Lindskog *et al.*, 2017) one single VARBC predictor is applied by default. The use of multiple outer-loop iterations in HARMONIE-AROME 4D-Var imply a special handling of propagation of VARBC predictor coefficients in between different outer loops.

Table 2: Usage of of non-conventional types of observations in 4D-Var.

Observation type	Observed quantity
MODE-S	derived w and derived t
G-B GNSS	ztd, std
ASCAT	derived surface w
RADAR	derived rh, radial wind
AMSU-A, MHS, MWHS-2	microwave radiance
IASI, SEVIRI	infrared radiance

When it comes to specification of observation errors, identification of radiances contaminated by clouds, spatial thinning procedures and quality control there are no significant differences between HARMONIE-AROME 3D-Var and 4D-Var.

2 Demonstration of functionality

In this section HARMONIE-AROME 4D-Var functionality is briefly presented with a description of the cost function evolution, results from single observations tests and the consequences of enlarging the observation window from 2 hours to 3 hours.

2.1 Cost function evolution

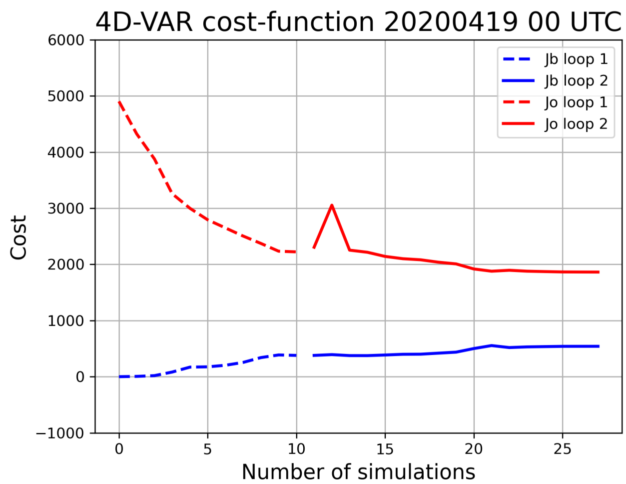

Figure 2: HARMONIE-AROME 4D-Var Jb and Jo parts of cost function for minimisation over MetCoOp domain for the 0000 UTC April 19, 2020 analysis using two loops at 6 and 3 times of the main forecast grid resolution of 2.5 km. For the first loop 10 iterations was used and for the second 15 (one iteration results in one or more simulations).

Figure 2 shows an example of the cost function, J, evolution during a HARMONIE-AROME 4D-Var minimization. The example is from the assimilation over a Nordic area using conventional as well as several non-conventional types of observations and a horizontal grid-distance of 2.5 km. Two outer loop iterations were used in the minimization of the cost function. Minimization in the first outer loop was applied at 15 km using a maximum of 10 iterations (15 simulations) and the minimization in the second outer loop was applied at 7.5 km using a a maximum of 15 iterations (20 simulations). Clearly the cost function values are mainly reduced in the first lower resolution loop, where larger scales in the background field are adjusted towards observations. The reduction of the cost function continues in the second, higher resolution loop, re-linearised around an updated nonlinear trajectory (see Eq. 1). It can be seen that at the end of the second outer loop the cost function does not change much so that the minimization has reached a satisfactory level of convergence. For both loops a preconditioning of the minimization using the square-root of the background-error covariance matrix was applied (Courtier *et al.*, 1998; Gustafsson *et al.*, 2001). There is ongoing work aiming at applying a preconditioning by normalisation of the second outer loop using the Hessian of the cost function (Akkraoui *et al.*, 2012).

2.2 Single observations and linear vs nonlinear evolution

In order to further test the functionality of 4D-Var a single observation experiment was carried out for the 2-hour assimilation window 4D-Var. A specific humidity observation at 850 hPa from a radiosonde valid at the middle of the observation window was assimilated. Figure 3 shows the resulting increment at the beginning of the window at 850 hPa for this particular observation (no other observations were used in the data assimilation) and its linear evolution during the length of the observation window. The red dot in the middle panel indicates the location of the observation. In Fig. 4 the linear (top panel) and nonlinear evolution (bottom panel) of the increment in terms of specific humidity is presented at analysis time by means of a zonal cross-section through the observation location. The nonlinear evolution is given by the difference between two full physics HARMONIE-AROME runs (4DVtraj, see Fig. 1) starting from the first-guess and the first-guess modified by the increment. Clearly the linearly propagated analysis increment resembles well the nonlinearly evolved increment.

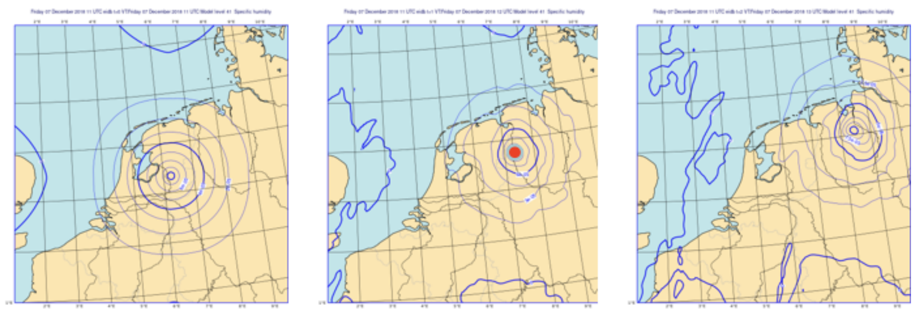

Figure 3: Linear evolution of the increment obtained from a 4D-Var single observations experiment. The 4D-Var observation window is 2 hours and the single observation, valid for the middle of the observation window, is for specific humidity at 850 hPa for a location denoted by a red dot. Panels show the increment at the beginning of the observation window (left), after 1 hour (middle) and after 2 hours (right).

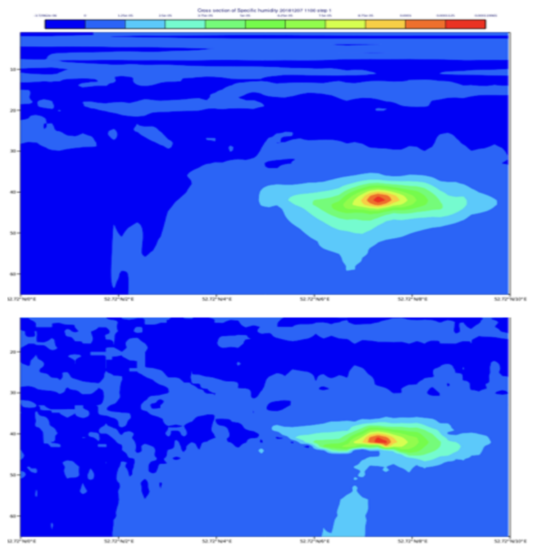

Figure 4: Cross section for specific humidity of the non-linear (top panel) and tangent linear evolution (bottom panel) of the increment shown in Fig. 3. The evolution is for 1 hour, which is the middle of the observation window (analysis time)

2.3 2-hour *vs*. 3-hour assimilation window

One of the recent enhancements of HARMONIE-AROME 4D-Var configuration was to apply a 3-hour assimilation window instead of 2-hour. The advantage of this configuration is shown for wind observations from ASCAT instruments on-board Metop satellites. Each day, these satellites overpass the Iberian domain between 09 UTC - 11 UTC and 21 UTC - 23 UTC. For the 2-hour window configuration, ASCAT winds between 10 UTC - 11 UTC and 22 UTC - 23 UTC are not considered. Fig 5 illustrates this point for 01 March 2020 at 12 UTC analysis. Although both configurations used observations from the two Metops available (Metop-B and Metop-C), for the 2-hour configuration, in contrast with the 3-hour one, only observations acquired between 11 UTC and 12 UTC were used in assimilation at 12 UTC analysis.

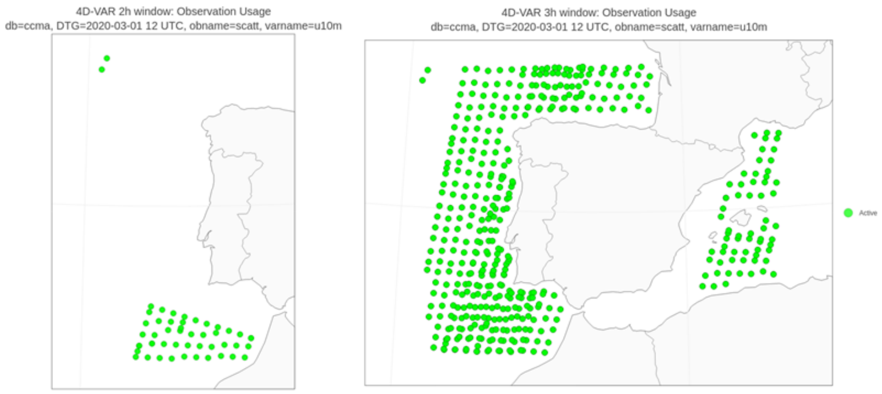

Figure 5: For 1 March 2020 ASCAT winds use in 4D-Var 2-hour window assimilation window (left) and 4D-Var 3-hour window (right) configurations, at analysis time 1200 UTC

3 Cooperation on three domains

3.1 Description of domains

An extensive evaluation of HARMONIE-AROME 4D-Var has been carried out for 3D-Var and 4D-Var by performing parallel data assimilation experiments over three different modelling domains centered around Iberian Peninsula (Iberia), the Netherlands (Netherlands) and Scandinavia (MetCoOp), respectively. The domains are illustrated in Fig 6. One advantage of running over a number of domains with different climates and characteristics is that this provides a more robust test of 4D-Var with respect to the typical local typical meteorological situations. It also prepares for a smoother local implementation in a pre-operational environment.

3.2 Experimental design

The evaluation of 4D-Var was partly through case studies investigating various aspects of HARMONIE-AROME 4D-Var, as demonstrated Section 2. We have also carried out a large amount of parallel experiments comparing 4D-Var with 3D-Var and also comparing various 4D-Var configurations over longer periods. Examples of such extended 4D-Var configuration comparisons are 2-hour *vs.* 3-hour observation window, impact of applying a Large Scale Mixing (LSM) of host model information into background state, utilisation of hourly SYNOP observations *vs.* utilisation at main analysis hour only, impact of applying the successive outer loop iterations at 15 km and 7.5 km *vs.* 15 km and 15 km, and assimilation of screen level $rh2m$ and $t2m$ observations. Here we will only briefly mention about some of these results but focus on three experiments comparing 4D-Var with 3D-Var. To make the comparison clearer LSM was not applied to either 4D-Var or 3D-Var in these experiments.

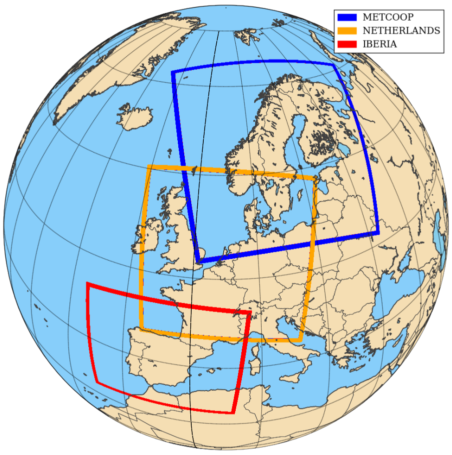

Figure 6: Domains used for the evaluation of HARMONIE-AROME 4D-Var.

The experiments were designed to use the same kind of observation in both the 4D-Var and the associated 3D-Var experiment. There were, however, some differences in configurations between the three different parallel experiments carried out. Each of the parallel 4D-Var *vs* 3D-Var experiments were carried out for a one-month period during 2020, covering three different seasons, and with 4D-Var configurations as summarized in Table 3. Before the start of each experiments a 10-day warm up-period was applied to spin-up surface fields and update VARBC-coefficients. The VARBC-coefficient files at the beginning of the warm-up period were taken from operational archive.

Table 3: Configuration of 4D-/3D-Var experiments carried out for 2020.

Conf	Iberia	Netherlands	MetCoOp
Period	07 Feb-07 Mar	14 Jun-14 Jul	20 Mar-20 Apr
Obs win (h)	3	3	2
Loop res (km)	15,7.5	15,7.5	15,7.5
Conv ob	all	all	all
Non-conv ob	ascat	mode-s ehs, ascat	amsu-a,mhs,iasi,ztd

4 Verification scores

Results from extended experiments carried out over the three domains reveal that 4D-Var produce forecasts that in general have better quality than the ones produced with 3D-Var.

For the experiment carried out over the MetCoOp domain 4D-Var produced clearly better atmospheric wind and humidity forecasts, as illustrated in Fig. 7. Temperature scores were rather neutral (not shown). The reason for the improved wind and humidity scores is most likely an improved use of wind and in particular satellite humidity-related observations taking the correct time of the observations into account and using the tangent-linear and adjoint of the forecast model within the minimization process. One problem with 4D-Var settings identified and solved while evaluating the coordinated experiments was that relaxation towards ECMWF host model information at the uppermost vertical levels was not applied in 4D-Var experiment, only in 3D-Var. This explains the worse 4D-Var forecasts at the uppermost levels seen in the left panel of Fig. 7.

Slightly worse scores for MetCoOp 4D-Var as compared to 3D-Var were obtained for short-range MSLP forecasts and standard deviation of forecasts of variables at two metre. This is illustrated in Fig. 8 for MSLP and rh2m forecasts. The reason for worse MSLP short-range forecasts is likely spurious wrap-around of surface

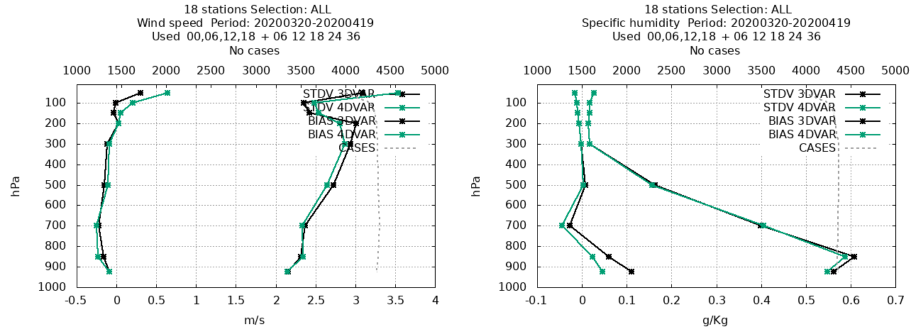

Figure 7: Verification statistics for MetCoOp domain, in terms of bias (BIAS) and standard deviation (STDV), of +06 to +36 h forecasts against radiosonde observations of wind speed (left, unit: m/s) and specific humidity (right, unit: g/kg) averaged over all observations within the domain and over the one month period. Scores are shown as function of vertical level and black full curves are for 3D-Var while green full curves represent 4D-Var. Grey dashed curve illustrates the number of observations used in the verification.

pressure analysis increments from one side of the domain to the opposite that can occur due to the use of bi-periodic spectral transforms in combination with large spatial surface pressure correlation length scales, a narrow extension zone with a relatively narrow redzone (in our case 150 km) and uneven distribution of surface pressure observations. The wrap-around problem is more pronounced in 4D-Var than in 3D-Var, because in 4D-Var the center of analysis increments may be projected significantly upstream of observation locations and well into the redzone area. This issue will be addressed in future versions by applying a wider extension zone. In addition there is a need for a revised blacklisting of z observations in MetCoOp 4D-Var as well as in 3D-Var. When it comes to relative humidity it can be seen that 4D-Var has slightly larger standard deviations than 3D-Var, in particular at short forecast ranges. However the bias is considerably smaller in 4D-Var. Regarding the standard deviations at two metre level, there is however room for improvement. With the Iberia experience in mind it is hoped that introduction of $rh2m$ and $t2m$ observations in 4D-Var as well as 3D-Var data assimilation will accomplish this.

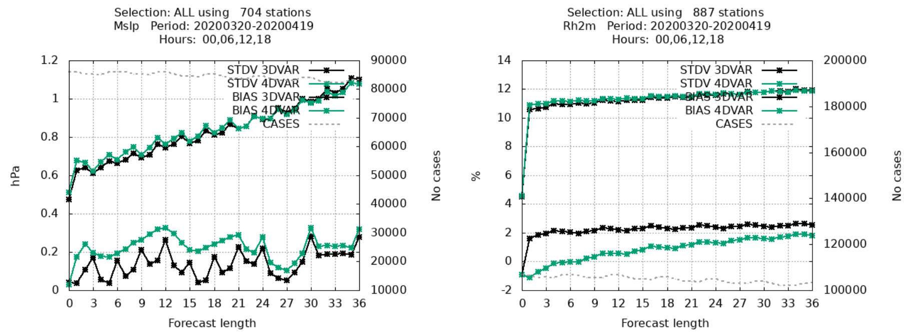

Figure 8: Verification statistics for METCOOP domain, in terms of bias (BIAS) and standard deviation (STDV) as function of forecast range for verification against SYNOP observations of $MSLP$ (left, unit: hPa) and $rh2m$ (right, unit: K) averaged over all observations within the domain and over the one month period. Black full curves are for 3D-Var while green full curves represent 4D-Var. Grey dashed curve illustrates the number of observations used in the verification.

Also for the experiments performed over Iberia, better wind forecasts were obtained with 4D-Var, as it is illustrated in terms of speed and direction in Fig. 9. In fact, comparing statistics for 3D-Var (black) and 4D-Var (green), improved scores are found for 4D-Var. In Iberia, apart from conventional observations, only ASCAT wind observations were used. A likely cause for the improved 4D-Var forecast scores is the 4D-Var ability to use these observations at the correct observation time.

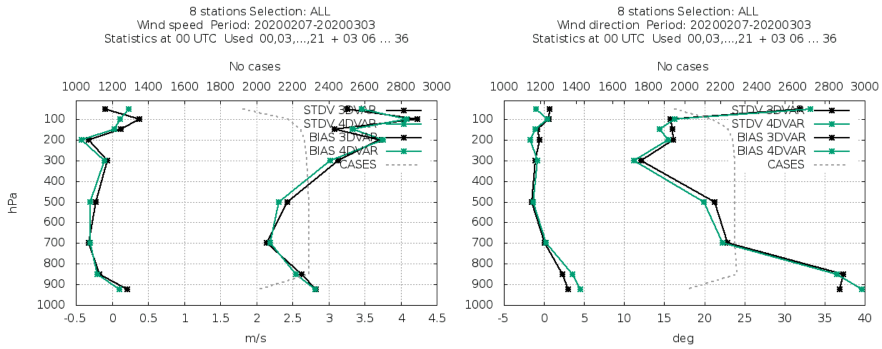

Figure 9: Verification statistics for the Iberian domain, in terms of bias (BIAS) and standard deviation (STDV) as function of forecast range for verification against radiosonde observations of wind speed (left, in m/s) and wind direction (right, in degrees) averaged over all observations within the domain From 07 Feb 2020 to 03 Mar 2020 period. Black full curves are for 3D-Var while green full curves represent 4D-Var (here the 3-hour configuration). Grey dashed curve illustrates the number of observations used in the verification.

For the Netherlands domain the performance for $MSLP$ improves with 4D-Var as compared to 3D-Var. This is most noticeable by a reduction of the bias, whereas the impact on standard deviation remains neutral, as is illustrated in Fig 10. The $MSLP$ forecasts do not seem to suffer from wrap-around issues as observed for the MetCoOp domain. With respect to screening level data the quality of $t2m$ forecasts improves as well, in particular for the bias. This is however not the case for $q2m$. Especially for the short range the 4D-Var forecasts are slightly worse both in terms of standard deviation as well as for bias, see Fig 10. Inclusion of $rh2m$ and $t2m$ observation in the future observation set may alleviate this.

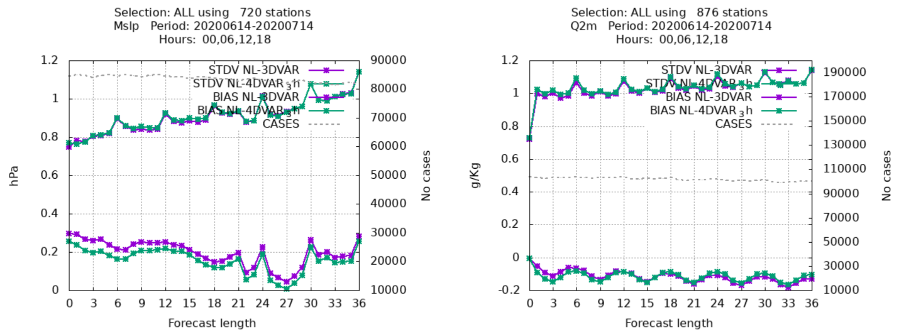

Figure 10: Verification statistics for the NETHERLANDS domain, in terms of bias (BIAS) and standard deviation (STDV) as function of forecast range for verification against SYNOP observations of $MSLP$ (left, unit: hPa) and $q2m$ (right, unit: g/kg) averaged over all observations within the domain and over the one month period. Purple full curves are for 3D-Var while green full curves represent 4D-Var. Grey dashed curve illustrates the number of observations used in the verification.

The large set of Mode-S EHS aircraft observations clearly has a positive impact on wind forecast performance in 4D-Var as shown in Fig 11. Note that in 3D-Var Mode-S EHS data is used only in a 30 minute interval around analysis time. Consequently roughly six times more Mode-S EHS observations are used in 4D-Var than in 3D-Var and at the appropriate observations time. In Fig. 11 scores for wind direction are shown indicating a decreased standard deviation and improved bias for 4D-Var. And although no additional humidity observations are assimilated other than from radiosondes, there is also a small improvement for 4D-Var specific humidity profiles as illustrated in Fig 11. This positive impact on humidity and associated parameters like cloud cover, fog and precipitation when using aircraft wind data has also been observed in earlier HARMONIE-AROME 4D-Var experiments and described in Gustafsson *et al.* (2018).

Additional sensitivity experiments carried out over the Iberian as well as over Netherlands domains revealed a benefit from using a using a 3-hour observation window as compared to using a 2-hour window. In addition, a positive impact from LSM, particularly for specific humidity was seen. This positive impact might decrease

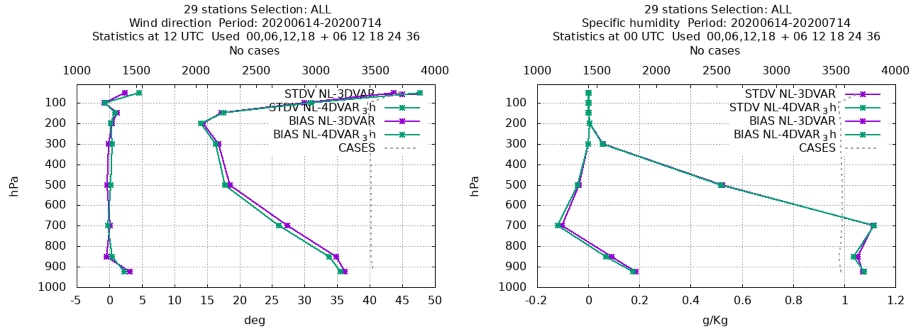

Figure 11: Verification statistics for the Netherlands domain, in terms of bias (BIAS) and standard deviation (STDV), of +06 to +36 h forecasts against radiosonde observations of wind direction (left, unit: m/s) and specific humidity (right, unit: g/kg) averaged over all observations within the domain and over the one month period. Scores are shown as function of vertical level and purple full curves are for 3D-Var while green full curves represent 4D-Var. Grey dashed curve illustrates the number of observations used in the verification.

when introducing assimilation of satellite-based radiances sensitive to atmospheric moisture, such as the MHS instrument. Finally a benefit of assimilating $rh2m$ and $t2m$ observations in HARMONIE-AROME 4D-Var experiments, in addition to their use in the surface analysis, has been demonstrated for Iberia.

5 Outlook

There are several ways in which HARMONIE-AROME 4D-Var can be further extended and improved. The various observation types which have not been explored yet provide an obvious route. We plan to extend the observation set with (not extensive) RADAR (both reflectivity and radial winds), AMDAR (humidity), GNSS STD, SEVIRI, AMV, MWHS-2, MHS, ATMS and on a longer term CRiS and MTG IRS.

Already mentioned are the introduction of a Hessian preconditioning to further speed up the minimization of the second outer loop, exploring the representation of serially correlated observation errors and adoption of a wider extension zone. Research versions with application of a wider extension zone (order of 50-100 grid-points) exists and will be further exploited. The larger extension zone framework requires more computer memory in minimization and also some transforms of domains (using the software tools GL or $FULLPOS$) in between 4D-Var and the surface analysis and forecast steps. It should be mentioned that the wider extension zone developments can be applied also in the context of 3D-Var. There have also been some early trials with weak constraint digital filter initialisation by introducing an additional Jc term to the cost function, penalising the divergent part of the flow-field. Longer term plans also include introduction of ECMWF simplified physics package and combining it with HARMONIE-AROME non-linear physics.

To benefit from high-quality large scale information provided by the ECMWF host model a spectral LSM might be applied to the background state (Müller *et al.*, 2017) in HARMONIE-AROME 3D-Var before upper-air data assimilation. Such a facility has also been introduced to 4D-Var, where the LSM is applied to the background state, valid at the beginning of the assimilation time-window and a positve impact have been seen over the Iberia. On the longer term one can as well think of introducing large scale host model information by introduction of additional constraints during the minimization of the cost function, as was done by Dahlgren and Gustafsson (2012). Another benefit from the large scale is the use of the optional relaxation to the ECMWF host model in the upper air levels (see 3D-Var experiment in Fig. 7.).

Based on ideas from HIRLAM 4D-Var (Gustafsson *et al.*, 2012) we are in the processes of enhancing HARMONIE-AROME 4D-VAR with an optional control of lateral boundary conditions. Some first results of controlling not only the initial state but also the lateral boundary conditions (at the beginning of the observation window) are illustrated in in Fig. 12. Shown are surface pressure analysis increments for one particular cycle without and with control of lateral boundary conditions. One can see that introduction of control of lateral boundary conditions control effects the initial state analysis increments in particular close to the lateral boundaries, but also in the inner part of the domain.

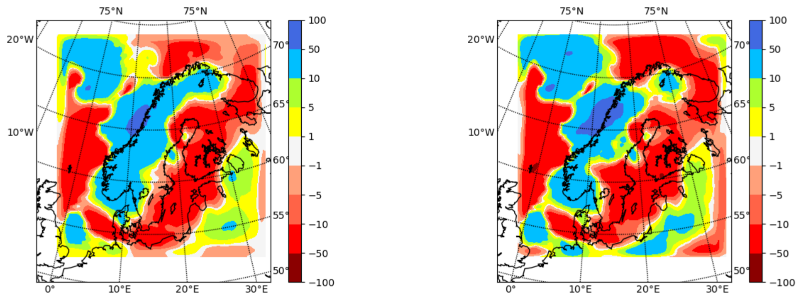

Figure 12: Two hour tangent-linear model development of surface pressure (unit: Pa) without (left) and with control of lateral boundary conditions. The propagation is for one particular assimilation experiment using one outer loop and 15 km assimilation grid distance and propagation of increments when convergence is reached.

One basic weakness of the default version of HARMONIE-AROME 4D-Var is the assumption of a perfect forecast model over the observation window – the forecast model is applied as a strong optimisation constraint. However, there exist possibilities to partly compensate for this weakness of 4D-Var. For example ECMWF has developed a method for controlling model errors during the data assimilation (Trémolet, 2006). This was in particular demonstrated beneficial in the stratosphere (Lindskog *et al.*, 2009), where it is now applied operationally at ECMWF. Related, the set-up of HARMONIE-AROME 4D-Var can also be used to determine a tendency increment that minimizes the cost function as given by Eq. 1 (Barkmeijer *et al.*, 2003). Then, instead of evaluating $\mathbf{M}_k^i \delta x^i$ we are interested in $\mathbf{M}_k^i \delta f^i$, where f^i is the tendency increment valid for loop i. In the current HARMONIE-AROME implementation the tendency increment does not change during the observation window, but is spatially varying both vertically and horizontally. In the case of opting for the tendency increment approach during the first outer loop, the subsequent nonlinear forecasts will apply a tendency increment for the appropriate lead time. For the forecast starting at analysis time this means that the tendency increment perturbation will not be active anymore after 1 hour into the forecast. Note that the part of the cost function associated with J_b remains constant during the minimization with respect to a tendency increment. In Fig. 13 the same single observation of specific humidity at 850 hPa valid for 12 UTC (middle of the observation window in this case) is used to determine the tendency increment. This tendency increment is plotted in the top left panel for specific humidity and differs for the analysis increment in the bottom left panel. It is slightly elongated and more located to the East. The middle panel slows the response of the linear model after applying this tendency increment for 1 hour. The maximum is located at the observation position and in fact J_o is zero. This linear response can be compared with the linearly evolved analysis increment as represented in the bottom row. The right panel shows the response at the end of the observation window.

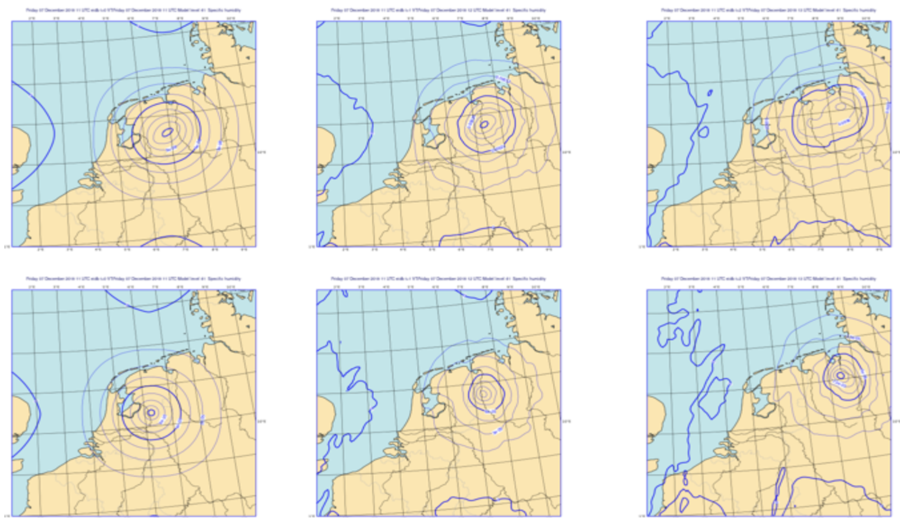

Figure 13: Top row. Tendency increment for the same single observation as used in Fig. 3 and its response after 1 hour (middle panel) and 2 hours (right panel) tangent linear integration. Bottom row. Identical to Fig. 3: the linear evolution of the analysis increment.

The main strengths of the 4D-Var scheme demonstrated so far comes from the possibility to assimilate observations at the proper observation time and from the flow-dependency of the analysis error structures due to tangent-linear and adjoint forecast model involved in the minimization process over a time window. The 4D-Var scheme will be further extended with the Hybrid EnVar functionality that allows for flow-dependent background error statistics. The Hybrid EnVar scheme based on an augmented control variable approach (Lorenc, 2003; Gustafsson *et al.*, 2014) has already been implemented in the HARMONIE-AROME forecasting system. It combines a full rank climatological background error covariance with ensemble-based flow-dependent evolution of the “error-of-the-day” uncertainty. The study to identify the best-choice initial conditions perturbations that are able adequately sample the “error-of-the-day” uncertainty for convective scale processes is on-going. On a longer time perspective we intend to apply a localisation including also hydrometeors (Destouches *et al.*, 2020) as developed for AROME 4D-Ens-Var and to enrich 4D-Var with a quasi-continuous overlapping window framework. We hope that nowcasting and very short range forecasting applications that are essential for modelling of convective scale processes will greatly benefit from this.

One particular challenge associated with initialisation of convective scale processes is different predictability time scales for different observed quantities. Temperature, wind and humidity profiles determine environmental conditions and have longer predictability time scales than for example cloud observations that bring in essential small scale details. An efficient data assimilation scheme on convective scales requires a long enough assimilation window to allow different model variables to influence each other and a short enough assimilation window to assure that controlled variables remain predictable over the window. The flexibility of HARMONIE-AROME 4D-Var and Hybrid EnVAR implementations allows to meet both requirements, which looks contradictory at first glance. An attractive feature of the Hybrid EnVar framework in the 4DVAR context is that the ensemble spans a space of non-linear model trajectories throughout that assimilation window. This provides flexibility to control some variables such as hydrometeors away from the start of the assimilation window.

Another idea is to develop for HARMONIE-AROME 4D-Var a tool to estimate the Forecast Sensitivity to Observation Impact (FSOI) with respect to short-range HARMONIE-AROME forecasts.

6 Conclusions

After several years of developments HARMONIE-AROME 4D-Var has now matured and is now at a stage where it can be considered for operational use. An added value as compared to 3D-Var has been demonstrated in terms of verification scores and there is ample opportunity for further improvement and applications of 4D-Var. In an operational framework it needs to be demonstrated that the benefit of 4D-Var remains when compared with a 3D-Var using LSM. In addition, computational aspects needs to be considered. The use of lower-resolution analysis increments, few iterations in the minimization of the cost function and only save the physics trajectory typically once every 30 minutes facilitate operational implementation. Some local optimization with regards to available computer capacity and observation cut-off will be needed.

7 References

Akkraoui, A.E., Trémolet, Y., Todling, R., 2012. Preconditioning of variational data assimilation and the use of a bi-conjugate gradient method. *Quart. J. Roy. Meteorol. Soc.*,**193**, 731–741. https://doi.org/10.1002/qj.1997

Barkmeijer, J., Iversen, T. and Palmer, T.N., 2003. Forcing singular vectors and other sensitive model structures. *Quart. J. Roy. Meteorol. Soc.*, **129**, 2401–2423, https://doi.org/10.1256/qj.02.126

Caumont, O., V. Ducrocq, E. Wattrelot, G. Jaubert, and S. Pradier-Vabre, 2010. 1d+3D-Var assimi- lation of radar reflectivity data: a proof of concept. *Tellus*, **62**, 173–187.

Courtier, P., Thépaut, J.-N. and Hollingsworth, A., 1994. A strategy for operational implementation of 4D-Var using an incremental approach. *Quart. J. Roy. Meteorol. Soc.*, **120**, 1367-1388.

Courtier, P., Andersson, E., Heckley, W., Pailleux, J., Vasiljevic, D., Hamrud, M., Hollingsworth, A., Rabier, F. and Fisher, M., 1998. The ECMWF implementation of three dimensional variational assimilation (3D-Var). Part I: Formulation. *Quart. J. Roy. Meteorol. Soc.*, **124**, 1783-1808.

Dahlgren, Per and Gustafsson, N, 2012. Assimilating Host Model Information into a Limited Area Model , *Tellus A* , **64**, 15836 DOI: 10.3402/tellusa.v64i0.15836.

Dee, D., 2005. Bias and data assimilation. *Quart. J. Roy. Meteor. Soc.*, **131**, 3323–334.

Destouches, M., Montmerle, T., Michel, Y., Ménétrier, B., 2020. Estimating optimal localization for sampled background-error covariances of hydrometeor variables. *Quart. J. Roy. Meteorol. Soc.*, https://doi.org/10.1002/qj.3906.

Gustafsson, N., Berre, L., Hörnquist, S., Huang, X.-Y., Lindskog, M., Navascués, B., Mogensen, K. S. and Thorsteinsson, S. 2001. Three-dimensional variational data assimilation for a limited area model. Part I: General formulation and the background error constraint. *Tellus*, **53A**, 425–446.

Gustafsson, N., Huang, X.-Y., Yang, X., Mogensen, K., Lindskog, M., Vignes, O., Wilhelmsson, T. and Thorsteinsson, S., 2012. Four-dimensional variational data assimilation for a limited area model. *Tellus A*, **64**, 14985, DOI: 10.3402/tellusa.v64i0.14985.

Gustafsson, N., Bojarova, J. and O. Vignes, 2014. Hybrid Variational Data Assimilation for High Resolution Limited Area Model (HIRLAM). *Non-linear Processes in Geophysics*, **21**, 303–323, https://doi.org/10.5194/npg-21-303-2014.

Gustafsson, N., Janjić , T., Schraff, C., Leuenberger, D., Weissmann, M., Reich, H., Brousseau, P., Montmerle, T., Wattrelot, E., Bučánek, A., Mile, M., Hamdi, R., Lindskog, M., Barkmeijer, J., Dahlbom1, M., Macpherson, B., Ballard, S., Inverarity, G., Carley, J., Alexander, C., Dowell, D., Liu, S., Ikuta, Y. and Fujita, T. 2018. Survey of data assimilation methods for convective-scale numerical weather prediction at operational centres. *Quart. J. Roy. Meteorol. Soc.*, **144**, 1218-1256, DOI: 10.1002/gj.3179.

Järvinen, H., Andersson, E. and Bouttier, F. 1999. Variational assimilation of time sequences of surface observations with serially correlated errors. *Tellus*, **51A**, 469–488.

Lindskog, M. Dee, D., Trémolet, Y., Andersson, E. Radnóti and Fisher, M., 2009. Weak-constraint 4D-Var in the stratosphere. Quart. J. Roy. Meteorol. Soc., **135**, 695–706.

Lindskog, M., Ridal M., Thorsteinsson S. and T. Ning., 2017. Data assimilation of GNSS zenith total delays from a Nordic processing centre. *Atmos. Chem. Phys.*, 17, 13983–13998,
https://doi.org/10.5194/acp-17-13983-2017.

Lorenc, A. C., 2003. The potential of the ensemble Kalman filter for NWP—a comparison with 4D-Var. *Quart. J. Roy. Meteorol. Soc.*, **129**, 3183–3203.
https://doi.org/10.1256/qj.02.

Müller, M., Homleid, M., Ivarsson, K.-I., Koltzow, M., Lindskog, M., Midtbo, K.-H., Andrae, U., Aspelien, T., Berggren, L., Bjorge, D., Dahlgren, P., Kristiansen, J., Randriamampianina. R., Ridal, M., Vignes, O., 2017. AROME-MetCoOp: A Nordic Convective-Scale Operational Weather Prediction Model. *Weather and Forecasting*, **32**, 609—627. doi:10.1175/WAF-D-16-0099.1.

Randriamampianina R, Iversen T, and Storto A., 2011. Exploring the Assimilation of IASI Radiances in Forecasting Polar Lows. *Quart. J. Roy. Meteorol. Soc.*,**137**, 1700–1715. DOI:10.1002/qj.838.

Ridal, M. and Dahlbom, M., 2017. Assimilation of Multinational Radar Reflectivity Data in a Mesoscale Model: A Proof of Concept. *J. Appl. Meteorol. Clim.*, **56**, 1739–1751. https://doi.org/10.1175/jamcd-16-0247.1

Sánchez Arriola, J., Lindskog, M., Thorsteinsson, S. and Bojarova, J.. 2016. Variational Bias Correction of GNSS ZTD in the HARMONIE Modeling System. *J. of Applied Meteorology and Climatology*. **55**, 1259–1276.
doi:http://dx.doi.org/10.1175/JAMC-D-15-0137.1.

Trémolet, Y. 2004. Diagnostics of linear and incremental approximations in 4D-Var. *Quart. J. Roy. Meteorol. Soc.* **130**, 2233—2251.

Trémolet Y. 2006. Accounting for imperfect model in 4D-Var. *Quart. J. Roy. Meteorol. Soc.* **132**, 2483-–2504.

Wattrelot, E., O. Caumont, and Mahfouf, J.-F., 2014. Operational implementation of the 1D+3D-Var assimilation method of radar reflectivity data in the AROME model. *Mon. Weather Rev.*, **142**, 1852-–1873.

Status of the NWP in Bulgaria during 2020

Boryana Tsenova, Andrey Bogatchev

1 Operational suites in Bulgaria

Two cannonical model configurations based on cy43t2 are run operationally twice daily at 06 and 18 UTC: ALADIN-BG (LONC=25.5, LATC=42.75, NDLON=256, NDGLG=200, NDLUX=245, NDGUX=189, NMSMAX=127, NSMAX=99, NFLEV=105, EDELX=5000) and AROME-BG (LONC=25.5, LATC=42.75, NDLON=320, NDGLG=240, NDLUX=309, NDGUX=229, NMSMAX=159, NSMAX=1199, NFLEV=60, EDELX=2500). From November 2020, two additional daily model runs are performed operationally at 00 and 12 UTC for the two models.

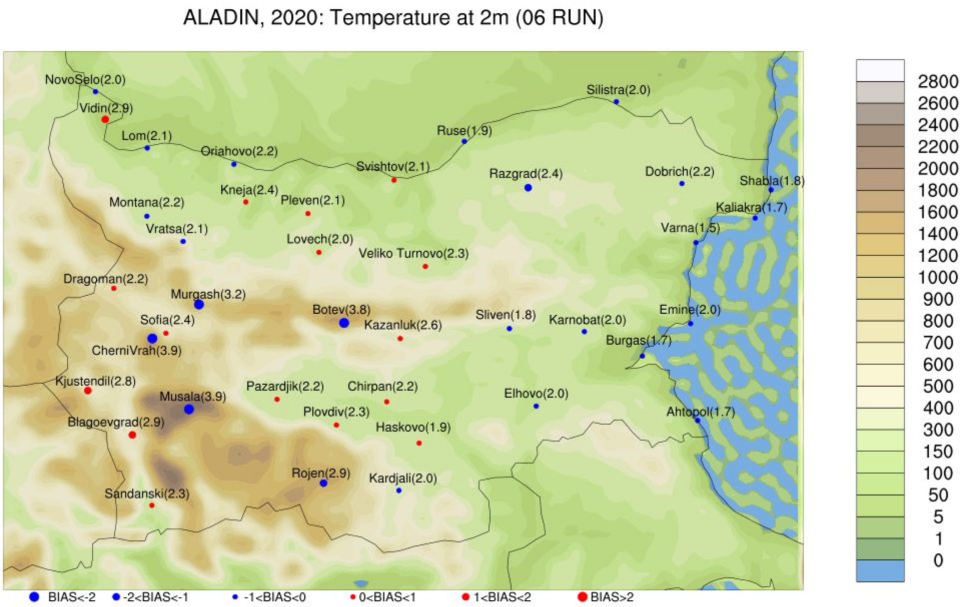

Figure 1: The mean BIAS and RMSE of the temperature at 2 m (in o C) forecasted by ALADIN-BG during 2020 for each station (coloured circles show the BIAS, while RMSE is indicated next to each station name)

In Figures 1 and 2 the mean annual BIAS and RMSE of the temperature at 2m for 2020 for each station is shown obtained respectively by ALADIN-BG and AROME-BG. In Tsenova and Valcheva, 2020, verification statistics of the operational forecasts for temperature and relative humidity at 2 m, wind velocity at 10 m and 12 hours accumulated precipitation are computed by interpolating ALADIN-BG output to observation points of 40 synoptic stations in Bulgaria. Results for the period between January and August 2020 showed diurnal and annual trends of the forecast accuracy, especially for the 2m temperature. Stations located at mountain peaks, as well some close to mountain massifs were pointed out with worse forecasts in comparison to others. It was established that for peak stations, ALADIN-BG underestimates significantly the night temperatures. Similar are results for AROME-BG and further in-deep investigations will be performed to explain such strong night temperature underestimations, that could be due to model physics, surface, forecast interpolation or any other reason.

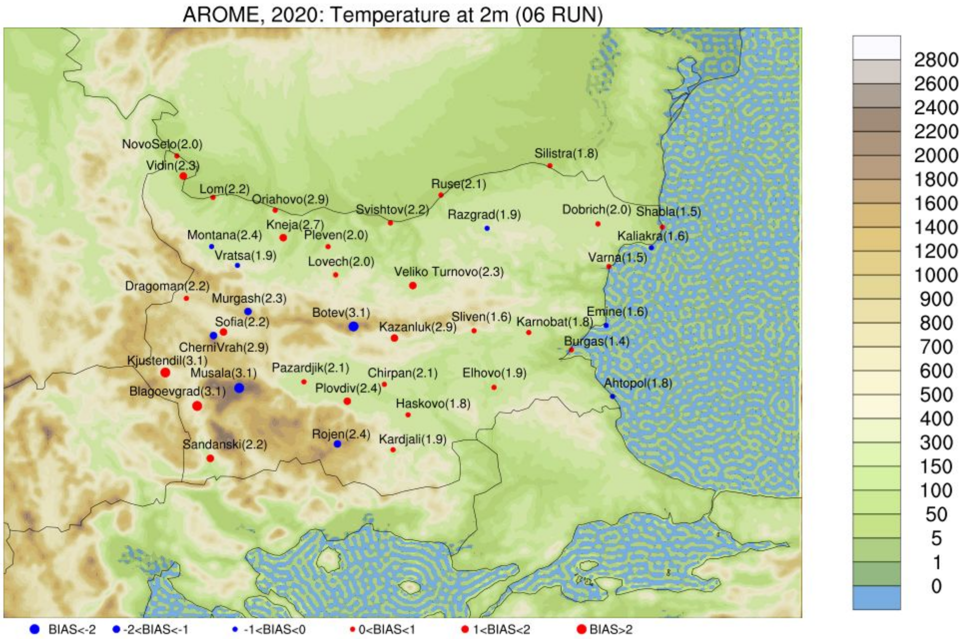

Figure 2: The mean BIAS and RMSE of the temperature at 2 m (in o C) forecasted by AROME-BG during 2020 for each station (coloured circles show the BIAS, while RMSE is indicated next to each station name)

2 Atmospheric instability forecast based on ALADIN-BG

In Tsenova and Bogatchev, 2020, the atmospheric instability over Bulgaria assessed based on ALADIN-BG forecast production for the warm half-year of 2018 and 2019 is evaluated and connected to the detected lightning data taken from ATDnet. Four instability indices, calculated based on forecasted thermodynamical fields in the atmosphere, showed a relatively good ability to discriminate thunderstorm cases from the non thunderstorm ones, depending on the month and could be considered for predicting thunderstorm probability formation over different regions. However, they should not be used as a sole tool for a more accurate thunderstorm forecast.

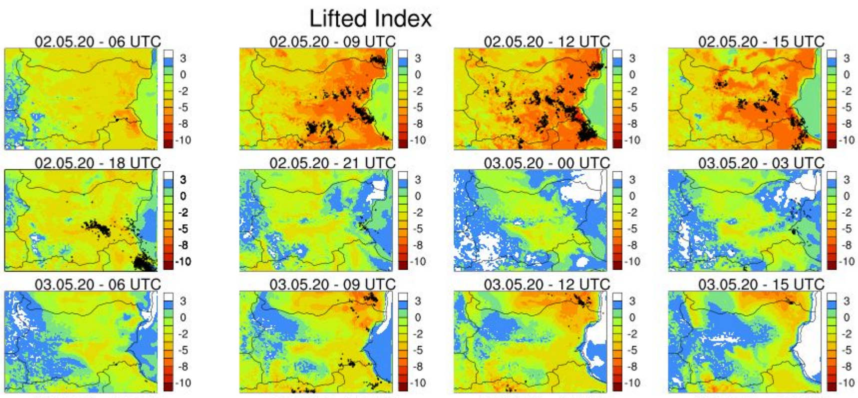

Figure 3: Lifted Index, calculated based on ALADIN-BG forecast on 02.05.2020 (06 UTC Run) with the corresponding lightning data detected by ATDnet

3 Probability of lightning activity forecasted by AROME-BG

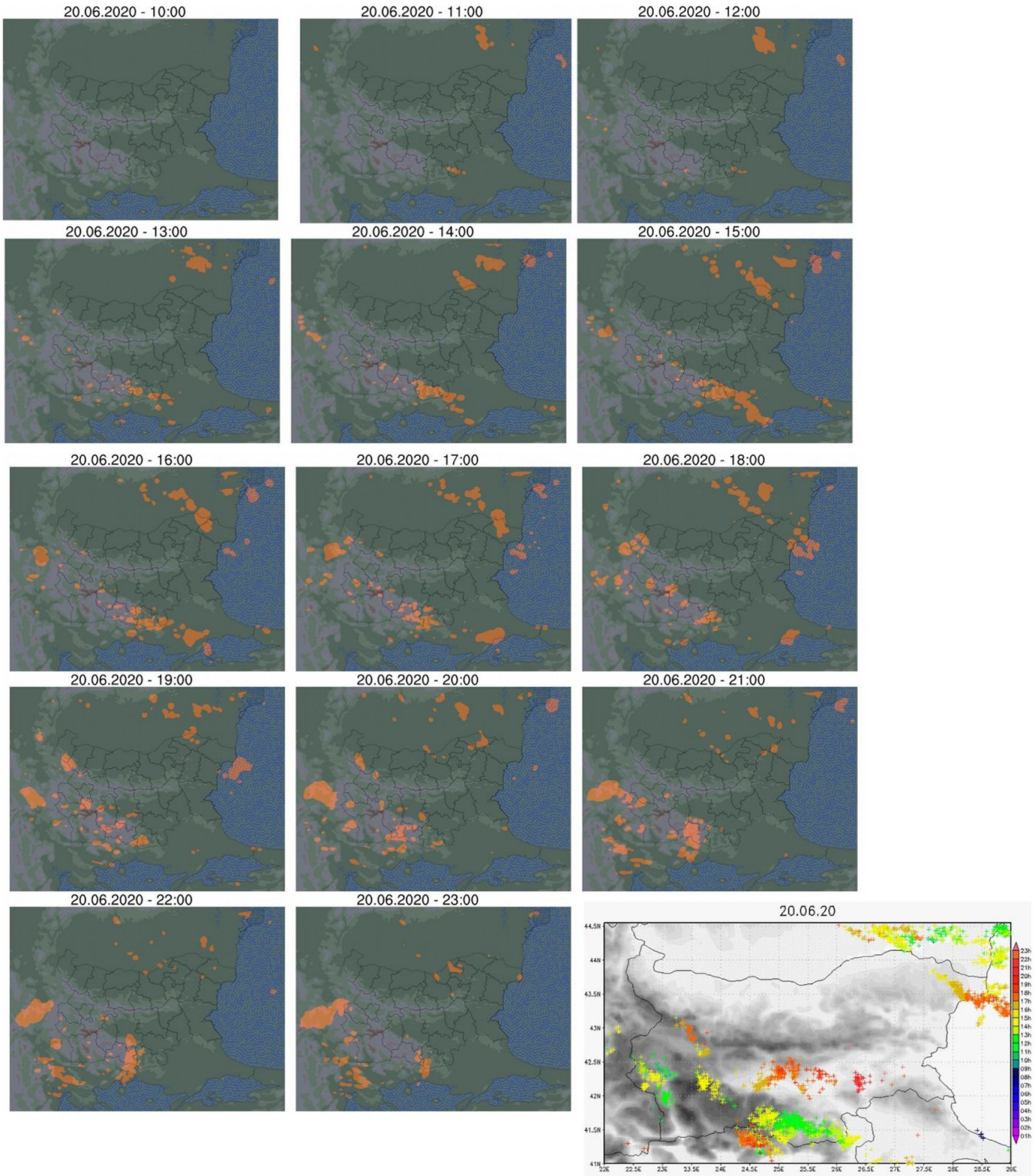

Figure 4: Lightning probability, evaluated based on AROME-BG forecast on 20.06.2020 (06 UTC Run) and lightning data detected by ATDnet with indicated time of strike detection (bottom right)

Since April 2020 a new tool for predicting lightning activity was added to the postprocessed model production at the institute. It is based on hydrometeors fields forecasted by AROME-BG. Its scores for the summer 2020 will be evaluated, as it was established based on results on the relationship between detected lightning and forecast production during 2018 and 2019, when the operational models were based on cy41t1.

4 References

Tsenova, B and R. Valcheva, 2020, Verification of the regional numerical weather prediction with
ALADIN-BG in Bulgaria, Bul. J. Meteo & Hydro, 24/2 (2020)
Tsenova, B and A. Bogatchev, 2020, On the use of atmospheric instability indices based on NWP model production for thunderstorm forecast, Bul. J. Meteo & Hydro, 24/2 (2020)

Summary of NWP related Highlights in Austria in 2020

Christoph Wittmann, Florian Meier, Clemens Wastl, Florian Weidle

1 Introduction

After major changes in the previous year with two new operational NWP systems at ZAMG (C-LAEF and RUC), major effort was invested in 2020 to increase the usability of the new systems for the ZAMG forecasting and warning applications. In the following, the major characteristics of the current NWP systems at ZAMG are briefly summarized (section 2) and an application of C-LAEF for a severe weather event is shown (section 3). In addition, section 3 summarizes the effects of Covid-19 pandemic and the loss of aircraft data for the ZAMG NWP models.
The year 2020 also brought the operational end of the 5km model in Austria. In January 2020, operations of the ALARO-Aut 5km version were finally stopped after approx. 10 years of operations.

2 Status operational models

Currently there are three NWP systems running in operational mode at ZAMG serving as the backbone for operational forecasts, warnings and a number of downstream applications. All systems are running under AROME configurations and are based on cy40t1. Besides the deterministic AROME-Aut setup, there is the ensemble system C-LAEF running on the same horizontal resolution as AROME-Aut and finally the nowcasting version AROME-RUC. The two latter systems were introduced to operations in December 2019 and the main target in 2020 was to enhance the usability of the new systems for downstream applications and forecasters. Table 1 summarizes the main characteristics of the three system setups.

Table 1: Operational AROME based NWP systems at ZAMG

	AROME-Aut	AROME-RUC	CLAEF
Model version	Cy40t1	Cy40t1	Cy40t1
Resolution	2.5 km	1.2 km	2.5 km
Levels	90	90	90
Grid points	600x432	900x576	600x432
Initialization	CANARI/OIMAIN, 3DVAR	CANARI/OIMAIN, 3DVAR, LHN, FDDA, IAU	EDA, surface EDA, Ensemble JK
Physics	AROME/MESO-NH	AROME/MESO-NH	AROME/MESO-NH incl. HSPP (stochastic Scheme)
Boundaries	ECMWF-HRES (hourly)	AROME-Aut (hourly)	ECMWF-ENS first 16 members (3 hourly)
Integration time	60h	12h	60h (00 UTC), 48h (12 UTC), 6h (6/18 UTC)
Initial times	00, 03, 06, … UTC	Every hour	00, 06, 12, 18 UTC
Member size	1	1	16 + 1
Computing site	ZAMG HPE Apollo	ZAMG HPE Apollo	ECMWF CRAY

AROME-Aut runs 8 times per day on a horizontal resolution of 2.5 km and 90 levels on a domain covering large parts of Central Europe (Fig. 1). The initial conditions are generated by a 3 hourly 3DVAR assimilation cycle and CANARI/OI for the surface.
The C-LAEF system is implemented on the ECMWF HPC and runs on the same domain and resolution as AROME-Aut, trying to consider all major sources of uncertainties in the forecast. The

method to address these uncertainties in C-LAEF are: Ensemble Data Assimilation (EDA) and Ensemble Jk to perturb initial conditions; hybrid stochastic scheme combining perturbations of tendencies in shallow convection, radiation and microphysics, with a parameter perturbation scheme in the turbulence to quantify model uncertainties; coupling with ECMWF-ENS member to address uncertainties at the boundaries. Since the resolution and integration domain of AROME-Aut and C-LAEF are identical, the C-LAEF control run serves as full backup for AROME-Aut.
The AROME based Nowcasting system AROME-RUC provides hourly updated forecasts for the next 12h on a 1.2km resolution. The initial conditions are created by running an hourly 3D-Var, Latent Heat Nudging of INCA 1km precipitation analyses and forecasts and FDDA nudging of surface stations (T2m, RH2m, u10m). Also additional observations like GNSS-ZTD and 3D RADAR are integrated into the system. To reduce the spin up a two-step IAU is implemented.

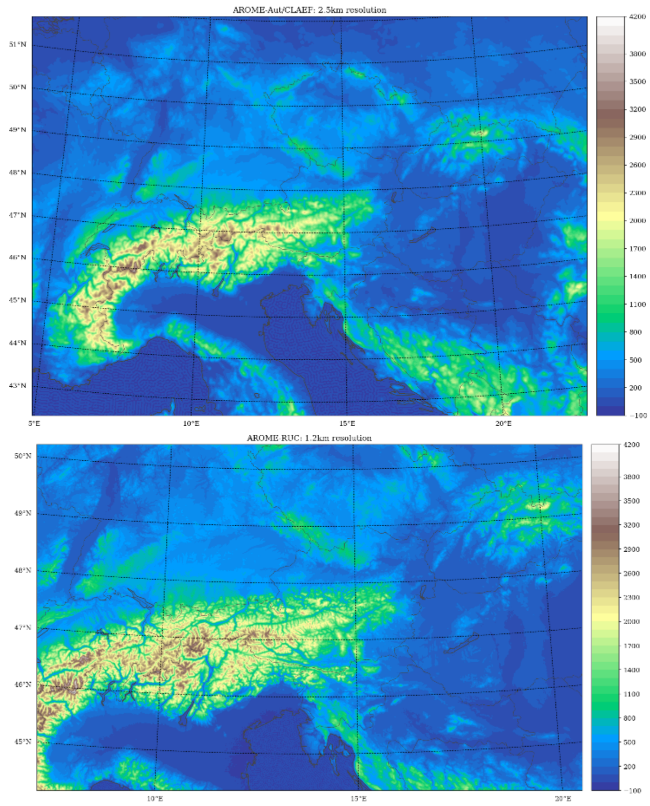

Figure 1: Integration domain of 2.5km AROME-Aut/C-LAEF (top) and 1.2km AROME-RUC

3 C-LAEF as major contributor to ZAMG warning system

Since its operational start in November 2019 C-LAEF has developed to an important tool in the daily routine forecast process at ZAMG. A survey among the operational forecasters at ZAMG has shown that it ranks among the three most used models in their routine activities. The acceptance and usage of this relatively new ensemble system is steadily growing which is also related to continuous improvements and the development of probabilistic products and maps in a close cooperation between model developers and users. Figure 2 shows an example for a wintertime EPSgram which is produced two times a day (00 and 12 UTC C-LAEF run) for more than 300 stations in the Alps. It contains probabilistic information about several parameters of the C-LAEF ensemble. The first row shows relative humidity and wind speed/direction in the vertical in dependence of the lead time (up to +60h). The second row contains the cloudiness, the third row the sunshine duration (hourly and 24h sum). The fourth panel gives information on freezing and snowfall level and the upper/lower limit of stratus. The probability of fog and low stratus is given in row five and panel six contains information on wind gusts (median and uncertainty information from the members). Temperature information for the upper

levels (panel seven) and the screen level (panel eight) is given as well. The last panel shows the precipitation amount (hourly, 6 and 24 hour sum) and the precipitation type (snow or rain).
During the summer season from April to September some parameters (snowfall/freezing level, stratus, etc.) are replaced by interesting parameters for convective situations like CAPE, lifted index, lightning and hail diagnostics etc.

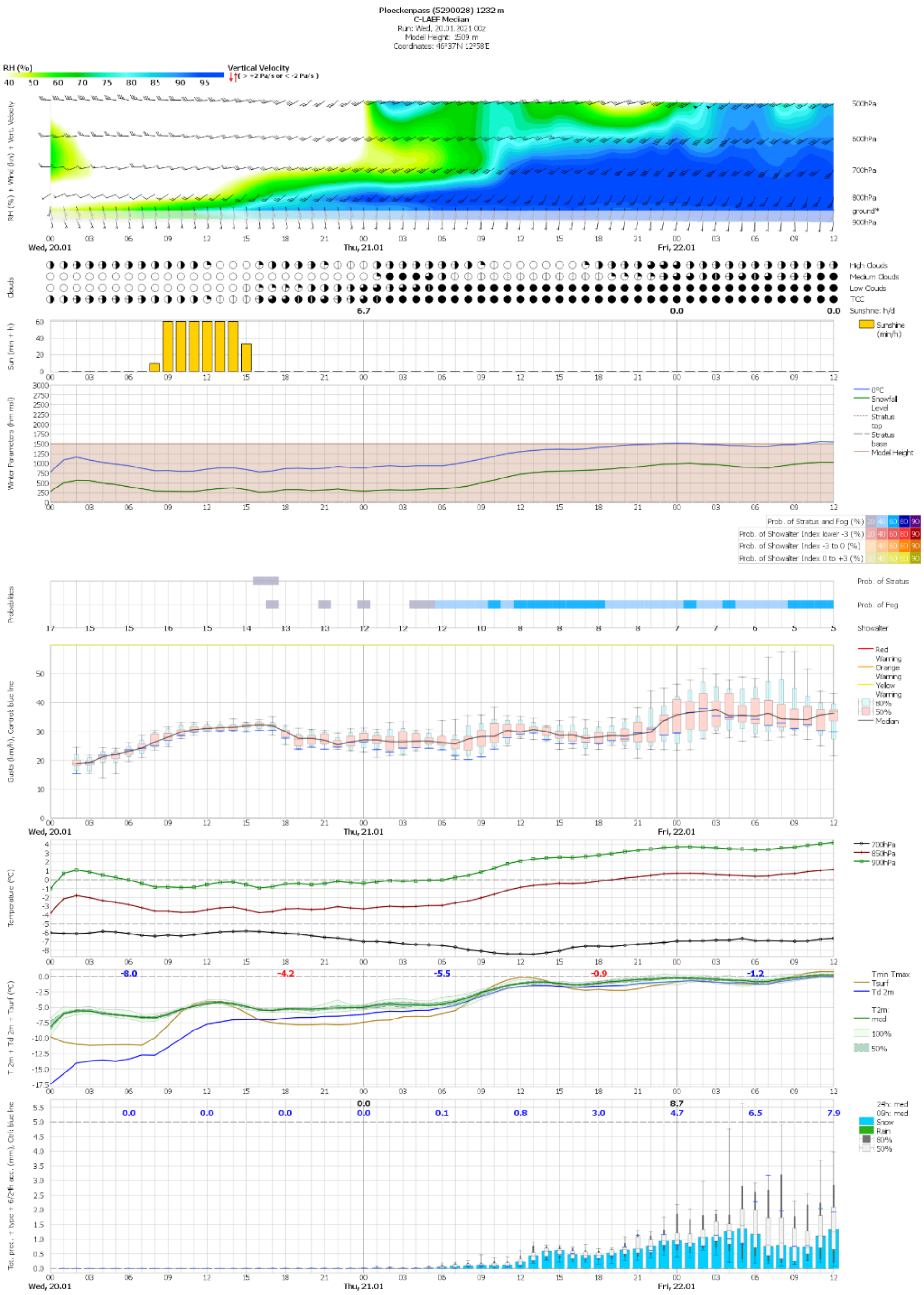

Figure 2: New VisualWeather based EPSgram for the station Plöckenpass for the C-LAEF 00 UTC run at Jan 20th, 2021.

The main application of the C-LAEF ensemble is for warning purposes as several severe weather situations during the past year have shown. The additional probabilistic information on exceeding warning thresholds or the plots of ensemble spread and extreme members are very helpful to better assess regional/temporal uncertainties as well as uncertainties in the intensity of severe weather. Figure 3 shows an example for a severe snow/rain event in southern Austria in December 2020.

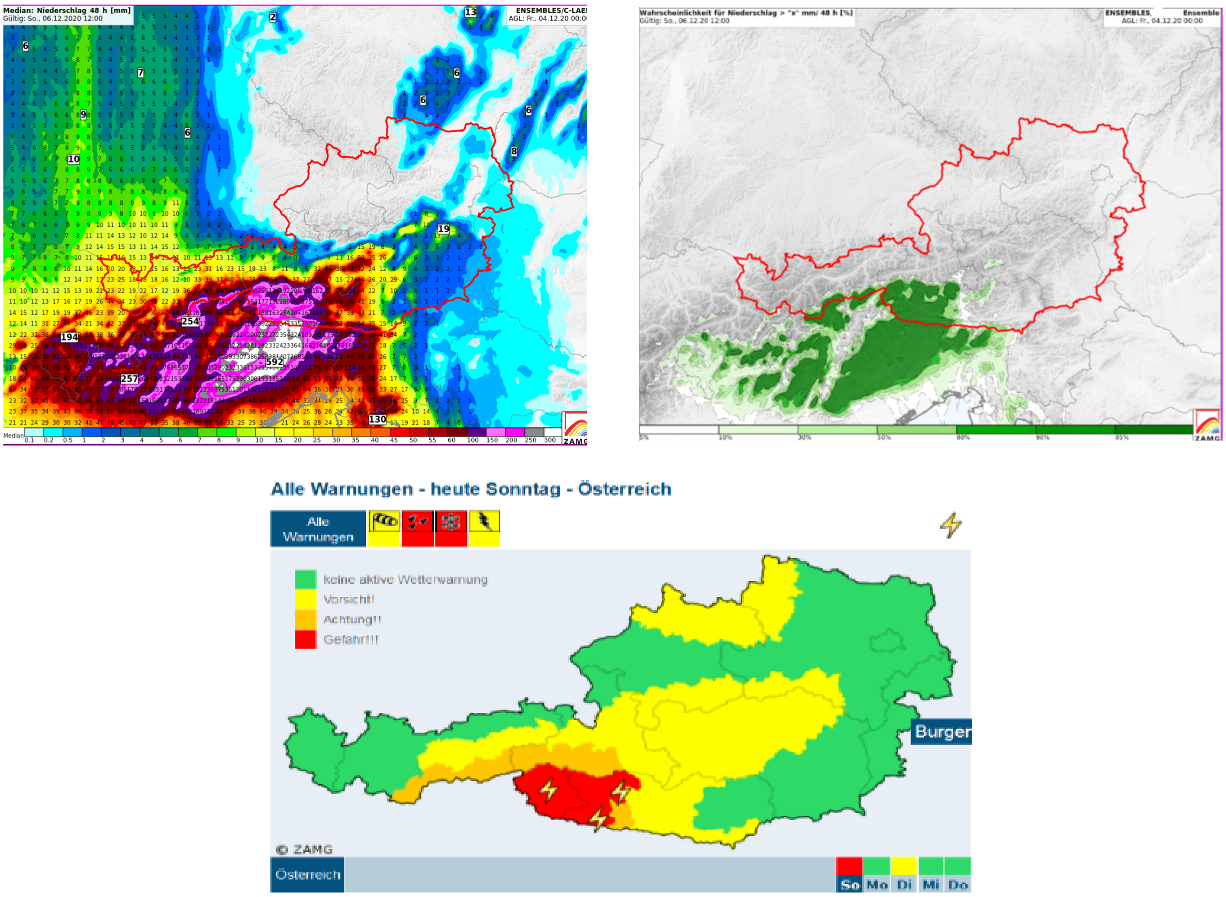

Figure 3: C-LAEF Median of 48h accumulated precipitation (upper left) and probability of exceeding 100mm/48h upper (right) for the 00 UTC run of Dec. 4th, 2020. Screenshot of ZAMG warning system (bottom).

4 Covid-19 effects

In 2020, the world was hit by the consequences of COVID 19 crisis. This had also direct implications on NWP systems beside organisation of work: The amount of commercial aircraft dropped drastically in times of strong travel restrictions in spring of up to 80-90% and after recovery in summer again in autumn over Europe and slightly less elsewhere. In consequence, the number of available AMDAR data assimilated in our AROME systems was also similarly reduced. To compensate the possible negative impacts, EUMETNET reorganised the AMDAR network and several National Meteorological Services launched temporarily additional radio soundings (ZAMG in Vienna 6 hourly instead of 12 hourly). Luckily, the EMADDC business case related to the exchange of MODE-S aircraft data coordinated by EUMETNET and KNMI was accelerated and therefore ZAMG made since spring profit receiving on top of data from Benelux, Germany, Slovenia und Czech Republic (the latter two via OPLACE) also centrally quality checked Austrian, Danish and Romanian MODE-S data (Figure 4).

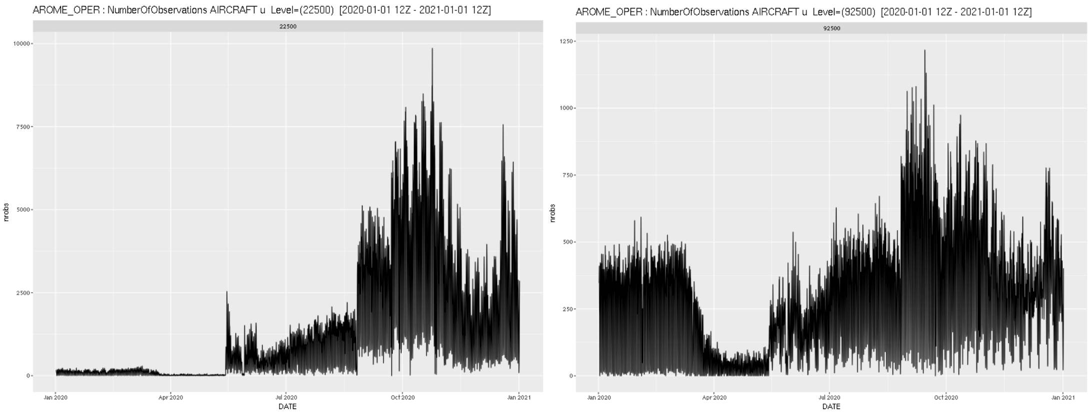

Figure 4: Number of aircraft observations in AROME-Aut 3D-VAR (12 UTC runs) for the year 2020 in 225hPa (left) and 925hPa (right). The number of AMDAR dropped during spring due to COVID-19 restrictions. The sudden increase in May is related to the activation of MODE-S observations from EMADDC (KNMI), which could compensate the loss except for the lowest levels. In autumn numbers decreased again due to less aviation activities with new travelling restrictions.

This could mostly compensate the loss of AMDAR wind and temperature data over Central Europe. Unfortunately, the AMDAR humidity measuring aircraft from LH were also grounded. In Austrian AROME-RUC we further activated assimilation of GNSS-RO from Metop as well as the assimilation of wind profilers (renewed profiler in Vienna airport since April 2020) and two Austrian SODAR profilers (Vienna, Linz). The wind profilers could be shown to be beneficial in several case studies regarding low level wind, while the SODARs needed an additional retuning of the observation error.

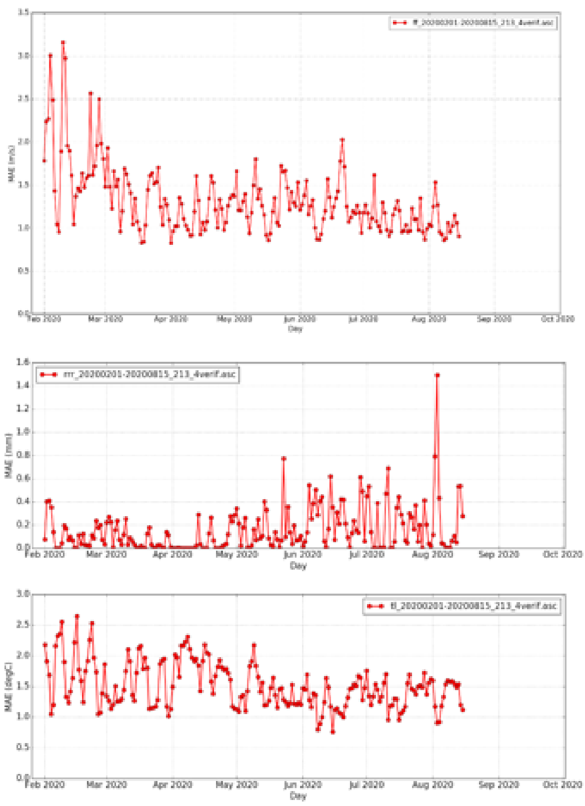

Figure 5: timeseries of MAE February to September 2020 for AROME-Aut 2.5km against SYNOP: 10m windspeed (top), precipitation (middle), T2m (bottom). No clear degradation related to loss of aircraft data in spring can be observed. Seasonal and synoptic scale variability dominate.

The profiler operator had to be updated in 3D-Var (hretr_conv.F90) to use for vertical interpolation first guess profile instead of standard atmosphere. The latter can be quite inaccurate especially in very low levels in case of strong inversions. All these measures and the calm weather in spring led to the fact, that our NWP validation scores showed no clear signal of degradation during the flight reduction in spring and is dominated by synoptical and seasonal variations (Figure 2). Only few single suspicious cases were observed before the activation of MODE-S assimilation. However, on short range the availability of aircraft data is still strongly affected. Therefore, adding new observation types and intensified MODE-S exchange via EMADDC could help to reduce the negative impact on NWP assimilation results also in the near future.

Benefit of early delivery ASAP data to LAM forecasts

Xiaohua Yang and Henrik Feddersen, Danish Meteorological Institute

1 Introduction

Apart from providing national weather services (NWS) in Europe with global medium range weather forecasts, ECMWF also plays a crucial role in supporting member NWS by providing its operational forecasts as coupling data to the limited area modelling (LAM) systems as lateral boundary conditions (LBC). Due to practical constraints, it has been necessary for LAM systems to time-lag the ECMWF coupling data using those initiated from earlier base-times, resulting in a base-time difference of 6 to 11 hours between local and coupling data. For a better LAM forecast quality, it is highly desirable to minimise such time lagging in coupling.

At the request of member services, ECMWF launched in June 2020 a pilot data dissemination project with early delivery data of operational data, ASAP ("As Soon As Possible"), in which gridded ECMWF operational data are disseminated to the participating services shortly after production, instead of the usual dissemination at fixed time points. ASAP is a test project for evaluation only, as such it is arranged in parallel to the normal, operational dissemination stream.

As one of the participating services to the ASAP pilot project, efforts have been spent at DMI to examine the ASAP stream from High Resolution 9 km dataset (HRES) and investigate potential use of such in the local operational LAM setup. By comparing arrival time of the HRES data with the ASAP vs "normal" streams, it is found that ASAP data is typically delivered substantially earlier than the operational stream, and as such it can be potentially used as LBC in some of the operational LAM suites at DMI. In this note, we report results from the parallel experiments with forecast systems at DMI using ASAP, in comparison to the corresponding operational forecasts with normal data streams.

2 Arrival time of ASAP vs normal stream

DMI started receiving HRES ASAP data from 06Z cycle on June 2 2020, in addition to the "NORMAL" stream. Looking at the overall ASAP data arrival situation during the first 50s days, it appears that in majority cases ASAP delivers HRES data 30 to 40 minutes earlier than NORMAL stream, but it also occurs, in a few occasions, that the ASAP data arrives merely a few minutes earlier than NORMAL one. Table 1 lists, as illustration, examples of arrival time with ASAP stream at the DMI HPC (Cray XC50) with the HRES data for various forecast lead-time 00h, 39h, 62h, 72h, in comparison to the corresponding NORMAL stream, for some randomly selected days (June 3, July 18 and July 19, 2020). Note that the last three columns of forecast lead-times as listed in the table are selected here due to their relevance for possible use as LBC for the operational LAM at DMI, see further discussions below.

Table 1. Arrival time of the ASAP data and gain in delivery time compared to NORMAL stream

	HRES an000		HRES fc+039		HRES fc+062		HRES fc+072	
	ASAP	Gain over Normal (minutes)	ASAP	Gain over Normal (minutes)	ASAP	Gain over Normal (minutes)	ASAP	Gain over Normal (minutes)
June 3 00	04:59	41	05:27	35	05:32	36	05:36	26
June 3 06	11:00	40	11:19	49	11:24	40	11:29	38
June 3 12	17:05	35	17:35	26	17:38	41	17:41	50
June 3 18	23:00	40	23:18	40	23:23	42	23:28	38
July 18 00	05:06	34	05:31	27	05:37	28	05:34	33
July 18 06	10:59	41	11:26	32	11:25	29	11:27	41
July 18 12	17:07	33	17:32	26	17:35	31	17:39	28
July 18 18	22:59	41	23:20	37	23:25	39	23:27	40
July 19 00	05:04	36	05:30	29	05:31	33	05:36	32
July 19 06	10:57	43	11:18	41	11:22	42	11:25	42
July 19 12	17:07	33	17:33	25	17:37	27	17:37	30
July 19 18	22:59	41	23:20	38	23:25	39	23:28	38

Although ASAP data arrives quicker, in comparison to the NORMAL stream, variation in delivery time of ASAP data is much more pronounced. Also, as shown in Table 1, delivery speed between those with different forecast lead-time also vary quite a lot. Presumably, while occasional delay with normal HRES stream is most likely associated with load issues on the receiving end (DMI-HPC), irregularity with ASAP stream may be caused by factors on both delivery (ECMWF HPC) and receiving (DMI-HPC) ends.

3 Importance of timeliness with ECMWF data to operational LAM systems

In operational NWP, due to different focus and service requirements, configurations about forecast lead time, update frequency, observation data cutoff and delivery time differ between global and LAM systems. Both of the operational ECMWF global HRES and ensemble system (IFENS) are run twice a day at 00 and 12Z. In addition, ECMWF runs at 06 and 18Z HRES shorter range forecasts for the member states optional Boundary Condition (BC) project. For the benefit of data assimilation, these setups are configured with relatively long observation data cutoff, hence with a delivery time of ca 6-h after nominal base time. In contrast, configuration characteristics with operational LAM systems at NWS are rather different in order to meet service needs and to achieve anticipated added values. At DMI, the focus of the operational forecast system (DMI-HARMONIE) has traditionally been on higher resolution and short range, emphasis on frequent update and early delivery, aiming to follow and predict evolution of rapidly developing weather in local scales, especially on severe convection. Accordingly, configuration of operational DMI-HARMONIE is characterised by a rather frequent data assimilation cycling with short observation data cutoff (Yang, 2017). Among the main operational setups at DMI, deterministic suites with 2.5 km grid resolution are run for regions centered over Denmark (“NEA” domain) and Greenland (“IGB” domain), respectively, at a 3 hour interval, 8 times a day. In addition, a 19 member ensemble forecast is made on NEA domain with an hourly interval through the COntinuous Mesoscale Ensemble Prediction System (COMEPS). For data assimilation in both deterministic and ensemble control members, 3DVAR is used in upper air analysis. In the ensemble system COMEPS, a novice, quasi-continuous, hourly update is achieved with control analyses launched each hour through three independent and consecutive 3DVAR suites, each with 3h assimilation cycling and configured on consecutively overlapped observation data window, and one hour apart from each other, see details in Yang et al (2017). In these setups, operational ECMWF HRES is used as LBC. Further, short range HRES boundary data valid at the analysis time are also used directly in the HARMONIE data assimilation through a background blending scheme LSMIX in which large scale information from the HRES data is utilised to improve the large scale background in 3DVAR. This has been shown to be effective to benefit from the high quality ECMWF data assimilation on synoptic scales.

The fact that operational ECMWF forecasts are delivered less frequently and with late arrival in comparison to the configuration in regional models which are run more often and with earlier delivery, entails that ECMWF data is used as LBC with time lagging. Table 2 lists some of the configurations in the IGB and COMEPS suites at DMI involving LBC coupling of HRES. As additional information, the scenario to use ASAP stream in some of these configurations has been marked in red colour within brackets.

Table 2. Coupling of lateral boundary in the operational IGB and COMEPS

Suite	Basetime (Z)	Forecast range	Launch time after basetime	Boundary data cut off after basetime	Age of the HRES boundaries
IGB (deterministic)	**00 06 12 18**	**66h**	**+1h36m**	**+1h46m**	**6h**
	03 09 15 21	**36h**	**+2h36m**	**+2h46m**	**9h (3h*)**
COMEPS (ensemble)	**00 06 12 18**	**57h**	**+0h36m**	**+0h46m**	**6h**
	01 07 13 19	**57h**	**+0h36m**	**+0h46m**	**7h**
	02 08 14 20	**57h**	**+0h36m**	**+0h46m**	**8h**
	03 09 15 21	**57h**	**+0h36m**	**+0h46m**	**9h**
	04 10 16 22	**57h**	**+0h36m**	**+0h46m**	**10h**
	05 11 17 23	**57h**	**+0h36m**	**+0h46m**	**11h (5h*)**

As shown in Table 2, the boundary "age" for the ECMWF HRES data in coupling to the operational suites at DMI vary between runs for different base time. E.g., the HRES 00Z data is used for IGB runs at both 06 Z and 09 Z, thus with a 6h and 9 h lagging, respectively. The 00Z data is also coupled to COMEPS ensembles for 06, 07, 08, 09, 10 and 11 Z, with a lagging between 6 and 11 hours.

As ECMWF data is coupled to regional models through lateral boundary, and, in some systems, also via initial condition through large scale constraint, the timeliness of HRES data delivery, especially those for the short range forecast, has a significant impact on quality of both data assimilation and forecast in the downstream LAM setups. As is well known, accuracy of NWP forecasts decreases with longer lead-time. All things being equal, a HRES boundary with shorter lead-time (earlier delivery, less lagging) is clearly preferable to those with longer lead-time (longer delivery, larger lagging). As an illustration, Figure 1 intercompares ECMWF HRES forecast with various lagging, in which observation verification on mean sea level pressure (MSLP) for Scandinavia stations during the month of Feb 2020 is compared between those with the most recent and those that are made 6 and 12h earlier. As shown in Fig 1, in comparison to the nominal HRES forecast quality (red colour, with 0h delay), forecasts with more aged HRES data clearly degrade forecast quality, and the more lagging, the more degradation. Such is especially clear for STD errors and for the short forecast ranges as shown in Fig 1a. From the daily error time series (Fig 1b), it is seen that the sensitivity of forecast errors to lagging appears particularly pronounced in some of the days (e.g. on around Feb 22, 2020), presumably reflecting the improved skills in later runs due to data assimilation. Obviously, especially during the period with rapid weather evolution, it is crucially important for the downstream applications to get timely global HRES updates.

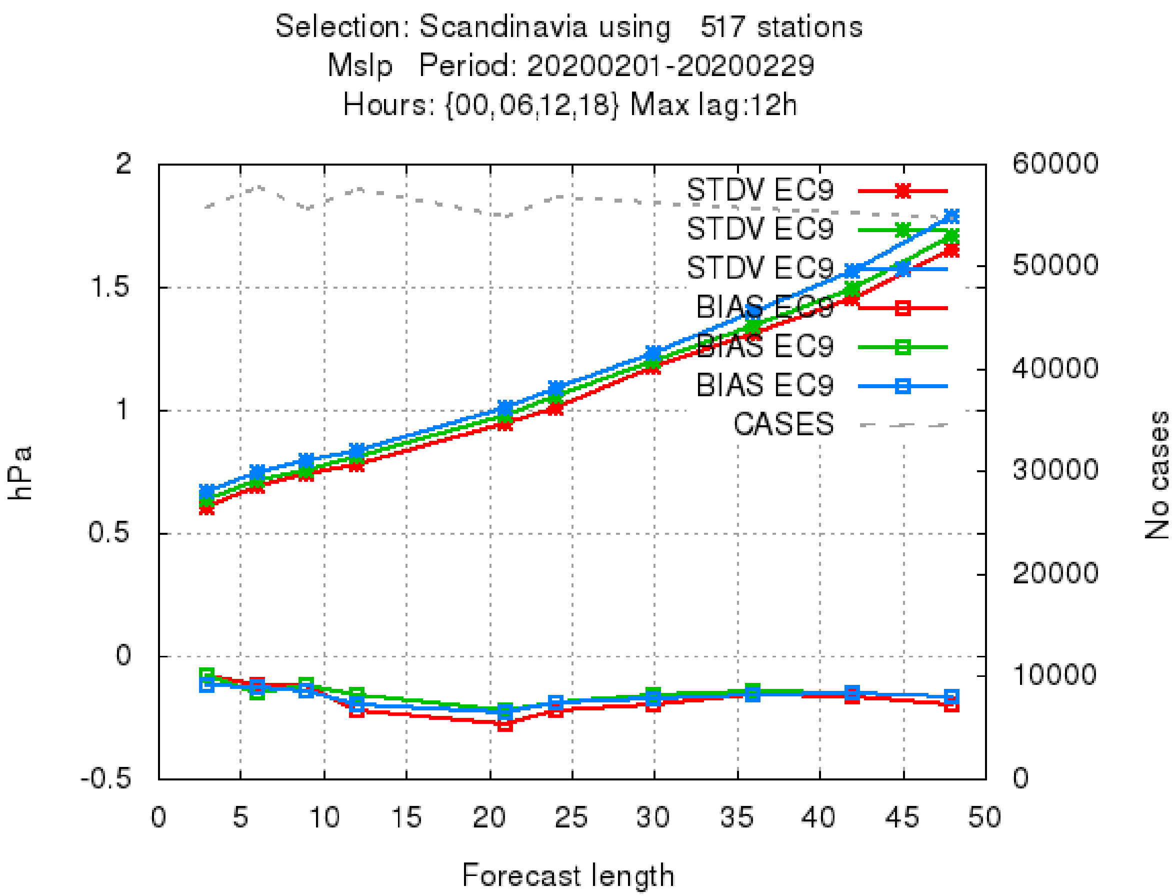
Selection: Scandinavia using 517 stations
Mslp Period: 20200201-20200229
Hours: {00,06,12,18} Max lag:12h
STDV EC9
STDV EC9
STDV EC9
BIAS EC9
BIAS EC9
BIAS EC9
CASES
hPa
No cases
Forecast length
2
1.5
1
0.5
0
-0.5
60000
50000
40000
30000
20000
10000
0
0 5 10 15 20 25 30 35 40 45 50

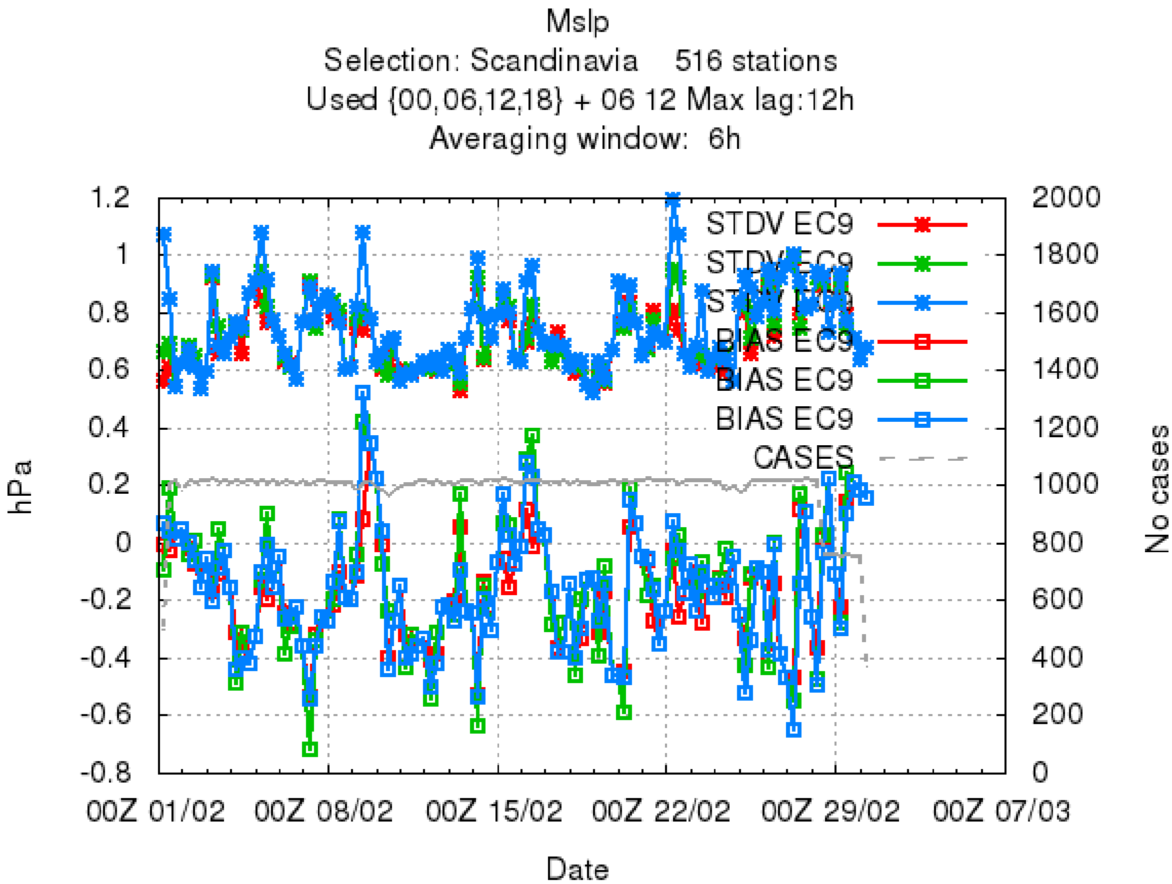

Figure 1. Inter-comparison of short range forecast errors in standard deviation (STD) and bias with ECMWF HRES forecasts of different time lagging, for mean sea level pressure in Scandinavia area during month of February, 2020, a) average errors along forecast lead-time, 2) daily averaged errors with short range forecasts. Model data in comparisons are those with latest forecast (with no lagging, in red), 6h earlier (in green) and 12h earlier (in blue). The last two approximate the data availability scenario at member services, which receive disseminated HRES data typically with 6 h delay relative to basetime. As such, HRES data has to be used in a lagged mode in coupling to regional models with a 6 to 11 h lagging.

Based on the above discussion, it is easy to derive that, with an earlier delivery of HRES data by 30 to 40 minutes with ASAP stream, for some of the operational forecast setup at member services, latest arrival ECMWF forecast may be used as coupling data, reducing the lagging time by 6h, which may improve overall forecast quality, and such improvement may become substantial in critical weather situations.

4 Impact of early delivery ASAP data on operational LAM systems

Examining arrival time of HRES data and coupling configuration as shown in Table 1 and 2, it is found that the earlier delivery HRES data with ASAP can be directly useful to optimise boundary coupling in IGB suite for the 03/09/15/21 cycles, and COMEPS for the 05/11/17/23 cycles, as those denoted in red by Table 2, where the latest HRES data is used as LBC with merely 3 to 5h lagging instead of 9 to 11h in the present setup, enhancing substantially quality of initial condition and boundary data in these forecast setup. These improvements will also be beneficial for later cycles through assimilation cycling.

To verify the hypothesis, real time experiments with IGB and COMEPS have been set up, in which the early delivery ASAP data is used to replace the operational NORMAL stream. These have been set up in strict parallel to the operational ones, so that the difference in observation verification, as presented below, reflects pure impact due to use of less aged LBC from HRES.

For IGB, ASAP data replaces operational HRES at 03, 09, 15 and 21Z, resulting in a boundary data age of 3 h instead of 9 h as in the operational. For IGB cycles at 00, 06, 12 and 18 UTC, configuration in boundary coupling remains unchanged, the benefit of ASAP data for these cycles are indirect, through a potentially improved background state from the runs using early delivery data. Figure 2 presents the averaged verification intercomparison of mean sea level pressure (MSLP) forecast for observation stations within IGB domains (Greenland and Iceland stations) during the month-long period between June 20 and July 20 2020. Short range forecasts up to 24h with IGB by both ASAP and operational runs have been included. Results in Fig 2 are clearly in favor of the use of ASAP data, showing a significantly consistent improvement in standard deviation errors of MSLP (Fig 2a, errors along lead time) and Fig 2b (daily time series of errors with 3, 6 and 24h forecasts). The advantage of ASAP data appears to increase with forecast lead time, reflecting the importance on large scales. From Fig 2b, the improvements on some of the days appear to be particularly significant, confirming the potential for the earlier delivery HRES data to enable effective reduction of forecast events with major failure/bust. For other forecast parameters, ASAP data also appear to be beneficial in general (not shown here).

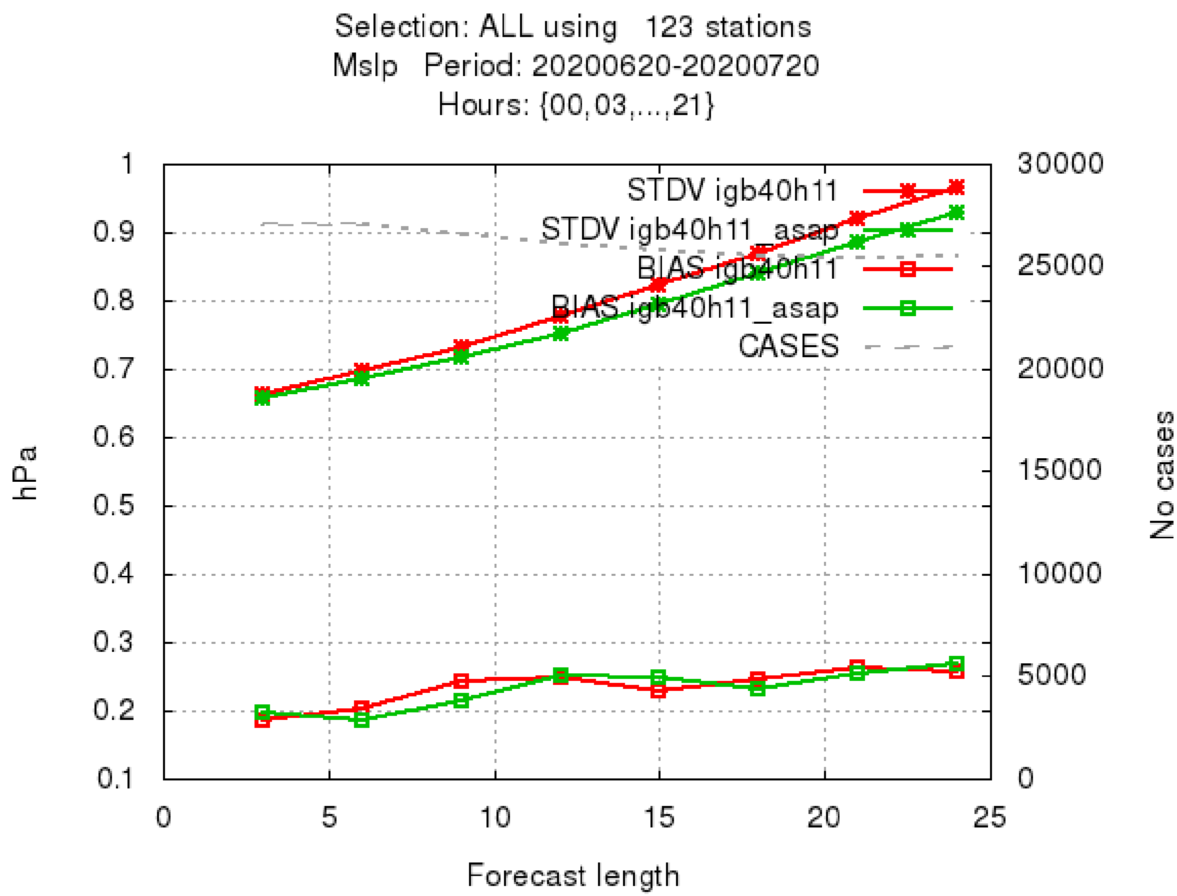
Selection: ALL using 123 stations
Mslp Period: 20200620-20200720
Hours: {00,03,...,21}
STDV igb40h11
STDV igb40h11_asap
BIAS igb40h11
BIAS igb40h11_asap
CASES
hPa
No cases
Forecast length
1
0.9
0.8
0.7
0.6
0.5
0.4
0.3
0.2
0.1
30000
25000
20000
15000
10000
5000
0
5
10
15
20
25

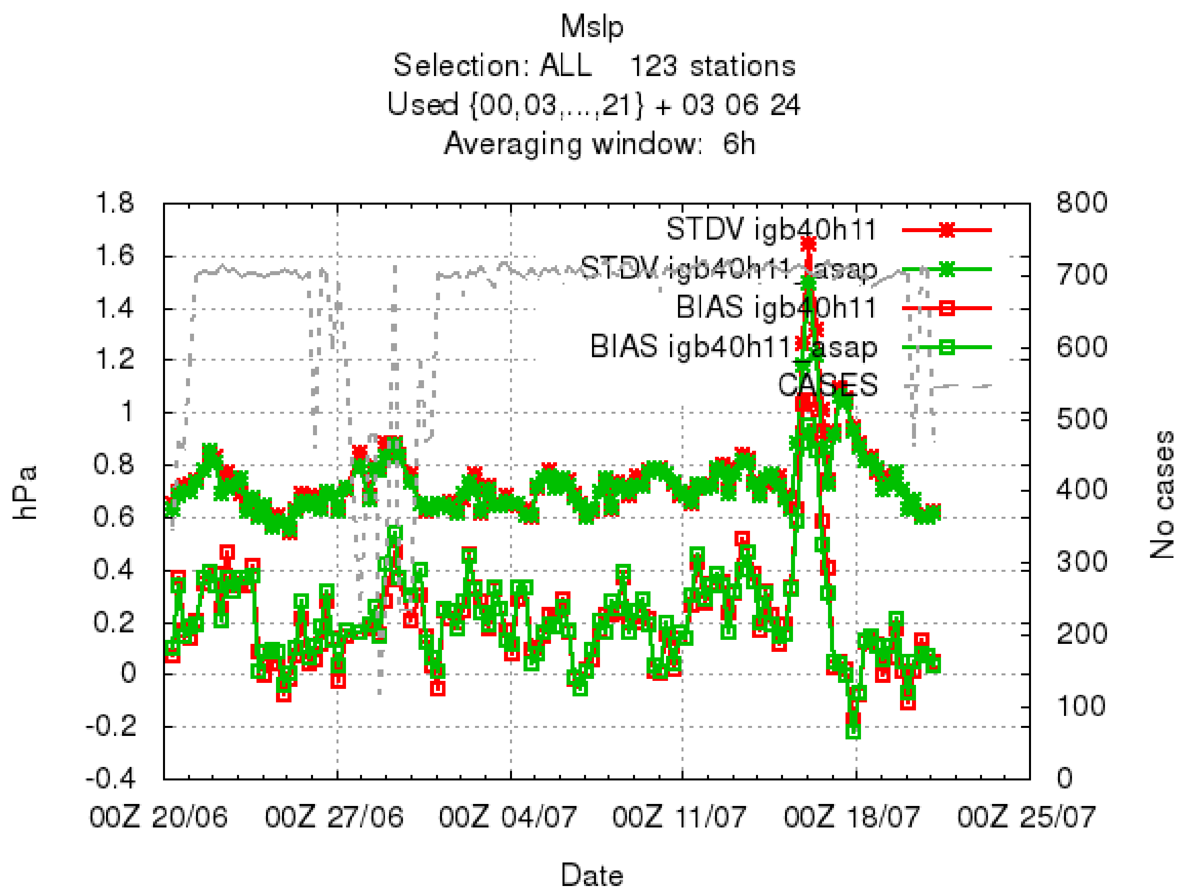

Figure 2. Inter-comparison of short range forecast errors in standard deviation (STD) and bias with IGB forecasts with lateral boundary data coupling to operational (in red) and early delivery ASAP (in green) streams, respectively, for mean sea level pressure in IGB domain for June 2 - July 24, 2020, a) average errors along forecast lead-time, b) daily averaged error time series with forecast ranges of 3h, 6h and 24h.

For the ensemble forecast system COMEPS with hourly launch and hourly data assimilation, it is found that the ensemble members with base times 05, 11, 17 and 23 Z can benefit from the earlier delivery ASAP data. Instead of coupling with 11-h old HRES boundaries, data from 5 h old cycle can be used as long as it arrives before boundary cutoff. For testing ASAP data, the starting time in COMEPS is changed to 5:41 (modulo 6h). For the 5-day experiment period, ~75% of the ASAP LBC arrived before 5:41 (modulo 6h). From averaged verification scores summarising control and perturbed ensemble members using LBC from ASAP (Figure 3), the reduced LBC lagging time results in a clear and substantial improvement in forecast skills as shown with reduced bias and rmse in MSLP. In addition, ASAP LBC is also seen to have improved COMEPS ensemble spread in 2-m temperature and 10-m wind in this test of short duration (not shown here).

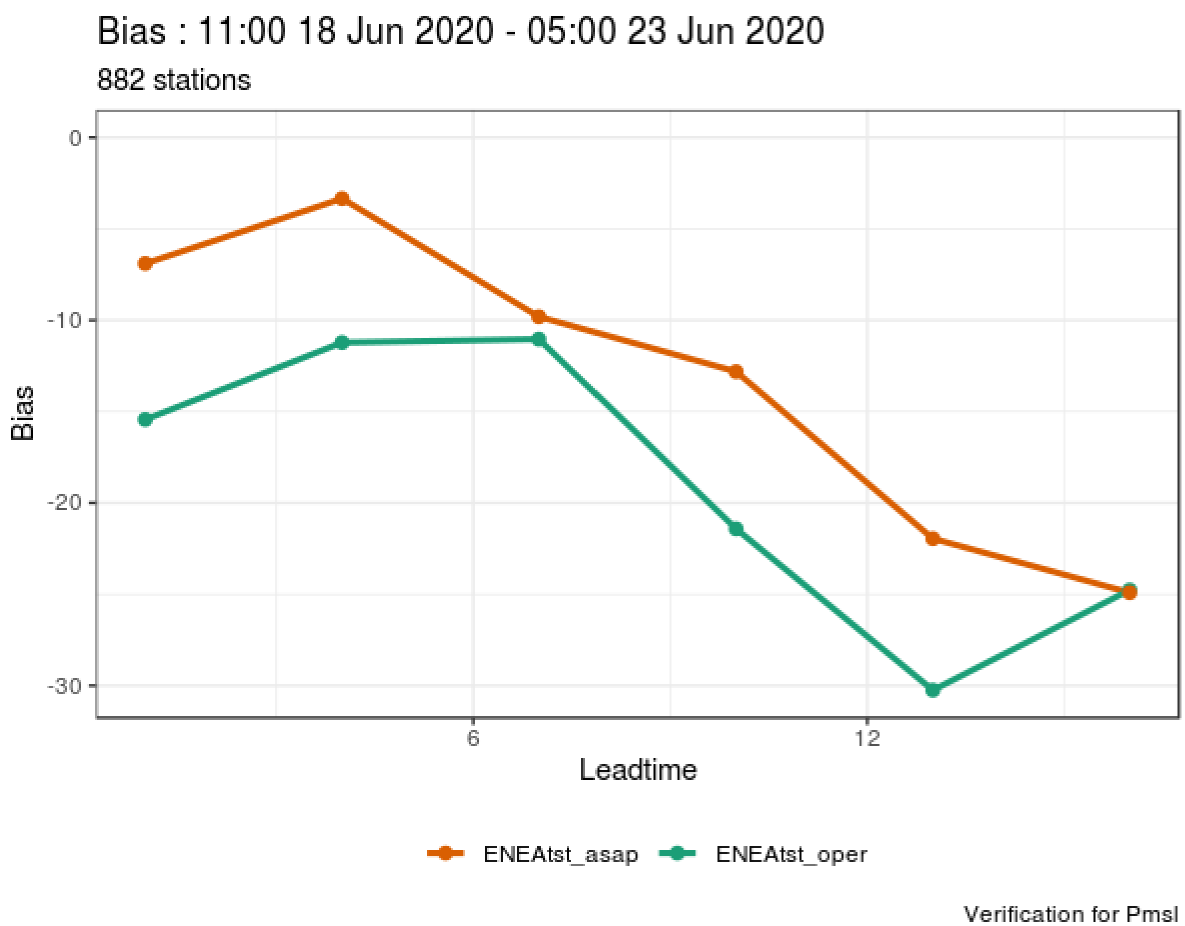
Bias : 11:00 18 Jun 2020 - 05:00 23 Jun 2020
882 stations
0
-10
-20
-30
Bias
6
12
Leadtime
ENEAtst_asap
ENEAtst_oper
Verification for Pmsl

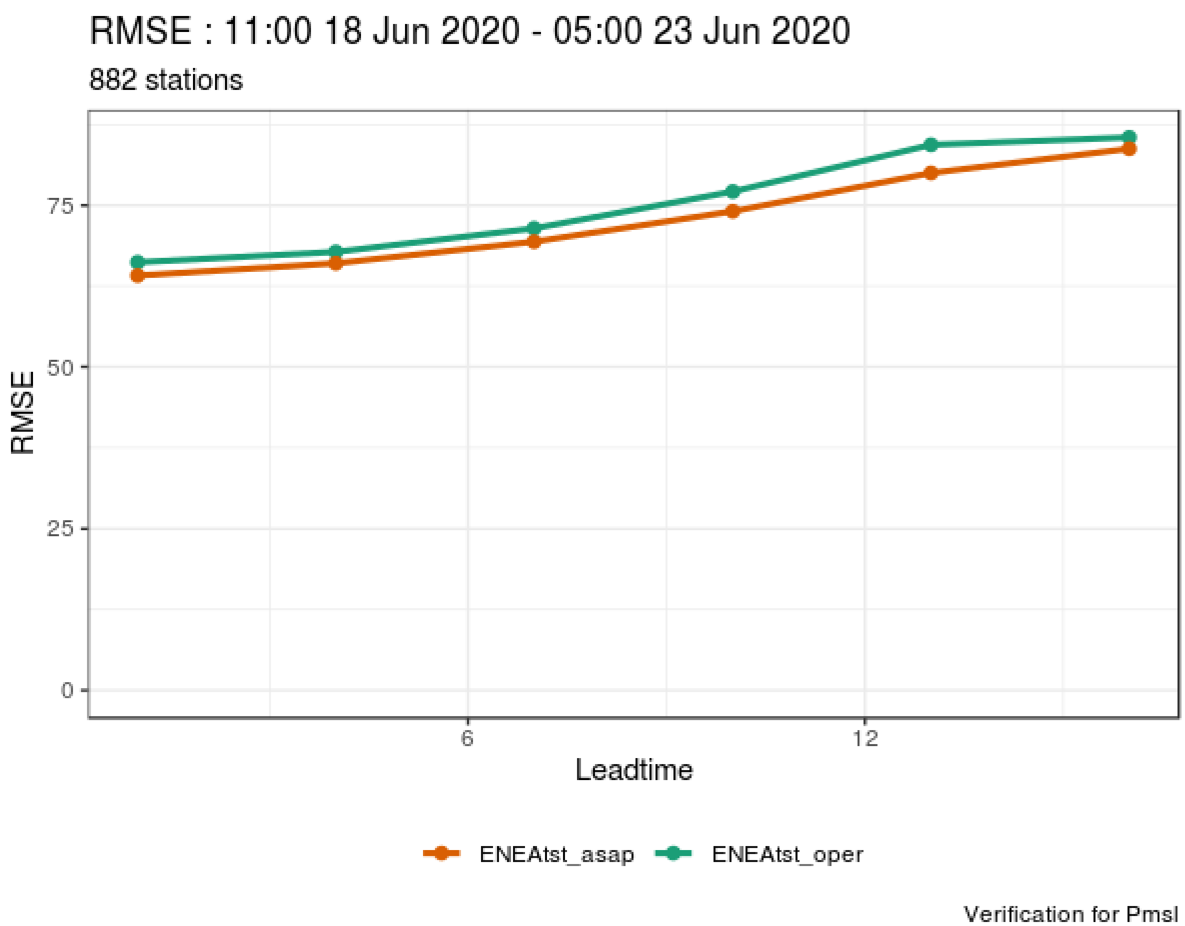

Figure 3. Inter-comparison of averaged forecast errors of up to 15 h with COMEPS controls and ensembles for which ASAP data is used, for (a) averaged bias error and (b) averaged Root Mean Square (rms) errors, on NEA domain, with 5-h lagged (ASAP, in red) and 11-h lagged (NORMAL, in green) LBC data from HRES. The experiment periods are for June 18-June 23, 2020 with a total of 84 control and perturbed forecasts compared.

5 Summaries and conclusions

Prediction skill of LAM systems rely crucially on the quality of coupling models which provide large scale constraints in initial and lateral boundary conditions. Due to various factors, delivery time of the operational ECMWF forecasts such as HRES and IFS-ENS is typically at the range of 6-h relative to the nominal basetime. Thus for users, the first 6 h of ECMWF forecasts can not be used for forecast purposes, as they arrive only after real time. Further, the operational ECMWF forecast data are updated no more than 4 times a day. Thus, the availability with ECMWF data entails that operational services using ECMWF LBC need to configure real time LAM systems with a lagging of 6 to 11h for LBC data. This is a major disadvantage for some of the member state NWS like DMI, especially for those of the LAM configurations which are airmed for continuous data assimilation with rapid/frequent cycling and for nowcasting. By comparing ECMWF HRES with various lengths of lagging, it is easy to see that short range forecast quality degrades rather significantly along lead time, and such degradation may be substantial in critical weather situations.

Using early delivery ASAP data from ECMWF HRES, a feasibility investigation of applying early delivery LBC data in operational LAM configurations has been conducted at DMI. It is found that the ASAP data can be available typically 30 to 40 minutes earlier than the normal operational HRES data, although the actual delivery time is not as stable and may occasionally deviate rather substantially. ASAP data enables a changed configuration for some of the runs in DMI's operational suites (IGB for Greenland-Iceland domain and COMEPS for Danish domain). In these setups, the age of coupling LBC data can be reduced by 6 hours in most cases when ASAP data arrives before LBC data cutoff. In the few cases when such data do not arrive, normal HRES data from older base-time is used. The test demonstrates a clear and consistent improvement in forecast quality, especially for large scale parameters such as MSLP. In some individual cases, such improvements appear to be rather substantial. The experiences show that, although the speed-up by ASAP stream is limited to 30 to 40 min compared to normal stream, the speed-up is sufficient to enable a substantially improved coupling for some operational configurations at DMI, which not only improves forecast skill of the runs using early delivery data themselves, but also the quality of other runs indirectly through assimilation cycling. On the other hand, even with the early delivery data such as ASAP, the age of LBC may still be as long as 10 hour given the current 6-hourly forecast update frequency at ECMWF. This is hardly satisfactory when applying such data to drive LAM applications with a more frequent assimilation cycling. Clearly, the shorter forecast lead time, the better accuracy. From the member service LAM perspectives, especially for quasi-continuous LAM forecast systems including those of nowcasting applications, it is hugely beneficial for ECMWF to develop data assimilation setup which provides a more frequent update, such as every 3 to 1 h.

6 Reference

Yang, X., 2017: The 2016 upgrade of the operational NWP at DMI. The WGNE Bluebook 2017, http://bluebook.meteoinfo.ru/uploads/2017/sections/BB_17_S5.pdf

Yang, X., H Feddersen, B H Sass and K Sattler, 2017: Construction of a continuous mesoscale EPS with time lagging and assimilation on overlapping windows. Joint ALADIN-HIRLAM Newsletter 8, 2017.

Recent Activities with AROME-Turkey at TSMS

Yelis Cengiz, Meral Sezer, Metin Emre Yakut

1. Introduction

Since Mid-October 2020, Arome-Turkey surface assimilation system has been running every 3 hours in the pre-operational mode as a result of the work done (Cengiz and Sezer, 2020) to set up the surface assimilation system for AROME-Turkey with the support of DAsKIT programme.

2. Basic Structure of AROME-Turkey Surface Assimilation System and Verification Experiment

Arome-Turkey (cy43t2) is running at 1.7 km of horizontal resolution and the model has 72 vertical levels and a 60 second time step. The pre-operational suite was generated by using ecflow script. The ecflow suite includes only production cycle. The surface assimilation system is running every 3 hours and producing a forecast with a 24 hour lead time.

In the surface assimilation system, lateral boundary condition data is obtained from ECMWF IFS model. And sea surface temperature is updated by the IFS coupling file. The SAPP system developed by ECMWF (Fucile et al., 2014), was installed at TSMS for the pre-processing of the observations and synop observations in bufr format processed by this system enter Arome-Turkey surface assimilation cycle (Cengiz et al., 2020).

AROME-Turkey uses CANARI-OIMAIN method to produce soil and surfex fields (T2m, H2m, TG1, TG2, WG1, WG2) analysis. In the CANARI namelist LMESCAN is set as .TRUE. .

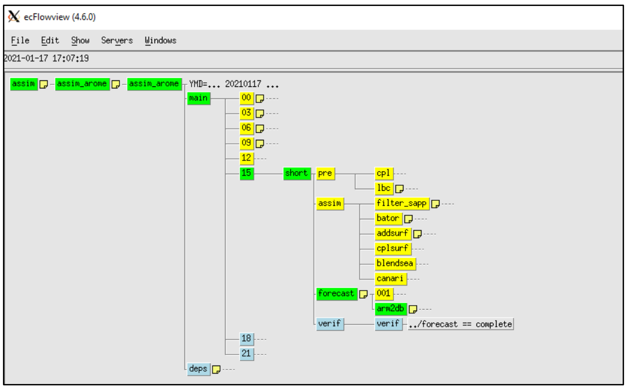

Figure 1: Screenshot of ecflow of AROME-Turkey Surface Assimilation System

In the verification experiment, Arome-Turkey surface assimilation system was compared to Arome-Turkey operational system. The differences between Arome-Turkey operational and Arome-Turkey surface assimilation system are as follows: The operational Arome-Turkey does not include a surface assimilation and using ARPEGE coupling file.
In the experiment, operational Arome-Turkey is named as ARM_OPER and Arome-Turkey surface assimilation system is named as ARM_OIMAIN. The time period of the experiment is 20210105-20210120. HARMONIE verification monitor was used for the verification (Yang, 2008).

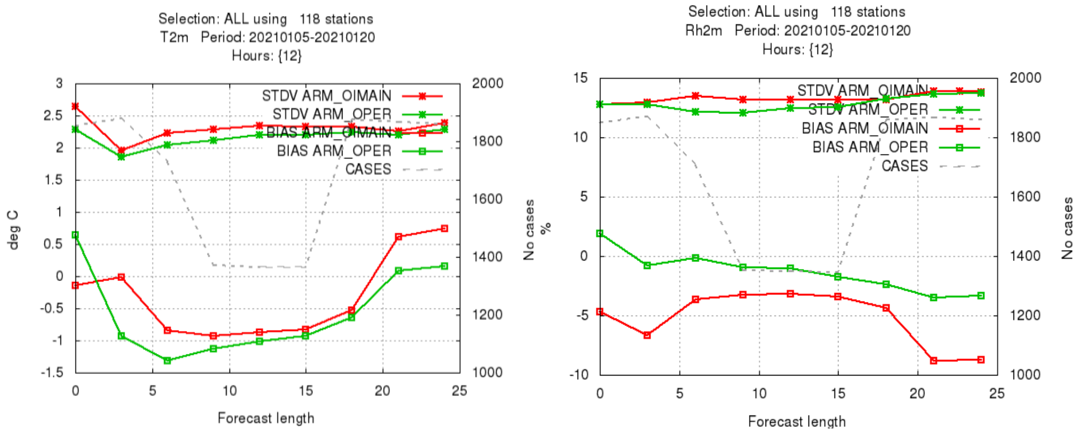

Figure 2: The verification results of experiments of 2 meter temperature and 2 meter relative humidity of 12 UTC are shown. The green line represents ARM_OPER and the red line represents ARM_OIMAIN.

It is possible to conclude that the bias values of ARM_OPER rh2m of 12 UTC are closer to zero than the bias values of ARM_OIMAIN rh2m of 12 UTC and the bias values of ARM_OIMAIN t2m of 12 UTC are closer to zero than the bias values ARM_OPER t2m of 12 UTC until the forecast length of 18.

3. Acknowledgements

The authors would like to thank all the participants of DAsKIT and Eoin Whelan for his support of using SAPP observations in the data assimilation system and for sharing the necessary files.

4. References

Cengiz, Y. and Sezer, M. (2020, January). Implementation of CANARI in AROME TURKEY. ALADIN-HIRLAM Newsletter, No 14, 151-153. https://www.umr-cnrm.fr/aladin/IMG/pdf/nl14.pdf

Cengiz, Y., Akdağ, G. H., Sert, M., Sezer, M.,. (2020, June). SAPP (Scalable Acquisition and Pre-processing System) at TSMS. ALADIN-HIRLAM Newsletter, No 15, 63-65. https://www.umr-cnrm.fr/aladin/IMG/pdf/nl15.pdf

Fucile, E. et al., 2014:SAPP: a new scalable acquisition and pre-processing system at ECMWF. ECMWF Newsletter No. 140 – Summer 2014, pp. 37–41. doi: 10.21957/3ylomoa6. https://www.ecmwf.int/sites/default/files/elibrary/2014/17341-sapp-new-scalable-acquisition-and-preprocessing-system-ecmwf.pdf

Yang, X. 2008, Development of Hirlam/Harmonie monitoring system. HIRLAM Newsletter no 54, 62-65.

ALADIN related activities @SHMU (2020)

M. Derková, M. Belluš, K. Čatlošová, M. Dian, M. Imrišek, M. Neštiak, A. Simon, J. Vivoda

1 Introduction

A summary of ALADIN related activities at Slovak Hydrometeorological Institute in 2020 is presented below. The setup of ALADIN operational system is described and some research and development activities are highlighted.

2 The ALADIN/SHMU NWP systems

The ALADIN/SHMU system setup

The operational ALADIN/SHMU system is ALARO 4.5 km/L63, as detailed in Table 1 below. Its setup is unchanged since the last report in the AH newsletter No. 14. The operational version was upgraded to new code version **CY43t2bf11** on **12/01/2021**. Upgrade and validation of CY43t2 was complicated due to an obsolete version of the gcc compiler. Several problems in assimilation jobs, partially linked to OMP parallelization, had to be solved locally.
The experimental convection permitting version ALARO 2.0 km/L87 is running in parallel. For setup details and model domain refer to Table 1 and Figure 1.

Table 1: ALADIN/SHMU operational (left column) and experimental system (right)

CMC	ALARO	ALARO
status	operational	experimental
code version	CY43t2bf11	
physics	ALARO-1vB	
resolution	4.5 km	2.0 km
levels	63	87
points	625 x 576	512 x 384
boundaries	ARPEGE, 3h frequency	Arpege, 1h frequency
initial conditions	CANARI & upper-air spectral blending by DFI	downscaling
initialization	none	DFI
surface scheme	ISBA	ISBA
starting times	00, 06, 12, 18 UTC	
cycle interval	6 hours	
forecast length	+78 h/+72 h/+72 h/+60 h	

3 Research and development activities

Most of research and development activities were ongoing within the RC LACE programme - stays or local work.

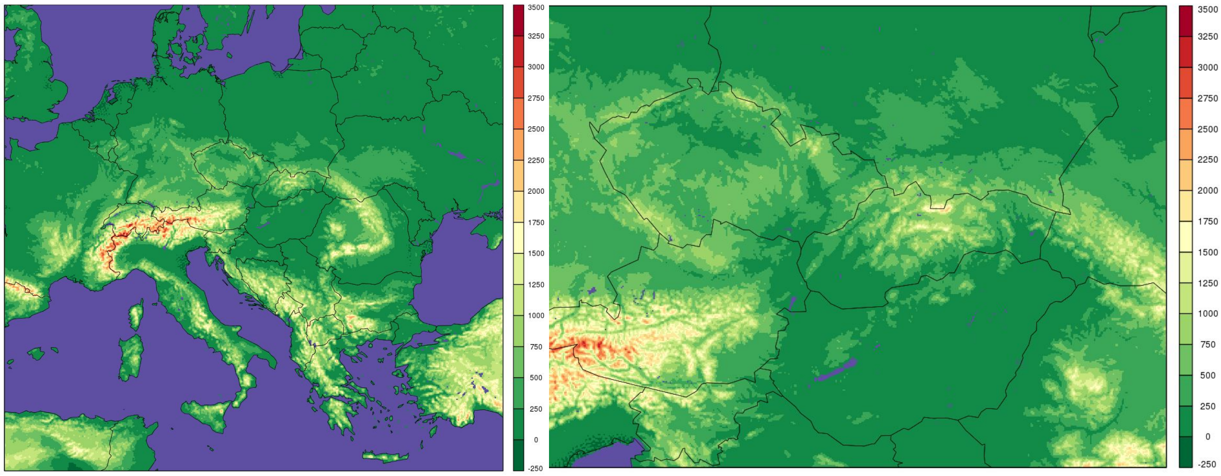

Figure 1: The domains and topography of ALADIN/SHMU operational system 4.5 km/L63 (left) and experimental convection permitting scale version 2.0 km/L87 (right).

Upgrade of the A-LAEF system (M. Belluš)

A-LAEF is a common RC LACE ensemble prediction system based on ALARO physics. It has been running at ECMWF as a TC2 application since 22/07/2020 (at 00 and 12 UTC up to +72 h). The 16+1 members with 4.8 km/L60 are coupled to ECMWF ENS via c903. The EPS system contains ensemble of surface data assimilation (ESDA) with internally perturbed screen-level observations, upper-air spectral blending, stochastic perturbation of physics tendencies (SPPT) for ISBA prognostic fields and new ALARO-1 multiphysics on CY40t1. The EPS output gribs are distributed to RC LACE members (CZ, SI, SK, RO, PL, and TK)**.**

At SHMU a preprocessing and visualisation of A-LAEF gribs based on R has been developed. A-LAEF maps are available for public at http://www.shmu.sk/webapps/#/sk/nwp/alaef. An example of A-LAEF products is shown on Figure 2 for a case study of night storms on undulated cold front associated with strong wind gusts (28/07/2020): precipitation totals (mean, spread, max), RADAR image [left], and wind gust probabilities for significant thresholds [right].

HARP based verification is under preparation.

More details about the new A-LAEF system including results of selected case studies can be found in [Belluš, M., 2020](#) (in Slovak).

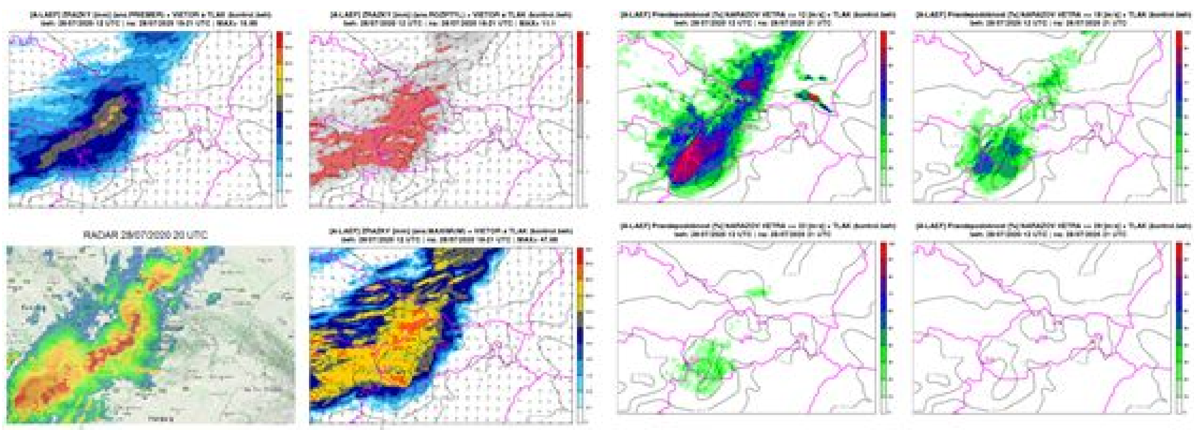

Figure 2: An example of the A-LAEF products for a case study of 28/07/2020: precipitation totals (mean, spread, max) & RADAR image [left], and wind gust probabilities for significant thresholds [right]

High resolution data assimilation activities (M. Imrišek, K. Čatlošová, M. Neštiak, M. Derková)

Several parallel activities are ongoing with the aim to prepare the high resolution data assimilation suite.

The operational scripting system was adapted in order to include 3D-Var modules (bator, screening and minimisation), all on CY43t2bf11. The 3Dvar assimilation of conventional data was implemented and validated in the experimental suite. The validation was performed by comparison of the single observation experiments and full observation experiments with beaufix reference. In the next step, the full BLENDVAR chain was tested. The actual experimental setup is canari > blending > 3Dvar > integration > verification. Preliminary results indicate improvement in the initial analysis, however the benefit from 3D-Var is lost during the first hours of subsequent model integration. Further work aims to test utilization of local Mode-S data from Slovak ATC (Čatlošová and Derková, 2020), processing and assimilation of GNSS data (Imrišek et.al., 2020), assimilation of radial winds from radars (Čatlošová, 2000), and to propose setup and tuning for operational BLENDVAR application.

Local quality control of automatic weather station (AWS) measurements based on A-LAEF was proposed. The experiences gained through INCA nowcasting and high resolution ALARO-1 reanalyses on 1-2 km grids led to a necessity of automatic quality control (QC). Without a proper QC, the automatic weather station measurements often brought a spurious signal into the analysis. A physically consistent spread of the meteorological fields provided by the A-LAEF ensemble was the main motivation for its use in an automatic QC procedure (in a new software level above MySQL database). As a first attempt the QC of 2m temperature was tested at SHMU. The suspicious AWS measurements with values out of the A-LAEF spread were identified. An example of 2m temperature measurements at Slovak AWS is shown on Figure 3 together with A-LAEF ensemble max and min values departures.

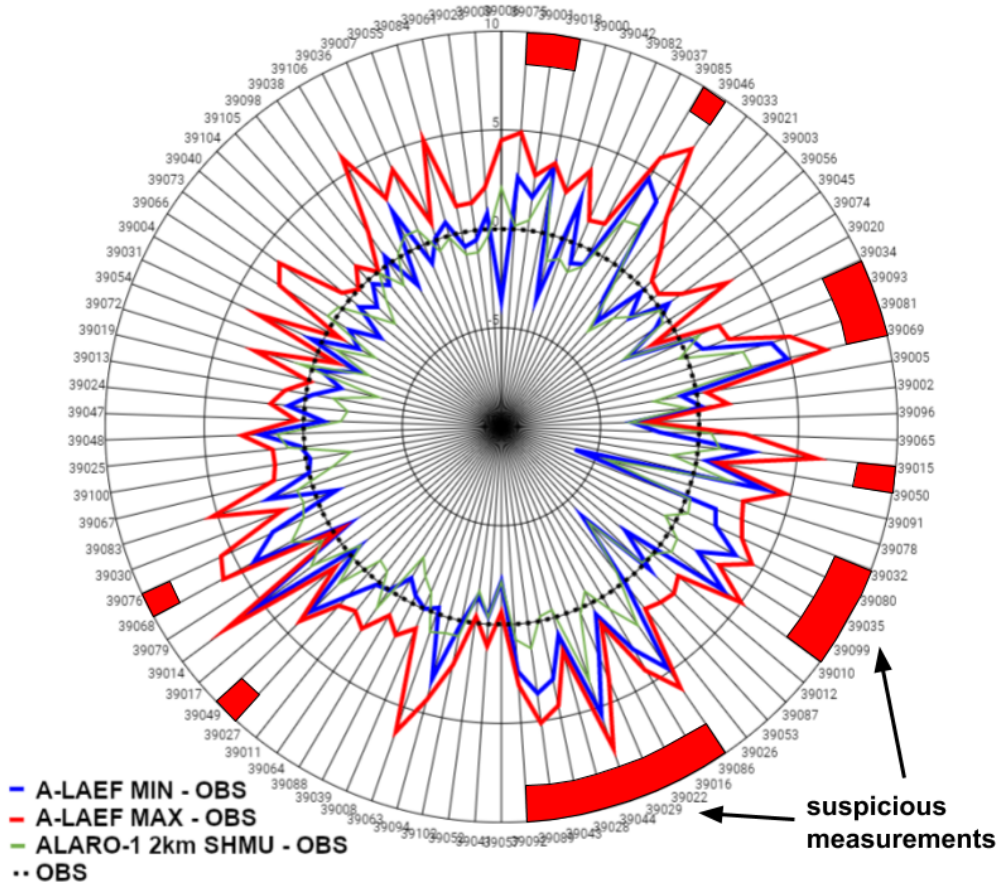

Figure 3: An example of the2m temperature observations for automatic weather stations in Slovakia compared to A-LAEF ensemble forecasts.

Stabilisation of SI scheme in NH model at 2km resolution (J. Vivoda)

ALADIN/HIRLAM partners exploit operationally predictor corrector (PC) scheme in their operational suites. I found that at resolutions 2km, the forecast computed with the PC scheme contains residual instabilities in the whole troposphere profile. These are not severe enough to cause "explosion" during forecast computation but are apparently visible in model results. This is presented on Figure 4.

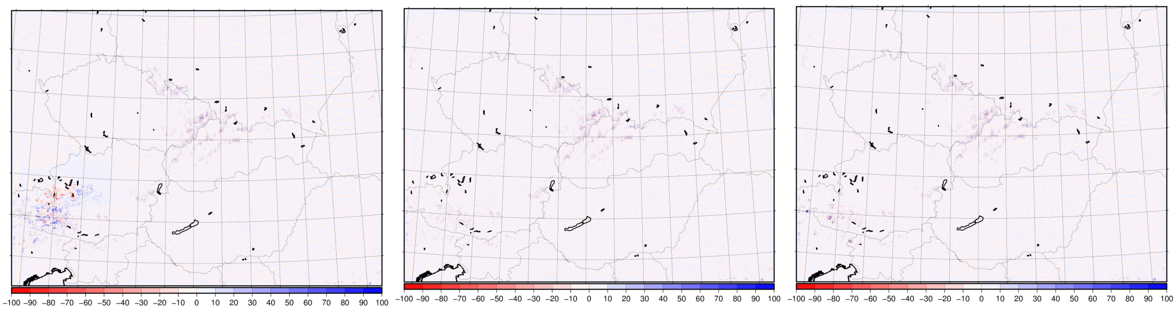

Figure 4: NH pressure departure at lowest model level in 12h prediction of ALARO model with 2km resolution. The left figure PC scheme, middle PC scheme with 3 iterations (reference) and the right figure is the SI SETTLS scheme with modified SI linear model.

We see that the prediction obtained with the PC scheme contains instability patterns above the Alpine region. When we use 3 iterations to improve stability those patterns disappear. We therefore modified SI linear system in a way that we subtract hydrostatic part of system from NH one, and NH departure we multiplied by constant parameter. Setting parameter higher than one (1.05) was sufficient to stabilize the SI SETTLS scheme. However, this must be combined with horizontal diffusion applied consistently at wind representation (divergence, vorticity and vertical divergence must be diffused with the same intensity) and also consistent treatment of temperature and pressure departure (both quantities must have same intensity of diffusion).
We see that the SI SETTLS scheme in our case provides the same results as reference in the majority of area, except for a few points usually above very steep regions. This is shown on Figure 5.

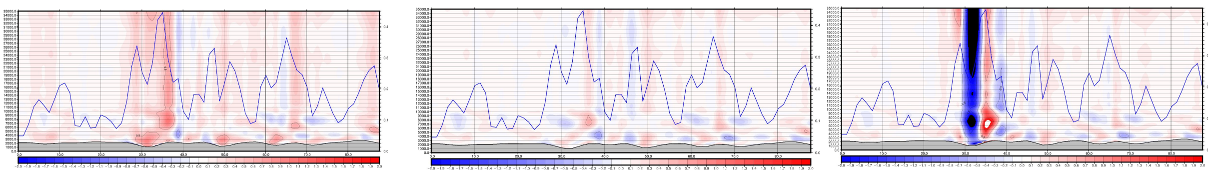

Figure 5: Vertical cross section of w via Alpine region. 12h prediction of ALARO model with 2km resolution. The left figure PC scheme, middle PC scheme with 3 iterations (reference) and the right figure is the SI SETTLS scheme with modified SI linear model.

We see that the SI SETTLS scheme is closer to reference in the major part of the domain except for a few model points where very severe vertical velocity develops. We are now investigating what are specific properties of location where such behaviour appears, resp. if such behaviour is a consequence of BCs mistreatment. There were around 10 such points in the whole model domain with such behaviour.

Investigation SURFEX in ALARO-1 (J. Mašek, M. Dian, M. Neštiak, M. Derková)

Continuing ISBA versus SURFEX validation, it was found that since ARPEGE switched to SURFEX at 05-Dec-2017 06 UTC production, total soil ice in ARPEGE coupling files are corrupted. Produced coupling files contain old ISBA fields with two ice reservoirs:

SURFRESERV.GLACE - ice in surface soil layer of depth d1 = 0.01m [kg/m^2]
PROFRESERV.GLACE - ice in whole soil column of depth d2 (including surface layer) [kg/m^2]

Therefore, PROFRESERV.GLACE is always greater than or equal to SURFRESERV.GLACE and the ice in the deep soil layer (i.e. between depths d1 and d2) is given by their difference.

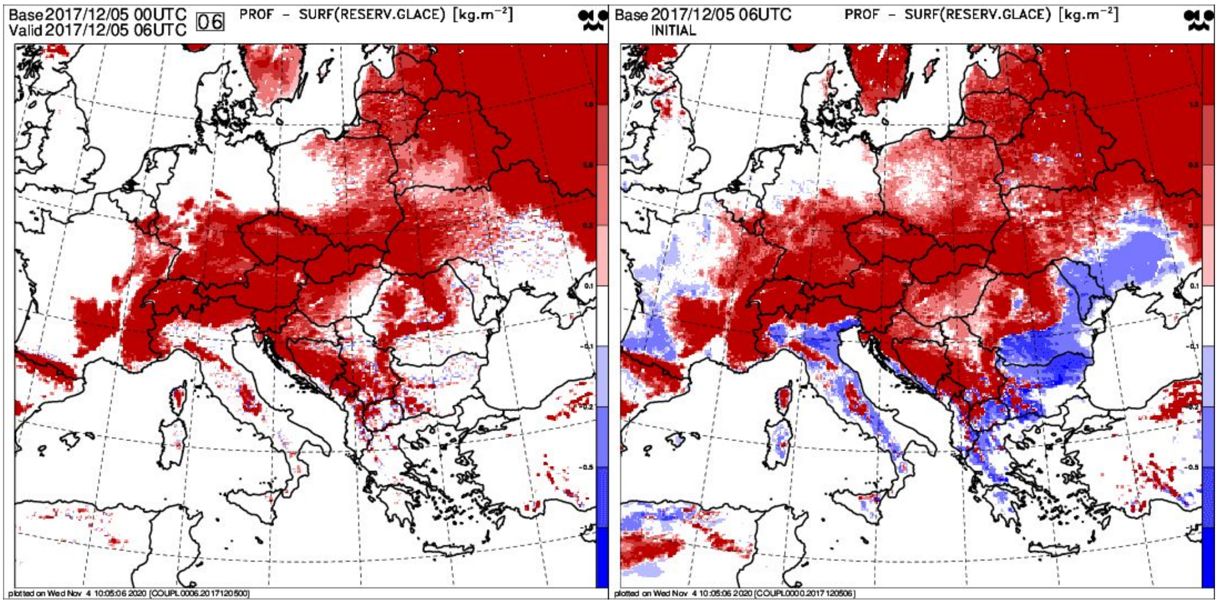

Figure 6: Difference PROFRESERV.GLACE - SURFRESERV.GLACE. Left: before switching ARPEGE to SURFEX. Right: after switching ARPEGE to SURFEX.

On Fig. 6 (left) is LACE LBC file from run preceding the switch of ARPEGE to SURFEX, valid at the time of switch. That difference PROFRESERV.GLACE - SURFRESERV.GLACE is positive (red) except from some points with slightly negative values caused by packing of subtracted fields. On Fig. 6 (right) is the same field from ARPEGE with SURFEX run. And here the problem comes - total soil ice in large areas can be less than surface soil ice! The problem is persisting and is easily seen every winter.

It has different consequences in ISBA and SURFEX:

In ISBA case unphysical negative values of deep soil ice are further evolved, which is not correct and it contaminates the forecast.

In the SURFEX case, negative deep soil ice is diagnosed and truncated to zero at the beginning of integration (in SURFEX subroutine ICE_SOILFR). However, change in deep ice reservoirs due to this truncation is interpreted as a phase change, kicking deep soil temperature by several degrees. This kick is then slowly contaminating the forecast via heat conduction in the soil.

This means that anybody coupling with ARPEGE and running AROME or ALARO in dynamical adaptation mode is affected, regardless of using ISBA, SURFEX.

Negative difference PROFRESERV.GLACE - SURFRESERV.GLACE persists also in CHMI and SHMU Alaro operative models, however both run surface CANARI. But this issue is caused by CANARI itself, independent of coupling from ARPEGE and was present before ARPEGE switch to SURFEX.

Anyway, the issues are urgent and it is possible that there are similar problems with soil water, not only ice.

Experimental runs of dynamic adaptation with 325m horizontal resolution (A. Simon)

In the operational ALARO-SHMÚ model, we still encounter large deviations between the forecast and observed 10m wind speed, mainly in mountain territories. One of the causes of this problem is the large under- and overestimation of the height of the orography, which can be several hundreds of meters at the current (4.5 km) resolution. Therefore, very short range (about 15 min.) forecasts of high-resolution (325m in horizontal) dynamic adaptation were tested. For computational reasons, we used a reduced number of vertical levels (37) and a domain (1600x950 points) just covering the area of Slovakia (see Figure 7 below). The adaptation was run on the cycle 43t2 with LBC from ALARO-SHMÚ, non-hydrostatic dynamics and with full physics. This configuration (with 12s timestep) seems to be numerically stable and was already run on more than 80 different situations, mostly with strong wind (selected from the 2016-2020 period). Although the representation of the terrain was improved compared to both operational and experimental 2 km model runs, it must be stressed that even at 325 m resolution we were not able to reproduce wind speed observed at the most extreme meteorological stations in Slovakia (e.g. at the station 11916 Chopok, 1998m ASL). This problem can partially be turbulence-related, since the model has a tendency to create a relatively thin (few hundreds of m deep) boundary layer around the mountain crests, although the observed wind records are closer to the free-atmosphere conditions at 10m or even lower height. Sensitivity tests were provided with different setups of the turbulence and mixing length parameterization (e.g. MD2+CG mixing length, MD2+BL89 mixing length, QNSE). However, the highest impact on wind speed could be found when changing the representation of the terrain roughness and when using the ECOCLIMAP II files for both surface roughness and thermal roughness length (see the presentation of Brožková and Mašek, 2020, from the Joint 30th ALADIN Workshop and HIRLAM ASM for more details). One of the goals of the ongoing research is to get information on the variation of the wind within an area corresponding to current subgrid scale and, if possible, to find relationships with respect to surface ruggedness and meteorological conditions. Modelling wind and several other meteorological parameters at high resolution at SHMÚ is the result of the project implementation: „ Scientific support of climate change adaptation in agriculture and mitigation of soil degradation" (ITMS2014+ 313011W580) supported by the Integrated Infrastructure Operational Programme funded by the ERDF.

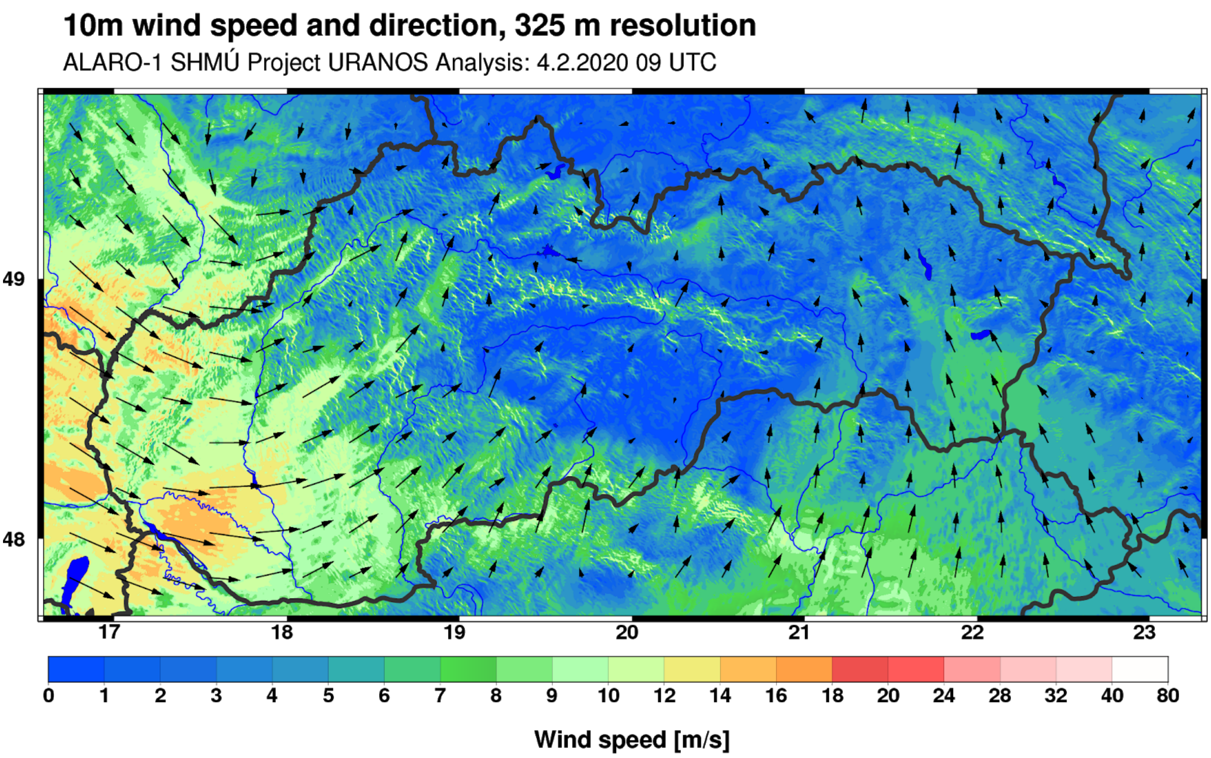

Fig. 7: 10 m wind (arrows) and wind speed (shades, m/s) in the 15 minute forecast of dynamic adaptation with 325m resolution over the area of Slovakia (referred as an analysis valid to 4 February 2020 09 UTC).

4 References

Belluš, M., 2020: NEW HIGH-RESOLUTION ENSEMBLE FORECASTING SYSTEM A-LAEF (in Slovak). METEOROLOGICAL JOURNAL 2020, VOLUME 23 – NUMBER 2, pp 75-86.

Čatlošová, K. and Derková, M., 2020: EXPLOITATION OF AIRCRAFT MODE-S DATA IN AROME/SHMU NUMERICAL WEATHER PREDICTION MODEL. METEOROLOGICAL JOURNAL 2020, VOLUME 23 – NUMBER 2, pp 65-74.

Čatlošová, K., 2020: Assimilation of radial velocity from radars. Report on stay at CHMI, August 2020, Prague, Czech Rep., (available on www.rclace.eu)

Imrišek, M, Derková, M. and Janák, J., 2020: Estimation of GNSS tropospheric products and their meteorological exploitation in Slovakia, *Contrib. Geophys. Geod.*, vol. 50, no. 1, pp. 83-111.

Assimilation of Doppler Radar Radial Winds data in the HARMONIE-AROME model configuration run at AEMET

J. Sánchez-Arriola and B. Navascués

1 Introduction

The current HARMONIE-AROME (Bengtsson et al., 2017) operational suite in AEMET that runs on the Nimbus supercomputer is based on a 3DVar data assimilation with a 3h cycle and the large scale mixing for humidity activated. It assimilates conventional observations from SYNOP, SHIP, DRIBU, AMDAR, and TEMP reports, GNSS ZTD data, ATOVS satellite radiances from AMSUA and AMSUB/MHS instruments, ASCAT, 2 meter temperature and relative humidity assimilated in upper air and radar reflectivity from 40 radars from three countries: Portugal, Spain and France.

As a mesoscale convection-permitting model, it is important to assimilate observations containing detailed information on appropriate scales (Ballard et al. 2016; Gustafsson et al. 2018,). Both the reflectivity and the Doppler radial winds (DRWs) from radars are high resolution observations and as have been demonstrated for different mesoscales systems like MM5, WRF, HIRLAM or HARMONIE, (Xiao et al. 2007, Wang et al. 2013, Lindskog et al. 2004; Salonen et al. 2011, Wattrelot et al. 2014 they have proven to be beneficial to numerical weather prediction systems.

The introduction of the radar reflectivity in AEMET operational HARMONIE-AROME system in 2019 has demonstrated to be beneficial, and to complement other humidity data assimilated from GNSS ZTD, ATOVS and Radiosonde observations. It produced a positive impact on HARMONIE forecasts, especially on precipitation. This improvement was mainly associated to a decrease of the False Alarms ratio. The assimilation procedure for radar reflectivity and some results can be found in Sánchez-Arriola et al. (2019).

DRWs are currently assimilated operationally at several centres (Xiao et al. 2008; Simonin et al. 2014) and a significant positive impact on the forecast (Montmerle and Faccani 2009; Xue et al. 2013, 2014) has been demonstrated. Once reflectivity data started to be assimilated operationally, efforts in AEMET have been devoted to also assimilate DRWs data from Spanish, French and Portuguese radar networks.

This document describes the process followed to assimilate these data processed and disseminated by OPERA, and the results obtained with respect to the current AEMET operational NWP run configuration.

2 Radar observations assimilated

Currently, the AEMET HARMONIE-AROME operational run assimilates reflectivity data from Portuguese (2), Spanish (15) and French (23) weather radars (Sánchez-Arriola et al., 2019). In this study, the additional DRWs observations that have been assimilated come only from the Spanish and French networks.

Data from Portuguese, Spanish and French radars are routinely exchanged by EUMETNET OPERA program (Saltikoff et al., 2019). These data are processed and pass a quality filter common to all the other radars of the European National Meteorological Services, so to be harmonized. As a result, homogeneous files are produced and disseminated at European level in conditions to be assimilated by NWP models.

The Spanish network is composed of C-band Doppler radars covering the Spanish peninsular territory (13), and the Balearic and Canary Islands respectively. They operate at 5620MHz except that at the Basque Country that does it at 5600MHz. Each radar makes a complete volume scan every 10 min, performing 19 different elevations (PPIs), from 0.5º to 25º. PPI sweeps are performed with two maximum ranges: 240km (long range products) and 120km (short range products). Short-range products use a dual PRF (900/1200Hz) which allows the Nyquist velocity of these short-range products to be 48.1 m/s. Radial wind is one of them. It is obtained at 0.5km resolution.

AEMET is sending to OPERA corrected (Z) and uncorrected (T) reflectivities at 1km resolution (240km range) coming from 0.5º, 1.4º and 2.3º elevations, and Doppler radar radial winds at 0.5km resolution (120km range) coming from 0.5º and 1.4º elevation angles.

Both reflectivities and radial winds at a larger number of elevation angles coming from the French radars network are exchanged by OPERA. They have been also used in this study.

The OPERA data received in AEMET has been preprocessed and quality controlled by BALTRAD software (Michelson et al., 2018). Some minor changes have been needed to adapt the reference cycle 40h.1.1 HARMONIE-AROME code to the operational context in AEMET to be able to assimilate these observations.

When using volume data of both reflectivity and radial velocity from OPERA there are a few challenges that needs to be taken into account. One of them is that the data is of a very high spatial resolution and need to be reduced to avoid representativeness errors and correlated observations. To face this and a few other caveats, a preprocessing tool for the OPERA data is included within HARMONIE system. This tool harmonizes the input data and creates super observations (SO) in order to reduce the density (Ridal et al., 2017). It has been seen that quality control of the radar observations is really important and it has also been shown that using super observations gives better scores than a simple thinning (Martin Ridal, personal communication). Radar reflectivities are used in operational or pre-operational production in most HIRLAM/HARMONIE countries following this approach.

The radial velocity observations present also other things that complicates the usage. One of these is the Nyquist velocity of the observations; if it is too low aliasing effects can occur and they will destroy the wind fields. There are de-aliasing methods available but the results from these are still not stable and therefore HARMONIE only use radial wind observations with a Nyquist velocity higher than 30 m/s. This is the case of DRWs from the Spanish and French radars.

Another issue to take into account is to quality control the radial velocities. So, HARMONIE only use wind information that are accompanied by a co-located reflectivity observation. Then the quality information from the reflectivities can be applied to the wind observations. Only the observations with an elevation angle higher than 1 degree have been selected. SO are generated with the ones whose quality "flag" assigned in the OPERA pre-processing exceeded a fixed threshold.

3 Data assimilation experiments

Several parallel experiments have been designed and carried out in AEMET to test the assimilation of DRWs with respect to the present configuration of the operational run. They have been run over one month long period: from 1st to 31 March 2020. This period was very rainy over the Iberian Peninsula. It should be noticed that during the last week of this period the number of available aircraft observations dropped drastically due to the reduction in flights caused by the COVID pandemic.

The CONTROL (AIBe) experiment run for this study is the operational suite based on HARMONIE-AROME cycle40h1.1. 3DVar data assimilation is used as upper analysis, with a 3h cycle and a large scale mixing of short range HARMONIE forecasts with ECMWF fields to create the first guess for the analysis. This procedure is also activated for humidity. The analysis assimilates conventional observations from SYNOP (including 2 meter temperature and relative humidity), SHIP, DRIBU, AMDAR, and TEMP reports, GNSS ZTD data, ATOVS satellite radiances from AMSUA and AMSUB/MHS instruments, ASCAT, and all the available radar reflectivity observations from the 40 radars from three countries: Portugal, Spain and France that cover the model area. The model runs at 2.5 horizontal resolution and 65 vertical model levels extending up to 10 hPa, over a geographical domain centered on the Iberian Peninsula that includes the Balearic Islands.

A preliminary experiment has been conducted introducing additionally DWRs from the French and Spanish radars. It was not necessary to run a spin up period, because it started from the same variational bias correction coefficients (to correct the bias from ATOVS and GB GNSS ZTD observations) and first guess from the operational suite. DWRs had already been assimilated passively over a different period, but the experiment was not parallel to the operational run. During this previous period, quality control of these data was an issue.

In this preliminary experiment over March 2020, default values in the HARMONIE-AROME code for relevant parameters for the assimilation of DRWs were kept. Most of them are documented in Montmerle y Faccani (2009). In particular, a value of 20m/s is used as rejection limit for DRWs innovations in the first guess check. DRWs are also thinned to avoid correlated observation errors by retaining the best data within 15 × 15 km^2 boxes. Observation error standard deviation is formulated following a linear increase with distance to radar. With the default formulation, it oscillates between 1m/s and 2m/s at 120km. Notice that this increase rate is half than the proposed in Montmerle and Faccani (2009).

Diagnostic of the preliminary assimilation of Doppler radar radial winds

The main goal of this preliminary experiment was to investigate the quality of the data itself, both for each radar separately and for all the data together. Plots of histograms of innovations for the different radars showed that the quality of the DRWs data could differ between radars (not shown here), and that not all of them seem to have the required Gaussian distributions. Also the number of data was highly variable among them. We observed these features both at Spanish and French radars.

Figure 1 (left) shows the total number of DRWs SO per analysis time that entered the data assimilation (and were not rejected by quality control checks) at different heights for the whole period. The highest number of them is found at around 3000m, whereas the lowest one corresponds to the uppermost levels (7000-1000m). AEMET is only exchanging radial winds obtained at two low elevation angles, and SO from Spanish radars are created from only one of them (1.4º). These figures may be compared to the number of assimilated wind observations from aircraft and from radiosondes to see the differences between them. On one hand, DRW SO are available at all analysis times (whenever there is reflectivity data) although this is not the case for aircraft observations at night, and of course for radiosondes, which are only launched at 00 and 12UTC. On the other hand, before the coronavirus pandemic produced a drastic decrease in aircraft data, the number of radal wind SO was 2 to 4 times greater than that of aircraft wind observations, depending on the level (not shown).

Figure 1 (right), displays the RMS of innovations per analysis time at different height levels. It can be observed that the size of innovations is higher at 7000-10000m height layers, where the number of DRW observations is also smaller. Nevertheless, too high innovations are found at the rest of levels in the atmosphere, but in a lesser percentage. We have not investigated the origin of this big innovation size, so we cannot discard, e.g. the data preprocessing, the SO creation and the observation operator apart from data quality.

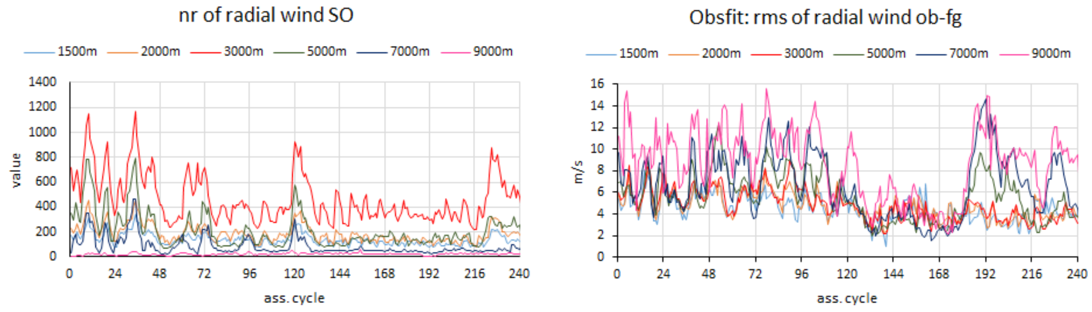

Figure 1: Time series of the number of radial wind observations (left), and of RMS of the innovations of DRWs at different vertical levels for the preliminary experiment carried out to assimilate DRWs.

In order to improve the first guess check decisions in the screening part of assimilation, histograms and transformed histograms of all innovations for DRWs observations assimilated have been obtained to identify the first guess departures of observations having gross errors according to Andersson and Järvinen (1999). They are shown in **Figure 2.** Extended tails at both sides of the innovations distribution (left) show clear non-Gaussian innovations corresponding to data with gross errors. The transformed histogram of innovations (right) reveals that the rejection limit value used for DRW observations in these experiments (the threshold where innovations apart from Gaussian) should be more restrictive (around 5m/s) than the one used by default (20m/s).

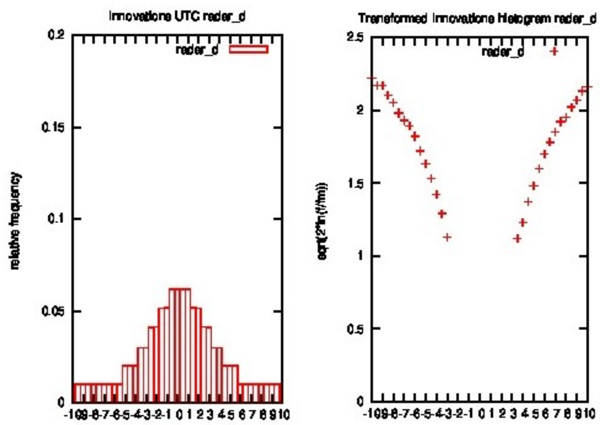

Figure 2: Histogram (left) and transformed histogram (right) of all innovations of Doppler Radar Radial Winds for March 2020

A new experiment was then conducted using this adjusted first guess check limit (5m/s) and assimilating these observations actively. It led to some decrease of the number of assimilated observations and innovation size was controlled, but it resulted in a forecasts deterioration with respect to the CONTROL AlBe forecasts skill (not shown).

More diagnostics were obtained to understand the assimilation performance of these observations. Although SO had been created trying to avoid it, and these SO data were also thinned in the screening step, we investigated if horizontal error correlation still existed in these data. The idea was to better tune the thinning of data in the screening, if these diagnostics indicated that this was needed. Then the Desroziers technique (Desroziers et al., 2005) was applied to obtain the horizontal error correlation of DWRs. The results obtained are displayed in **Figure 3.** It shows that observation error correlation drops to 0.2 around 20km distance. This horizontal distance is close but slightly larger than the thinning distance value applied in the screening to radar data (15km).

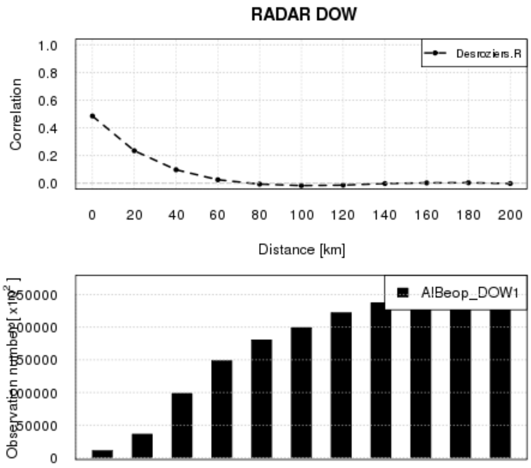

Figure 3: Estimation of horizontal error correlations based on Desroziers et al.(2005) (top) and the number of collocations (bottom) as a function of separation distance for DRWs observations

We additionally looked at the values of observation errors for DWRs and compared them to those of radiosonde and aircraft wind. **Figure 4** (left) shows that the observation error assigned to Doppler winds, although its increase with distance to radar, is much lower than the one assigned to the other two observation types, and therefore the model trusted wind data from DRWs more than from radiosonde and aircrafts whose innovations size was smaller/similar to that of DWRs. Taking also into account the huge DWRs spatial density, and that perhaps these scales are not being represented enough in the background error covariance matrix used, the DWRs weight in the analysis could be overestimated.

Design of a refined data assimilation of Doppler radar radial winds

Taking into account the conclusions achieved with the diagnostics obtained, a new experiment called AIBeop_DOW16 was designed and run.

This experiment modifies the default setup in respect to:

- The first guess check limit has been increased to 5m/s (instead the former 20m/s).
- The thinning distance has been increased to 25km (instead the former 15km).
- The formula for observation error standard deviation has been modified. The rate of error increase with distance to radar has been kept, but the independent term has been inflated after some empirical tuning. In this way, DRWs error ranges between 3-4m/s (instead the former 1-2m/s). It should be noticed that, although their data assimilation systems are different, other NWP centers (DWD, UKMO) give DRWs an observation error value larger than the one used by default in the HARMONIE-AROME code (Waller et al., 2019).

Figure 4 (right) displays values of sigmao for DRWs observations in this new experiment as compared to those assigned to radiosonde and aircraft wind.

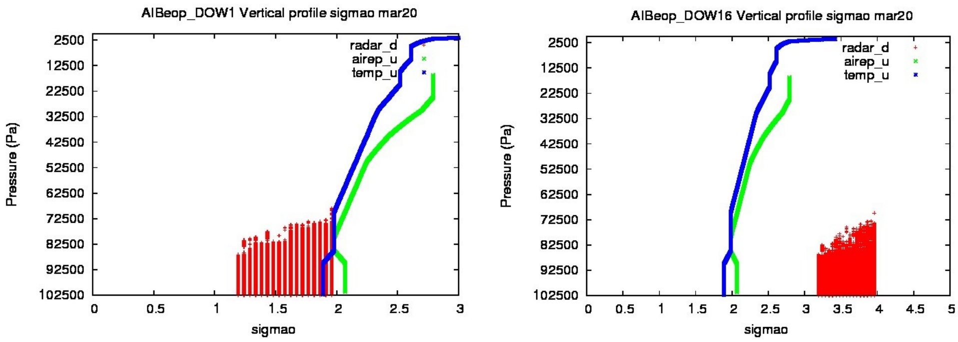

Figure 4: Vertical profile of observation error standard deviation (sigmao) values for wind observations from Doppler Radar radial Wind (only up to 700hPa), AIREP and radiosondes. Default values (left), and modified values used in AIBeop_DOW16 experiment (right).

The new experiment called AIBeop_DOW16 with these updates has been run over the same period of study.

Data assimilation performance in AIBeop_DOW16 experiment

Some additional diagnostics have been obtained to check the functionality of the changes introduced in the experiment AIBeop_DOW16.

Figure 5 shows the observation fit of DRWs to the first guess and to the analysis for the different height levels in the atmosphere corresponding to AIBeop_DOW16 experiment with tuned parameters of the DRWs data assimilation. It can be observed that innovations size has substantially decreased with the new first guess check limit applied (in comparison to **Figure 1**, right). The analysis increments are also smaller due mainly to the inflated sigmao for DRWs in AIBeop_DOW16 (not shown). It also allows to see that many DRWs with high innovations at the uppermost levels have been filtered out by the usage of the new rejection limit value. At any case, inspection of the analysis residual and innovation of individual data shows that some DRWs that were actively assimilated were not supported by the rest of observations, indicating that their quality might not be good or there are deficiencies with data processing (not shown).

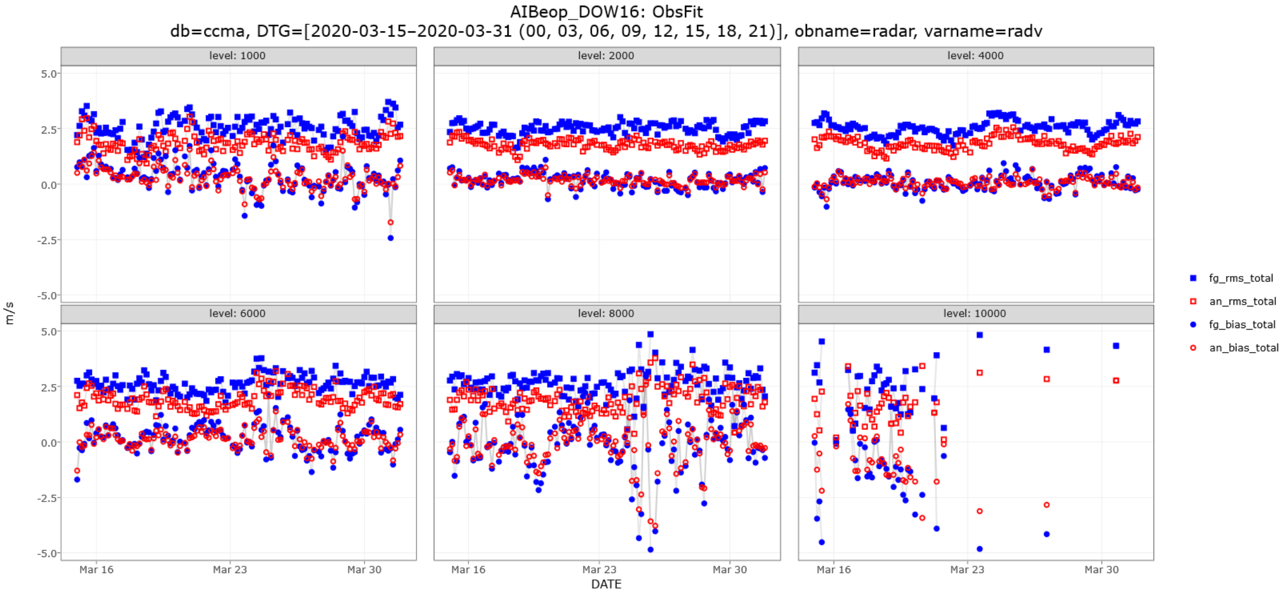

Figure 5 Observation fit to the first guess (blue) and to the analysis (red) for AIBeop_DOW16 experiment at different height levels

The Absolute Degree of Freedom for Signal (DFS) diagnostic is shown for AIBeop_DOW16 experiment (**Figure 6**). It allows to see the information content of all observation types assimilated. The impact of both Radar-Z and Radar-DOW has decreased in AIBeop_DOW16 experiment with respect to previous ones due to the larger data thinning of radar observations (the same thinning is applied to reflectivity derived relative humidity profiles and to radial winds). In case of RADAR-DOW it is also due to the higher observation error assigned to these data in this experiment. The total weight of Doppler radar radial winds in this experiment is comparable to that of aircraft wind observations (slightly smaller), although the larger number of DRWs observations compared to that of aircraft data.

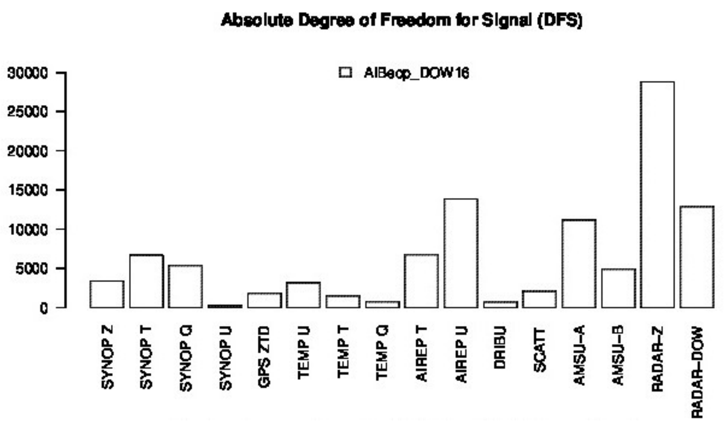

Figure 6: DFS plot showing the Absolute Degree of Freedom for Signal of AIBeop_DOW16 experiment

4 Results: impact on forecasts

The impact of the assimilation of Doppler radar radial winds has been assessed by means of the objective verification of model forecasts against SYNOP and TEMP observations over the four weeks period of study. The following figures show the most relevant features found. They display verification scores reached by the two experiments described in the text: CONTROL (AIBe, in red) and the revised assimilation of DRWs (AIBeop_DOW16, in green).

The revised assimilation of DRWs seems to be positive for precipitation and surface wind forecasts of high impact events. At **Figure 7,** the Kuiper Skill Score for 10meter winds, and 12h accumulated precipitation is shown. It can be seen how the skill of 10meter wind forecasts clearly improves for AIBop_DOW16 experiment for the stronger wind speed intervals. This is due to a better Probability of Detection since the False alarm rate is the same for both experiments. In case of precipitation, a positive impact is found for the largest precipitation amounts at the different accumulation intervals and the reason is the improvement of both the Probability of Detection and False Alarm rate. An improvement of 2 meter temperature forecast has also been found (not shown).

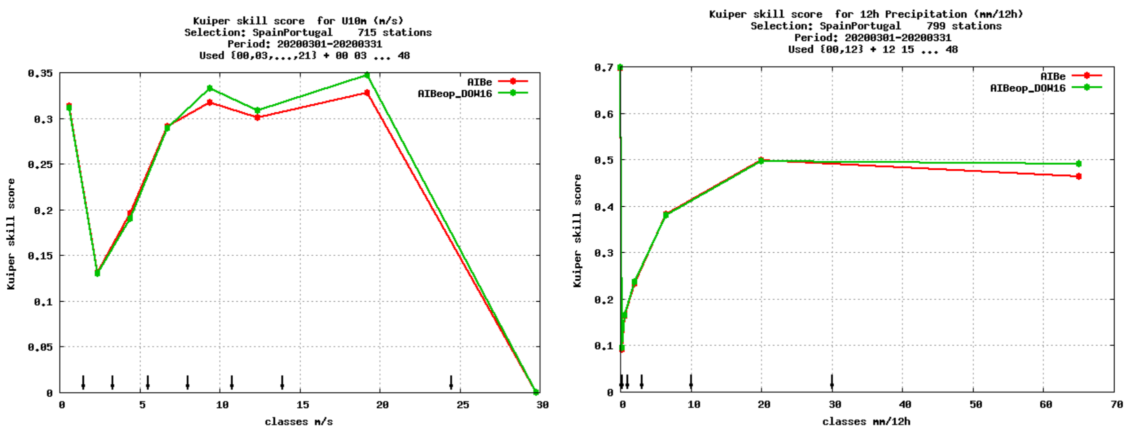

Figure 7: Verification of CTRL (red) vs AIBeop_DOW16 (green) forecasts. (a) Kuiper Skill Score of 10m wind, (b) Kuiper Skill Score of 12h accumulated precipitation,

The overall influence of this revised assimilation of DRWs has shown to be neutral for most of the variables. **Figure 8** displays the vertical profiles of forecast bias and error standard deviation for (a) wind speed and (b) relative humidity, obtained by comparison against observations from the 16 existing radiosonde stations in the domain. However, wind speed bias is slightly larger at 700 and 500 hPa. The wind speed weakening at these levels will be further investigated in a future work. On the other hand, a small positive impact is found for relative humidity at 850-700hPa, not statistically significant, at all forecast lengths. This improvement in humidity is more noticeable the last week of the period, when the number of aircraft data decreased drastically (not shown).

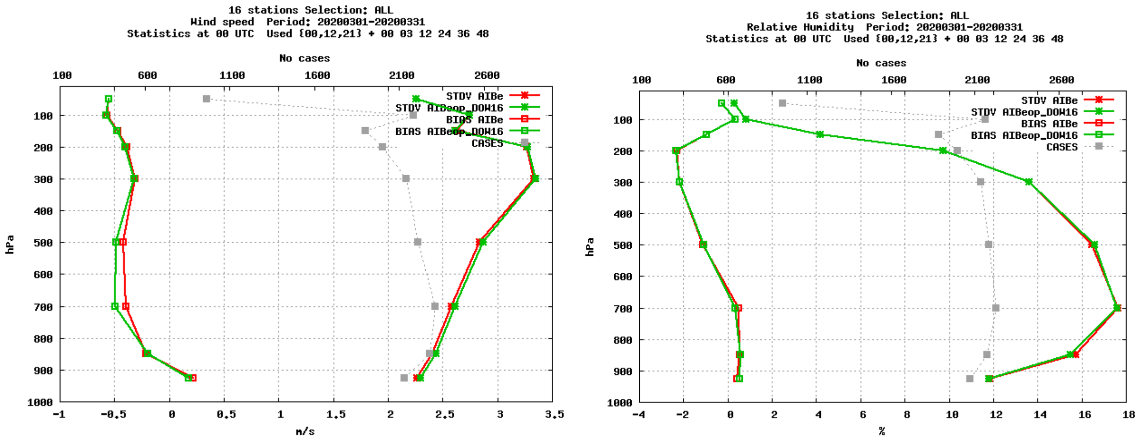

Figure 8: Vertical profile of verification scores (bias and standard deviation) obtained by CTRL (red) and AIBeop_DOW16 (green) forecasts using radiosonde observations: wind speed (left), relative humidity (right).

7 Conclusions and further work

Doppler radar radial winds (together with reflectivities) from the Spanish and French weather radars have been assimilated by two experiments parallel to the HARMONIE-AROME run operational in AEMET over one month long period (March 2020).

The preliminary experiment conducted to assimilate these new radial winds data with the default settings in cycle40h1.1 of HARMONIE presented very high radial wind innovations. Some tuning of first guess check limits has allowed to filter them, but active assimilation of the rest of DRWs data produced a negative impact on some forecasted parameters.

Additional diagnostics of the data assimilation performance have been obtained and have led to a larger revision of quality control and data thinning parameters. Observation error standard deviation for these data has been also empirically inflated, after comparing it against that of other observation types. The revised configuration of DRWs assimilation has been tested in a new experiment over the same period. A rather neutral impact is then found in forecasts of upper air parameters. However, the revised DRWs assimilation shows to improve surface wind speed and precipitation forecasts in high impact weather conditions.

Although the results finally found are rather promising, additional work is required to better understand the source of high innovations of DRWs, to tune the quality control of these data, to advance in characterizing its errors (the role of not only distance to the radar but also elevation angle similarly to Waller et al., 2019), to improve the construction of the SO (with regards to the size, quality index limit of the observations to include...), in connection with the data thinning strategy.

The background error covariances B matrix used by the assimilation algorithm when assimilating these observations having a high spatial density is also of paramount importance (Bojarova and Gustafsson, 2019), and must be taken into account. These experiments have used a B matrix calculated with downscaled ECMWF Ensemble Data Assimilation (EDA) members. Work is ongoing at AEMET to calculate it using BRAND (B-randomization) and HARMONIE EDA methods that might better represent small scale background errors, being more apropriate for radar data assimilation.

Acknowledgements

The authors would like to acknowledge Martin Ridal (SMHI) for helping with the radar data preprocessing in Cy40h11 and his explanations, Javier Calvo (AEMET) for his support in this work, Alberto Cansado (AEMET) for answering our questions about the Spanish radars characteristics and operation and Florian Meier (ZAMG) for advice concerning first guess check and errors of DRW observations.

References

Andersson,E. and Järvinen,H., 1999:Variational quality control. *Q.J.R. Meteorol. Society* 125, 697-722, https://doi.org/10.1002/qj.49712555416

Ballard, S. P., Z. Li, D. Simonin, and J.-F. Caron, 2016: Performance of 4D-Var NWP-based nowcasting of precipitation at the Met Office for summer 2012. Quart. J. Roy. Meteor. Soc.,142, 472–487, https://doi.org/10.1002/qj.2665.

Bengtsson, L., Andrae, U., Aspelien, T., Batrack, Y., Calvo, J., de Rooy, W., Gleeson, E., Hansen-Sass, B., Homleid, M., Hortal, M., Ivarsson, K.-L., Lenderink, G., Niemelä, S., Nielsen, K. P., Onvlee, J., Rontu, L., Samuelsson, P., Muñoz, D. S., Subias, A., Tijm, S., Toll, V., Yang, X., and Køltzow, M. Ø., 2017: The HARMONIE-AROME Model Configuration in the ALADIN-HIRLAM NWP System, *Monthly Weather Review*, **145**, 1919-1935 doi: 10.1175/MWR-D-16-0417.1

Bojarova,J., Gustafsson N., 2019: Relevance of climatological background error statistics for meso-scale data assimilation, *Tellus A: Dynamic Meteorology and Oceanography*, Volume **71**,1, 1615168 doi: 10.1080/16000870.2019.1615168

Caumont, O., V. Ducrocq, E. Wattrelot, G. Jaubert & S. Pradier-Vabre, 2010: 1D+3DVar assimilation of radar reflectivity data: a proof of concept. *Tellus A: Dynamic Meteorology and Oceanography*, Volume **62**, Issue 2

Desroziers, G., L. Berre, B. Chapnik, and P. Poli, 2005: Diagnosis of observation, background and analysis-error statistics in observation space. Quart. J. Roy. Meteor. Soc., 131, 3385–3396, https://doi.org/10.1256/qj.05.108.

Gustafsson, N., and Coauthors, 2018: Survey of data assimilation methods for convective-scale numerical weather prediction at operational centres.Quart. J.Roy.Meteor. Soc., 144, 1218–1256, https://doi.org/10.1002/qj.3179.

Lindskog, M., K. Salonen, H. Järvinen, and D. Michelson, 2004: Doppler radar wind data assimilation with HIRLAM 3DVAR. Mon. Wea. Rev., 132, 1081–1092, doi:10.1175/ 1520 0493(2004)132,1081:DRWDAW.2.0.CO;2.

Montmerle, T., and C. Faccani, 2009: Mesoscale assimilation of radial velocities from Doppler radars in a preoperational framework. Mon. Wea. Rev., 137, 1939–1953, https://doi.org/ 10.1175/2008MW-R2725.1.

Salonen, K., G. Haase, R. Eresmaa, R. Hohti, and H. Järvinen, 2011: Towards the operational use of Doppler radar radial winds in HIRLAM. Atmos. Res., 100, 190–200, doi:10.1016/ j.atmosres.2010.06.004.

Ridal, M., and M. Dahlbom, M., 2017: Assimilation of Multinational Radar Reflectivity Data in a Mesoscale Model: A Proof of Concept. *Journal of Applied Meteorology and Climatology*, 56(6), 1739-1751

Sánchez-Arriola J., Navascués B., Calvo J., 2019: Radar Reflectivity Impact study with HARMONIE-AROME in AEMET. ALADIN-HIRLAM Newsletter No.12, 112-118

Saltikoff, E. & Haase, Günther & Delobbe, Laurent & Gaussiat, Nicolas & Martet, Maud & Idziorek, Daniel & Leijnse, Hidde & Novák, Petr & Lukach, Maryna & Stephan, Klaus. 2019. OPERA the Radar Project. Atmosphere. 10. 320. 10.3390/atmos10060320.

Simonin, D., S. P. Ballard, and Z. Li, 2014: Doppler radar radial wind assimilation using an hourly cycling 3D-Var with a 1.5 km resolution version of the Met Office Unified Model for nowcasting. Quart. J. Roy. Meteor. Soc., 140, 2298–2314, https://doi.org/10.1002/qj.2298.

Wang, H., J. Sun, X. Zhang, X.-Y. Huang, and T. Auligné, 2013: Radar data assimilation with WRF 4D-Var. Part I: System development and preliminary testing. Mon. Wea. Rev., 141, 2224–2244, doi:10.1175/MWR-D-12-00168.1.

Wattrelot, E., O. Caumont, and J.-F. Mahfouf, 2014: Operational implementation of the 1D13D-Var assimilation method of radar reflectivity data in the AROME model. Mon. Wea. Rev., 142, 1852–1873, doi:10.1175/ MWR-D-13-00230.1

Xiao, Q., and J. Sun, 2007: Multiple-radar data assimilation and short-range quantitative precipitation forecasting of a squall line observed during IHOP_2002. Mon. Wea. Rev., 135, 3381– 3404, doi:10.1175/MWR3471.1.

Waller, J. A., and coauthors, 2019: Observation Error Statistics for Doppler Radar Radial Wind Superobservations Assimilated into the DWD COSMO-KENDA System. Mon. Wae. Rev., 147, 3351-3364, https://doi.org/10.1175/MWR-D-19-0104.1

Xiao, Q., and Coauthors, 2008: Doppler radar data assimilation in KMAs operational forecasting. Bull. Amer. Meteor. Soc., 89, 39–43, https://doi.org/10.1175/BAMS-89-1-39.

Xue, M., F. Kong, K. Thomas, J. Gao, Y. Wang, K. Brewster, and K. Droegemeier, 2013: Prediction of convective storms at convection-resolving 1-km resolution over continental United States with radar data assimilation: An example case of 26 May 2008 and precipitation forecasts from spring 2009. Adv. Meteor., 2013, 259052, https://doi.org/10.1155/2013/259052.

——, M. Hu, and A. Schenkman, 2014: Numerical prediction of 8 May 2003 Oklahoma City tornadic supercell and embedded tornado using ARPS with assimilation of WSR-88D radar data. Wea. Forecasting, 29, 39–62, https://doi.org/10.1175/WAF-D-13-00029.1.

Assimilation of IASI radiances in AEMET operational suite

Joan Campins, Beatriz Navascués

1 Introduction

Infrared Atmospheric Sounder Interferometer (IASI) is an infrared Fourier-transform spectrometer on board the MetOp polar orbiting meteorological satellites which make up the EUMETSAT Polar System (EPS) series.

IASI measures in the infrared part of the electromagnetic spectrum at a horizontal resolution of 12 km over a swath width of about 2,200 km, in a sun-synchronous mid-morning orbit (9:30 Local Solar Time equator crossing, descending node), providing global observations twice a day. It provides information on the vertical structure of the atmospheric temperature and humidity in an accuracy of 1° Kelvin and a vertical resolution of 1 kilometre and profiles of humidity with an accuracy of 10% and a vertical resolution of 1-2 kilometres, which has given significant positive forecast impact at NWP centers in both global and regional models (Collard and McNally, 2009, or Randriamampianina et al. 2011).

The aim of this short contribution is to present the implementation and assessment of the assimilation of IASI clear-sky radiances from METOP-B in the AEMET HARMONIE-AROME system. First, IASI radiances assimilation has been prepared by executing an experiment where these data were assimilated passively. Then, these data have been actively assimilated to test their impact on model forecasts.

2 IASI passive data assimilation experiment

The current HARMONIE-AROME cycle 40h1.1 (Bengtsson et al., 2017) operational suite in AEMET that runs on the local HPCF. The model runs at 2.5 horizontal resolution and 65 vertical model levels extending up to 10 hPa, over two domains: one centered on the Iberian Peninsula that includes the Balearic Islands (called AIB), and other centered on the Canary Islands (called AIC). AEMET HARMONIE-AROME is based on a 3DVar data assimilation with a 3h cycle. Until recently, it assimilated conventional observations from SYNOP, SHIP, DRIBU, AMDAR, and TEMP reports, GNSS ZTD data, and ATOVS satellite radiances from AMSUA and AMSUB/MHS instruments. A later major update of this system added the assimilation of radar reflectivities, scatterometer winds, and 2-meter temperature and relative humidity data in upper air, and activated the large-scale mixing with ECMWF fields in the first guess also for humidity (Sánchez-Arriola et al., 2020). Now, clear-sky IASI radiances from METOP-B have been incorporated to the assimilation system at 09, 12, and 21 UTC for AIB and at 00, 09, 12, and 21 UTC for AIC. A thinning distance of 80 km is used to reduce the original spatial resolution of IASI data.

The preparation of IASI data assimilation has mainly consisted in selecting the set of channels to be assimilated, checking the cloud detection scheme results and tuning the bias correction variational algorithm (VarBC). Passive assimilation of IASI radiances in a parallel experiment to the operational configuration has allowed to perform it.

Data and initial channel selection

The IASI L1c product (provided by EUMETCAST) contains 8461 channels (between 645.0 cm-1 and 2760 cm-1 at 0.5cm-1 resolution). For numerical weather prediction data assimilation purposes, this high volume of data was reduced to 366 channels by Collard (2007) and Collard and McNally (2009).

This large number of channels must be checked and evaluated for each model. This is a hard task which we decided not to perform initially. Instead, we used the reduced channel selection performed by MetCoOp that is available in the HARMONIE-AROME set-up. This comprises 30 channels for the long-wave CO2 band and 25 channels for the water-vapour band (see Table 1). In this study IASI data from METOP-B satellite are used.

Table 1: Selection of IASI channels used for passive IASI data assimilation experiments.

Band	Peaking Level	Channel
CO2	High	38, 51, 63, 85, 104, 109, 167
	Middle	173, 180, 185, 193, 199, 205, 207, 212, 224, 230, 236, 239, 242, 243, 249, 296, 386
	Low	333, 337, 345, 352, 389, 432
Water vapour		2701, 2819, 2910, 2919, 2991, 2993, 3002, 3008, 3014, 3098, 3207, 3228, 3281, 3309, 3322, 3438, 3442, 3484, 3491, 3499, 3506, 3575, 3582, 3658, 4032

Variational bias correction and cloud detection scheme

Satellite bias for IASI radiances is corrected using a Variational Bias Correction scheme (VarBC) in a similar way as for ATOVS radiances (Campins et al., 2017). We use a set of 6 predictors (0, 1, 2, 8, 9, and 10; see Table 2) which were initialized from a cold-start and updated with a 24-h cycling.

Table 2: Description of predictors used in VarBC.

Number	Predictor
0	Constant
1	1000-300 hPa thickness
2	200-50 hPa thickness
8	Nadir viewing angle
9	Nadir viewing angle **2
10	Nadir viewing angle **3

As the current assimilation of IASI deals with clear-sky radiances, the cloud contaminated channels must be rejected. To discriminate between clear-sky and cloud-affected channels the scheme described by McNally and Watts (2003) was used. This algorithm works with observation minus first-guest departures, but these departures must be unbiased. However, that is not the case for a cold start passive assimilation, until regression bias correction coefficients are updated. Biased data can be evaluated as cloudy data and rejected through quality control checks, mainly for low and middle peaking channels. To diminish this issue, we followed the procedure described in Benacek (2013). It mainly consists in selecting a few clear sky days to relax cloud detection algorithm and accelerating the bias coefficients convergence during these days in order they may adapt faster. The objective is to prevent in subsequent assimilation cycles, when both cloud detection and bias coefficients are reset to their default values, that cloud detection decisions may reject radiances affected by strong biases.

Final channel selection

The aim of passive assimilation is to spin-up VarBC coefficients and to ensure the suitability of the IASI observations that will be further assimilated as active. For all channels in Table 1, time series of (bias corrected) observations minus first guess were examined. We expect a bias reduction in time, from zero (cold-start) to a small mean value of observation minus guess (OMG) departures (i.e., 0.1-0.2 K). After the 40-day period this is the case for almost all the channels, except for some low-peaking levels as 333, 352, 389, and 432 (see the difference between channel 205 and 389 in Figure 1). For these low-peaking channels (more affected by cloud contamination) the number of observations is very low, preventing an appropriate bias correction. For this reason, these channels are discarded in both domains. Besides, channel 85 exhibits a large OMG standard deviation in the AIB domain, and it seems reasonably to reject it too. As a consequence, the final channels selection is reduced to 50 channels for AIB and 51 channels for AIC.

We have not found any significant difference between corrected first-guess departures over land and sea, thus the selected channels are assimilated over both surfaces.

The assimilated clear-sky radiances for different channels were validated against cloud-top-pressure images (a product derived from MSG-SEVIRI by EUMETNET Nowcasting-SAF) along the passive, and active data assimilation periods. Overall, cloud detection scheme and variational bias correction are able to identify clear channels and reject those affected by clouds, specially in the mid and upper troposphere.

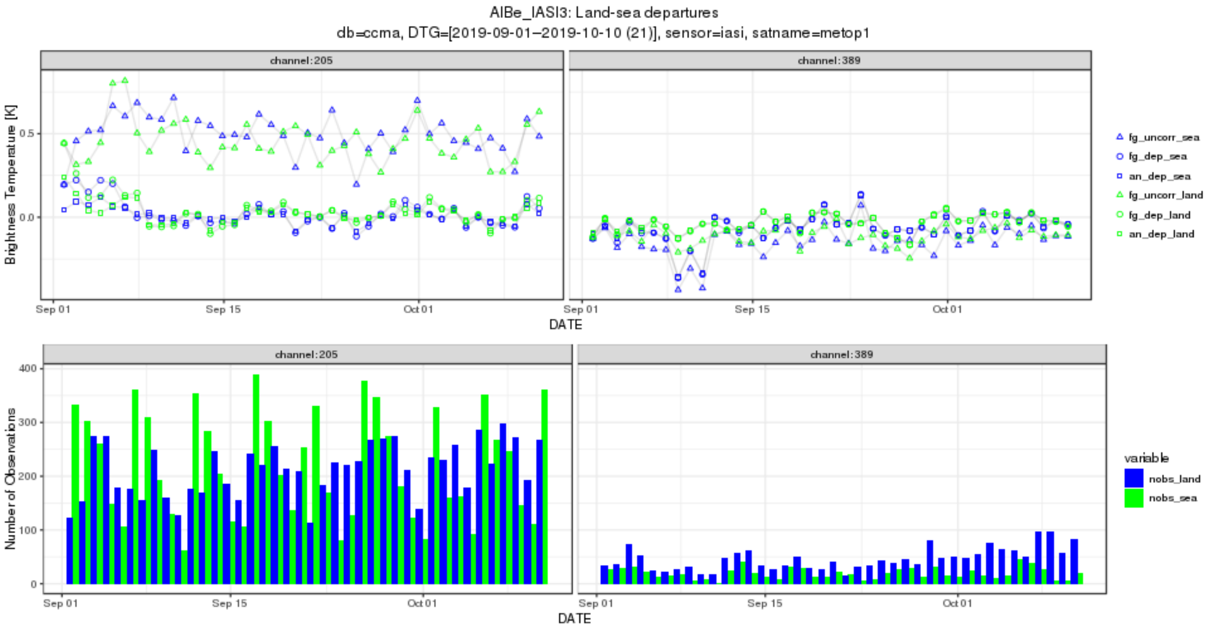

Figure 1: Time series of: top) uncorrected and corrected first-guess departures (fg_uncorr and fg_dep), and analysis departures (an_dep), and bottom) number of assimilated observations for channel 205 (left), and channel 389 (right) over land (in green) and sea (in blue) at 21 UTC.

3 IASI active data assimilation experiment: impact on the forecast

Once the bias for clear-sky IASI radiances is being corrected properly because bias coefficients are tuned, the next step is to assimilate these observations in active mode, and to evaluate their impact on the forecast. Two parallel experiments have been run, one without IASI radiances (which is used as control), and another one assimilating actively IASI radiances in long wave CO2 and water vapour bands. This procedure is applied over the Iberian Peninsula domain (AIB vs AIBe), and Canary Islands domain (AIC vs AICe) over a long study period. For the first domain, forecast verification is split in two consecutive periods (from 10th June to 31st August 2020, and from 1st to 30th September 2020), and for the second domain forecast verification is performed over one single period (from 10th June to 9th September 2020). The forecast lead time is 24 hours for analysis time at 00, 06, 12 and 18 UTC; and 3 hours for analysis time at 03, 09, 15, and 21 UTC.

It should be mentioned that previously the impact of the assimilation of only CO2 band radiances had been evaluated in a different shorter period. The best scores obtained when the radiances of the two bands were assimilated decided the final configuration of the experiments presented here.

The impact of the assimilation of IASI data has been assessed through the forecast objective verification of the parallel experiments against SYNOP and TEMP observations, and for both domains.

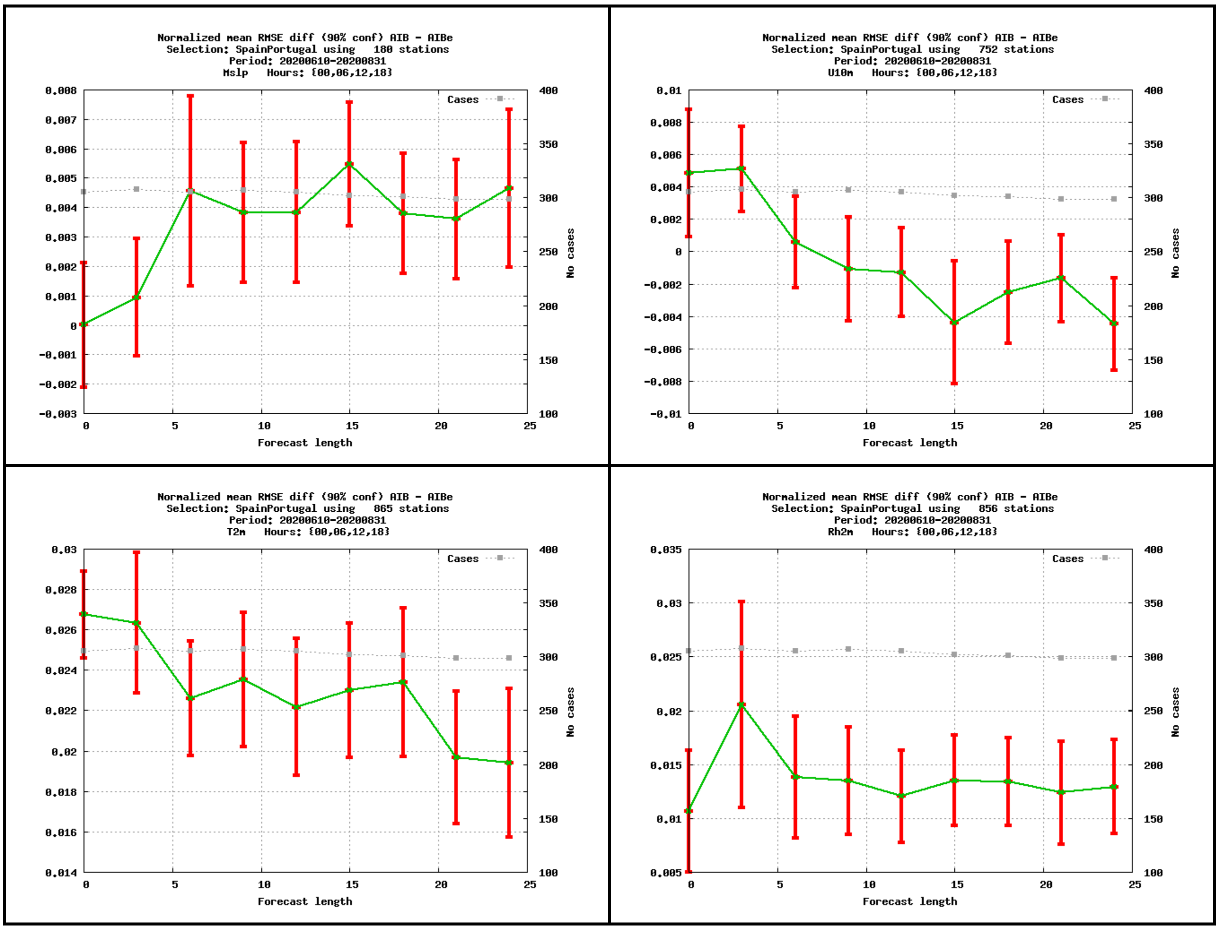

Figure 2: Normalized mean Root Mean Square Error (RMSE) difference between AIB and AIBe for mean seal level pressure (top-left), 10-meter wind (top-right), 2-meter temperature (bottom-left), and 2-meter relative humidity (bottom-right).

AIB-AIBe: 10th June to 31st August 2020

The impact of the active assimilation of clear-sky ASI radiances on surface parameters is shown in Figure 2, where normalized mean Root Mean Square Error (RMSE) differences between AIB and AIBe are calculated for different forecast lengths (positive/negative values correspond to larger/lower RMSE for AIB respect to AIBe). For mean sea level pressure (top-left), and 2-meter temperature and relative humidity the impact found is positive, and it is statistically significant for most of the forecast lengths (bottom panels). For 10-meter wind (top-right), the impact found is positive only for short forecast lengths (H+0 and H+3, statistically significant), but negative thereafter.

At upper-air, vertical profiles of temperature and wind speed verification scores do not reveal any impact on forecast during this summer period, but for relative humidity a slight positive impact can be underlined (Figure 3).

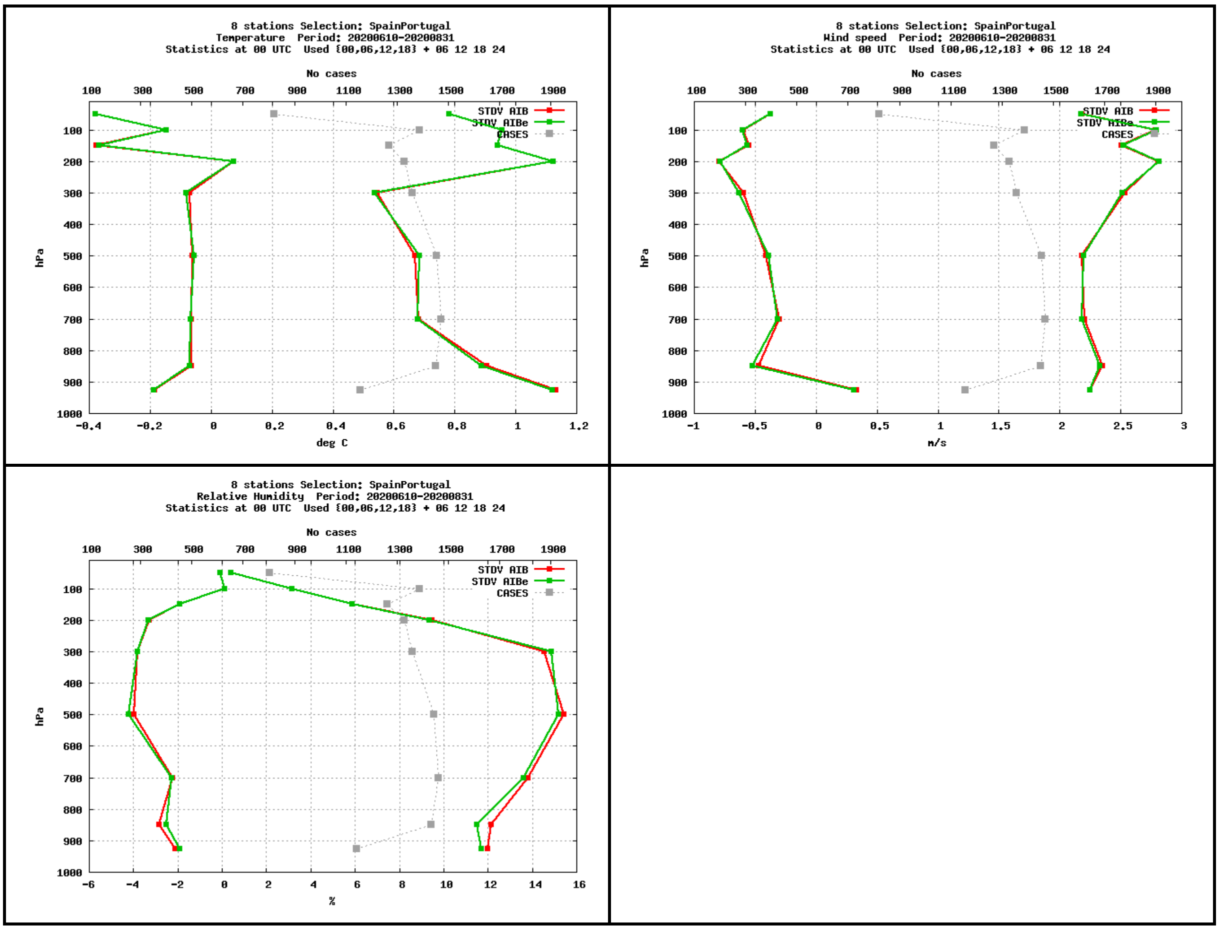

Figure 3: Vertical profiles of standard deviation and mean error for temperature (top-left), wind speed (top-right), and relative humidity (bottom-left) for AIB (in red) and AIBe (in green) at 00 UTC.

The skill of precipitation forecasts is very similar for AIB and AIBe, except for high precipitation amounts (> 60 mm in 6 and 12 h) where the active assimilation of IASI observations improves the forecast (not shown). Similar results are obtained in this period for False Alarm Ratio and Probability of Detection (not shown).

AIBe-AIB: 1st to 30th September 2020

Forecasts objective verification has been carried out for this month separately because it is representative of rainy conditions over Spain. For this period, the impact of IASI data assimilation has shown to be slightly positive for mean sea level pressure, statistically significant for some forecast lengths (not shown). On the contrary, for 10-meter wind the overall impact is negative (statistically significant), but it seems related to light winds, which are dominant, while for strong winds the impact is positive (not shown). For 2-meter temperature and relative humidity the impact is either positive or negative depending on the forecast length (not shown).

The assimilation of IASI data slightly improves precipitation forecasts. As an example, in Figure 4, the forecast skill (measured by the Equitable Skill Score) and the probability of detection for 6h accumulated precipitation are presented. The improvements are obtained at almost all the accumulated precipitation amount intervals.

Along this period the impact of IASI data assimilation is found to be neutral for all the upper air parameters (not shown).

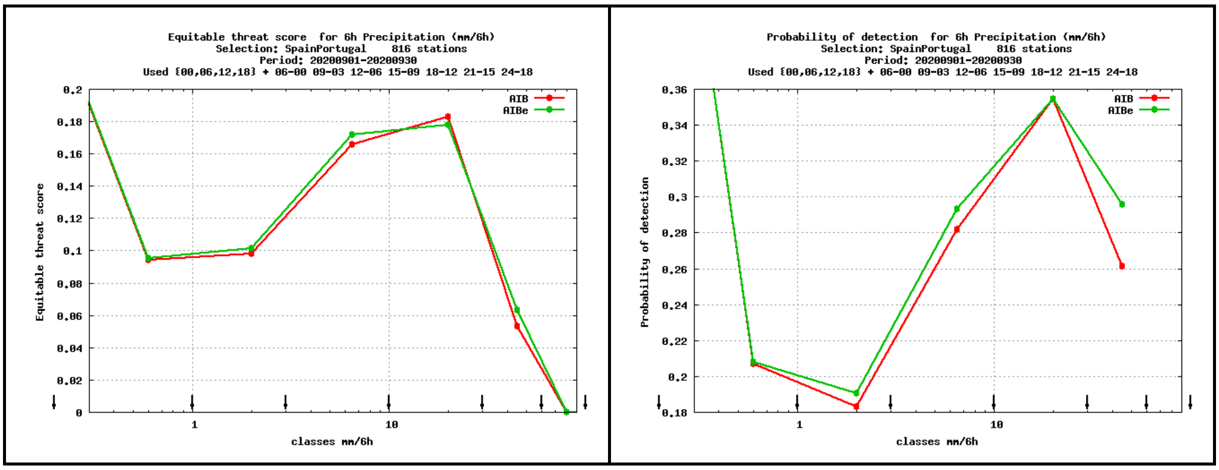

Figure 4: Equitable Threat Scores (left) and Probability of detection (right) of 6h accumulated precipitation for AIB (in red) and AIBe (in green).

AIC-AICe: 10th June to 9th September 2020

The impact of IASI data assimilation in the Canary Islands forecasts is very similar to that obtained for the Iberian Peninsula domain. That is, IASI data assimilation slightly improves mean sea level pressure, 2-meter temperature and relative humidity forecasts, but impact is found to be negative on 10-meter wind (statistically significant for almost all forecast times; Figure 5). Verification scores for vertical profiles of meteorological parameters indicate no impact neither at temperature nor at relative humidity, but a small improvement is observed for low-level wind speed (not shown).

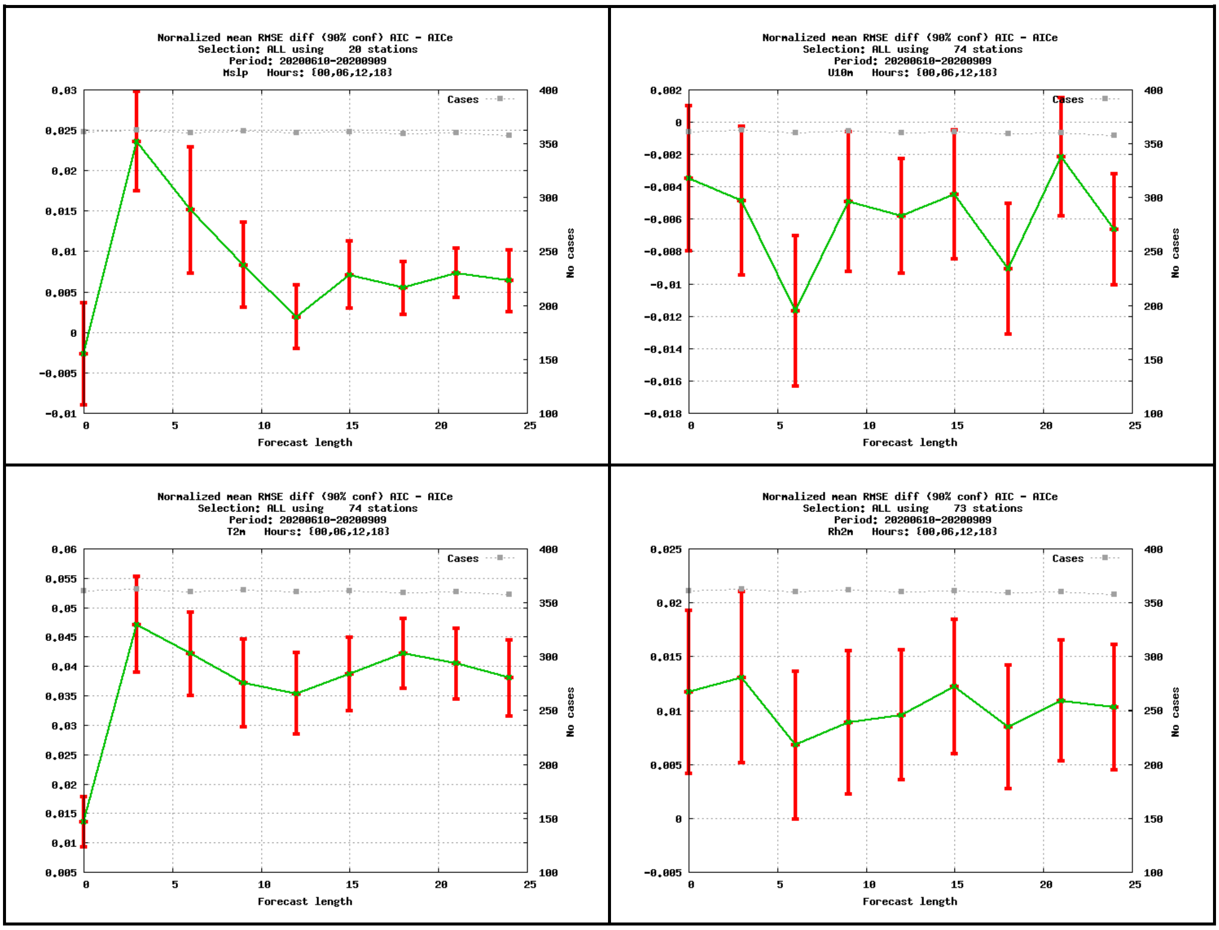

Figure 5: As Figure 1 for AIC and AICe.

4 Conclusions and outlook

We shortly presented the implementation of clear-sky IASI radiances from Metop-B into the AEMET HARMONIE-AROME system. Firstly, we passively assimilated a pre-selected set of channels to spin-up and update bias coefficients included in VarBC files. Then, the quality of bias correction over these channels was investigated, and a few channels (most of them low-peaking) were discarded. Radiances from the final selection of channels were actively assimilated during a long period, and we have assessed their impact on forecasts. These two steps were done over the two domains used in the actual AEMET set-up.

Overall, the assimilation of IASI radiances from long-wave CO2 and water vapour bands channels has a neutral or slight positive impact on forecasts for both domains. In more detail, for surface parameters, there is an improvement on mean sea level pressure, and 2-meter temperature and relative humidity, but the impact is negative on 10-meter wind. Vertical profiles of verification scores for upper air parameters do not show any impact, except a slight positive one for relative humidity at the Iberian Peninsula domain, and for low-level wind at the Canary Islands domain. Finally, it is observed that precipitation forecasts are slightly improved over the Iberian Peninsula domain (the Canary Islands domain was not evaluated due to the small number of cases).

Accordingly, the assimilation of IASI observations became operational in AEMET on 15th December 2020.

AEMET is currently implementing the cycle43 of HARMONIE system. This new run is being prepared to additionally assimilate METOP-C ATOVS radiances, METOP-B IASI and Doppler radar radial wind data. It is also foreseen to run this new cycle over a single geographical domain covering the current AIB and AIC geographical areas.

Acknowledgements

The authors wish to acknowledge Javier Calvo, who carried out the forecast objective verification of the parallel experiments against SYNOP and TEMP observations, and Gema Morales for maintaining the obsmon tool in AEMET.

References

Benacek, P., 2013: Assimilation of IASI data III. Report from LACE.

Bengtsson, L., Andrae, U., Aspelien, T., Batrack, Y., Calvo, J., de Rooy, W., Gleeson, E., Hansen-Sass, B., Homleid, M., Hortal, M., Ivarsson, K.-L., Lenderink, G., Niemelä, S., Nielsen, K. P., Onvlee, J., Rontu, L., Samuelsson, P., Muñoz, D. S., Subias, A., Tijm, S., Toll, V., Yang, X., and Køltzow, M. Ø., 2017: The HARMONIE-AROME Model Configuration in the ALADIN-HIRLAM NWP System, Monthly Weather Review, 145, 1919-1935.

Campins, J., J. Sánchez-Arriola, M. Díez, J. Calvo and B. Navascués, 2017: Assimilation of ATOVS and GNSS ZTD data in the HARMONIE-AROME model configuration run at AEMET. ALADIN-HIRLAM NewsLetter No.8, 40-50.

Collard, A.D., 2007: Selection of IASI channels for use in numerical prediction. Q. J. R. Meteorol. Soc. 133: 1977-1991.

Collard, A.D., and McNally, A. P., 2009: The assimilation of Infrared Atmospheric Sounding Interferometer radiances at ECMWF. Q. J. R. Meteorol. Soc. 135: 1044–1058.

McNally, A.P., and Watts, P.D., 2003: A cloud detection algorithm for high-spectral-resolution infrared sounders. Q. J. R. Meteorol. Soc., 129: 2411-2323.

Sánchez-Arriola, J., Escribà, P., Monteiro, I., Campins, J., Díez, M., Martín, D., Costa, V., Navascues, B., and Calvo, J., 2020: A major update in AEMET operational suite including radar reflectivity, ASCAT data, humidity in the large-scale blending and assimilation of screen level variables in 3DVar. ALADIN-HIRLAM NewsLetter No. 14, 128-137.

Randriamampianina, R., Iversen, T., and Storto, A., 2011: Exploring the assimilation of IASI radiances in forecasting polar lows. Q. J. R. Meteorol. Soc. 137: 1700–1715.

2020 ALADIN Highlights for IPMA, I. P.

Maria Monteiro, João Rio, Isabel Monteiro, Vanda Costa, Nuno Lopes

1 Introduction

Assembling a Data Assimilation (DA) system for the local version of the AROME model at 2.5km horizontal resolution over the Iberian domain (locally designated AROME-PT2), has gathered the majority of the efforts of the local ALADIN team. This effort was embedded in a wider ALADIN's Project effort, the so-called 'DAsKIT' programme [1] which joins synergies from the ALADIN-HIRLAM communities to support countries' members which do not have a local DA system in operations. During the period 2018-2020, the programme was coordinated by Portugal. Therefore, the local methodology followed a common step-by-step implementation approach, of a solution of combined DA algorithms, to know: surface, by OI_MAIN [2] plus upper-air, by 3D-Var [3,4]. The following implementation aspects were tackled: i) the porting and validation of the individual numerical system configurations, as the model time integration, the ingestion of different types of observations, the surface DA cycling and the upper-air DA cycling; ii) the local implementation of the cross-consortia pre-processing, monitoring and diagnostic tools, in particular the Scalable Acquisition and Pre-Processing (SAPP) system, the monitoring package known as OBSMON (HIRLAM) and the verification package known as HARP. In the meantime, the actual local IBM-P7+ machine has been considered obsolete to cope with the installation of new cycles, therefore the development associated with these developments was moved to the ECMWF HPC platforms. The following Portuguese NWP configurations of the ALADIN-HIRLAM shared system at CY43T2_bf10 are now being tested, tuned and validated over the Iberian domain at 2.5km of horizontal resolution and 60 vertical levels: AROME dynamical adaptation; AROME surface DA (OI_MAIN); AROME combined DA (OI_MAIN+3D-Var). This report summarily describes these efforts in the following sections: Section 2 illustrates the preliminary results on the porting of the model integration in comparison with previous cycles; Section 3 illustrates the added value (over dynamical adaptation) of assimilating conventional and radar Iberian observations on a combined DA solution; Section 4 gives the status of the local implementation of pre-processing, monitoring and diagnostics tools; and finally in Section 5 a short overview on new developments is foreseen.

Other research activities, yielded in the context of HARMONIE-AROME and of HIRLAM's HARMONIE-AROME 4D-VAR project, were devoted to the optimal use of observations in HARMONIE-AROME. The later activities are extensively described in a dedicated article [5] in this newsletter edition. More studies addressing the optimal use of observations in HARMONIE-AROME currently focus on the use of ocean winds from scatterometers in the model and are performed in the framework of EUMETSAT funded project MIDAS (Proj. Ref. No. EUM/CO/1/19/4600002345/EO). Further details about the MIDAS project can be found in https://www.eumetsat.int/MIDAS.

2 Local porting and validation of CY43T2

In this Section, preliminary conclusions are given on the porting of the basic dynamic adaptation configuration of AROME-PT2 to CY43T2_bf10. The experimental work was performed on ECMWF computing platforms; CY38 and CY40 results were obtained with the local IBM-p7+ machine;

statistical scores were performed with the home-made verification software, IPRODS-IVERIF, over a Winter period (20181216-20190210) and a Summer period (20180801-20180909), for the model runs starting at 00UTC and up to 48-hour leading time. ARPEGE is the coupling model used at 10km horizontal resolution as it is disseminated operationally by Météo-France over the Portuguese domains (Iberia+Adjacent Atlantic).

The illustration on Figure 1 shows, for comparison, the model scores, when different code cycles are in use for the same 40-day Summer period. On each day, the observations set used as reference to the scores calculations' is the same for the 3 cycles and covers only Portugal Mainland (around 130 weather stations). Previous cycles' 38T2 and 40T1 lines correspond to the historical operational configurations and its respective tunings; CY43T2 is still under study.

We can see that the model performance seems to show an improvement in screen-level parameters, in the latest version upgrade (the panel illustrates this result for 2-metre temperature) when compared with the previous cycles, for the period and geographical region under study.

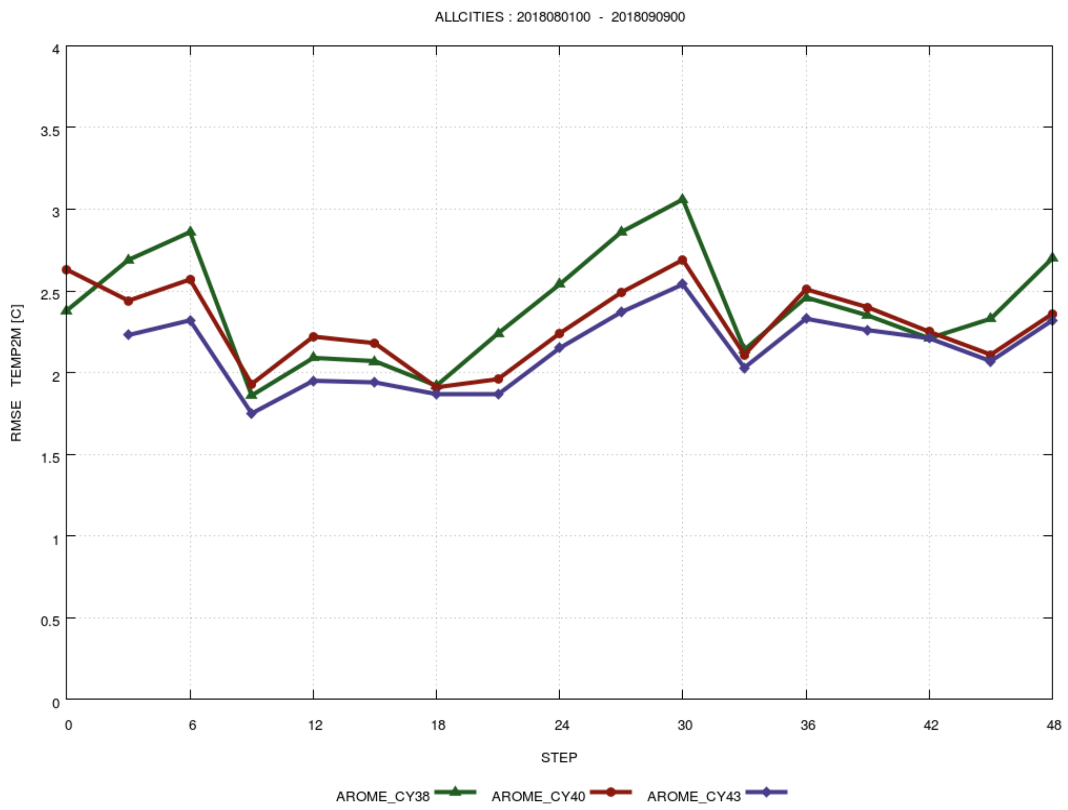

Figure 1: 40-day time series of horizontal RMSE scores for AROME-PT2 2-m temperature (C) forecasts over Portuguese Mainland using local (conventional) surface observations network as reference, on the Summer period 20180801-20180909, obtained with different AROME code cycles: CY38 (green line); CY40 (red line); and CY43 (blue line).

The improvement shown in Figure 1 also applies to the 2-m relative humidity and the 10-m wind speed in the Summer period. In the Winter period, however, the improvement is negligible, regardless of the parameter being assessed.

3 Towards a combined surface+upper-air DA solution for AROME-PT2

The goal of the on-going work is to set up a combined surface plus 3D-Var experiment for AROME-PT2 (Iberia). A feasibility test was performed on the OLIVE reference environment of Météo-France: a cycling of the combined surface plus 3D-Var setup for AROME-PT2 (CY42T2) was performed and its added value was analysed during the 20-day rainy period: 20190122 – 20190210. In this experiment, conventional observations and OPERA Iberian volumetric radar data were assimilated. During the period under study, two 48-hour forecast experiments were run, initialised at 00UTC by two different processes: i) the analysis obtained by the assimilation cycling; ii) the dynamical adaptation of ARPEGE fields. The latest simulated the actual local operational configuration and was used as a reference. The preliminary results have shown neutral or slightly positive impact on the 24-hour precipitation forecasts when the model is initialized by the DA cycling instead of initialized by dynamical adaptation, specially for larger accumulated precipitation amounts.

In order to assess the impact of the DA experiment, the 24-hour precipitation performance was initially examined through several categorical scores. As an illustration, Figure 2 shows one example of the scores examined, the Probability of Detection (PoD) as a function of the False Alarm Rates (FAR). It shows that an added value over precipitation forecasts has been found when assimilating Iberian OPERA radar data. In particular, we can see the Probability of Detection increases keeping the False Alarm constant when the initialization of AROME-PT2 is done through the assimilation cycling.

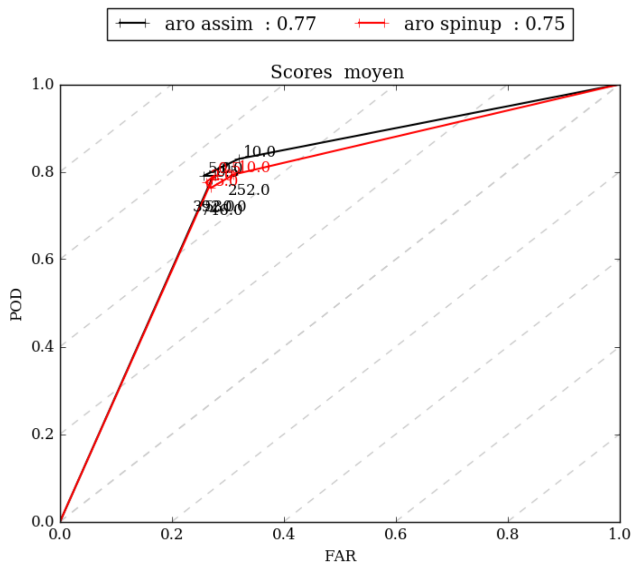

Figure 2: False Alarm Rate versus Probability Of Detection versus False Alarm Rate (right panel) averaged over the period 20190122 – 20190210 for different thresholds of 24-hour precipitation, for AROME-PT2 initialized by: dynamical adaptation (red line) and assimilation (black line).

At the time of writing this article, the assimilation experiment described above has been ported to CY43T2_bf10 and migrated to ECMWF. It is being cycled for testing purposes. Further work includes its validation and tuning.

4 Implementation of DA cross-consortia tools: SAPP, OBSMON, HARP

Local DA requires the availability of several tools for observations pre-processing, monitoring and diagnostic. As mentioned in [1], some cross-consortia tools for this purpose have been selected *a priori* on the DAsKIT programme, and their status implementation on IPMA is described in this section.

SAPP

The Scalable Acquisition and Pre-Processing system at ECMWF (SAPP) virtual machine (SAPP VM) was installed at IPMA's local environment in February 2019. So far, all the three stages, 'Acquisition', 'Processing' and 'Extraction' have been tested, as shown in Table 1.

Table 1: Status of local implementation of SAPP

SAPP (vsapp02)	**Maturity**
Acquisition Stage	mature and tested for GTS. Conventional observations received by GTS are adequately scanned, updated and ingested.
Processing Stage	tested but still some tailoring needed. Appropriate decoders are used and tested for BUFR and ASCII.
Extraction Stage	under development. The extracted data files are in a consolidated BUFR format (ECMWF local templates) that can be directly used in HARMONIE-AROME. Local source code BATOR from the latest 'export' version (CY43T2_bf10) has been adapted and tested to ingest SAPP BUFR data, after exercise prepared by Turkey (TSMS) for the ' 2020 LACE DAWD & DAsKIT WD' [see, for instance, 6].

Future work will encompass: the update of the current SAPP version to vsapp021.1 (ECMWF release May 2020) and the local tailoring of the daily suites.

OBSMON

OBSMON package generates statistics from the ODB and stores it in SQLite tables (pre-OBSMON). This software package allows the interactive visualization of data contained in the SQLite (shiny part). This can be done either offline or via a server daemon. At IPMA, only the offline option was implemented, OBSMON v3.11 (shiny part). For instance, is being used to regularly produce statistics for the HARMONIE-AROME data assimilation system; besides local source code BATOR from the latest 'export' version (CY43T2_bf10) has been updated and tested so that SQLite tables created with in this way may be read by OBSMON interactive visualization tool (shiny part), after the exercise prepared by Belgium (RMI) for the' 2020 LACE DAWD & DAsKIT WD' [7]. Future developments will include the update of the latest OBSMON version (which is ODB cycle dependent) and test under regular use of DA suites.

HARP

HARP is meant to become a common ACCORD verification (and validation) tool. HARP is able to directly ingest pre-MONITOR files.

MONITOR is a self-contained stand-alone verification package originally created for HARMONIE. It is composed in two parts: i) pre-MONITOR, which calculates several standard verification scores. The scores can be presented per station for the whole data set or filtered through different selection criteria; ii) WebgraF, a portable web interface, where the scores are presented and which allows the easy sharing of the validation information. Since the verification is station based it is less suitable for moving observation platforms or fields.

MONITOR is used regularly to verify and monitor all experimental HARMONIE suites of IPMA. For instance, the impact of including new observations in the HARMONIE-AROME system (eg. transition from ASCAT-A/B to ASCAT-A/B/C) was assessed using MONITOR.

Besides, AROME-PT2 suites at CY43T2 performed at ECMWF already create statistical pre-MONITOR files, suitable to be read either by the MONITOR web interface or by HARP, though HARP has not been installed at IPMA yet.

As future work is foreseen: the regular use of MONITOR up to the effective implementation of HARP as well as some progress onto the local implementation of HARP.

5 Outlook

As a direct consequence of the work done with CY43T2 at ECMWF it is expected to run the actual AROME-PT2 operational configuration (dynamic adaptation) as a time-critical (2) application, as a backup of the actual local production at 00 and 12 UTC.

Besides, the remaining AROME-PT2 configurations (surface DA and combined DA) should continue to be tuned and validated under the DAsKIT programme using conventional and radar observations. Finally, the local usage of the cross-consortia tools should become more regular.

Acknowledgements
To Pierre Brousseau, Wafa Khalfaoui and Maud Martet for the support when assembling the AROME-PT2 assimilation experiment under Météo-France’s reference environment. To Alena Trojáková for the support on the implementation of CY43T2_bf10 under ECMWF computing platforms. To Benedikt Strajnar and Jure Celdinik for the support with the adaptation of ARSO’s scripting system at ECMWF and the implementation of pre-MONITOR facility.

6 References

[1] Monteiro, M., Aitmeziane, O., Belghrissi, H., Bogatchev, A., Cengiz, Y., Deckmyn, A., Dehmous, I., Hdidou, F., Khalfaoui, W., Kolonko, M., Rio, J., Sahlaoui, Z., Sezer, M., Szczęch-Gajewska, M., Tsenova, B., 2020: The DAsKIT programme: status and plans, ALADIN-HIRLAM Newsletter No. 15, June 23rd, 2020.

[2] Giard, D. and Bazile, E., 2000: Implementation of a New Assimilation Scheme for Soil and Surface Variables in a Global NWP Model, Monthly Weather Review, Vol. 128, Issue 4, Page(s): 997–1015, https://doi.org/10.1175/1520-0493(2000)128<0997:IOANAS>2.0.CO;2.

[3] Fischer, C., Montmerle, T., Berre, L., Auger, L., Ştefănescu, S., 2005: An overview of the variational assimilation in the ALADIN/France numerical weather‐prediction system, QJRMS, Vol. 131, Issue 613, Pages 3477-3492, https://doi.org/10.1256/qj.05.115.

[4] Brousseau, P., Seity, Y., Ricard, D., Lége, J., 2016: Improvement of the forecast of convective activity from the AROME‐France system, QJRMS, Vol. 142, Issue 699, Pages 2231-2243, https://doi.org/10.1002/qj.2822.

[5] Barkmeijer, J., Lindskog, M., Gustafsson, N., Bojarova, J., Azad, R., Monteiro, I., Escribà, P., Whelan, E., Ridal, M., Sánchez Arriola, J., Vignes, O., Stappers, R.: HARMONIE-AROME 4D-Var [this newsletter].

[6] Cengiz, Y., Gökhan Akdağ, H., Sert, M., Sezer, M., 2020: SAPP (Scalable Acquisition and Pre-processing System) at TSMS, ALADIN-HIRLAM Newsletter No. 15, June 23rd, 2020.

[7] http://www.umr-cnrm.fr/aladin/spip.php?article364

Aladin in Poland - 2020

Bogdan Bochenek, Piotr Sekuła, Gabriel Stachura, Małgorzata Szczęch-Gajewska, Marcin Kolonko

1 Introduction

The ALADIN Poland team worked in 2020 on both operational changes to everyday use of ACCORD products (such as ALARO and AROME models) as well as on scientific and technical aspects of weather forecasting: the use of UAV (unmanned aerial vehicle) to investigate the foehn wind above Cracow and its influence at PM10 particle concentrations and random forest methods used to decrease RMSE error of temperature forecasts on a set of 35 Polish synoptic stations. These results will be published soon.

2 The Influence of Foehn Wind on the Concentrations of PM10 and Urban Boundary Layer Structure in the Complex Terrain

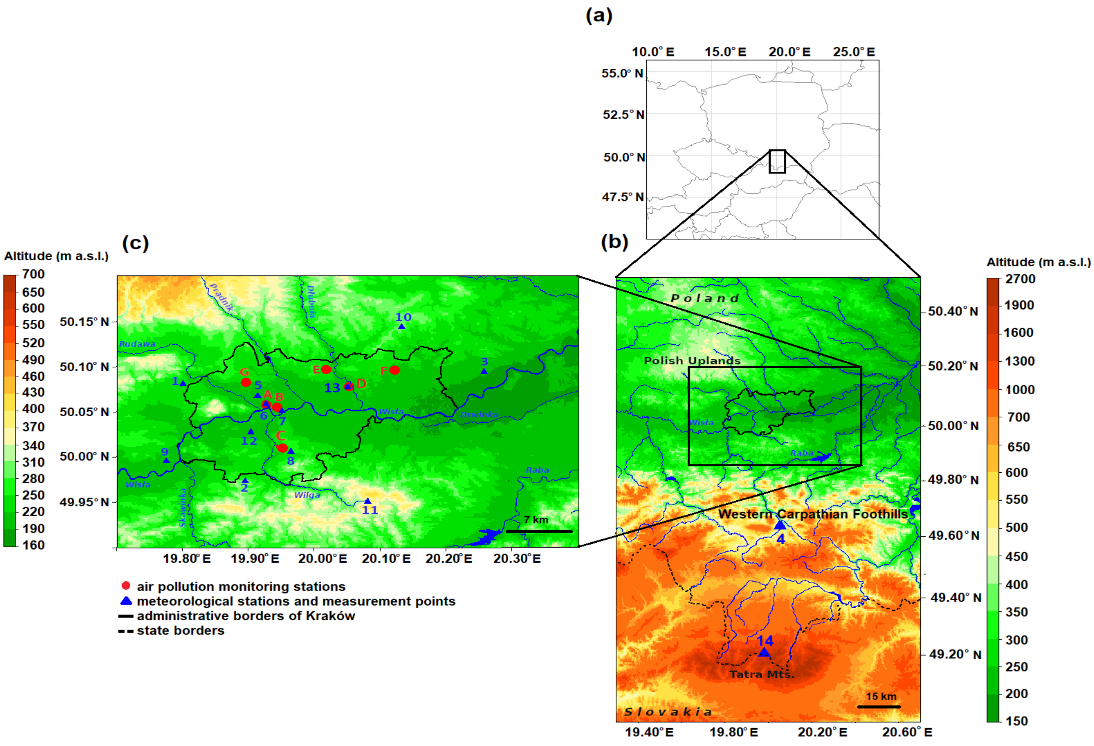

Figure 1: Topographic map of analysed area and location of meteorological and air pollution stations.

Introduction and AROME model support

The present work aims at better understanding of foehn wind's impact on urban air quality, due to modification of air pollution dispersion conditions in cities located in large valleys. Cracow, southern Poland, is an example of a city with poor air quality, mainly due to abundant PM10 concentrations, located in a large valley of the Vistula River, within the area affected by a foehn wind called 'halny' from the Carpathian Mountains. There were 14 long (i.e. >24h) episodes of 'halny' analysed (40 days, 591 hours in total), from the periods Sep. 2017-Apr. 2018 and Sep. 2018-Apr. 2019, for which sufficient measurement data were available. Numerical forecasts of model AROME cy40t1r1 (87 vertical levels, resolution 1km x 1km) were used to analyse meteorological conditions and dynamics of atmosphere at lowest part of troposphere.

Selected results

Among four spatial-temporal patterns of PM10 concentrations, two are described here: (**1**) sudden, large increase of PM10 concentrations at all measurement points, and (**2**) short-term peaks or long-term periods of high PM10 concentrations in the western part of the Cracow only.

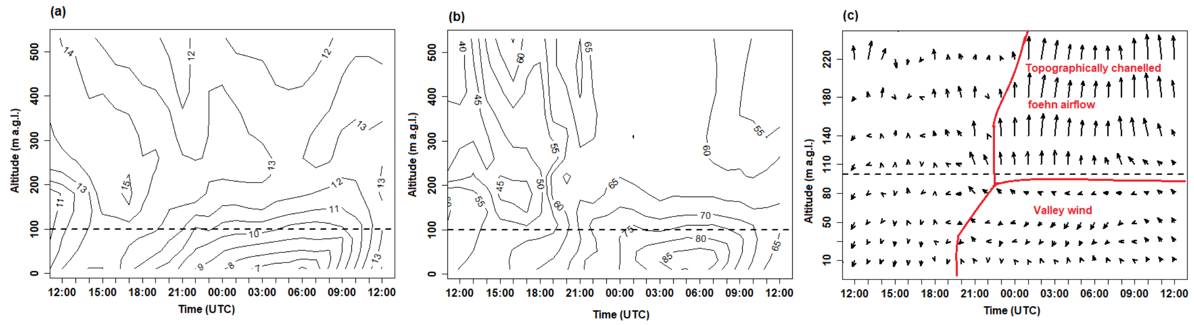

*Figure 2: Vertical profiles of: **a.** air temperature (°C); **b.** relative humidity (%); **c.** wind components, for the location of PM10 monitoring station in Krasińskiego Street (point B at topographic map), from AROME model, on 12-13.11.2018. Dashed line: Vistula River valley height.*

Pattern 1: Sudden, large increase of PM10 concentrations at all measurement points. PM10 increase was linked to the development of air temperature inversion in the Vistula River valley. At the same time, relative humidity reached 80-90% at the valley floor in rural areas which indicates fog occurrence, as the values were decreasing quickly with height. Wind speed inside the valley was below 3 m/s whereas around 100 m higher (i.e. above the valley) it increased to 6-8 m/s.

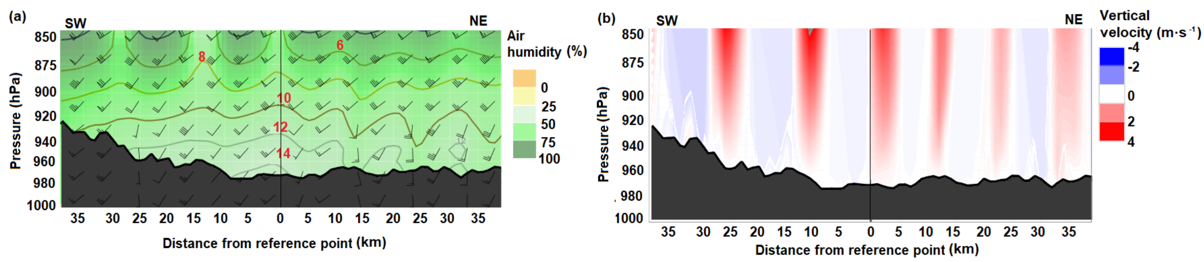

*Figure 3: Spatial pattern of: **a.** air temperature (contour lines), air humidity (background) and wind speed (in knots) and direction (graphical symbols) in the SW-NE cross section through Cracow and its vicinities, and **b.** vertical velocity, at 7 UTC on 12.12.2017*

Pattern 2: Short-term peaks or long-term periods of high PM10 concentrations in the western part of the city only. The differences in relief between the western and eastern part of the Vistula River valley in Cracow contribute to the occurrence of pattern 2. In all cases of pattern 2, much larger PM10 concentrations were observed in the western than in the eastern part of the valley. They were either long-lasting or occurred as concentration peaks. Such conditions were the effect the gravity waves impact. The gravity waves are one of foehn wind effects and can generate closed eddies in a valley which in turn leads to the accumulation of air pollution locally.

3 Improvement of Air Temperature Forecast at Post-processing Stage - Machine Learning Methods

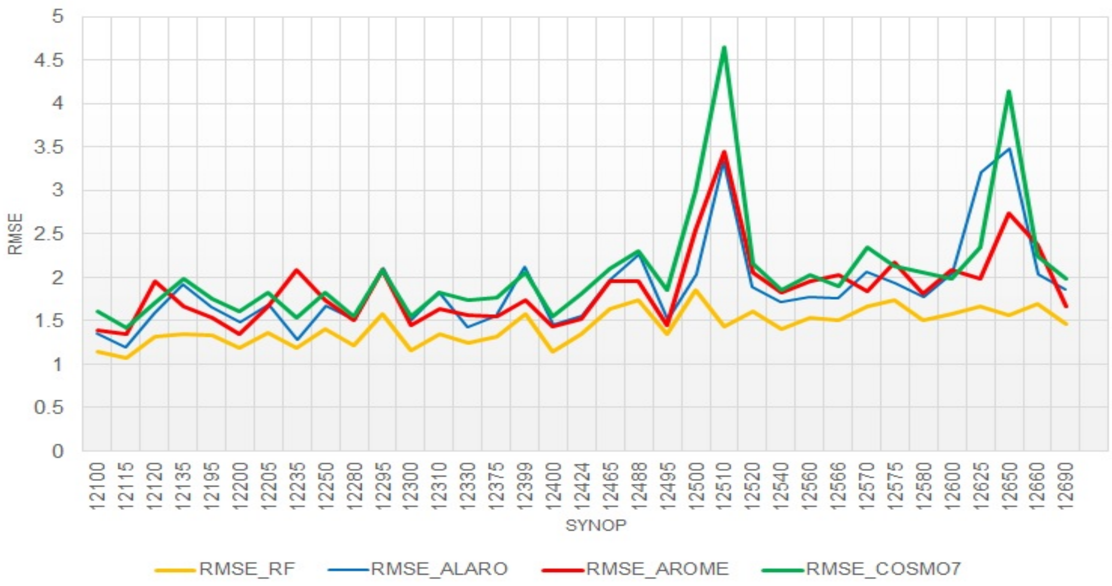

Figure 4: Averaged for each synop station (on all leadtimes and test days) 2m temperature RMSE of ALARO, AROME, COSMO forecasts and random forest (RF).

The sketch of methodology

In the experiment forecasted 2m temperatures from three operational models (ALARO-NH-v1B CY43T2 4km, AROME CY43T2 2km and COSMO 7km) were compared with observed 2m temperature SYNOP values. A machine learning algorithm *Random Forest* was applied (package *randomForest* in R), which uses a collection of decision trees (random forest) with increased performance and can use both classification and regression techniques depending upon the user and target or categories needed. In our case each decision tree, based on the respective predictor variables, was trained on different model and finally *Random Forest* took the average of the results from all the decision trees.

For building a random forest all models datasets were used with the same specification:

- sampling frequency:3h
- leadtime: 3-30h;
- predictors comprise also month, day of the year, hour and leadtime;
- training was conducted on the two years period (2018-2019), which gave around 6800 cases.

Built random forest was tested on the period from 2020 (until August 13th) and compared with forecasts of each of previously used models. Results were verified by calculating RMSE for 35 selected SYNOP stations from different regions in Poland (lowlands, uplands and mountains). On figures they are named by its numbers.

Figure 5: Comparison of random forest RMSE with respect to best performing model RMSE for certain station.

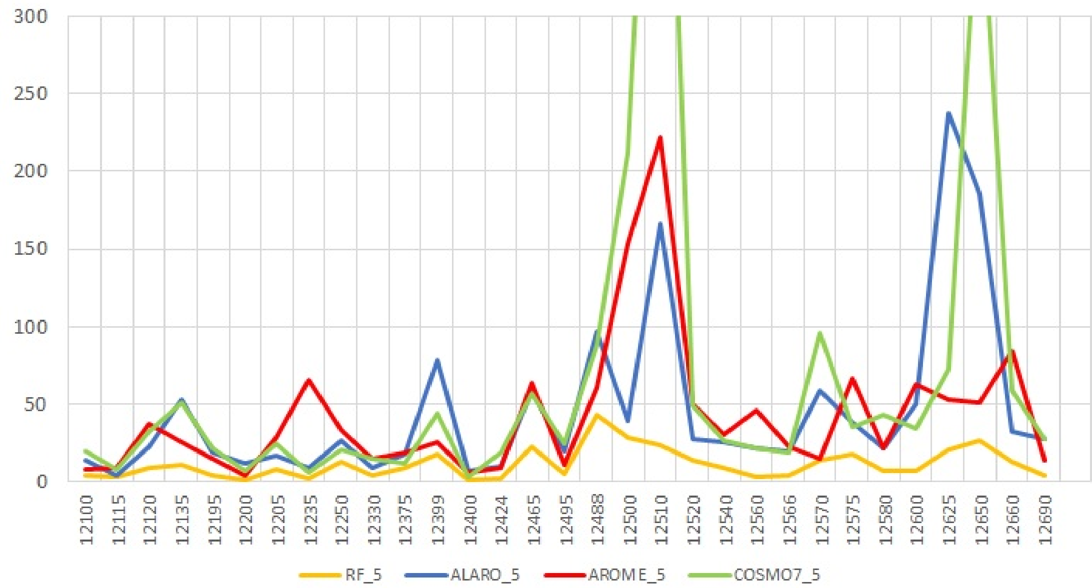

Figure 6: Number of forecasts of each model and random forest with absolute error value bigger than 5^{O}C. 12510 and 12650 are mountain-top stations.

Conclusions.

- RMSE reduction occurred at every station, with an avarage of 16%;
- The biggest improvement occurred for mountain-top stations (12510,12650), probably because models were strongly biased there;
- Some predictors with information about topography and cloudiness/insolation should be added to training data;
- Although random forest performs better than the best of three models only in 30-40% of forecasts, its impact is the most visible when considering big errors (over 5°C) – e.g. for Cracow (12566) random forest made such an error only 4 times, while COSMO 20 times, ALARO – 21 and AROME – 23.

ALADIN highlights in Slovenia - 2020

Benedikt Strajnar, Neva Pristov, Jure Cedilnik, Nina Črnivec, Jana Čampa

1 Overview

This contribution describes two recent NWP developments at the Slovenian Environment Agency (ARSO): definition and evaluation of a high-resolution NWP suite with hourly data assimilation cycling, intended for nowcasting, and implementation of ALADIN/ALARO model over a large south-eastern Europe region in the scope of SEE-MHEWS-A project.

2 The NWCRUC model

System design

A new convection-permitting model setup at ARSO, called NWCRUC, was set up with the intention to more precisely simulate complex precipitation events in the northern Mediterranean and the eastern Alps. The area is known for complex orography and coastline as well as frequent and occasionally severe precipitation events. This is especially pronounced during the secondary cyclogenesis which contributes to longer lasting and intensive rain/snow events south of the main Alpine ridge and over the Dinaric Alps. The prevailing atmospheric flow is southwesterly during the prefrontal phase of those cases, which is very challenging for NWP models in terms of properly simulating precipitation occurrence and intensity. Taking this into account, the model domain is centered over the northern Adriatic Sea in order to better simulate this sensitive area. Slovenia is located in the north-eastern part of the domain (Fig. 1, left). The model has 1.3 km horizontal resolution and 87 vertical levels.

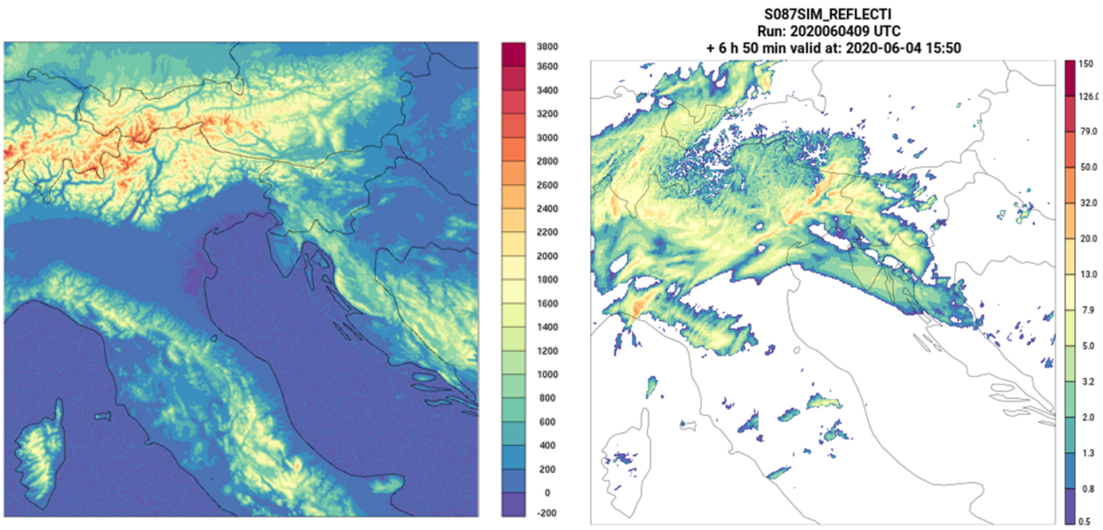

Figure 1: (Left) NWCRUC model domain with orography. (Right) forecast of simulated radar reflectivity, computed every 5 min during a model run.

The NWCRUC system includes similar components as the operational ALADIN 4.4 km. These are ALARO-v1B model physics package and code version cy43t2_bf10. It is run with a time step of 60s.

LBC coupling, applied in a space consistent way, is provided by ECMWF/IFS in a lagged mode. The hourly analysis using 3D-Var and OI for soil is carried out with a cut off time of 35 minutes after the nominal analysis time. This is followed by a production forecasts up to 36 h, which provide a selection of meteorological variables every 5 min (e.g. simulated radar reflectivity, Fig. 1) on top of the hourly model output. This forecast is currently run every 3h and it is planned to increase this to every hour in the preoperational phase. The analysis step is repeated 35 min later (70 min after the nominal analysis time), and this second analysis is used to compute the first guess for the next production run.
The observation data set includes all types of the ALADIN 4.4 km plus the radar reflectivity. Observations, such as Mode-S datasets, are used with a higher spatial resolution.

Validation results

Apart from daily runs which were assessed subjectively by the NWP department, an objective verification period was carried out for a summer (1-15 August 2020) and winter (1-15 December 2020) period. For these two periods, four experiments were prepared: both reference operational ALADIN 4.4 km setup (3h DA cycling) and the new hourly NWCRUC (1h cycling) were rerun twice, with and without radar reflectivity data assimilation, which is experimental at ARSO. Forecasts were computed twice a day.

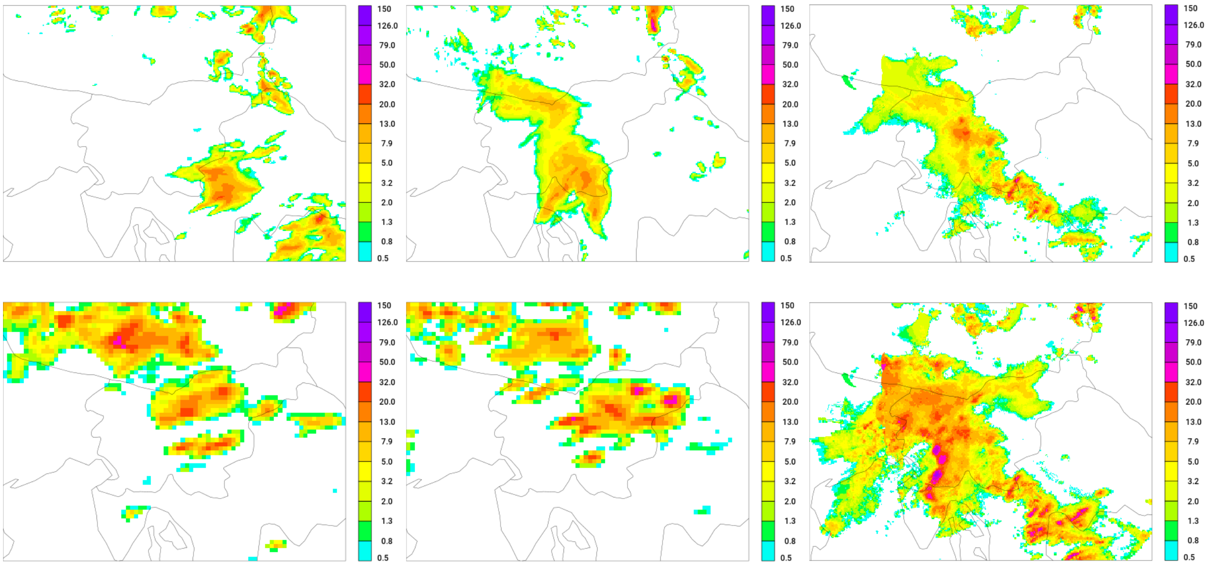

Figure 2: Top row: precipitation sums in the 1h first guess for NWCRUC without (left) and with radar reflectivity assimilation (middle) and reference hourly INCA analysis (right). Bottom row: precipitation sums in the 3 h first guess for ALADIN 4.4 km without (left) and with radar assimilation (middle) reference 3 h INCA analysis (right). The case is from August 14 2020 18 UTC.

The validity of assimilation cycle was evaluated by plotting hourly and 3-hourly precipitation sums in the first guess (depending on the model setup) and comparing them to INCA analyses over Slovenia and the surroundings (quantitative precipitation analysis based on rain gauges and radar). It was observed that the impact of radar data assimilation on precipitation field was generally more visible in the NWCRUC setup. Fig. 2 shows an example case when a passage of a convective system was better captured by the NWCRUC when radar reflectivity was assimilated. One can note that there is only a very limited effect of radar reflectivity DA in the 4 km suite for the same event. It was generally observed that the radar DA is able to dry-out the spurious precipitation signal produced by the model, and this contributes to significant reduction of the false alarm rate. On the other hand the radar DA struggled with isolated and sparse convection where in most cases the dry pixels were chosen for assimilation and we observed no or less rain in the next first guess, compared to the experiment without radar assimilation.

The 36h forecasts were verified against Synop stations over the whole domain plus automatic surface stations in Slovenia, Austria and Italy, and radiosondes. A comparison between reference operational ALADIN 4.4 km and NWCRUC (both without radar data assimilation) for the summer period is shown in Fig.3, in the form of a scorecard. The NWCRUC system clearly outperforms the ALADIN 4.4 km for all main surface variables in terms of standard deviation and also bias with exception of wind speed. The upper-air verification, which suffers from a very limited number of available soundings over the domain, suggests a slight degradation of standard deviation mainly at ranges 3h and 6h. This may also be related to increased fit to Mode-S aircraft observations which are, despite the COVID-19 epidemic in 2020, the main source of hourly upper-air information. Notable degradation is seen also for cloudiness and needs further attention. The situation is relatively similar in the winter period. Impact of radar reflectivity data assimilation was relatively neutral for both 1.3 and 4.4 km resolutions.

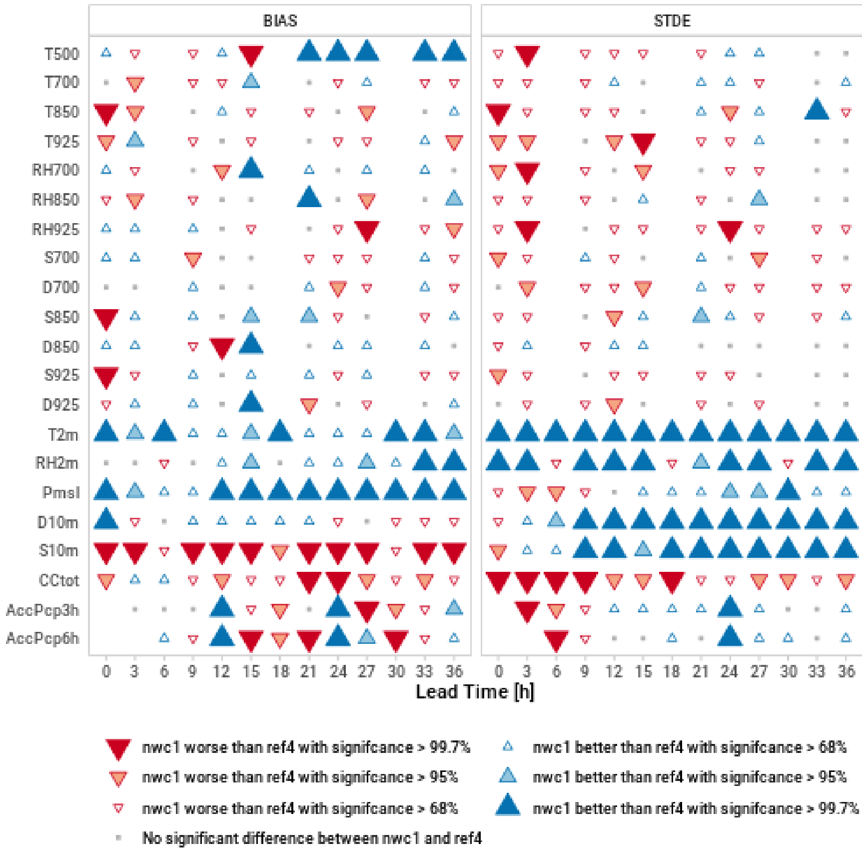

Fig. 3: Comparison of scores for NWCRUC (denoted nwc1) and reference ALADIN 4.4 km (denoted ref4), for main surface and upper-air variables.

The impact on precipitation forecasts was further assessed using the categorical verification. Fig. 4 shows the frequency bias of 1 h precipitation sums over the winter period, for various thresholds. It is evident that all models tend to overestimate the precipitation amounts for precipitation intensities below 5 mm/h. The 1.3 km runs however decrease this bias for about one half in comparison to 4.4 km model. The NWCRUC also performs better for precipitation between 5 and 10 mm/h where ALADIN 4.4 is negatively biased. NWCRUC predicts more precipitation events in the class above 10 mm/h. This results in overall slightly better equitable threat score (ETS) for the NWCRUC. Another interesting feature can be observed in the first 7h of forecast where both experiments with radar DA are more balanced in terms of bias and this also results in an improved ETS, especially for the first two precipitation classes (light rain). The point verification of precipitation as presented here potentially suffers from the double penalty issues and is not optimal for verification of convective scale precipitation. Spatial verification is also planned.

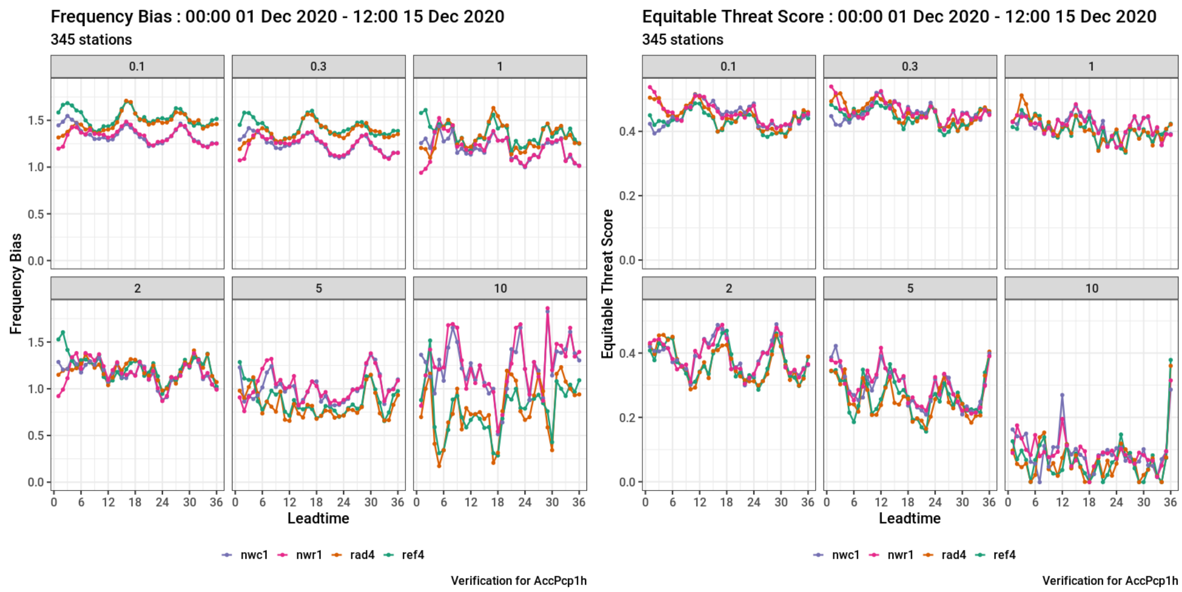

Fig. 4: Frequency bias (left) and equitable threat score (right) for hourly precipitation and different intensity classes. Experiments are NWCRUC without (nwc1) and with radar DA (nwr1) and reference ALADIN 4.4 km without (ref4) and with radar DA (rad4).

3 The SEE25 model

The SEE-MHEWS-A project

One of the main components of the project South-East European Multi-Hazard Early Warning Advisory System (SEE-MHEWS-A) was to set up multiple regional LAM NWP models. Four countries in this region participate with their operational or custom NWP results: Greece with COSMO, Israel with ICON, Serbia with NNMB and Slovenia with ALADIN/ALARO.

Model setup

ALADIN-based modelling system called SEE25 for production of short range meteorological forecast, covering a large domain (SEE region as defined by WMO) with high horizontal resolution of 2.5 km, including data assimilation and basic post-processing, was developed specifically for the purpose of the SEE-MHEWS-A project. The model version, physics package (ALARO-1vB) and the data assimilation set-up used are the same as in the operational ALADIN-SI system. The model suite is running at ECMWF HPC infrastructure. The model domain has 1429 x 1141 horizontal grid points at 2.5 km resolution (Fig. 5), and 87 vertical model levels. Forecast time step is 90 s. For the time integration the iterative centered implicit (ICI) temporal scheme with one iteration in the non-linear model part with the semi-Lagrangian (SL) advection is used. The LBC coupling is provided by IFS ECMWF at 1h (assim. cycle) and 3h (forecast) temporal resolution.

Observations for SEE25 model, the only system within the project with applied DA, currently come entirely from the OPLACE preprocessing system (with approval by RC LACE members). All conventional and remote-sensed observations as typically assimilated in RC LACE data assimilation system are used, including surface observations (GTS SYNOP, automatic station network from many central-European countries), aircraft observations (AMDAR, Mode-S MRAR, Mode-S EHS), radiosonde data (TEMP), NWC-SAF atmospheric motion vectors, wind profilers and satellite radiances (MGS SEVIRI, and AMSU, MHS from various polar satellites) and scatterometer data (ASCAT). The density is higher over central Europe (example Fig. 6) and decreases towards south-east.

Meteorological forecast fields are available on the model and pressure levels for visualization and various applications with hourly output resolution. Selected fields are encoded to GRIB2 format and processed. Post-processing into regular latitude-longitude grid is also performed. The system runs in real time mode and its performance is very stable. Consumption of computational resources is deliberately kept as low as possible because a high-speed dissemination is currently not of high priority (yearly estimation is 50 M SBU).

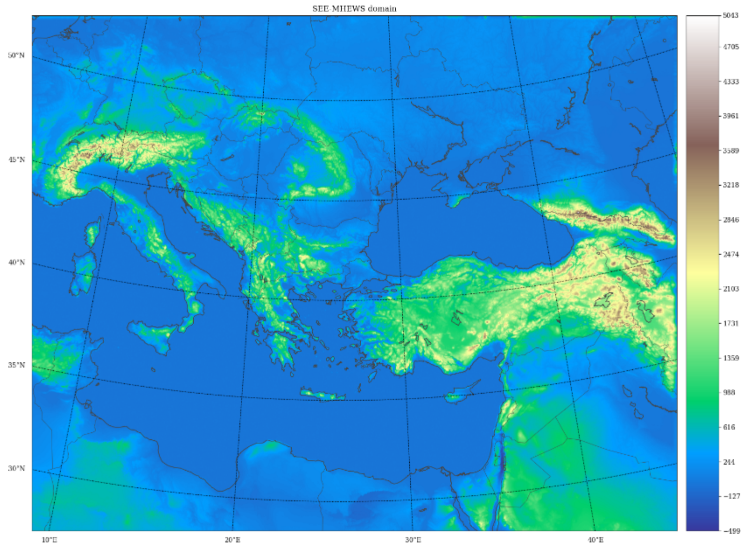

Figure 5: SEE25 model domain with the height of model orography.

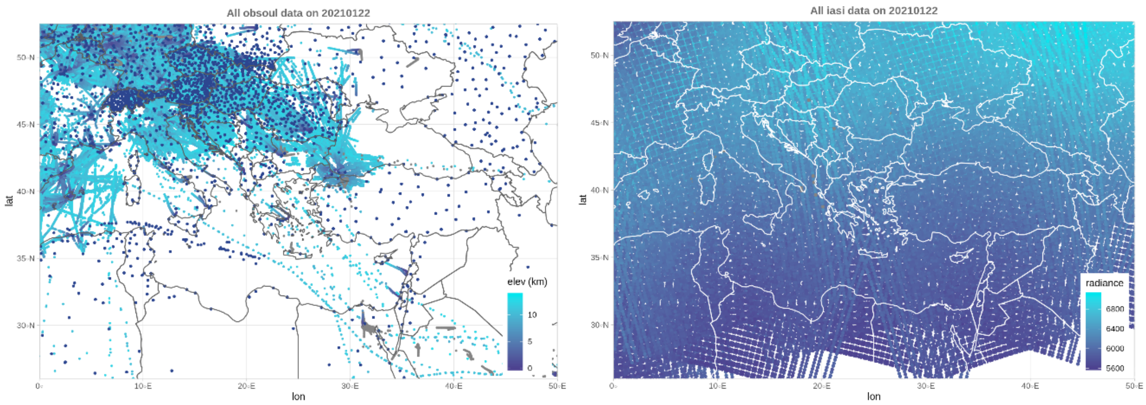

Figure 6: (left) Conventional (Synop, aircraft) observations and (right) IASI radiances over the SEE25 domain. Example from January 22, 2021.

Initial validation

During the assembly phase of the suite some issues were encountered. The initial ambition was to cover the vast and rather non-orthogonal SEE region with an optimally (in the meteorological NWP context) sized computational domain. Such domain would cover some parts towards the west to allow for meteorological systems' smooth transition from the driving model, but would be somewhat rotated as the SEE region is oriented quite diagonally with the main axis direction from the north-west to the

south-east corner. However, during the initial regular trial runs with this model configuration some strange patterns were emerging that were later attributed to the rotation of the domain and more exactly to non-negligible map factor. This was more precisely diagnosed by examining the kinetic energy (KE) spectrum pattern, which exhibited an excessive energy accumulation at smaller scales. This fact forced us to slightly modify the domain and its magnitude of rotation and unfortunately also increase the size of the model domain and hence slightly increase computational time. Eventually, this did remove the problematic patterns and improved the spectral representation of KE in the model (Fig. 7).
A short objective validation of near-surface and upper-air forecast fields was carried out in the period of 1-15 December 2020, in comparison with operational and experimental suites at ARSO. This verification was therefore limited to eastern Alps and the northern Mediterranean. The SEE25 performance is comparable to other model setups in terms of typical model biases. The slightly positive bias in 6, 12 and 24 h precipitation accumulation was also noted. Somewhat larger RMSE error for certain surface variables compared to operational models at ARSO indicates some room for improvement mainly for soil or near surface variables, in terms of performance surface data assimilation or realism of input physiographic data.

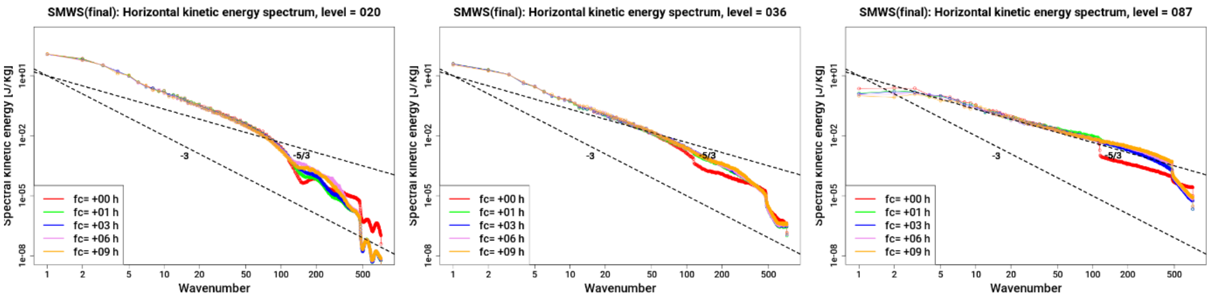

Figure 7: Horizontal kinetic energy spectra in the SEE25 model configuration at three different levels: 20 (left panel), 36 (middle panel) and 87 (right panel) during initial 9 hours of integration. The theoretical limits K^{-3} and $K^{-5/3}$ are shown for comparison.

4 Outlook

The first results with the hourly NWCRUC system at 1.3 km are quite encouraging, and the development will continue by defining products for users. It is planned that the first version of the system will be fully operational before summer. Further optimization includes tuning of the observation error standard deviation which is currently the same as in the 4.4 km model version. We also hope to be able to gradually increase the number of assimilated observations, especially over Italy and the Adriatic Sea where there still are significant observation gaps.
The SEE-MHEWS-A project activities will continue in 2021 by providing daily model outputs to the project members. Continued validation and further optimization are also planned. One important goal would be to extend the observation data set by use of higher number of local ground observations (such as those exchanged by participating partners and ECMWF) and other data types (radar, GNSS data, more satellite radiances).

ALADIN activities in Romania

Alina Dumitru, Răzvan Dobre, Simona Tașcu, Alexandra Crăciun

1 Introduction

During last year, a significant amount of the team's efforts was dedicated to the migration, optimization and reorganisation of the entire operational suite on the new computer platform [1], as well as changing the operational model version. These changes were determined by the technical characteristics provided by the new computing infrastructure, along with the necessity to design a more flexible, portable scripting system that is also able to deliver the output faster.

2 Description of the changes in the operational suite

The former ALADIN/ALARO operational suite was implemented on the old IBM cluster, starting 2016 until the beginning of the year 2020. There, 5 nodes (each having 12 processors) were available. The operational version employed was based on cy40t1 of the model and ALARO-0 baseline physical package.

The transition to the current operational suite was established along several steps. Firstly, the compilation and installation of the ALARO model version cy43t2_bf10 on the new platform was done. There, 10 nodes (2 processors, each 32 cores with HyperThreading) are assigned for the group's activity. Afterwards, the whole scripting system was reorganised to better fit the capabilities of the new computing resources. This approach would also lead to a more portable and increased flexibility of the operational system and applications.

2.1 Implementation of the model code

For compilation of the model code and necessary dependencies, the rpm spec file type was used. Together with the *rpmbuild* tool, this type of files creates native packages for the operating system RedHat/Centos available on the new platform that can be further installed on all computer nodes and even on personal computers. The spec file type contains a sequence of information which describes, in the code, the necessary steps for obtaining the specific library or model version in binary format. The spec files currently used are available on GitHub.

2.2 Optimization of the operational scripts

The new structure enables data pipeline facilities [2], which means the deconstruction of a process in several successive sub-processes, each sub-process requiring the output of the previous one as input files. In some cases, independent processes may run in parallel, in a data pipeline structure. This concept consists of three key elements: a source, one or more processing steps and a destination (figure 1).

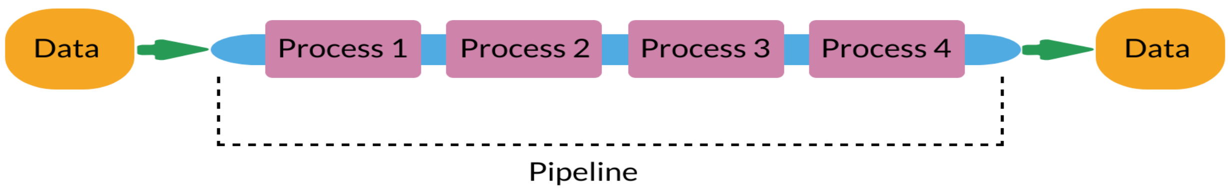

Figure 1: Data pipeline architecture. Adapted from https://hazelcast.com/glossary/data-pipeline.

The new cluster management and job scheduling system - *slurm workload manager* allows similar parallel tasks submission through the *Job Array* feature, provided that those tasks have the same initial options [3]. A general representation of the jobs involved in the operational system, as well as the links between them is shown in figure 2.

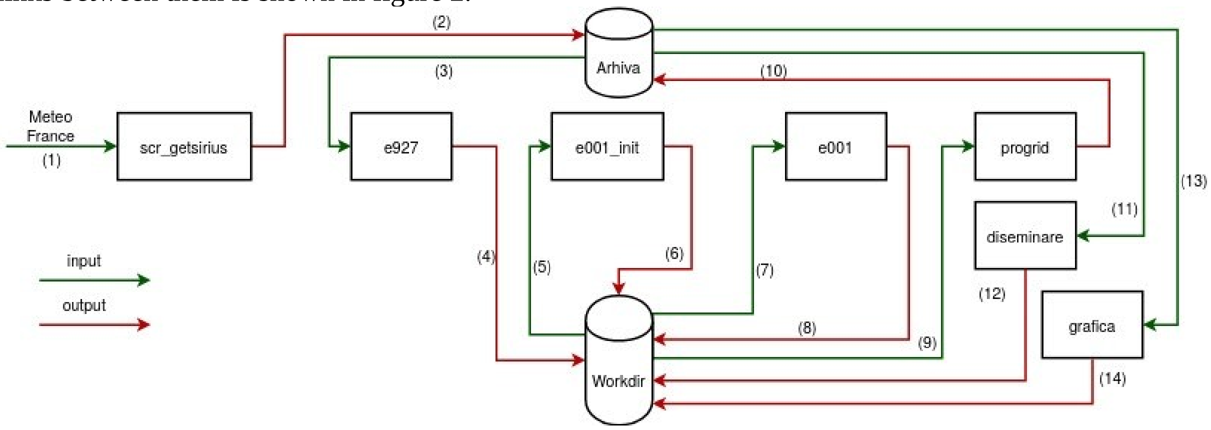

Figure 2: Workflow diagram of the ALADIN/ALARO operational suite.

It can be observed that the first step *scr_getsirius* consists in fetching the coupling files (LBCs from the global model ARPEGE) from Meteo-France. This is one of the tasks that was parallelized through the *Job Array* component, resulting in a decrease in the execution time required for this job. The next operational step (configuration *e927)* was changed in the same manner. Figures 3 and 4 show the execution times spent by these tasks.

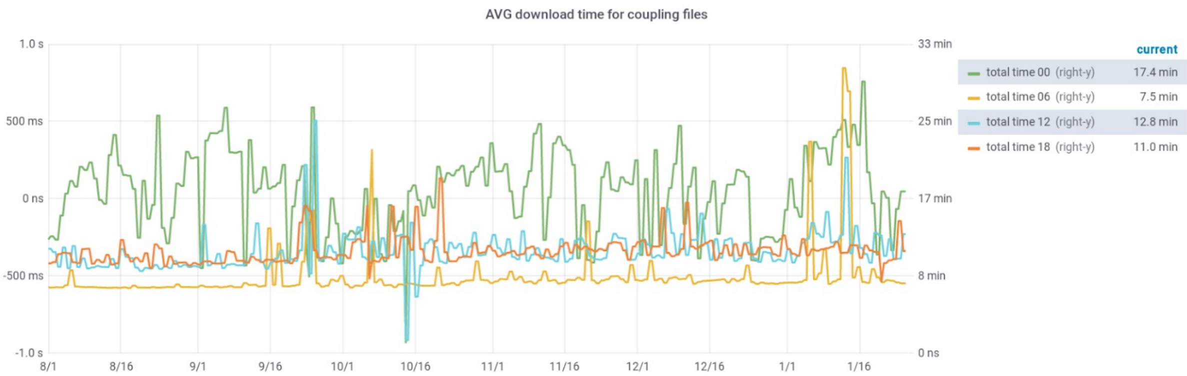

Figure 3: Execution time for task scr_getsirius, for each run (1 Aug 2020 - 24 Jan 2021).

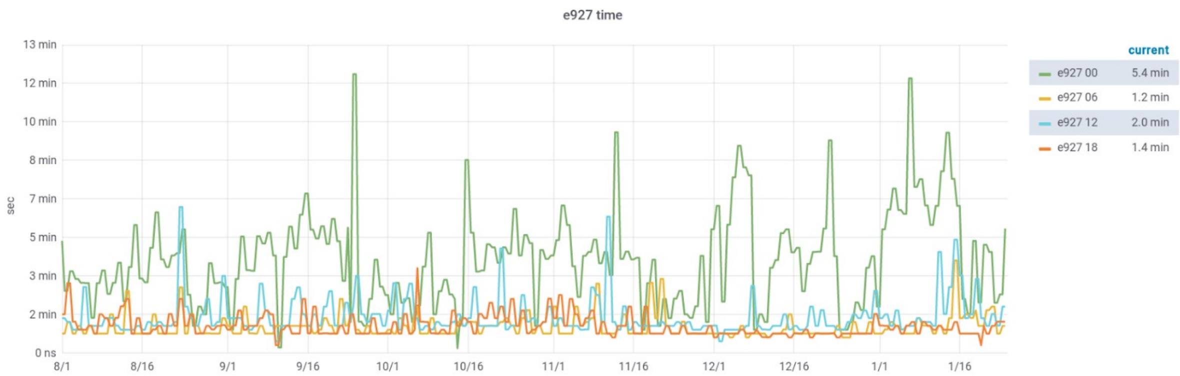

Figure 4: Execution time for task e927, for each run (1 Aug 2020 - 24 Jan 2021).

On the new platform, configurations *e001_init* and *e001* require 3 computer nodes (96 cores). This number of nodes was established following preliminary scalability tests conducted in order to find the best version for optimal execution time. The setup on the new platform results in significantly less compute time (of the order of minutes) spent for obtaining the standard hourly historical and *fullpos* files (*ICMSH* and *PFLALO*), in comparison with the former operational platform. Figure 5 shows the execution times obtained in step *e001*.

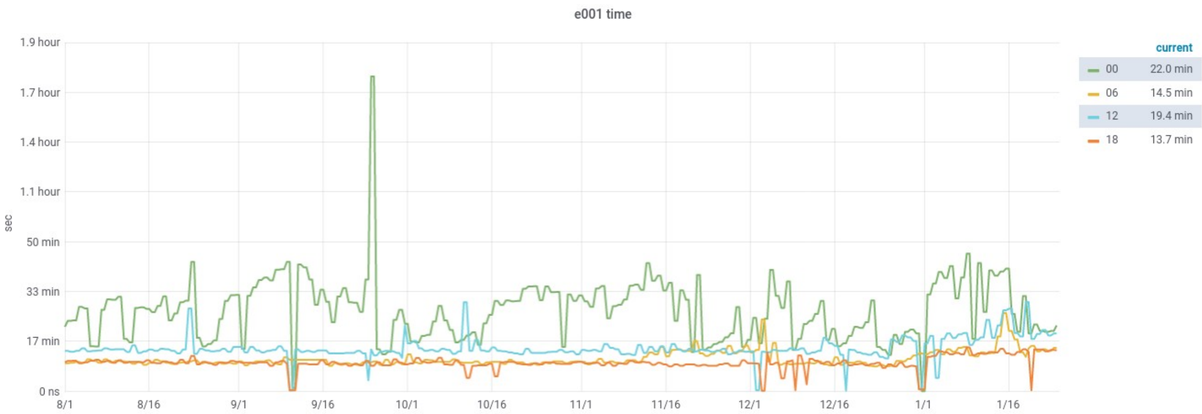

Figure 5: Execution time for task e001, for each run (1 Aug 2020 - 24 Jan 2021).

The next step, the data dissemination for different customers was mostly reshaped as well. The data are extracted from grib files (following progrid task in figure 2) by means of ECMWF's *ecCodes* package *(eccodes-2.13.0-gcc6.5.0).* Furthermore, different data computations and writing of the output files adapted to each customer requirements were modified and optimised. For instance, previous FORTRAN programs were replaced with more flexible *Linux Shell* scripting. All these changes proved beneficial for obtaining smaller execution times for these tasks, compared to the former operational suite.

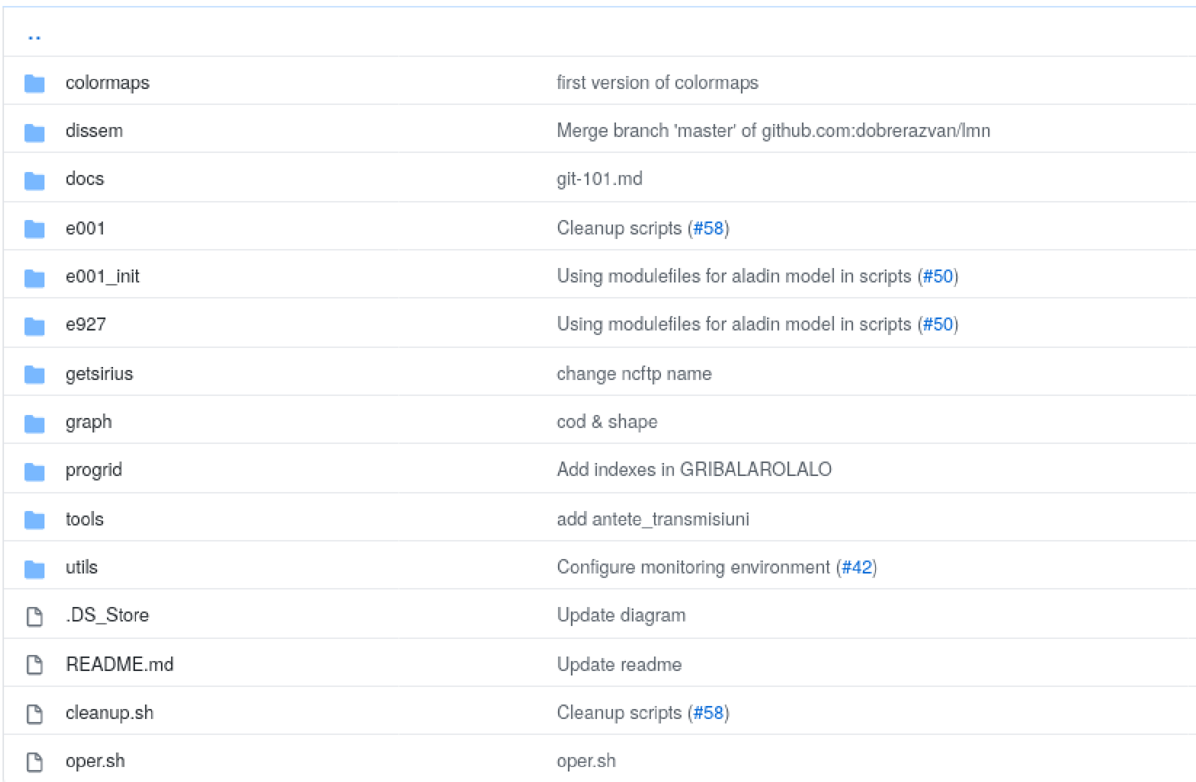

..	
colormaps	first version of colormaps
dissem	Merge branch 'master' of github.com:dobrerazvan/lmn
docs	git-101.md
e001	Cleanup scripts (#58)
e001_init	Using modulefiles for aladin model in scripts (#50)
e927	Using modulefiles for aladin model in scripts (#50)
getsirius	change ncftp name
graph	cod & shape
progrid	Add indexes in GRIBALAROLALO
tools	add antete_transmisiuni
utils	Configure monitoring environment (#42)
.DS_Store	Update diagram
README.md	Update readme
cleanup.sh	Cleanup scripts (#58)
oper.sh	oper.sh

Figure 6: Operational file structure on GitHub platform.

In order to better facilitate the whole migration and reorganisation process, the open-source GitHub platform was used. In this manner, all users have access to the common repository, can see the status and download the latest version of the code (figure 6).

2.3 Monitoring system and alert manager

An additional component was introduced to the operational suite: a monitoring and alert procedure. The idea was to gain more visibility in case of technical errors occurrence and assess the performance in terms of CPU time and memory used. In this manner, we can obtain metrics that show the time spent by different operational tasks which can be analysed in relation to server computer metrics, to identify causes for any delays encountered when dealing with each task. The following open source software tools [4] were used for this endeavour:

- *Prometheus* - records metrics generated by data collectors installed on computer nodes; also, it handles and generates alerts further processed by the *AlertManager* application;
- *Push Gateway* - necessary for batch type tasks that can send data to this collector, though they are not continually running;
- *Grafana* - used for the visualisation of the recorded metrics;
- *VictoriaMetrics* - allows storage of the metrics for a longer period of time (currently this period is 1 year);
- *AlertManager* - forwards alerts received from Prometheus to users in charge of the concerned task, either by email or SMS (using RaspberryPI and a GSM modem). The operational tasks are designed to “fail fast” (to stop at first encountered error), in order to be resumed from the last successfully completed step.

The list of metrics that are currently collected are: status of the jobs, Aladin node (10G, IB traffic, CPU usage); download time, number of downloading retries and download errors for coupling files; time and errors for: ee927, e001_init, e001, progrid, dissem processes. An example of the information obtained from this type of metrics can be observed in figures 3, 4 and 5 previously introduced.

3 Forecast validation

As previously mentioned, the new operational suite is based on the cy43t2_bf10 model version. However, other integration settings and characteristics are not changed in the new configuration. The operational setup runs in 6.5 km horizontal resolution and 60 vertical levels. Validation of the new cycle was performed for a two month period, June and July 2018 over the same operational integration domain (figure 7). Verification scores were computed for the forecast of several meteorological parameters: 2 m temperature, 6 h accumulated precipitation, mean sea level pressure, as well as 10 m wind speed, and were compared with the results obtained with cy40t1. The verification was performed using observation data from 157 synoptic stations in Romania.

The 2-month period was chosen due to its synoptic events. Over the last weeks of May, June and mid-July 2018, a particularly large number of thunderstorms occurred mostly in western and central parts of Europe, causing severe wind gusts, large hail, excessive precipitation and a considerable number of flash floods. During this time, more than 2500 reports of hazardous weather events were collected and registered by the European Severe Weather Database (ESWD: https://eswd.eu/cgi-bin/eswd.cgi).

Figure 8 shows the BIAS and RMSE scores for 2 m temperature, 6-hour accumulated precipitation, mean sea level pressure and 10 m wind speed. The verification was done for a forecast length up to 78-hour lead time and 00 UTC run is considered for this study. It can be noticed that generally these two scores are comparable between the two model versions, with small differences for 10 m wind speed.

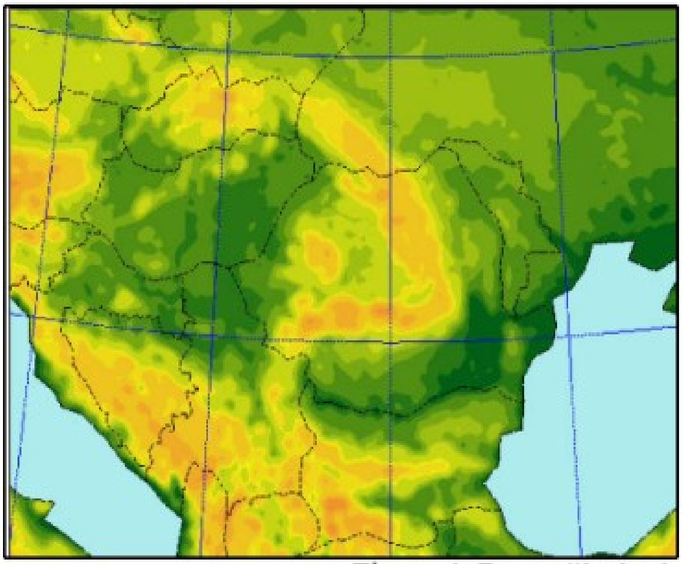

Figure 7: Operational integration domain.

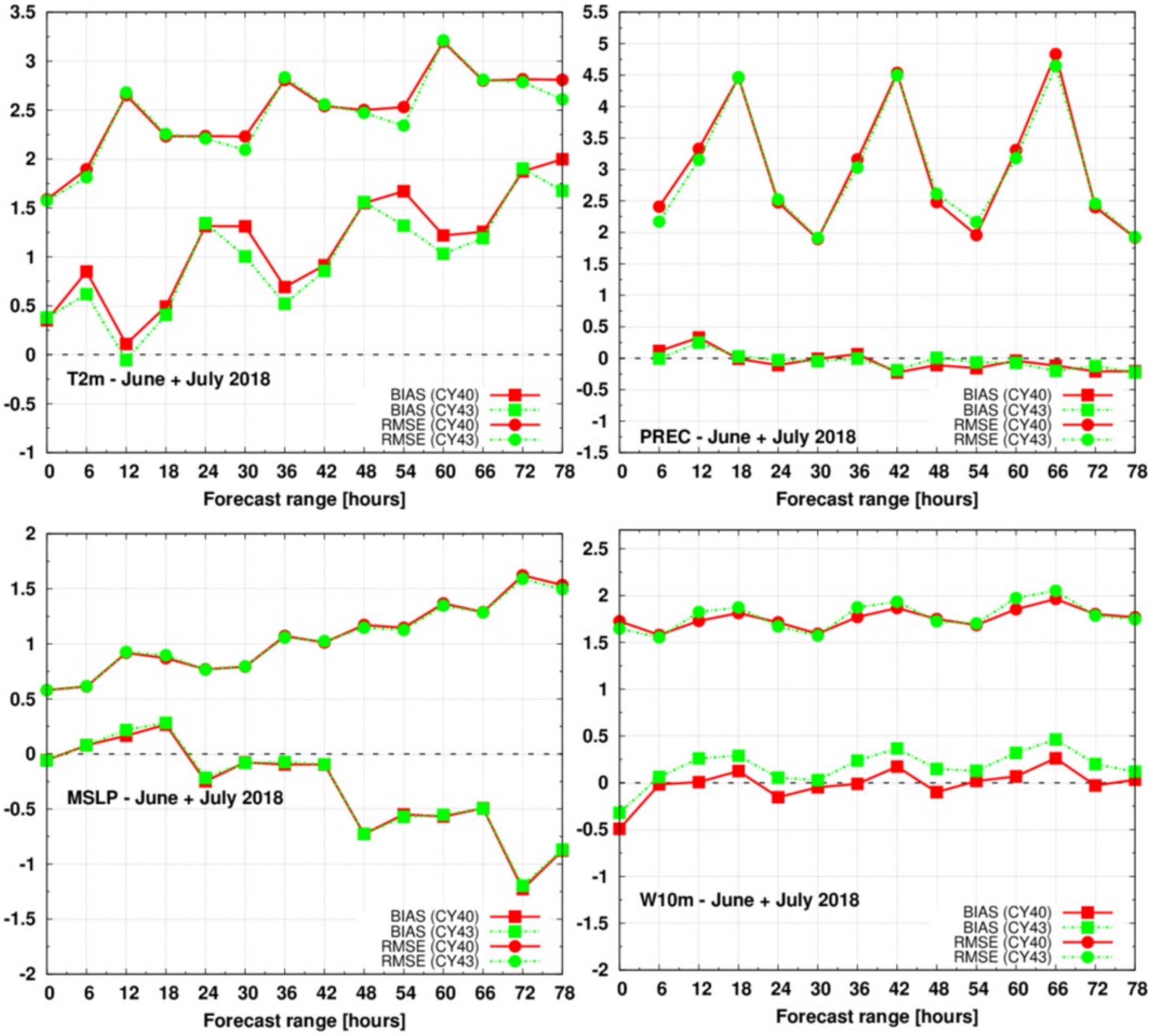

Figure 8: BIAS and RMSE, first row: 2 m temperature (ºC) and 6-hour precipitation (l/m²); second row: mean sea level pressure (hPa) and 10 m wind speed (m/s); cy40 (red) and cy43 (green), June and July 2018, 78h forecast range, 00 UTC run.

4 Conclusion

Many changes have been made to the structure of the operational scripting system over the past year. Either computational platform itself, workflow rearrangement or change in model version, all modifications led to a more efficient operational implementation. Although rather technical, all this work facilitates further developments, as well as better management of all tasks involved in the operational duties.

5 References

[1] Dumitru, A., Tascu, S., and Craciun, A. (2020). ALADIN activities in Romania. ALADIN-HIRLAM Newsletter 14:113-114, https://www.umr-cnrm.fr/aladin/IMG/pdf/nl14.pdf.

[2] What Is A Data Pipeline? Considerations & Examples | Hazelcast, https://hazelcast.com/glossary/data-pipeline.

[3] Slurm Workload Manager - Job Array Support, 2019, https://slurm.schedmd.com/job_array.html.

[4] Prometheus - Monitoring system & time series database. https://prometheus.io/.

Very high-resolution experiments at AEMET

David Suárez-Molina, Javier Calvo

1 Introduction

The accuracy of Numerical Weather Prediction (NWP) models in complex terrain is lower than over flat and homogeneous terrain. This discrepancy is attributed to the fact that boundary-layer processes in complex terrain are not well represented by NWP models (Suárez-Molina et al. 2021). Test bed over the Canary Islands (challenging orography) has been stablished with 1 and 0.5-kilometre (km) resolution.

The main objective has been to run a very high-resolution stable version. This version has been called High-Resolution Reference Version), is based on Harmonie-Arome cycle 43h2.1and includes:

- First order in SETTLS for the first steps (NFOST=10),
- Adding diffusion in Pressure Departure (RDAMPPD=20)
- Adding diffusion in Vertical Divergence (RDAMPVD=10) and Vorticity (RDAMPVOR=10)
- Activating COMAD

In addition, several sensitivity tests have been carried out to tests different resolutions and model configurations.

2 Study area

This research is focused on the Canary Islands (Figure 1). This archipelago is in front of the west coast of North Africa in the subtropical zone (27°37′–29°25′N and 18°10′–13°20′W). The archipelago is formed by seven islands of volcanic origin that present a complex orography.

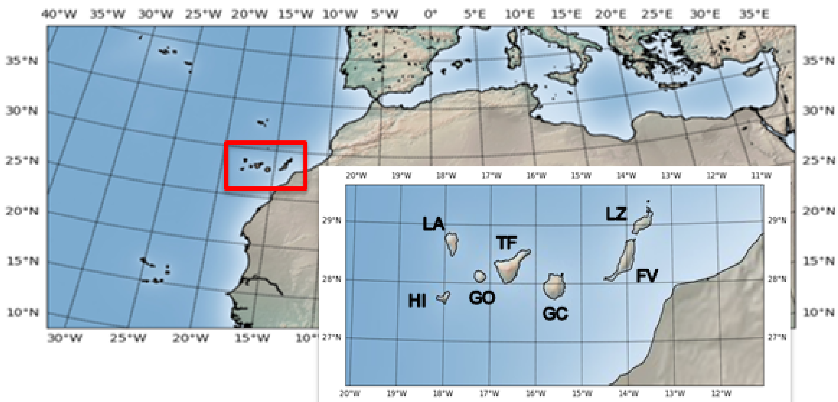

Figure 1. Location of Canary Islands in the Subtropical Eastern Atlantic. The zoom shows the study area in more detail.

The highest point is Mount Teide (3718 m) on Tenerife (TF). With Tenerife being by far the highest island, La Palma (LA), Gran Canaria (GC), La Gomera (GO) and El Hierro (HI) constitute a medium cluster with highest heights of: 2423 m (Roque de los Muchachos, LA), 1948 m (Pico de Las Nieves, GC), 1501 m (Pico de Malpaso, HI) and 1487 m (Garajonay, GO). Lanzarote (LZ) and Fuerteventura (FV) are much flatter with maximum heights of 671 m and 807 m, respectively.

3 Experimental setup

Preliminary tests

A previous study (Subías *et al.,* 2019) performed several sensitivity tests at 1 km resolutions:

- Spectral truncation: linear, quadratic and cubic.
- Time scheme: SETTLS and Predictor/Corrector.
- Nesting strategy: IFS and AROME 2.5 km.
- Single and double precision.

From these test, our recommended configuration at 1 km resolution in dynamical adaptation mode includes SETTLS time scheme, Single precision, Linear grid and IFS nesting.

Sensitivity tests

Based on the High-Resolution Reference Version, different experiments have been created in order to discern the feasibility of increasing the resolution of the operational model in the Canary Islands. Table 1 summarizes the main characteristics of the sensitivity experiments. Al experiments are based on cycle 43h2.1 version. The 1 and 0.5 km resolution experiments run with Single Precision, Linear Grid, SETTLS, surface analysis and blending for upper levels.

Table 1: Experiments and settings

Experiment	1km	1km_L90	0.5km	0.5km_L90
Nesting	IFS	IFS	Arome 2.5 km	Arome 2.5 km
Resolution	1 km	1 km	0.5 km	0.5km
Vertical levels	65	90	65	90
Time step	30	15	10	10

The 90 level integrations used a smaller time step than the 60 level ones to avoid crashes from time to time. In Figure 1 we can see the positive impact of increasing both horizontal and vertical resolution, especially, the wind bias is significantly reduced.

Besides, two additional experiments have been setup at 1 km with 90 levels to check the impact of applying SLDH diffusion also Pressure Departure, Vertical Divergence, Temperature and Vertical Velocity (1km_L90_SLHD) and of using Predictor/Corrector scheme instead of SETTLS (1km_L90_SLHD_PC). Figure 2 shows that wind speed decreases with the additional SLHD and that T2m degrades unless using Predictor/Corrector scheme. In principle, we will not use this additional diffusion in our km and sub-km settings.

Figure 4 show the performance of the 0.5 km versions compared with the 2.5 km one that is the host model. Both wind speed and temperature improve at 0.5 km with the 90 level version performing slightly better than the 60 level one. An especially interesting feature of the 0.5 km versions is their ability to capture the very strong wind events as can be seen in the scatterplot observation-forecast shown in Figure 3.

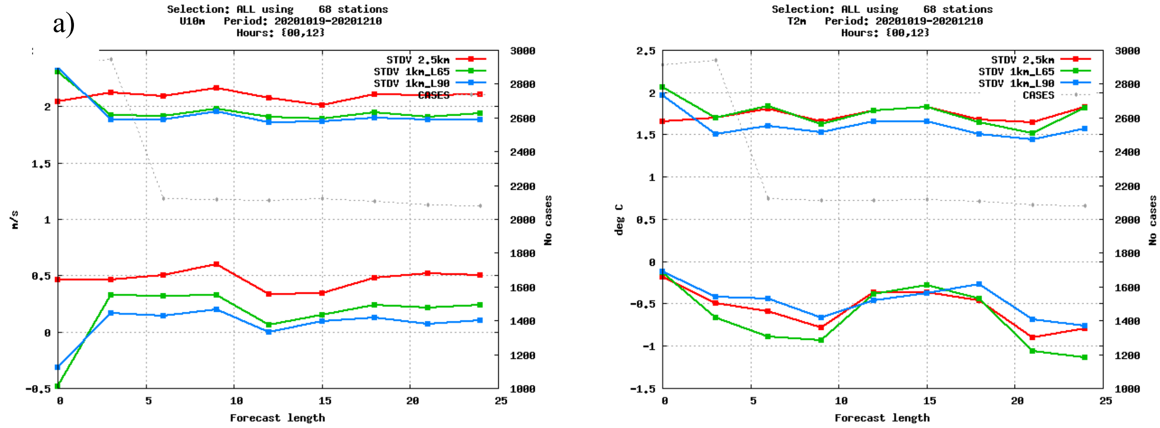

Figure 1: *STDV and BIAS function of the forecast length. Comparison for different horizontal and vertical resolutions: 2.5km is the reference with 65L and complete DA, 1km_L65 and 1km_L90 are the 1 km versions with 65 and 90 levels: (a) 10 m wind speed, (b) 2m temperature.*

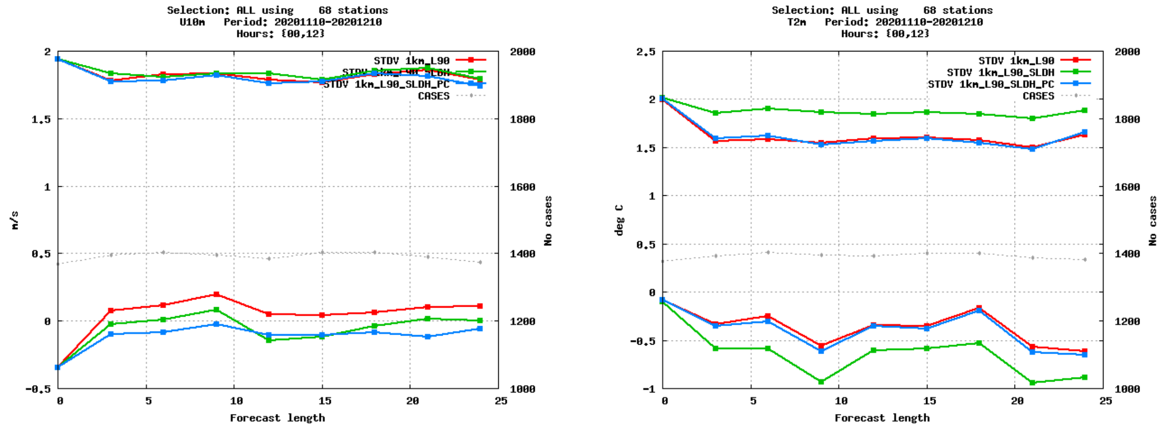

Figure 2: *As Fig. 1 for the experiments at 1 km and 90 levels: 1km_L90 is the reference with SETTLS, 1km_L90_SLDH includes SLDH in all variables and 1km_L90_SLDH_PC uses Predictor /Corrector.*

Validation of the precipitation forecast for the Canary Islands is difficult because it is a scarce phenomenon and because of the very local features. In order to have a flavour about the behaviour of precipitation for the different setups we show the precipitation on the 2nd December 2020 at 15 utc associated with cyclone Clements. In Fig.5 we analyse the effect of resolution that is more realistic at 1 km than at 2.5 km resolution. The precipitation at 0.5 km is strongly conditioned by the size of the domain which only allows convection to develop far from the borders.

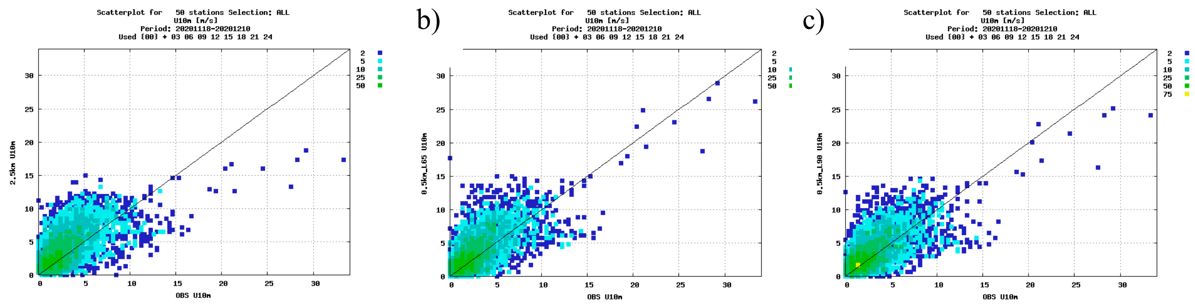

Figure 3: *Scatterplots observation-forecast of wind speed: (a) Reference 2.5 km, (b) 0.5 km 60L and (c) 0.5 km 90L.*

a)

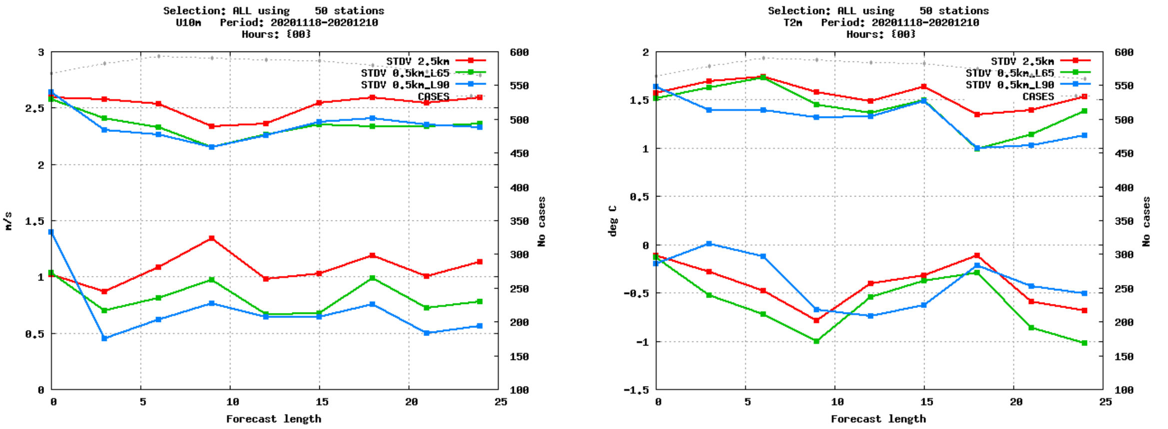

Figure 4: *As Fig. 1 comparing the reference version (host model) at 2.5 km (2.5km) with the ones at 0.5 km with 65 levels (0.5km_65) and 90 levels (0.5km_L90).*

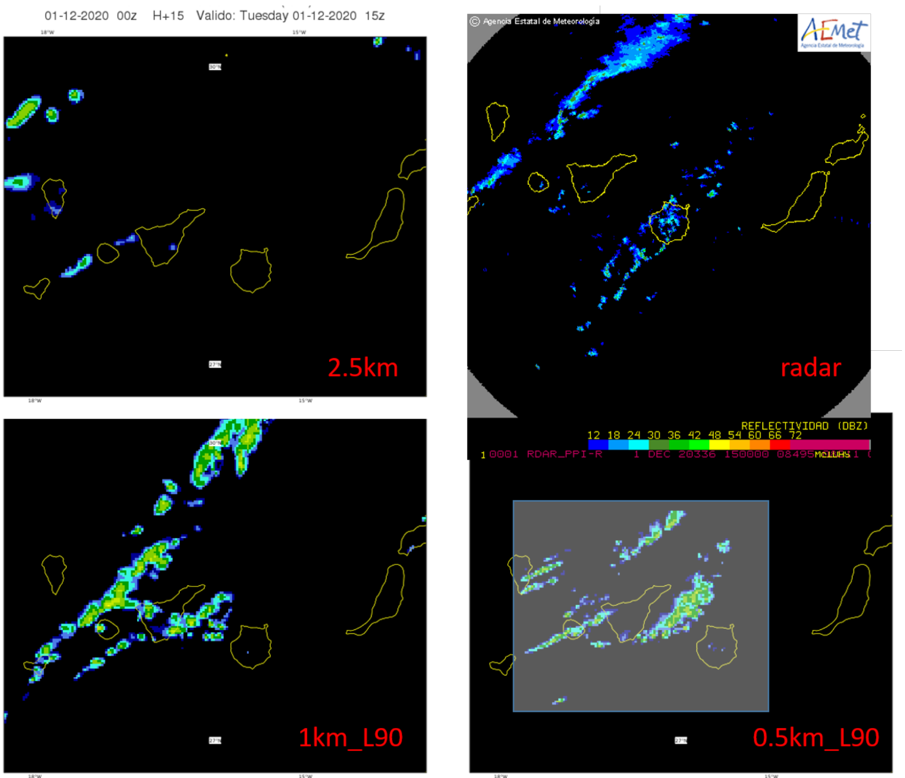

Figure 5: *Reflectivity the 2nd December 2020 at 15 utc. Comparison of (a) H+15 prediction at 2.5 km, (b) radar observation, (c) 1km L90 prediction and (d) 0.5 km L90 forecast (the square shows the model domain).*

Concerning the impact of different setups at 1km on precipitation (Fig. 6), the differences are small between the 65 and the 90 level versions. Besides, it can be seen that applying SLDH in all variables produces structures of smaller size and turns out in higher precipitation maxima. Predictor/Corrector scheme seem to increase a little the size of the precipitation cells.

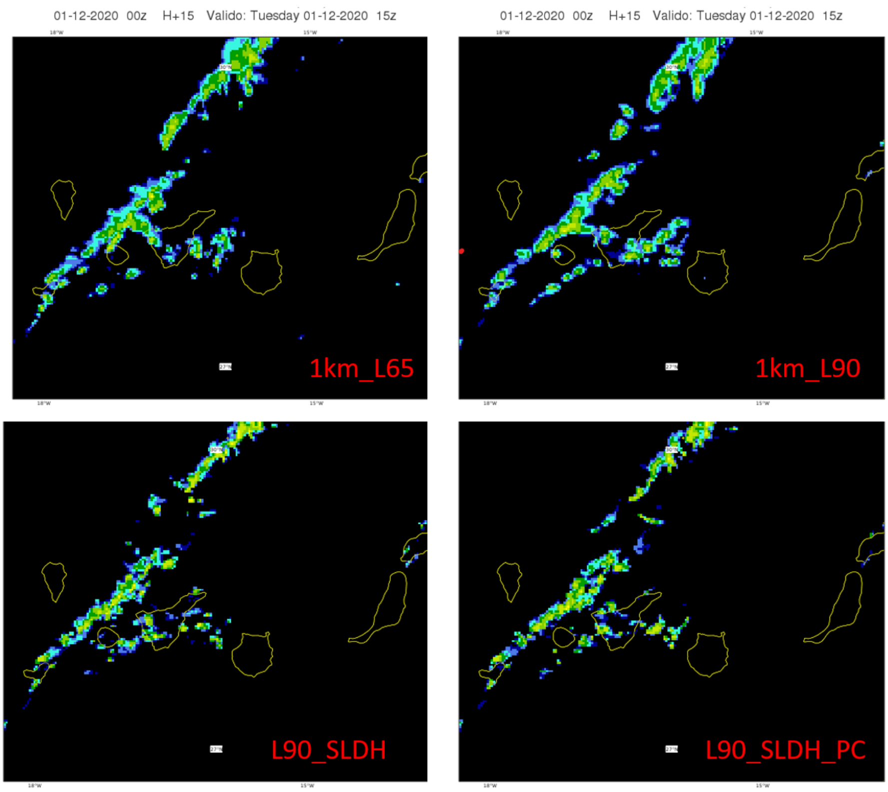

Figure 6: *As Fig. 5 for different setups at 1 km resolution: (a) L65, (b) L90 and (c) L90 with SLDH in all variables (d) L90 SLDH with Predictor/Corrector instead of SETTLS*

4 Conclusions

We have been able to define stable versions at 1 and 0,5 km resolution for the challenging orography of the Canary Islands. The increase in horizontal and vertical resolution improves the forecasts and, therefore, the increase in the resolution of the operating model could represent a better representation of weather phenomena in the domain of the Canary Islands. The added value of the 0.5 km resolution is not so clear, probably because the setup and the parameterizations are not well prepared for this resolution and because of the limitation of the domain size.

The increase of vertical resolution from 65 to 90 levels is beneficial but it is less stable and may need to lower the time step or using Predictor/Corrector time scheme. In our experience, SETTLS is slightly better than P/C so our recommendation would be use P/C only for specific more unstable situations or time steps.

Although, applying SLDH diffusion to all variables may be beneficial for 10 m wind, overall we think is detrimental.

5 References

Suárez-Molina, D., Fernández-González, S., Montero, G., Oliver, A., & González, J. C. S. , 2021: Sensitivity analysis of the WRF model: Assessment of performance in high resolution simulations in complex terrain in the Canary Islands. *Atmospheric Research*, 247, 105157.

Subías, A., Suárez, D. and Calvo, J., 2019: High resolution experiments at AEMET. *HIRLAM-ALADIN High Resolution and Nowcasting Workshop*, Las Palmas de Gran Canaria, 12-14 December 2019 (https://hirlam.org/trac/wiki/Meetings/HR/HR_2019_LasPalmas

Summary of the activities for AROME at Météo-France.

Eric Bazile, Pierre Brousseau, Yann Seity, Salomé Antoine, Etienne Arbogast, Loik Berre, Yves Bouteloup, Rachel Honnert, Quentin Libois, Yann Michel, Thibault Montmerle, Adrien Napoly, Jean-Marcel Piriou, Sébastien Riette, Benoit Vié

1 Introduction

In this newsletter, the next version of the operational AROME system, based on cy46t1_op1, is briefly described, following by some results from more medium/longer terms activities: 4DEnVar, fog forecast with the SOFOG field experiment, soil diffusion scheme, EC-Rad, 3D-turbulence, cold clouds.

2 Main update for the next operational AROME

- Semi-Lagrangian interpolator: since the increase of the horizontal resolution to 1.3km of AROME, some forecasters complains about the underestimation of diurnal convection in case of weak forcing. Causes of this problem has been understood, thanks to academic 3D tests with AROME on a small domain (48x48x90 grid points @1250m) with a very simple initialization for cloud variables: $q_c=q_i=q_r=q_s=q_g=0$ except for q_r=1g/kg at 2000m height in the center of the domain. All the physical parameterization are switch off except the rain sedimentation, in order to study the mass conservation during the fall of rain droplets. Figure 1 shows the impact of the use of the linear interpolator (right) versus the quasi-monotum (QM) default one (left) for the total rain (green line). After 5 time steps, the total rain is increased by 50% with the (QM) interpolator (left) whereas it remains constant with the linear one, indicating a perfect mass conversion in this case. Of course, this academic case is extreme with large discontinuities, however in case of weak forcing in summer, it is characteristics of small convective cells. The impact of this change in the operational configuration (Fig. 2) is significant and fix the underestimation problem reported by forecasters.

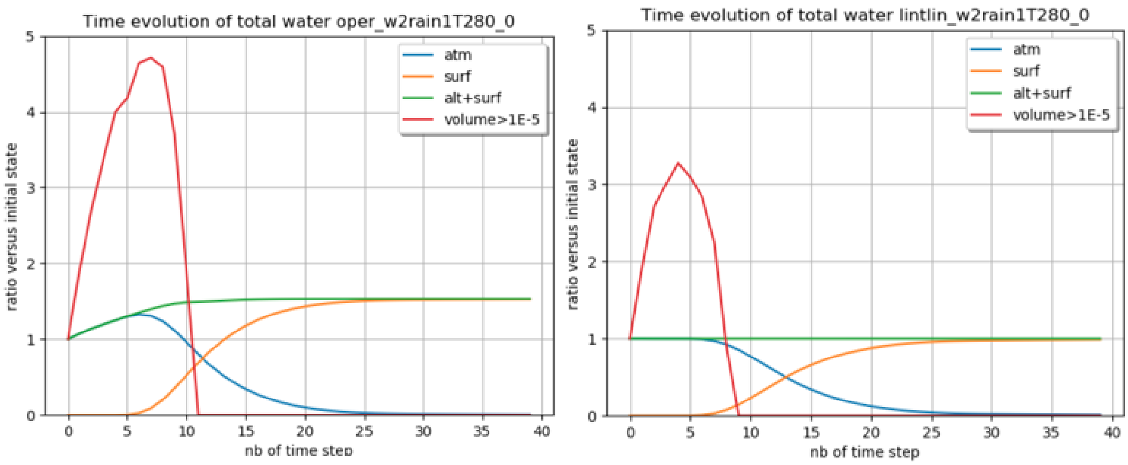

Figure 1: Total rain content in the atmosphere (blue) and surface (orange) normalized by the initial value. Left : with the QM-interpolator and right with the linear-interpolator

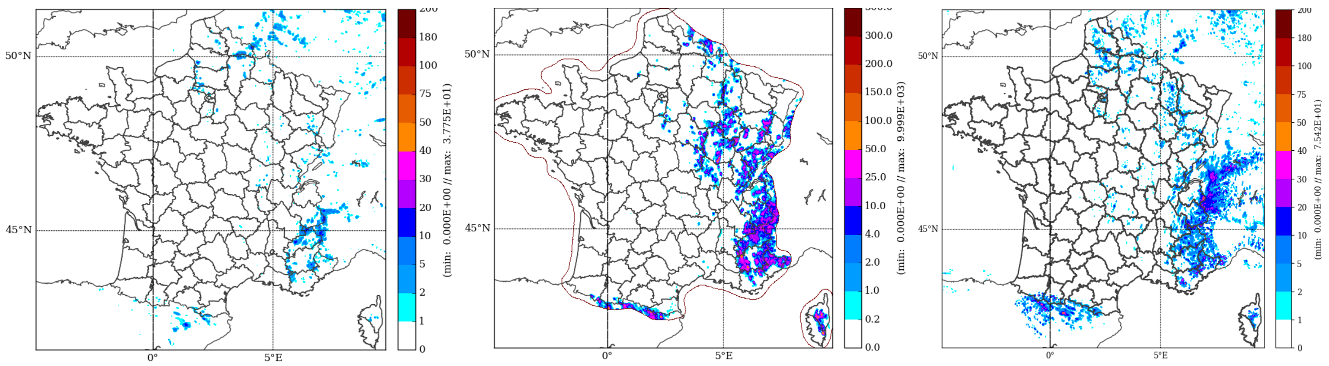

Figure 2: 24h accumulated rainfall. Left: AROME oper. Middle: Radar obs.. Right: AROME with linear interpolator in the semi-lagrangian.

- Ecume V6 will be used in the next operational ARPEGE system with positive impact and also in AROME with a very small and neutral impact at least for the two month periods tested.
- A lightning diagnostic (Fig. 3) has been implemented based on Mc Caul (2009).

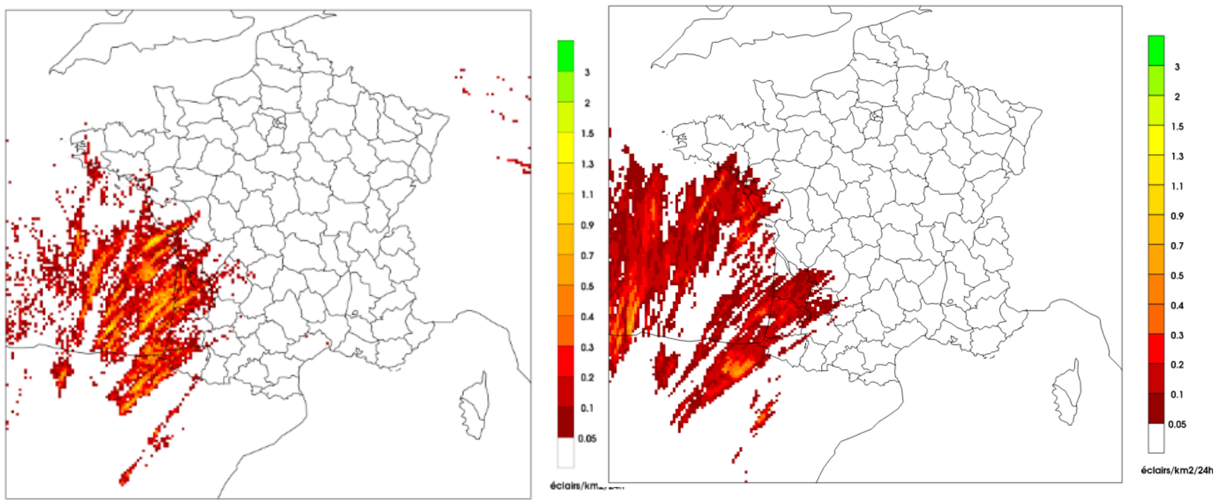

Figure 3: Left: Observation Right: AROME Lightning diagnostic

3 Further developments:

- **4DEnVar**: Since April 2015, the Arome-France data assimilation is based on 1h cycle, instead of 3h, to allow assimilation of more informative observations especially at the convective-scale, such as radar measurements, with a higher temporal frequency. To further use of these high temporal frequency observations, 4D schemes are now investigated in the AROME-France. First, a 4D-Var scheme, has been developed to assimilate radar observations every 15 minutes, however this first 4DVar scheme described by Brousseau et al. (2015) is not a "real full" 4DVar AROME for some technical/scientifical aspect: the minimisation can not run with the AROME physics with SURFEX and the specific humidity in grid point. To fix this weaknesses, the minimisation uses the ARPEGE/ALADIN physics without SURFEX and the specific humidity in spectral, in addition, the tangent linear and adjoint model is the hydrostatic one developed by Soci et al. (2006) for ALADIN. Finally, despite of this, the results are encouraging. Nevertheless, to avoid this kind of inconsistency between the "real" forecast model and the

one used in the minimisation, the 4DEnVar framework is investigated under OOPS. In such a system, an AROME EDA allows: the uses of flow-dependant background error covariances and the temporal dimension within the assimilation window, is managed by temporal correlations of these error covariances computed with a 3.2km Ensemble Data Assimilation (EDA).
A prototype of a 4DEnVar system has been developed at 1.3km horizontal resolution, with 15 minutes timeslots in an hourly cycle, using perturbations from a 3.2km EDA. Preliminary results obtained from the simulation of a strong convective event are illustrated on the situation of the 26 of May 2018 (Fig: 4). The sum of the 1h precipitations simulated by the 1h forecasts from the data assimilation cycle for the whole 26th of May from the 4DEnVar experiment gives a better agreement of the 24h accumulated precipitation than the 3dvar experiment one compared to the radar network.
On going works concern now the evaluation of this system for more situations and long periods at different season.

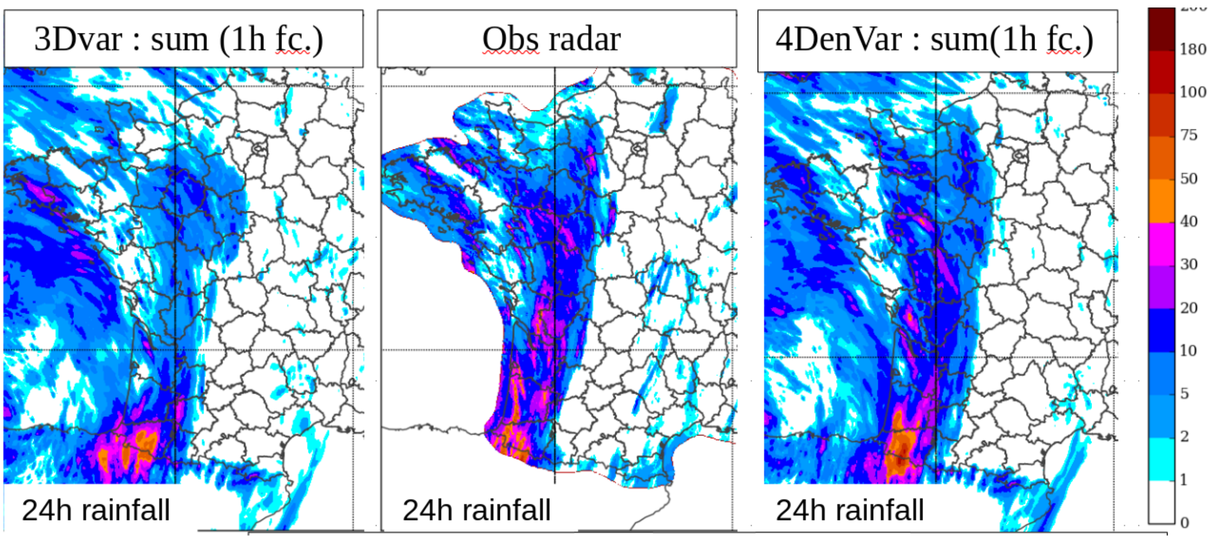

Figure 4: Accumulated 24 1h precipitation. Left: 3Dvar . Middle: Radar. Right: 4DEnVar

- **SOFOG:** During the SOFOG field campaign (Oct.2019-March 2020), 15 IOPs have been performed. Three AROME configurations have been created on the SOFOG domain in a dynamical adaptation from the operational AROME-France:
  - AROME-ref: 1.3km L90 = AROME oper.
  - AROME-500-L156: 0.5Km with 156 vertical levels with 1st one at 1m (from Philip. et al. 2016)
  - AROME-500-L156 with the LIMA scheme (Vié et al. 2016)

  The preliminary results shows that AROME-500-L156 improves the fog detection however with an increase of the false alarm rate. The fog duration is mainly overestimated with ICE3 (Fig. 5), the LIMA scheme improves this aspect with more short events in better agreement with the observation (Fig. 5 right).

- **3D turbulence:** Thanks to the availability of the horizontal gradients in the AROME physics several actions can start to improve the mixing in the deep cumulus clouds following Verelle et al. (2015) and to increase the TKE production with an additional term of the shear production due to the orography (Goger et al. 2018) .

- **EcRad, ISBA-Diff:** EcRad is now available in cy46t1 for AROME and ARPEGE, preliminary results are encouraging, nevertheless more experiment are necessary before the use in operations. For the explicit soil (DIF) and snow (ES) scheme, a 3Dvar have been performed for 6 months in summer without specific re-tuning for the surface assimilation (soil moisture assimilation). The first results are positive but longer evaluation at least one year is required.

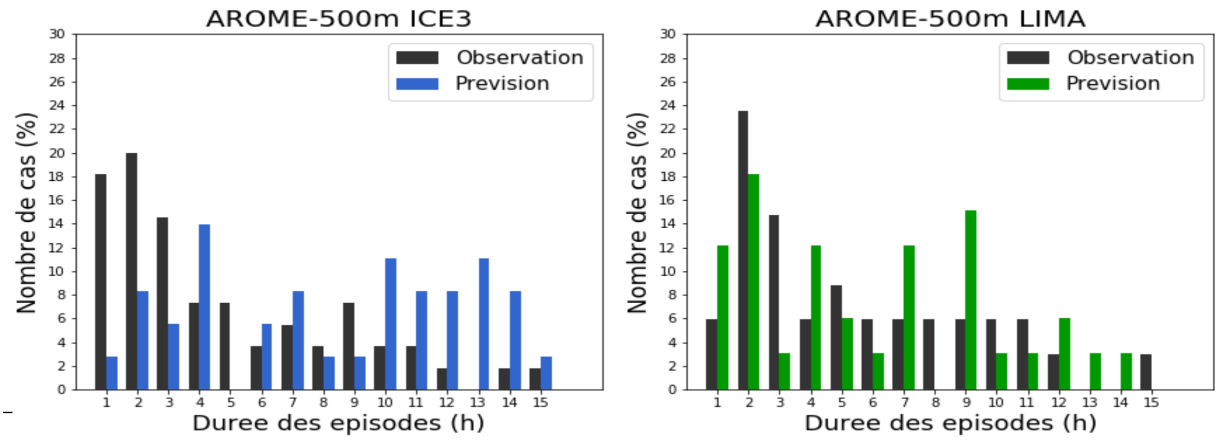

Figure 5: Histogram for fog function of fog duration. Left with ICE3 right with LIMA

More details can be found in the presentation given at the EWGLAM meeting by Yann Seity and Pierre Brousseau. http://srnwp.met.hu/Annual_Meetings/2020/

4 References

Brousseau et al. 2015. http://www.data-assimilation.riken.jp/isda2015/program/pdf//4-3.pdf

Goger, B., Rotach, M.W., Gohm, A. *et al.* The Impact of Three-Dimensional Effects on the Simulation of Turbulence Kinetic Energy in a Major Alpine Valley. *Boundary-Layer Meteorol* 168, 1–27 (2018). https://doi.org/10.1007/s10546-018-0341-y

Philip, A., Bergot T., Bouteloup Y., and Bouyssel F. The Impact of Vertical Resolution on Fog Forecasting in the Kilometric-Scale Model AROME: A Case Study and Statistics. Weather and Forecasting. (2016). https://doi.org/10.1175/WAF-D-16-0074.1

McCaul, E.W., Jr.; Goodman, S.J.; LaCasse, K.M.; Cecil, D.J. Forecasting Lightning Threat Using Cloud-Resolving Model Simulations. *Weather Forecast.* 2009, *24*, 709–729

Soci, C., C. Fischer and Andras Horanyi. Sensitivity of High-Resolution Forecasts Using the Adjoint Technique at the 10-km Scale (2006) MWR. DOI: https://doi.org/10.1175/MWR3091.1

Verrelle, A., Ricard, D., and Lac, C.: Evaluation and Improvement of Turbulence Parameterization inside Deep Convective Clouds at Kilometer-Scale Resolution. (2015) Mon. Weather Rev., 145, 3947–3967

Vié, B., Pinty, J.-P., Berthet, S., and Leriche, M.: LIMA (v1.0): A quasi two-moment microphysical scheme driven by a multimodal population of cloud condensation and ice freezing nuclei, Geosci. Model Dev., 9, 567–586, https://doi.org/10.5194/gmd-9-567-2016, 2016.

Physically based stochastic perturbations and applied machine learning

Michiel Van Ginderachter, Lisa Commerman, Joppe Massant, Milan Vispoel,
Joris Van den Bergh, Daan Degrauwe, Stephane Vannitsem, Piet Termonia

1 Introduction

Recently, much effort has been put into the development of schemes that simulate the random component of the errors of the model tendencies. Keeping in mind the purpose of stochastic perturbations, which is to represent forecast uncertainties originating from model errors, the perturbations ideally have the same statistics as the error source. Since the model error sources are diverse and their statistical characteristics only partially known (Boisserie et al., 2014), most methods resort to pragmatic solutions: the amplitude of the perturbations or their spatial patterns are usually chosen such that a satisfactory reduction of ensemble under-dispersion is obtained (Berner et al., 2017).
Recent methods to assess sources of model uncertainty and their statistical properties are based on a comparison between perfect and target forecasts (Nicolis, 2003, 2004; Nicolis et al., 2009). The aim of the present paper is to use this method to characterize the model error related to convective transport by comparing two forecasts which differ only in the representation of the deep convective processes. Once the model error is characterized, it is reintroduced under the form of stochastic perturbations and the impact on the upper air scores in investigated. Finally, the use of a generative adversarial network (GAN) (Goodfellow et al. 2014) for generating new perturbations is investigated.

2 Methodology and results

The above described methodology is applied as follows. The reference model is a configuration of the ALADIN model with a parameterization of deep convection. An identical configuration is also run with the deep-convection parameterization scheme switched off, degrading the forecast skill. The model error is then defined as the difference of the energy and mass fluxes between the reference model with scale-aware deep-convection parameterization and the target model without deep-convection parameterization.
The diagnosed model-error characteristics are used to stochastically perturb the fluxes of the target model by sampling the model errors from a training period in such a way that the distribution and the vertical and multivariate correlation within a grid column are preserved. By perturbing the fluxes it is guaranteed that the total mass, heat and momentum are conserved.
The tests, performed over the period 11 - 20 April 2009, show (see Fig. 1) that the ensemble system with the stochastic flux perturbations combined with the initial condition perturbations not only outperforms the target ensemble, where deep convection is not parameterized, but for many variables it even performs better than the reference ensemble (with scale-aware deep-convection scheme). The introduction of the stochastic flux perturbations reduces the small-scale erroneous spread while increasing the overall spread, leading to a more skilful ensemble. The impact is largest in the upper troposphere with substantial improvements compared to other state-of-the-art stochastic perturbation schemes. At lower levels the improvements are smaller or neutral, except for temperature where the forecast skill is degraded. While these results are promising, the sampling methods has the computational drawback that the database needed for the sampling has to be kept in memory.
In 2020 three students at Ghent University (Lisa Commerman, Joppe Massant and Milan Vispoel) trained the GAN on the database of the model errors described above. The machine learning technique was then applied

Table 1: 250 hPa Temperature scores for the different experiments at lead time +24h. BS is calculated at threshold 233K.

	TARGET	SAMPLED	PC20	GAN
RMSE	0.880	0.803	0.803	0.832
BIAS	-0.308	-0.221	-0.222	-0.264
SPREAD	0.305	0.310	0.309	0.299
BS	0.272	0.233	0.233	0.247

within the model to generate the stochastic perturbations and the performance was compared to the sampling method. This alleviates the cumbersome task of storing and loading all perturbations fluxes, as perturbations can now be generated 'on-the-fly'. First tests with these generated fluxes, even though the generated spread is generally lower compared to the sampled perturbations, show promising results. It can be seen from Table 1 that, while the sampling method compensates for the absence of the deep convection parameterization, the machine learning technique does it much less. Nevertheless, there is some potential in it and this will be further investigated.

More detailed information can be found in:
Van Ginderachter, M., Degrauwe, D., Vannitsem, S., and Termonia, P.: Simulating model uncertainty of subgrid-scale processes by sampling model errors at convective scales, Nonlin. Processes Geophys., 27, 187-207, https://doi.org/10.5194/npg-27-187-2020, 2020.

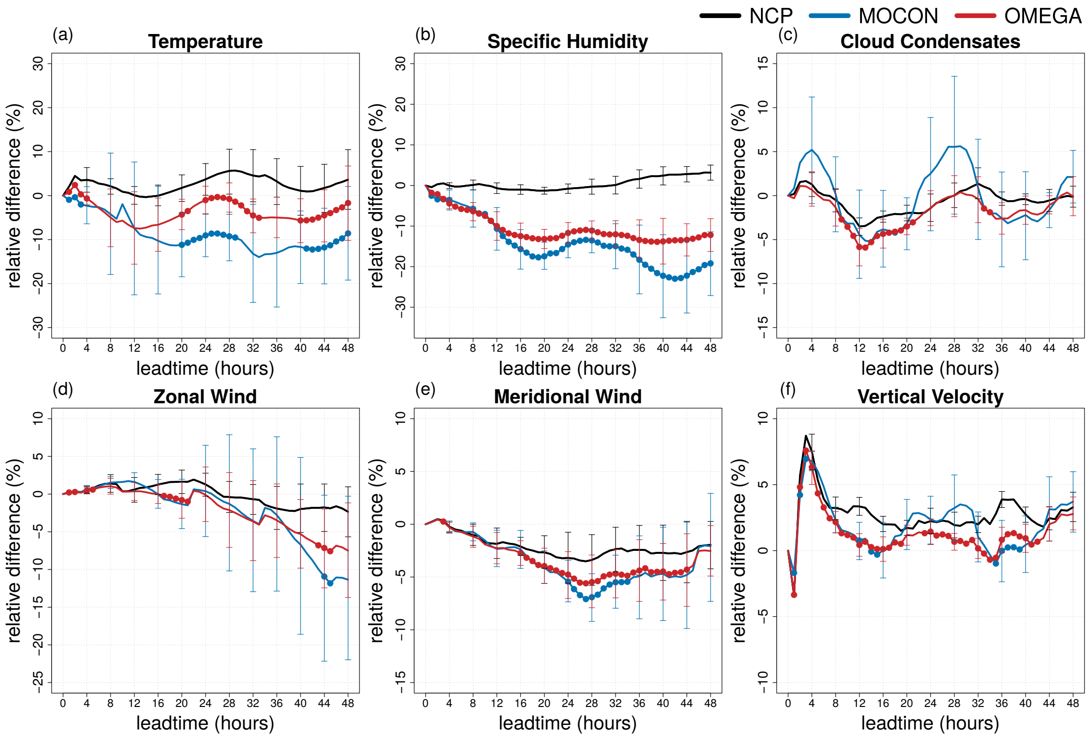

Figure 1: Relative CRPS difference (in percentage with respect to the reference configuration) of the target NCP (black), MOCON based perturbations (blue) and OMEGA based perturbations (red) ensemble for temperature (a), specific humidity (b), cloud condensates (c), zonal (d) and meridional (e) wind, and vertical velocity (f) at 250 hPa. All ensemble forecasts are performed with perturbations in ICs and LBCs. Error bars show the 95 % confidence interval. Lead times where the CRPS is significantly lower than the NCP CRPS at the 95 % confidence level are indicated with a filled circle.

3 References

Berner, J., Achatz, U., Batté, L., Bengtsson, L., Cámara, A. D. L., Christensen, H. M., Colangeli, M., Coleman,D. R. B., Crommelin, D., Dolaptchiev, S. I., Franzke, C. L. E., Friederichs, P., Imkeller, P., Järvinen, H., Juricke, S., Kitsios, V., Lott, F., Lucarini, V., Mahajan, S., Palmer, T. N., Penland, C., Sakradzija, M., von Storch, J.-S., Weisheimer, A., Weniger, M., Williams, P. D., and Yano, J.-I.: Stochastic Parameterization: Toward a New View of Weather and Climate Models, B. Am. Meteorol. Soc., 98, 565-588, https://doi.org/10.1175/BAMS-D-15-00268.1, 2017.

Boisserie, M., Arbogast, P., Descamps, L., Pannekoucke, O., and Raynaud, L.: Estimating and diagnosing model error variances in the Météo-France global NWP model, Q. J. Roy. Meteor. Soc., 140, 846-854, https://doi.org/10.1002/qj.2173, 2014.

M. M. I. Goodfellow, J. Pouget-Abadie, Generative adversarial networks, Proceedings of the International Conference on Neural Information Processing Systems (NIPS 2014), p. 2672-2680, 2014.

Nicolis, C.: Dynamics of Model Error: Some Generic Features, J. Atmos. Sci., 60, 2208-2218, https://doi.org/10.1175/1520-0469(2003)060<2208:DOMESG>2.0.CO;2, 2003.

Nicolis, C.: Dynamics of Model Error: The Role of Unresolved Scales Revisited, J. Atmos. Sci., 61, 1740-1753, https://doi.org/10.1175/1520-0469(2004)061<1740:DOMETR>2.0.CO;2, 2004.

Nicolis, C., Perdigao, R. A. P., and Vannitsem, S.: Dynamics of Prediction Errors under the Combined Effect of Initial Condition and Model Errors, J. Atmos. Sci., 66, 766âĂŞ778, https://doi.org/10.1175/2008JAS2781.1, 2009.

Met Éireann Updates

Geoffrey Bessardon, Colm Clancy, Tiziana Comito, Conor Daly, Rónán Darcy, James Fannon, Emily Gleeson, Alan Hally, Eoghan Harney, Dáire Healy, Ewa McAufield, Eoin Walsh, Eoin Whelan

1 Introduction

Cycle 40h1 of HARMONIE-AROME has been operational at Met Éireann since May 2018, with the short-range Irish Regional Ensemble Prediction System (IREPS) running since October 2018. A description of the most recent technical upgrade to the suite can be found in Bessardon et al., 2020 and an overview is provided below in Section 2.

Throughout 2020 and early 2021, extensive development and testing has been carried out on an e-suite based on Cycle 43h2.1. Details of this testing are given in Section 3. Some of the research activities that we are involved in are summarised in Section 4.

2 Operational Suite

For reference, we present below in Table 1 the details of the operational IREPS suite in its current configuration since the last technical upgrade in August 2019.

Table 1: Configuration of the operational IREPS suite

Component	Description
Code	HARMONIE-40h1.1
Domain	1000×900×65, model top 10 hPa
Grid	2.5 km, quadratic truncation
Cut-off	20 mins (perturbed members), 45 mins (control)
Observations	SYNOP, SHIP, AIREP, BUOY, TEMP, ASCAT, AMSU-A, MHS, IASI
Data assimilation	Surface OI & 3D-Var (control), Surface OI & blending (members)
Cycle	3-hourly: 54 hour forecasts at 0000/0600/1200/1800 UTC
LBCs	IFS-HRES
EPS	1+10 members, SLAF & surface perturbations

2.1 Deterministic performance

We present here point verification of the IREPS control member from the operational suite. Figure 1 shows statistics for 2 m temperature for July and October 2020. The model continues to show a cold bias, with strong daily variation. Post-processing using a Kalman filter is seen to ameliorate the cold biases somewhat.

Wind-speed results are shown in Fig. 2. On the top panel, forecasts during February 2020 are compared with observations for IFS-HRES and HARMONIE-AROME. The lower panel shows frequency biases during three named storms in February: Ciara, Dennis and Jorge. While HARMONIE-AROME exhibits more undesirable

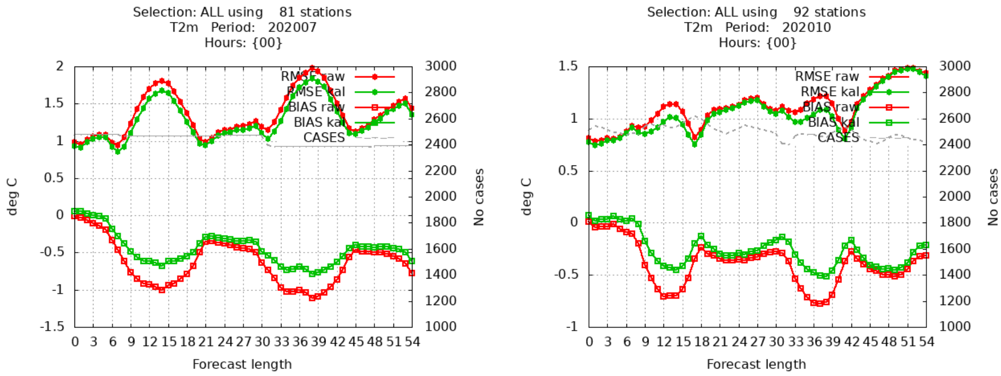

Figure 1: Point verification of the operational 2 m temperature forecasts for July (left) and October 2020 (right). The raw model forecast is shown in red; the Kalman-filtered post-processed data is in green.

variability and shows more of a positive bias at lower wind speeds, it is much more likely to capture the extremes for such windstorms.

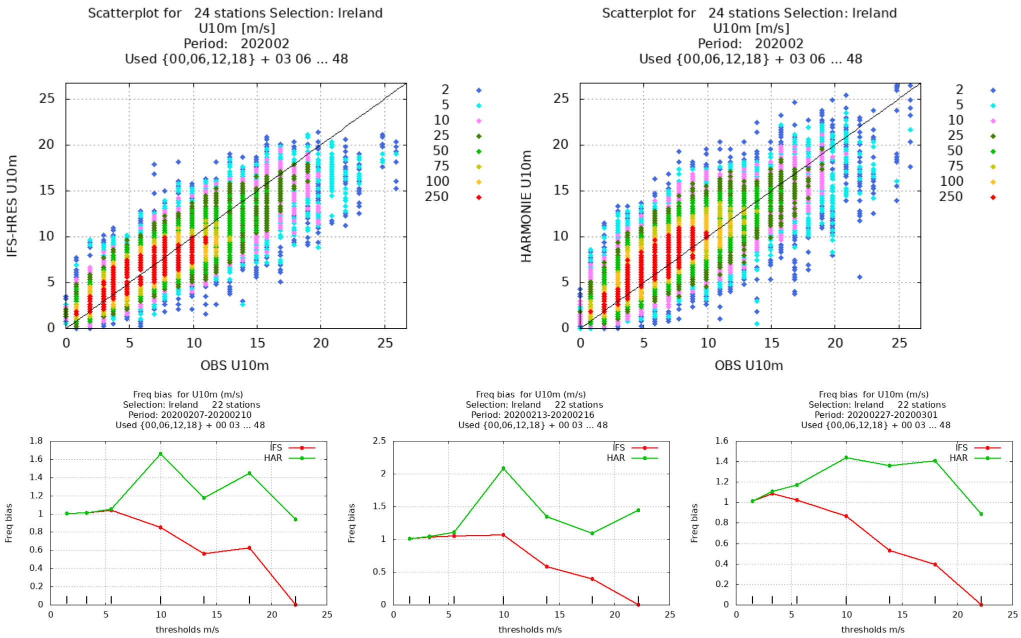

Figure 2: Point verification of 10 m wind forecasts from the operational suite. Above: scatter plots for February 2020 for IFS-HRES (left) and HARMONIE-AROME (right). Below: frequency biases during Storms Ciara, Dennis and Jorge.

2.2 Verification of IREPS

Probabilistic verification of IREPS is carried out using the latest version of harp (`https://github.com/harphub`), the ALADIN-LACE-HIRLAM 'software for NWP analysis, verification and visualization'. Below are two spread/skill plots illustrating IREPS' performance when compared to the ECMWF ensemble prediction system (EPS), IFS-ENS.

IFS-ENS continues to outperform IREPS when it comes to mean sea-level pressure (MSLP) scores. However, IREPS displays both increased spread and reduced error when compared to IFS-ENS for 10 m wind speed (see Fig. 3). The known negative 2 m temperature bias over Ireland in HARMONIE-AROME Cycle 40h1 typically leads to a degradation in IREPS performance relative to IFS-ENS which increases with forecast length. IREPS demonstrates a higher spread-skill ratio for 2 m relative humidity when compared to IFS-ENS.

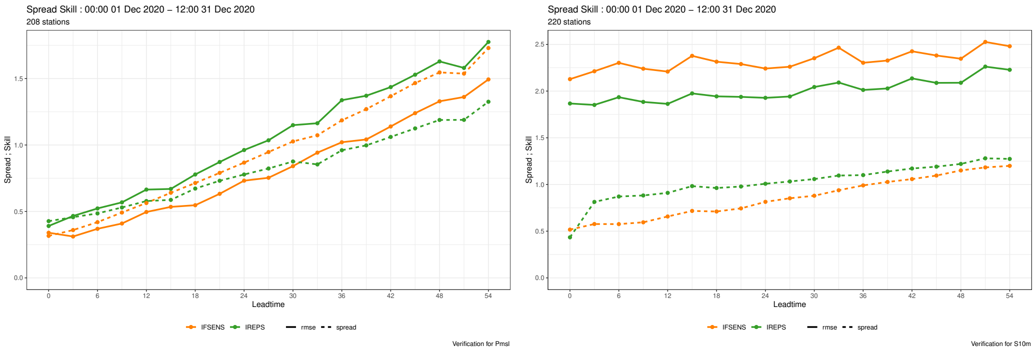

Figure 3: Spread-skill scores for mean-sea-level pressure (left) and 10m wind speed (right) for IREPS (green) and IFS-ENS (orange) for the month of December 2020.

3 Upgrade to Cycle 43

3.1 Initial Tests

Cycle 43h2.1 of HARMONIE-AROME was released by HIRLAM-C at the end of July, 2020 and more extensive testing for operational use by Met Éireann began soon after. The initial phase of testing consisted of four two-week long experiments, corresponding roughly with the four seasons, carried out using a 540x500 domain centred on Ireland. The results were compared with the default configuration of Cycle 40h1.1 in order to assess the general performance and highlight any significant biases. This phase of testing was also used to confirm the continued use of the quadratic grid.

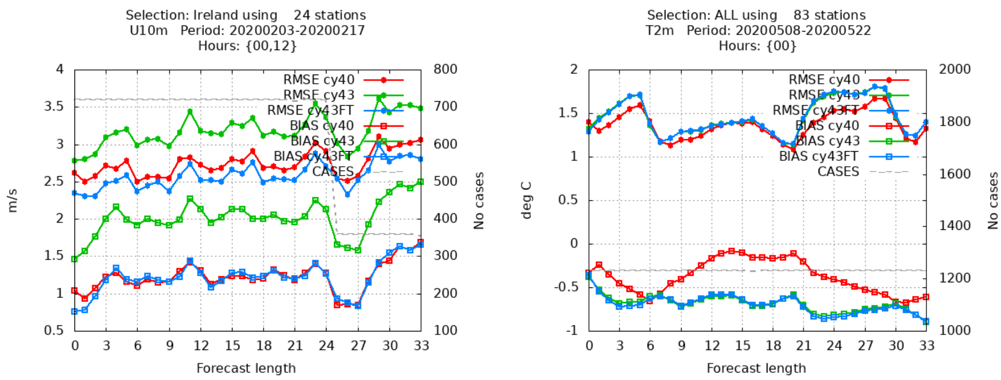

Figure 4: Point verification of wind-speed (left) and temperature (right) during the initial phase of Cycle 43 testing. The experiments are as follows: Cycle 40h1.1 (red), Cycle 43h2.1 (green), Cycle 43h2.1 with LFAKETREES=.TRUE. option (blue).

It was quite clear that, while many parameters showed broadly similar results, there was a much larger positive bias in 10 m wind speeds in Cycle 43h1. The LFAKETREES option, developed by Samuel Viana (AEMET), was found to be necessary to correct the bias. In Fig. 4 we see the strong effect of LFAKETREES on wind-speed, while not affecting 2 m temperature. The LFAKETREES option makes physical sense for our domain as ECOCLIMAP Second Generation classifies much of Ireland as grassland. Such a classification misses out on the fact that most fields in Ireland are surrounded by hedgerows and trees. LFAKETREES allows for a statistical reintroduction of such roughness elements reducing the model near-surface winds speeds appropriately.

3.2 e-suite preparation

Following the initial tests of the new release the use of observations by HARMONIE-AROME's 3D-Var data assimilation system and forecast model performance were evaluated using the larger operational (1000x900) domain.

With Cycle 43h2.1 comes the possibility to assimilate Metop-C radiances and data from MWHS2 and ATMS instruments. The assimilation of ATMS and MWHS2 data will fill early-morning gaps in radiance data. The availability of Mode-S EHS aircraft data (winds and temperatures) from the European Meteorological Aircraft Derived Data Centre (EMADDC) made it possible to test the impact of these data in an operational context. A test period in October/November 2020 was used to spin up the VarBC coefficients and evaluate the impact of these new observation types. Figure 5 shows the impact of assimilating non-conventional data (AMSUA-A, MHS, IASI, ATMS, MWHS2, and ASCAT) by HARMONIE-AROME Cycle 43h2.1 on the quality of MSLP forecasts. There were neutral impacts on the quality of near-surface parameters but moderately positive impacts in the lower atmosphere (not shown).

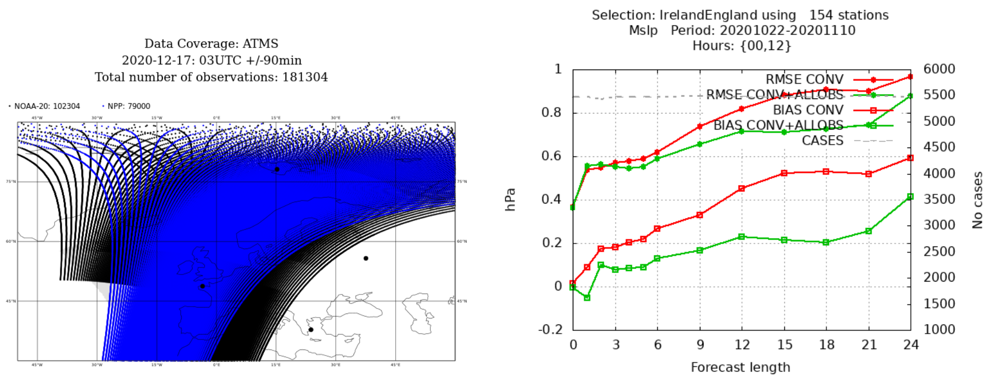

Figure 5: Left: Data coverage map of ATMS data from NOAA-20 and NPP at 0300 UTC. Right: MSLP forecast bias and RMSE for HARMONIE-AROME 43h2.1 assimilating conventional observations only (red) and assimilation of conventional and non-conventional observations (green).

A longstanding issue in HARMONIE-AROME has been the overestimation of fog, both in terms of its optical depth and extent. Work by many within the consortium led to a suggestion to reduce the land, sea and urban cloud droplet number concentrations (CDCN) used by default in the model. Further information on this is available at `https://hirlam.org/trac/wiki/Meetings/Physics/FOG2020`. Sample visibility output from our Cycle 43 e-suite (reduced CDCN) and Cycle 40 o-suite is shown in Figure 6. A notable decrease in regions with very low visibility can be seen in the e-suite compared to the o-suite. While fog was recorded at many of our synoptic stations the increased visibility in the e-suite is closer to observations than the very low visibilities forecast by the o-suite.

Despite the additions and adjustments made to Cycle 43h2.1, a significant bias in night-time 2 m temperature forecasts persisted. In previous cycles (37h1.1 and 40h1.1.) changes were made to surface data assimilation code in order to increase the response of lower layer temperatures to 2 m temperature increments. For this cycle it has also been necessary to apply this change using XSODELX settings in the SURFEX NAM_ASSIM namelist.

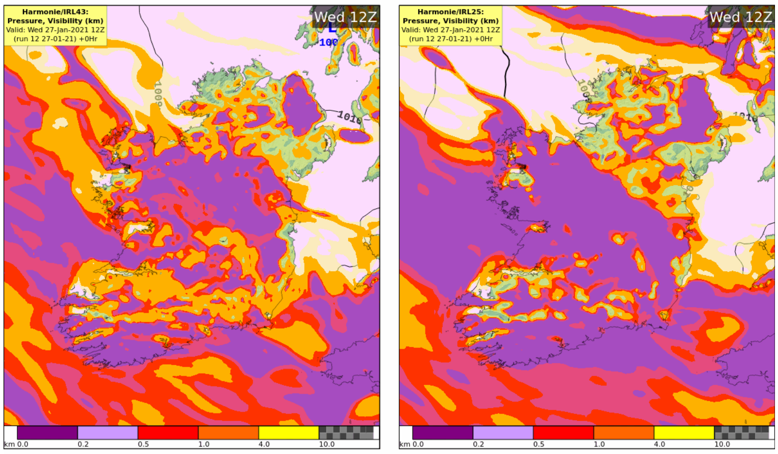

Figure 6: Visibility (m): (left) Cycle 43 e-suite. (right) Cycle 40 o-suite.

3.3 EPS configuration

The upgrade to Cycle 43 sees the introduction of a number of new perturbation techniques to IREPS as well as a lagged configuration that will produced a 1+15 member EPS updated every three hours. Initial condition perturbations have been included in the form of an ensemble of data assimilations (EDA). Using this approach, perturbations are applied to the assimilated observations which form part of the CCMA database. More technical details on EDA can be found in (Frogner et. al, 2019). The positive influence of EDA perturbations on ensemble verification scores can be seen in Fig. 7.

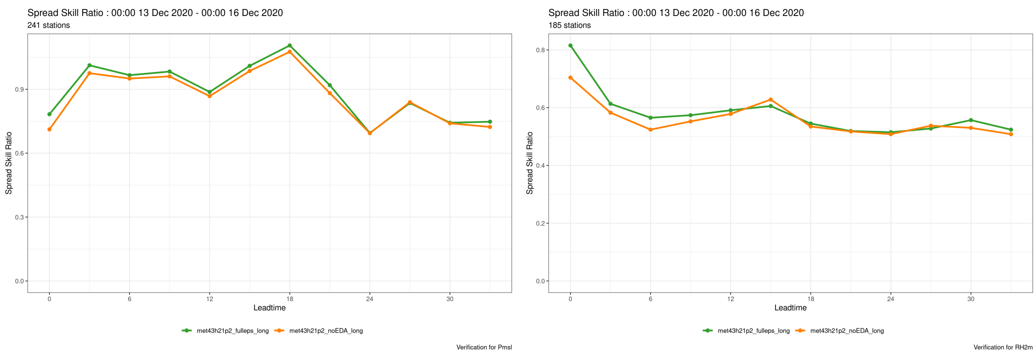

Figure 7: Spread-skill ratios for MSLP (left) and 2 m relative humidity (right) for an experiment with EDA (green) and without EDA (orange).

Other upgrades to IREPS include multi-physics perturbations (using various settings for CROUGH=NONE/OROT and XRIMAX=0.0/0.1/0.2) and the use of a total energy norm function for calculating the SLAFK coefficients (Keller et. al 2008). In general, the multi-physics settings gave satisfactory ensemble scores. However, using a setting of $\mathrm{CROUGH} = \mathrm{Z01D}$ produced a clear negative wind-speed bias. Therefore, the setting of $\mathrm{CROUGH} = \mathrm{Z01D}$ was omitted from the IREPS multi-physics perturbations.

3.4 Final proposed e-suite

Table 2 shows the final list of changes to the default settings used by Cycle 43h2.1, which were implemented in a parallel e-suite beginning on the 20th of January 2021. Some promising preliminary verification results are shown in Figs. 8 and 9 below. In Fig. 8 we see notable improvements in the biases of MSLP and 10 m wind-speed. Figure 9 suggests that the changes to the surface data assimilation described in the previous section have helped somewhat with the 2 m temperature forecasts.

Table 2: Changes from default Cycle 43h2.1 in proposed e-suite

Model Component	**Description**
Observations	CONV, MODES (winds only), AMSU-A, MHS, IASI, ATMS, MWHS2, ASCAT
Surface DA	XSODELX(0)=1.0, XSODELX(1)=2.0
Dynamics	Quadratic grid
Dynamics	LGWADV=T, LRDBBC=F (to control MSLP noise)
Surface	LFAKETREES=T
Surface	XRIMAX=0.0
Microphysics	CDCN=50
EPS	EDA, multi-physics, scale_pert=yes, WG perturbations off
EPS	Lagged 1+15 EPS: 1+10 at 0000/0600/1200/1800; 1+5 at 0300/0900/1500/2100 UTC

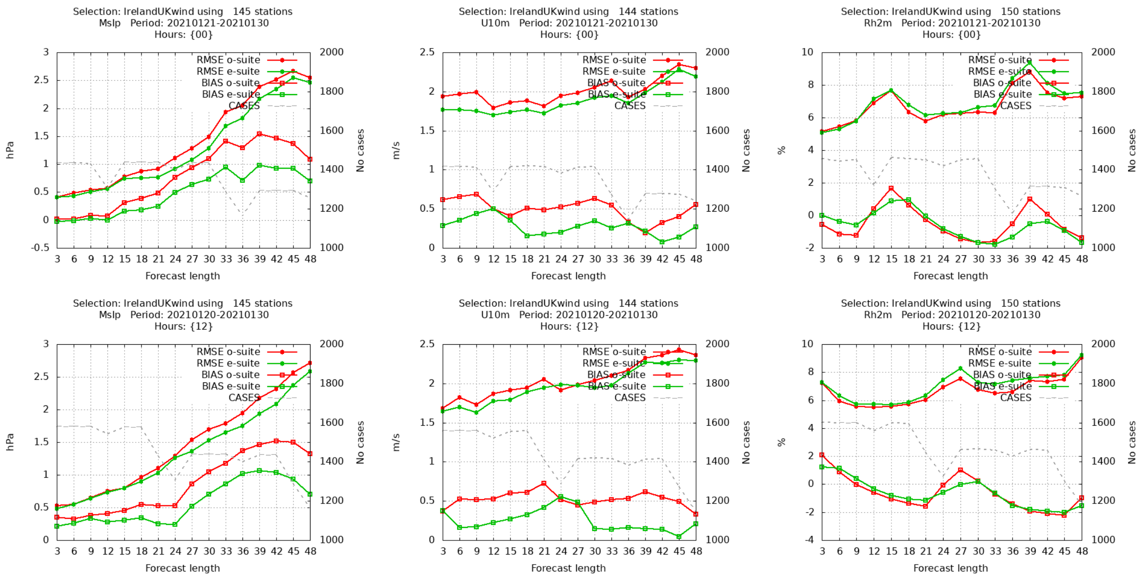

Figure 8: Verification at Irish and UK stations, comparing the proposed e-suite (green) with the operational o-suite (red) for the first week of parallel cycling. Shown are scores for the 0000 UTC (top) and 1200 UTC (bottom) cycles, for parameters (left to right) MSLP, 10 m wind-speed, 2 m relative humidity.

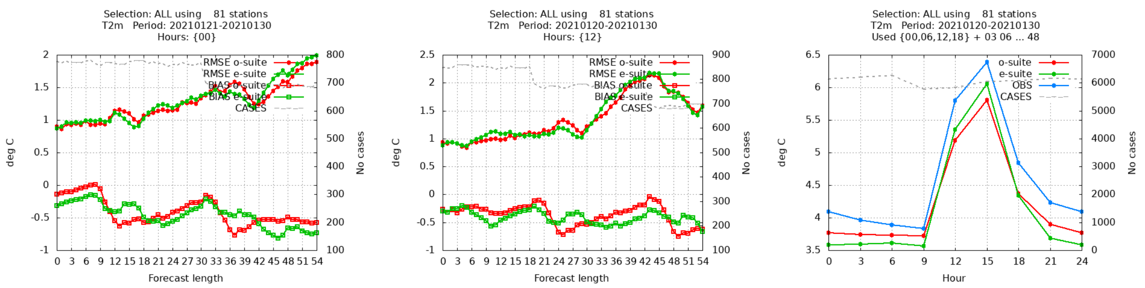

Figure 9: Verification of 2 m temperatures at Irish stations, comparing the proposed e-suite (green) with the operational o-suite (red) for the first week of parallel cycling. Shown are scores for the 0000 UTC (left) and 1200 UTC (middle) cycles, as well as the daily variation for all (right).

4 NWP Research Activities

4.1 Single precision testing

As part of our initial testing phase of HARMONIE-AROME Cycle 43h2.1, several experiments investigating the option to run HARMONIE-AROME in single precision (SP) were carried out. Some verification results for a two-week winter period experiment, for which only the Forecast model was run in SP, are given in Fig. 10. The SP option was found to have a neutral impact on the surface verification scores, with a slight degradation in the humidity at 700 hPa. Initial results suggested a run time reduction of $\approx 20\%$ when utilising the SP option. This option will be investigated further in Cycle 46h1.

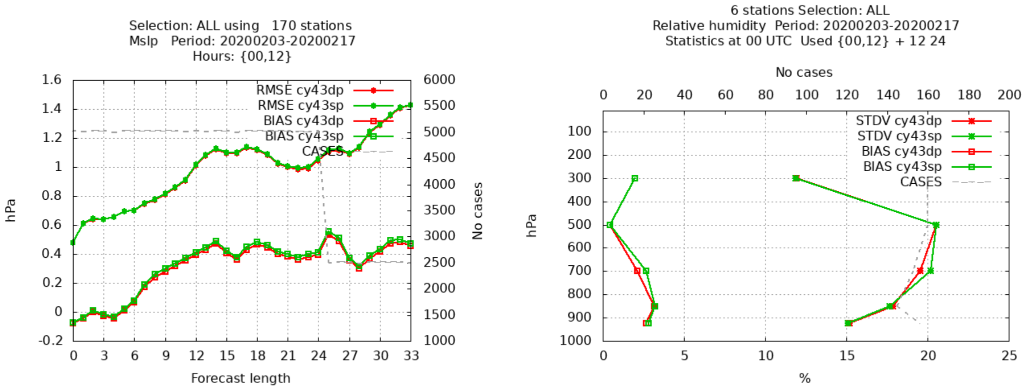

Figure 10: Verification results for MSLP (left) and RH sounding (right) comparing the Cycle 43h2.1 double precision (red) and single precision (green) experiments.

4.2 Fog studies

As described in the previous section, the forecasting of fog is an ongoing issue for HARMONIE-AROME. Met Éireann has dedicated staff resources to further investigate fog problems. Some initial tests involved an investigation of the effect of the different settings on fog development for some specific fog cases, compared to the default settings. One such fog case was an over-prediction of fog over land on November 6th, 2018 (Fig. 11 top-left panel). No fog was detected by satellite at that time (not shown). Cycle 43h2.1 showed a considerable reduction in fog over land compared to Cycle 40h1.1. A further substantial reduction in the fog extent was observed in Cycle 43h2.1 when CDCN was reduced to 50cm^{-3}. In contrast, the ACRANEB2 radiation scheme options slightly increased the extent of fog over land compared to the default Cycle 43h2.1. For a summer case (June 3rd, 2018) Cycle 43h2.1 predicted, on average, less sea fog over the Irish Sea throughout the day compared to the Cycle 40h1.1 (not shown). However, visibility diagnostic values at 1200 UTC (Fig. 12) suggest that local effects may play a role in fog development, as some locations show increases and some locations show decreases in the amount of fog over the sea in Cycle 43h2.1 compared to Cycle 40h1.1.

4.3 Physiography - Land Cover and Machine Learning

In summer 2020 Eoin Walsh, a data science PhD student from the University of Limerick, worked with us on creating a land cover map for Ireland using machine learning techniques along with Sentinel-2, CORINE and the BigEarthNet dataset. This work was important to us as we found deficiencies in ECOCLIMAP Second Generation (ECO-SG) for Ireland, mainly that too much of Ireland was classified as pure grassland.

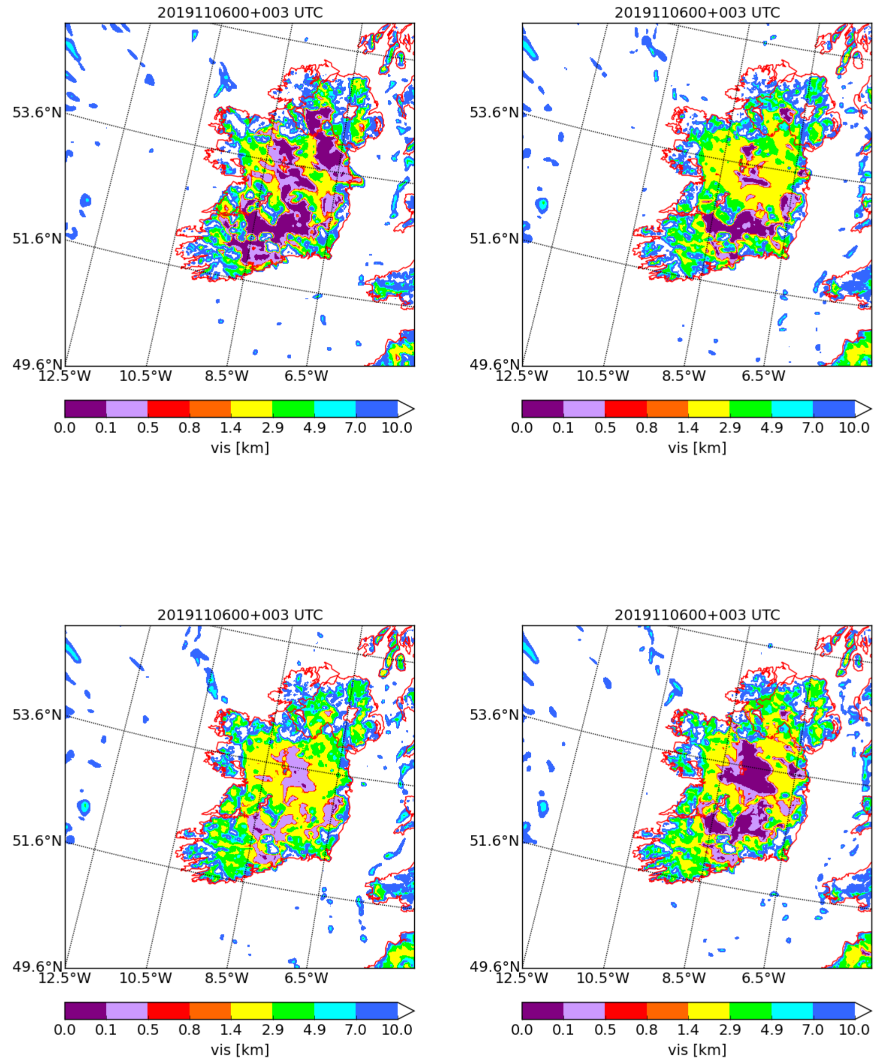

Figure 11: Visibility diagnosed at 0003 UTC Novemvber 6th, 2018 in the experiments: Cycle 40h1.1 (top-left), Cycle 43h2.1 (top-right), Cycle 43h2.1 with CDCN=50cm^{-3} *(bottom-left) and Cycle 43h2.1 with ACRANEB2 radiation scheme (bottom-right).*

A comparison between the Prime2 land-cover map (Ordnance Survey Ireland, 2014), considered to be Ireland's reference land-cover map (Green, 2015), and ECO-SG suggested that sparse urban areas are underestimated and instead appear as vegetation in ECO-SG (Bessardon and Gleeson, 2019). Figures 13 shows that grassland tends to be overestimated and appears in place of sparse urban areas and other vegetation. For example, everything within the white polygon is classified as grassland.

Recently, Ulmas and Liiv (2020) used a machine learning (ML) algorithm architecture, normally used mainly for computer vision tasks, called a convolutional neural network (CNN) to create a land-cover map over Estonia with CORINE labels using Sentinel-2 satellite imagery (Bertini et al., 2012). This method showed a capability of increasing the accuracy of CORINE which is estimated to be more than 85% accurate (European Environment Agency, 2017). This is superior to the 75.4% estimated accuracy of the ESA-CCI 2015 land cover dataset, the base map for ECO-SG (European Space Agency, 2017). This method can consequently significantly improve on the accuracy of ECO-SG and can produce a land-cover map at Sentinel-2 resolution (10 x 10 m)

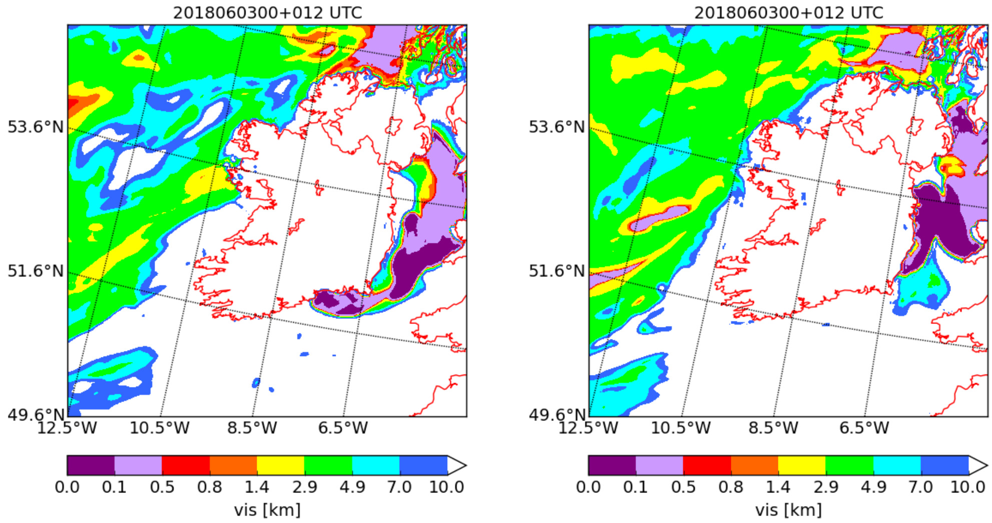

Figure 12: Visibility at 00UTC+012 on 03/06/2018 in Cycle 40 (left) and Cycle 43 (right).

Figure 13: ECOCLIMAP-SG covers (left) and Google Earth view (centre) around Ballyhaise (County Cavan) with a closer zoom (right) over the white polygon

which is 900 times higher than that of ECO-SG (300 x 300 m). The method has the potential to be used for any area covered by Sentinel-2 and offers the possibility of frequent updates to account for seasonal changes in land-cover.

Some sample results are included here. Figure 14 shows three land cover maps each plotted using CORINE primary land cover labels. The ECO-SG map is shown on the left, CORINE in the centre and the machine learning model predicted map on the right. A pixel-wise comparison showed that the predicted map is 92.6% similar to CORINE whereas ECO-SG is 89.8% similar to CORINE. This shows that, as expected, the predicted map is closer to CORINE than ECO-SG is, because it was trained using CORINE. However, it also shows that the model picked up different details through the Sentinel-2 imagery and some of the differences between the predicted map and CORINE are in fact correct in the predicted map.

Figure 15 shows a Sentinel-2 satellite segment of Killaloe/Ballina on the river Shannon (Ireland) and the corresponding ECO-SG and model prediction labels showing that the prediction represents the details of the area better thanks to its higher accuracy. Similar results and improvements were found when secondary land cover labels were used. Figure 16 shows the ECO-SG and the predicted secondary label map of Dublin. Again this figure shows that the model captures finer details than ECO-SG. For example, the Phoenix Park in the centre of the map clearly appears as forest in the model prediction while it is considered to be urban in ECO-SG.

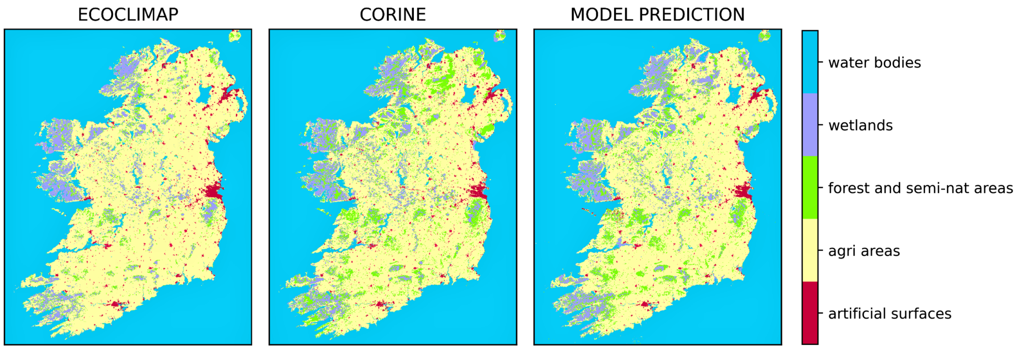

Figure 14: Land-cover maps of Ireland: (left) ECO-SG, (centre) CORINE and (right) the predicted map from the model. Pixel-wise, ECO-SG was found to be 89.8% similar to CORINE. The predicted map was found to be 92.6% similar to CORINE

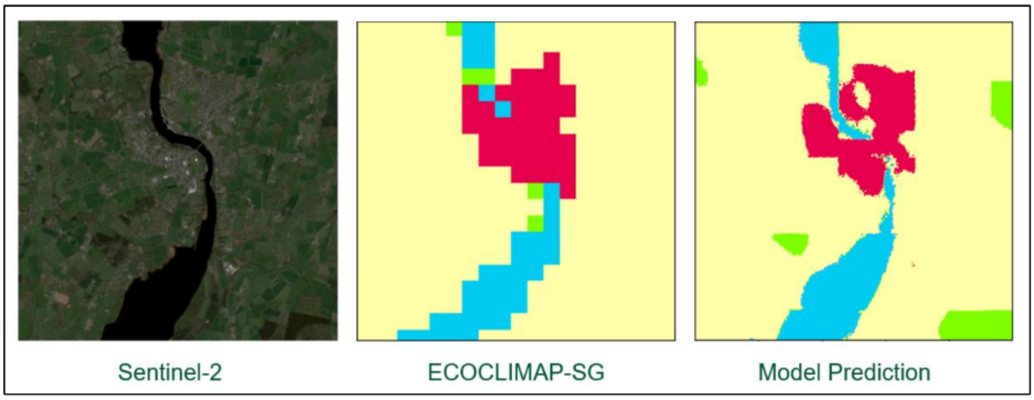

Figure 15: Sentinel-2 satellite image segment of Killaloe/Ballina on the river Shannon (Ireland), along with the corresponding ECO-SG and model prediction segment.

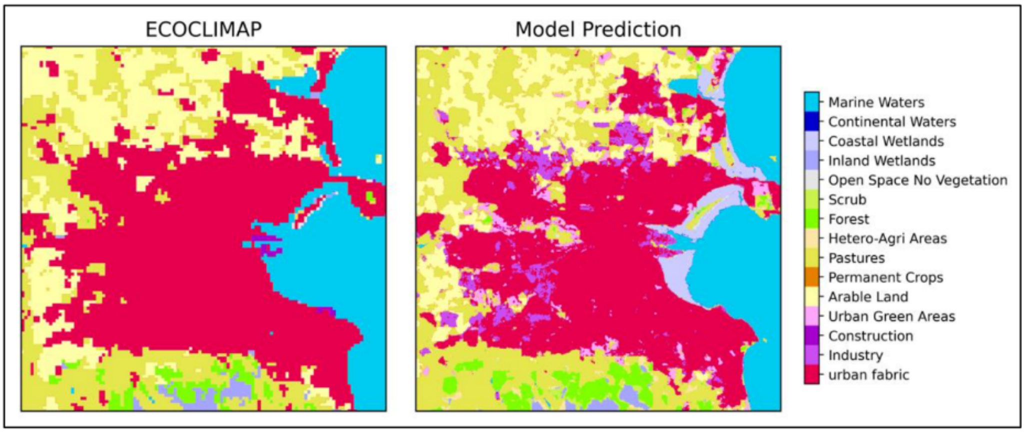

Figure 16: ECO-SG and the model prediction secondary labels for county Dublin.

Based on these results, the use of machine learning algorithms associated with satellite imagery is a viable method to improve ECO-SG accuracy and resolution. The method applied here is potentially applicable for any region covered by CORINE and Sentinel-2 imagery. A manuscript describing the method in greater detail, as well as presenting further analysis, was submitted for peer review and possible final journal publication in Advances in Science and Research (ASR).

Further work is ongoing for the application of the method with tertiary labels as well as over other HIRLAM regions. Further complementary machine learning work involving building heights and urban densities is underway in order to help with urban land cover labelling.

4.4 Surface roughness and machine learning

Initial tests of HARMONIE-AROME Cycle 43h1 indicated an overestimation of 10 m winds prior to the development of the LFAKETREES option. Results showed that over Spain this wind overestimation was associated with changes in surface roughness length (z_0). These changes in z_0 are due to the use of the ECO-SG physiographic map. This result led to ongoing work on z_0 tuning and redefinition (Viana Jiménez 2020). In physically-based roughness length models the incomplete physical understanding of z_0 led to the introduction of some critical constants for the quantification of z_0. These constants lead to considerable uncertainties. For example, in HARMONIE-AROME z_0 for grassland is defined by equation 1:

$$z_0 = 0.13 * LAI/6 \tag{1}$$

The value of 6 in Equation 1 is tunable - tests using values lower than 6 led to better results in Cycle 43h1 (Viana Jiménez 2020). Moreover, some of the underlying assumptions of physically-based models may not always hold in a real-world situations (Hu et al. 2020). These issues show the need for alternative solutions that fill gaps in the physical understanding and facilitate model input updates.

While further in-depth research on the surface roughness mechanism is needed, machine learning techniques offer an alternative solution to physically-based model limitations. A recent study combining satellite imagery from Moderate Resolution Imaging Spectroradiometer (MODIS) and surface fluxes measurements from the FLUXNET2015 dataset `https://fluxnet.fluxdata.org/data/fluxnet2015-dataset/` shows promising results. The data-driven surface roughness out-performed the physically-based models and improved the accuracy of turbulence flux estimations.

During a 12-weeks placement Dáire Healy (Maynooth University) trained a random forest machine learning algorithm following the Hu et al. 2020 method to estimate surface roughness length at Irish sites. This model was trained using 45 FLUXNET2015 stations and 5 Irish flux stations from the CelticFlux and CCFlux projects with land cover and LAI information from ECO-SG.

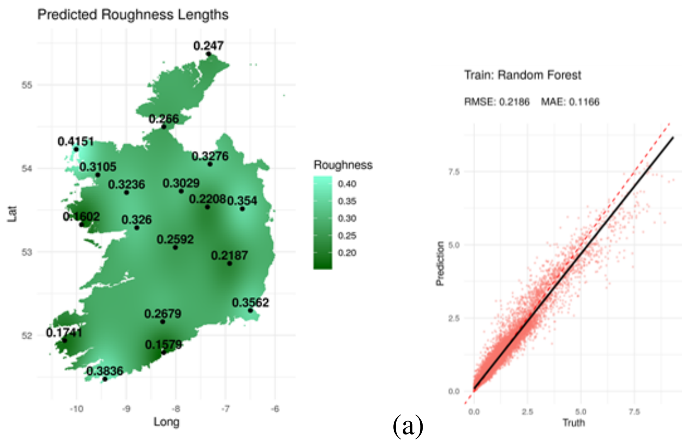

(a) (b)

Figure 17: Estimated roughness length at Irish Synoptic stations (a), Predicted values (prediction) against estimated z_0 values at all the flux stations used to train the algorithm (b)

Figure 17a shows the resulting estimated roughness map. While these values seem quite large, they are consistent with the high estimated z_0 values at the flux stations which were used to train the model. The result of a random forest prediction will always tend to have a bias towards its training dataset as it is considered as the truth. Consequently, additional analysis will be performed to make sure the estimated z_0 values used for this first simulation are relevant for the Irish synoptic stations. We also hope to investigate the use of satellite data regarding roughness lengths.

4.5 Post-processing EPS precipitation forecasts using machine learning

Post-processing of IREPS precipitation forecasts applies the use of fixed radius up-scaling (5 grid-points). This is carried out in order to overcome the 'double penalty' problem from which all high-resolution models suffer. However, uncertainty surrounds the number of grid-points that should be used in such up-scaling approaches.

During the course of a 12-week placement Tiziana Comito (University College Dublin) utilised various statistical and machine learning tools in order to uncover an optimum up-scaling radius for IREPS' precipitation forecasts. In particular, Tiziana investigated the appropriateness of a dynamical up-scaling approach as well as a hierarchical clustering technique based on a pattern recognition algorithm. The algorithms were tested on an IREPS dataset which contained summertime convective episodes.

Results demonstrated that the statistical and machine learning approaches were capable of out-scoring the operational fixed up-scaling approach (see Fig. 18). However, it was also concluded that the suitability of the approach depends strongly on the meteorological scenario in question.

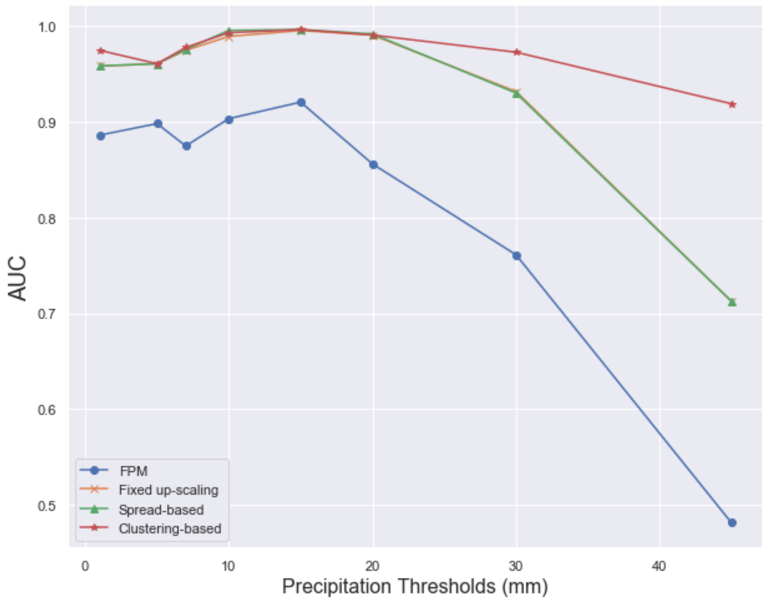

Figure 18: Area under the ROC curve (AUC) scores as a function of precipitation threshold for 24-hour IREPS precipitation forecasts for a case of summertime convection. The various curves represent raw model output (blue), current operational up-scaling (orange), a dynamical up-scaling approach (green) and a hierarchical clustering approach (red).

5 Summary and Outlook

Following a summer of exciting data science activity in Met Éireann, NWP staff started to prepare for the operational implementation of Cycle 43h2.1 during the second half of 2020. Following many tests, a few additions and some tweaks Cycle 43h2.1 was made ready for operational use by Met Éireann.

For 2021 it is hoped to further explore the possibilities provided by HARMONIE-AROME and the release of Cycle 43h2.2 in the areas of use of observations (GPS-RO, AMV, GNSS and Radar), data assimilation (4D-Var), EPS (Stochastically Perturbed Parameters (SPP), IFS-ENS LBCs and further explore multi-physics options) and forecast model settings (the ECUME6 sea flux scheme, review the CDCN changes, review model settings (LICERAD, LMIXUV) and the KPN LW cloud-liquid optical properties).

6 References

Bertini, F., Brand, O., Carlier, S., Del Bello, U., Drusch, M., Duca, R., Fernandez, V., Ferrario, C., Ferreira, M., Isola, C., Kirschner, V.,Laberinti, P., Lambert, M., Mandorlo, G., Marcos, P., Martimort, P., Moon, S., Oldeman, P., Palomba, M., and Pineiro, J.: Sentinel-2 ESA's Optical High-Resolution Mission for GMES Operational Services, ESA bulletin. Bulletin ASE. European Space Agency, SP-1322,2012

Bessardon, G. and Gleeson, E.: Using the best available physiography to improve weather forecasts for Ireland, in: Challenges in High-Resolution Short Range NWP at European level including forecaster-developer cooperation, European Meteorological Society, Lyngby, https://presentations.copernicus.org/EMS2019/EMS2019-702_presentation.pdf, 2019.

Bessardon, G., Clancy, C., Daly, C., Darcy, R., Gleeson, E., Hally, A. and Whelan, E., 2020: Met Éireann Updates. ALADIN-HIRLAM Newsletter No. 14.

European Environment Agency: Copernicus Land Service- Pan-European Component: CORINE Land Cover, https://www.eea.europa.eu/430data-and-maps, 2017.

European Space Agency: Land Cover CCI PRODUCT USER GUIDE VERSION 2.0, http://maps.elie.ucl.ac.be/CCI/viewer/download/ESACCI-LC-Ph2-PUGv2_2.0.pdf, 2017.

Frogner, I.-L., Andrae, U., Bojarova, J., Callado, A., Escribà, P., Feddersen, H., Hally, A., Kauhanen,J., Randriamampianina, R., Singleton, A., Smet, G., van der Veen, S., and Vignes, O. (2019). HarmonEPS The HARMONIE Ensemble Prediction System. Weather and Forecasting, 34(6):1909-1937

Green, S.: ILMO : Irish Land Mapping Observatory, https://www.teagasc.ie/media/website/publications/2016/6405-ILMO.pdf, 2015.

Hu, X., Shi, L., Lin, L. and Magliulo, V. 2020. Improving surface roughness lengths estimation using machine learning algorithms. Agricultural and Forest Meteorology. 287 (September 2019), p.107956 https://doi.org/10.1016/j.agrformet.2020.107956

Keller, J. D., Kornblueh, L., Hense, A., and Rhodin, A. (2008). Towards a gme ensemble forecasting system: Ensemble initialization using the breeding technique. Meteorologische Zeitschrift, 17(6):707–718

Ordnance Survey Ireland: Prime2 - Data Concepts & Data Model Overview, http://www.osi.ie/OSI/media/OSI/Prime2_Docs/Prime2-V-2.pdf, 2014

Ulmas, P. and Liiv, I.: Segmentation of Satellite Imagery using U-Net Models for Land Cover Classification, pp. 1–11, http://arxiv.org/abs/2003.02899, 2020.

Viana Jiménez, S. 2020. Experiments with roughness length ECOCLIMAP-SG (in Harmonie-Arome) In: Joint 30th ALADIN Workshop and HIRLAM ASM 2020 [Online]. Available from:http://www.umr-cnrm.fr/aladin/IMG/pdf/asm2020_viana_final_1_.pdf

ALADIN 1991-2020: 30 years of working together

including 3 years with HIRLAM (2018-2020)

Patricia Pottier

1 Introduction

This article aims at presenting the manpower invested in ALADIN (and HIRLAM in the last 3 years) from the point of the view of the manpower dedicated to work on the common system (as defined in the ALADIN MoUs); it is neither a financial nor a scientifical report.
For ALADIN, a full report is presented over the 30 years of ALADIN existence and manpower recording. Since 2018, the manpower dedicated to the realisation of the common ALADIN-HIRLAM Rolling Work Plans (RWP) has been recorded and some statistics are presented below.
These two kind of data (1991-2020 statistics of ALADIN manpower and 2018-2020 on common ALADIN-HIRLAM RWP) will be proposed to the 1st ACCORD Assembly for validation and update of the Annex VII (ALADIN and HIRLAM legacy codes and repartition of their IP) and Annex VII (Manpower provided by Members since the creation of the Common Manpower Register) of the ACCORD MoU.

2 ALADIN 1991-2020

People
ALADIN adventure was shared by 730 persons, some of them only joined for one week teaching or workshop, others spent on ALADIN most of their working time along the last 30 years, some have been fully dedicated to ALADIN during a more or long period; others have partially, but very regularly, contributed to ALADIN during years.
Biggest contributors:

- Radmila Brozkova (Cz) spent the equivalent of 26 years working on ALADIN
- 20 years' work: Luc Gérard (Be), Neva Pristov (Si), Claude Fischer (Fr), Patricia Pottier (Fr)
- 15 to 19 years' work: Andrey Bogatchev (Bg), Piet Termonia (Be), Alena Trojakova (Cz), Jean-Daniel Gril (Fr), Ryad El Khatib (Fr), Thibaut Montmerle (Fr), Alex Deckmyn (Be)

Most faithful ALADINers:

- Radmila Brozkova (Cz) was there for ALADIN during the whole 1991-2020 period, together with Marek Jerczynski (Pl) and Alain Joly (MF), although Marek only dedicated half of his working time to ALADIN and Alain's contribution was smaller but very stable.
- 25 year ALADINers: Maria Derkova (Sk), Neva Pristov(Si), Jozef Vivoda (Sk), Oldrich Spaniel (Sk), Eric Bazile (Fr), Patricia Pottier (Fr), Andrey Bogatchev (Bg), Ryad El Khatib (Fr), Patrick Le Moigne (Fr).

"Full-time" ALADINers:

- besides the above mentioned colleagues, some ALADINers have contributed on shorter periods (as they joined later or left before 2020) but on a quasi "full-time' basis during those periods: Joël Hoffman (Fr), Cornel Soci (Ro), Jan Masek (Cz), Daan Degrauwe (Be), Pierre Brousseau (Fr), Bart Catry (Be), Jean-Daniel Gril (Fr), Florian Meier (Au), Filip Vana (Cz) …

The number of F.T.E. invested in ALADIN (fig.1) kept growing during these last 30 years, with around 100 F.T.E. during the last MoU (2016-2020), with an average partial time of 50%.

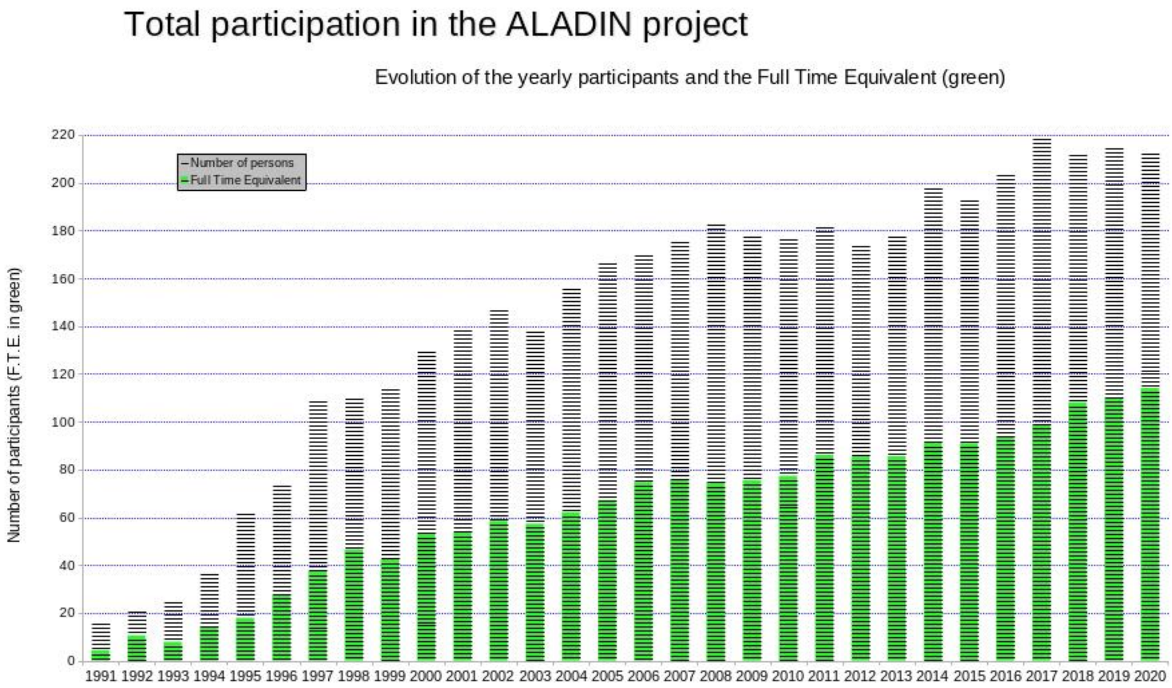

figure 1: evolution of the number of ALADINers and F.T.E

Working together of course also means meeting regularly (also with HIRLAM colleagues), i.e. at the annual Workshops in nice places or virtually (fig.2: in-situ meetings and covid-free virtual room).

figure 2: Annual meetings: people behind the manpower and F.T.E statistics !

Teams at Partners

The 16 Partners have contributed to the common work: the repartition of the IPR of the ALADIN legacy codes is based on the accumulated statistics since 1991 (fig.3). *Note: in Annex VIII, the statistics are "re-partitioned": the manpower funded by ALADIN, i.e. the Code Architect and the DAs-KIT coordinator, is not accounted as manpower of the NMSs who employ them but is distributed over the 16 ALADIN Members with the same weight as all 16 Members contribute the same to the ALADIN budget who pays these positions (these funded positions represent only 1/1000 of the total manpower).*

Figure 3:

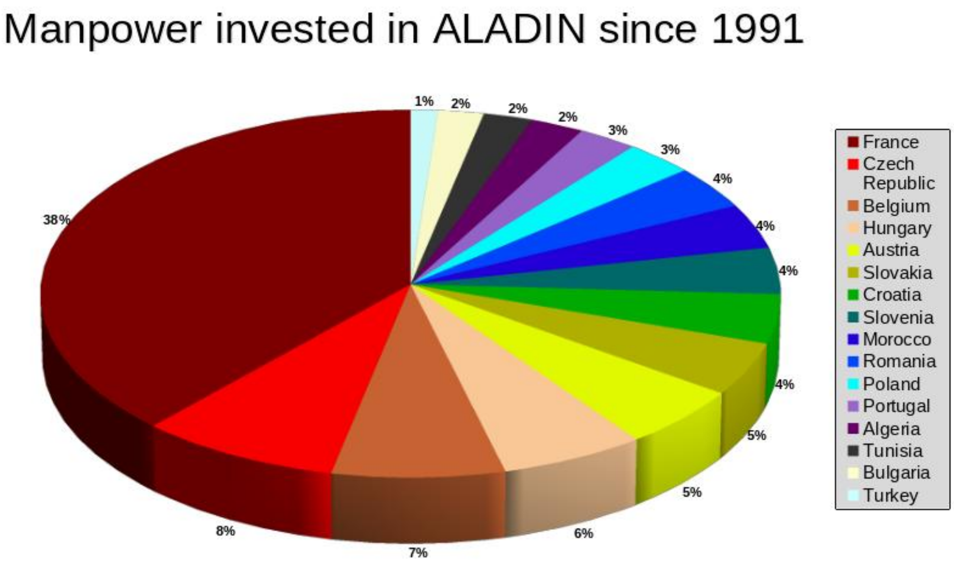

Breakdown of the manpower invested in ALADIN by Partners since 1991

These accumulated statistics may give a distorted view for the last countries who joined ALADIN more recently. See fig.4 for the statistics during the last five years (MoU5 period), for the F.T.E. and for the number of people involved.

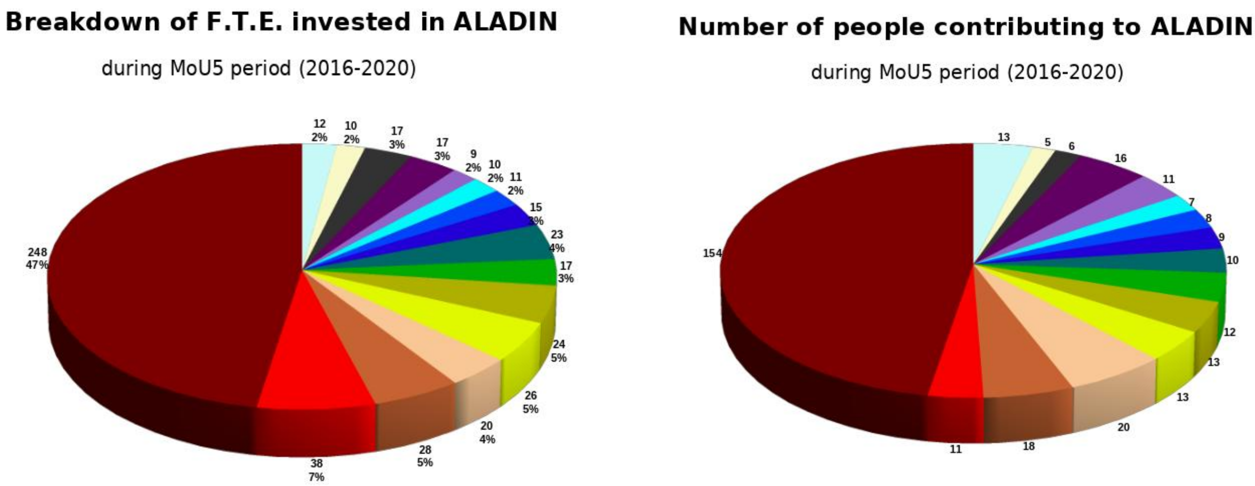

Figure 4: F.T.E. reported in ALADIN during MoU5 (left) and number of people involved (right) by Partners (with the same colour and in the same order than in the figure 3)

Families

ALADIN was composed of 3 families (or groupings):

- LACE Partners: initially composed of 6 Partners (Austria, Croatia, Czech Republic, Hungary, Slovakia, Slovenia), then Romania joined in 2007 and Poland in 2020,
- Flat-Rate countries: initially composed of 9 Partners (Algeria, Belgium, Bulgaria, Morocco, Poland, Portugal, Romania, Tunisia, Turkey), 7 in 2020 (with Romania and Poland in LACE),
- Météo-France.

The distribution of the manpower among these 3 components of the ALADIN Consortium evolved over (fig.5) but, it can be roughly considered that each of them contributed to 1/3 of the accumulated manpower (fig.6). Note that the contribution of Romania and Poland is accounted for as Flat-Rate countries before they joined LACE, and as LACE from 2007 and 2020, respectively.

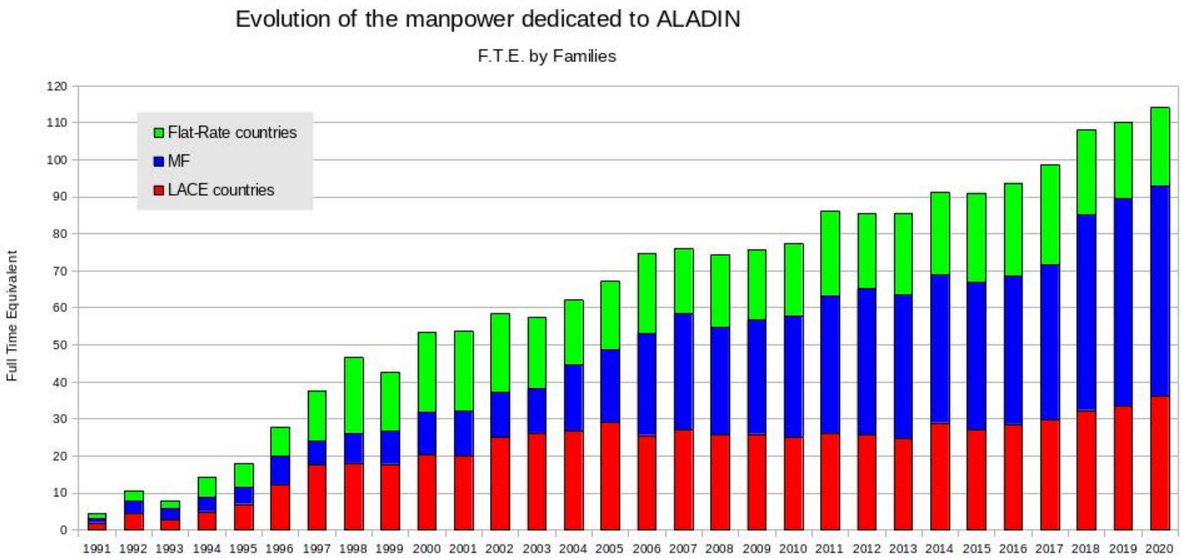

Figure 5: Distribution of the manpower over the years, by families

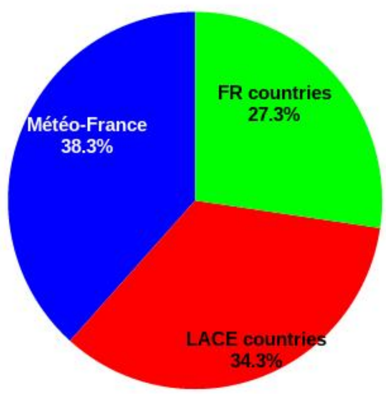

Figure 6: Breakdown of the accumulated manpower (1991-2020) by ALADIN components

Characteristics of the work

In 2001, new criteria were added to the manpower registration and accounting to characterise the registered manpower:

- Around ¾ of the reported work was done on the code/system, with potential benefice for all Partners whereas the maintenance of the local applications represents less than 20% (fig.7);
- Half of the work consists in R&D and 40% of the manpower is dedicated to more technical work (operational, maintenance, validation); the management represents 8% and a regular effort is done for capacity building (training/tuition)v(fig.8).

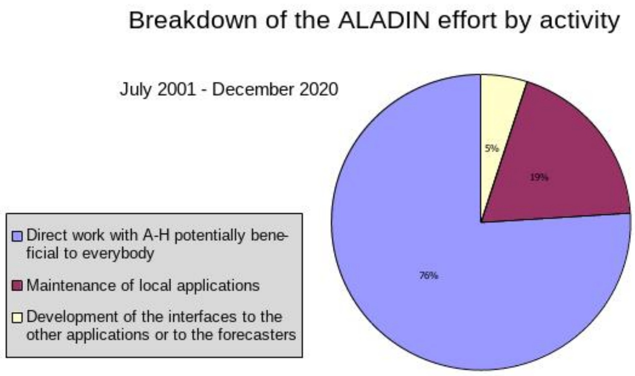

Figure 7: Scope of the ALADIN effort

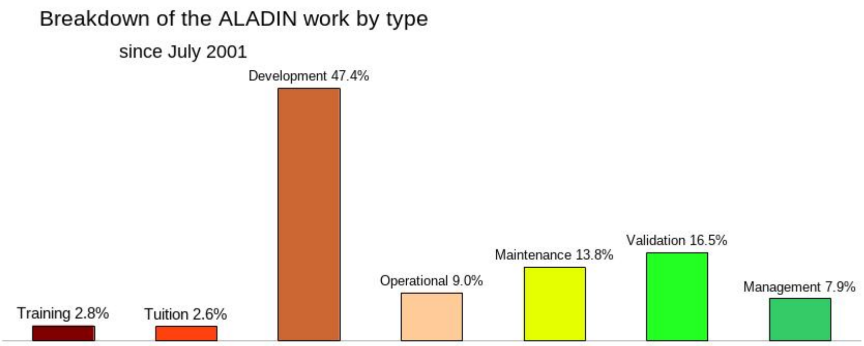

Figure 8: Type of the work reported in ALADIN framework

3 ALADIN-HIRLAM Rolling Work Plans: 2018-2020

ALADIN-HIRLAM-LACE Rolling Work Plans 2018-2020

In 2017, in the framework of the ALADIN-HIRLAM convergence towards a single consortium, the structure of the common Work Plan was renewed to describe the activities with a high level of details, with an organisation in Work Packages and tasks. A tight schedule (fig.9) follows the life of the Work Plans, from their redaction, the commitments from Partners to work on their different tasks, the manpower reporting and the assessment of their realisation. Besides the teams working along these plans and the redactors many people and bodies are involved in this process: PMs, HMG-CSSI, PAC-HAC, LTMs, Assembly and Council, …

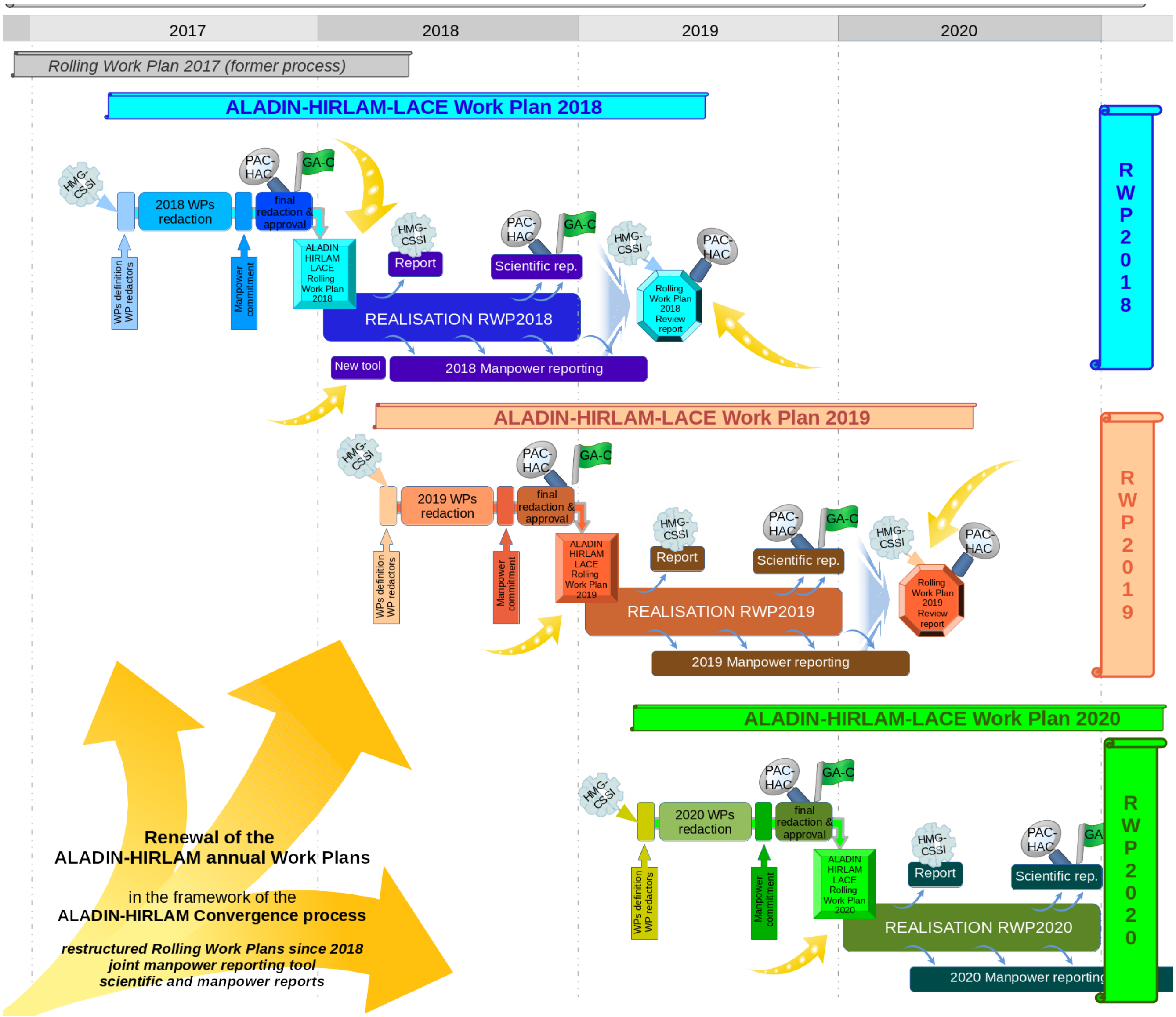

Figure 9: Preparation and assessment of the 2018-2020 Rolling Work Plans (the preparation of the RWP2021 is not included in this figure but took place according to a similar time-line as the previous RWPs, with additional input from the Strategy Workshop organised in February 2020

Common Manpower Register

Since 2018, the RWPs are supported by a Common Manpower Register containing the commitment of manpower from all Members (commitments are made annually) and the realization of the effort (monitored every three months). With this new tool, it is possible to estimate the distribution of the manpower by Work Package and to compare with the commitments.

In the ACCORD consortium, for important decisions, the relative manpower contributions to the Consortium during the last eight years, as measured by the common manpower register, will be taken into account in determining majorities. For the initial years of the Consortium, the scale of manpower contributions of Members in the ALADIN and HIRLAM consortia since the start of the common monitoring in 2018 will be used. *Note: in the MoU, these statistics are "re-partitioned": the manpower funded by ALADIN or HIRLAM is not accounted as manpower of the NMSs who employ the funded people but is distributed over the ALADIN, respectively the Members with the same weight in ALADIN as all 16 Members contribute the same to the ALADIN budget who pays these positions, with a weight proportional to the Members contribution to the HIRLAM budge*t. Fig.11 illustrates the effort done by each Partner (independently of the funding, thus before re-partioning). Fig.12 summarises these statistics by main components of the ACCORD Consortium (HIRLAM, and the three ALADIN components: Flat-Rate Partners, LACE Partners, Meteo-France).

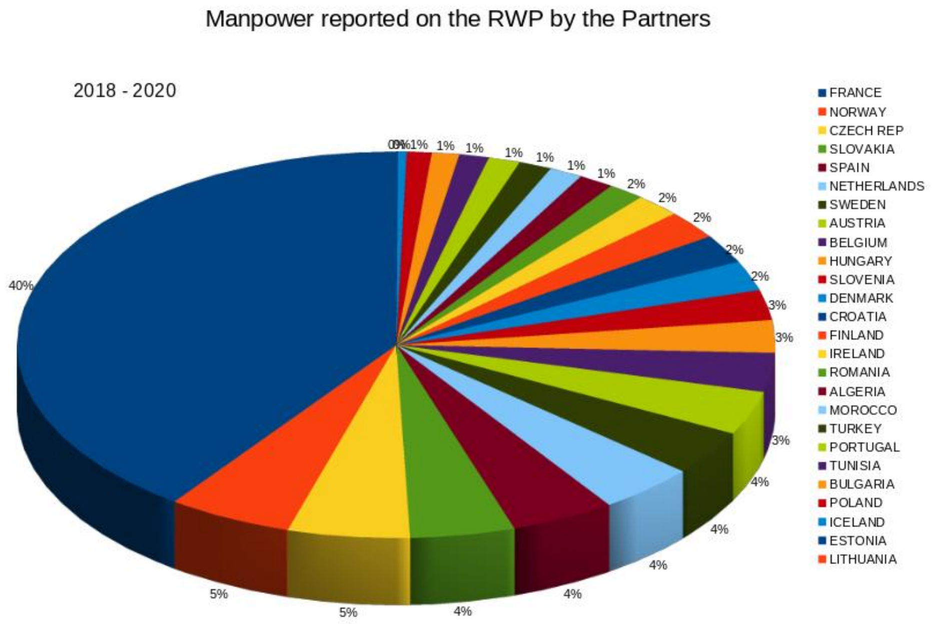

Figure 11: Accumulated Manpower dedicated on the RWPs in 2018, 2019 and 2020, by Partners

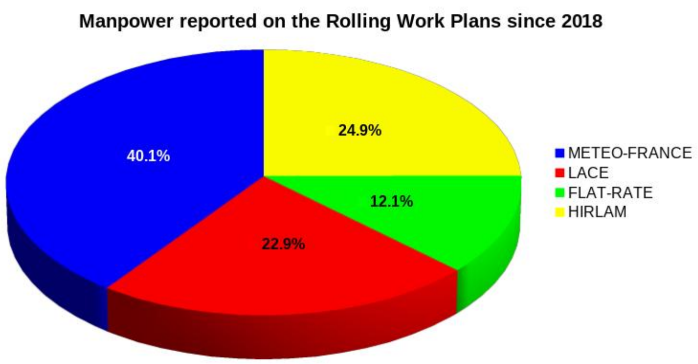

Figure 12: Accumulated Manpower dedicated on the RWPs in 2018, 2019 and 2020, by Groupings

Commitments and Realisation of the 2018-2020 Work Packages

The manpower committed to the RWP2018-19-20 has been compared with the manpower registered between 2018 and 2020 by the ALADIN and HIRLAM Partners (Fig.13). More work is realized than what was committed (as explained above, the preparation of the RWP follows a tight schedule and the teams may be cautious when committing for the following year in September when their internal plans and staffing are still locally under discussion).

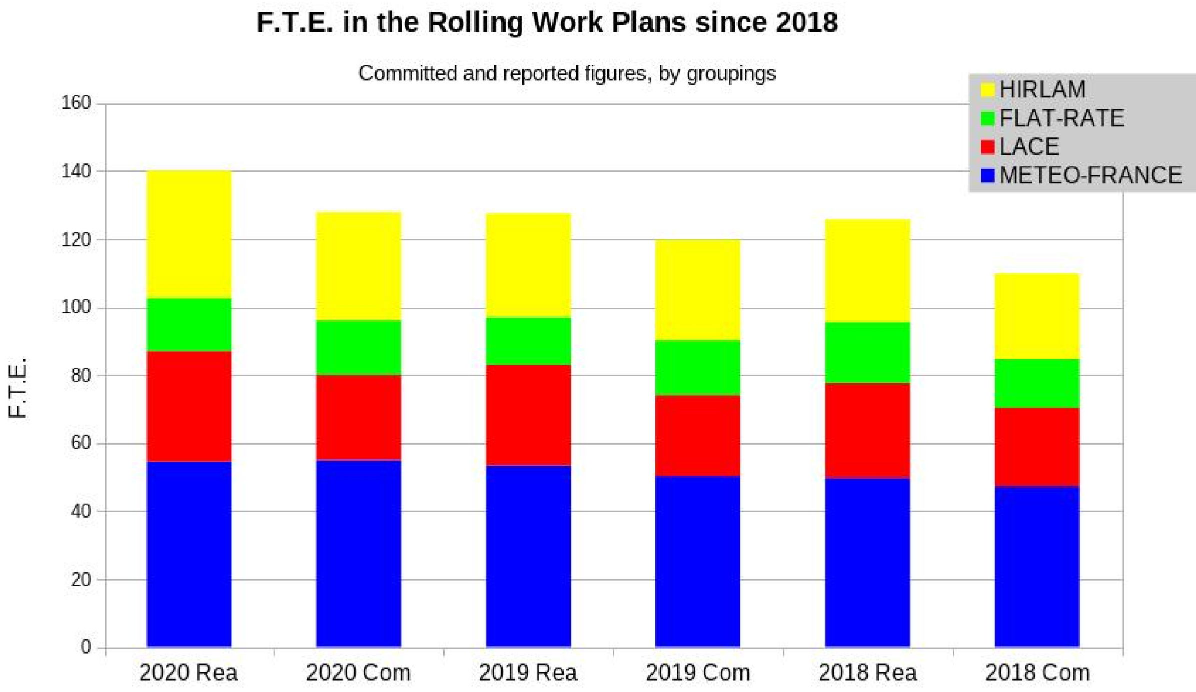

Figure 13: Comparison between the commitments and the reported manpower, by year

Precise commitment and reporting is done for each Work Package of the RWPs. The staffing of each WP is presented for 2020 (fig.14), with both commitments and realisation and over the whole 3 year period with the Work Packages grouped by thematic (fig.15): details inside the Work Packages differ between the 2018, 2019 and 2020 RWPs, new Work Package were added, some were removed, but the big thematics remained the same.

Three types of activities were distinguished in the three main parts of the RWPs:

- Management and support activities,
- Common activities on code design and engineering, generation of new CMC code and subsequent maintenance, general support provided to local implementations and troubleshooting, training,
- two strategic (core) programs: one on the scalability and efficiency of the dynamical core (with Work Packages grouped under SP dynamics) and one on providing a basic data assimilation setup for all members (Work package: SP data assimilation).
- Prospective R&D and/or operational activities described in the form of a set of work packages for each of the main areas of development: data assimilation, dynamics, physics parametrizations, surface analysis and modeling, ensemble forecasting, very high resolution modeling, quality assurance and technical code and system development. al

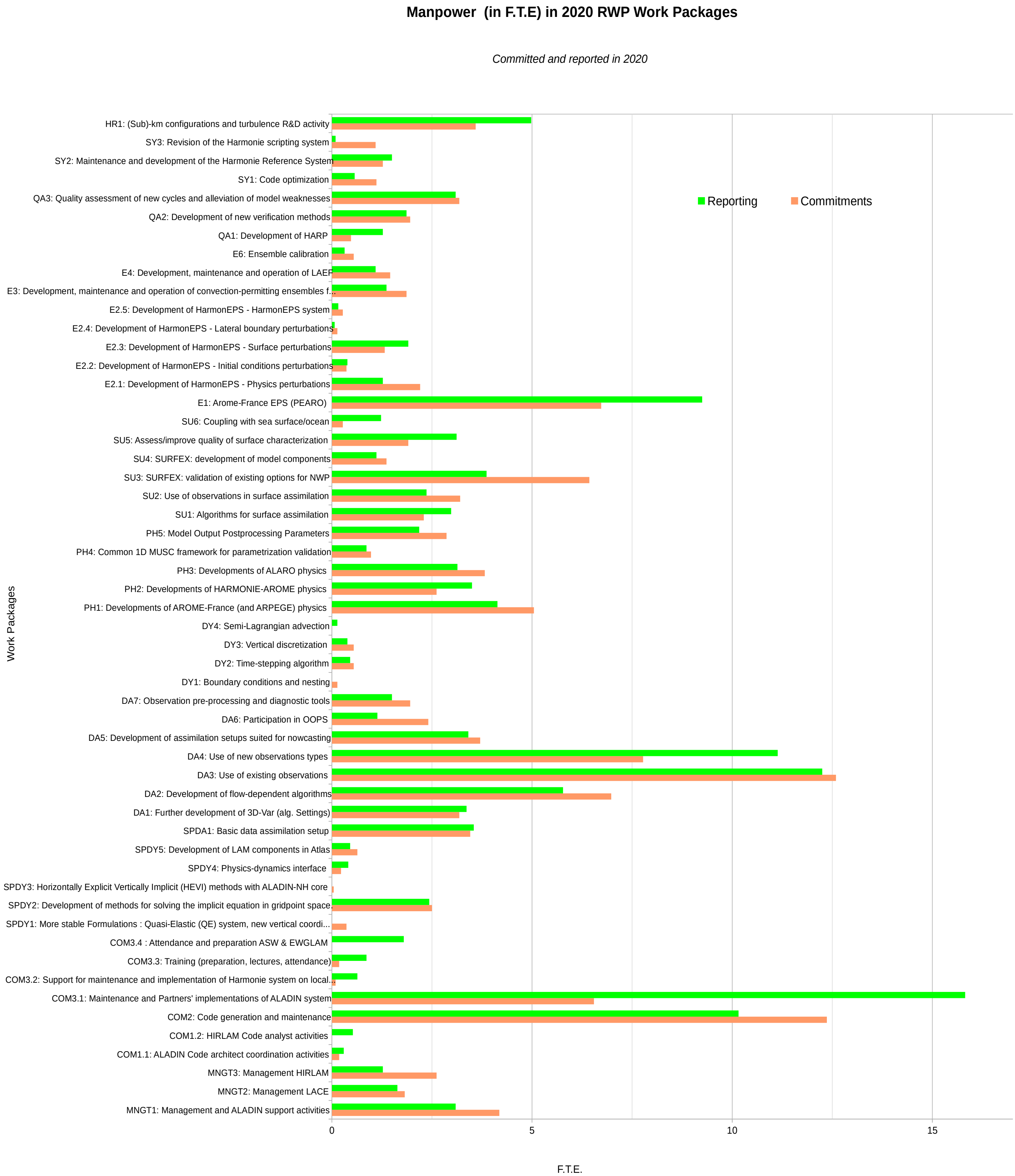

Figure 14: F.T.E. committed and reported on the Work Packages in 2020

Figure 15: accumulated F.T.E. committed and reported in 2018, 2019 and 2020 (Work Packages grouped by thematic)

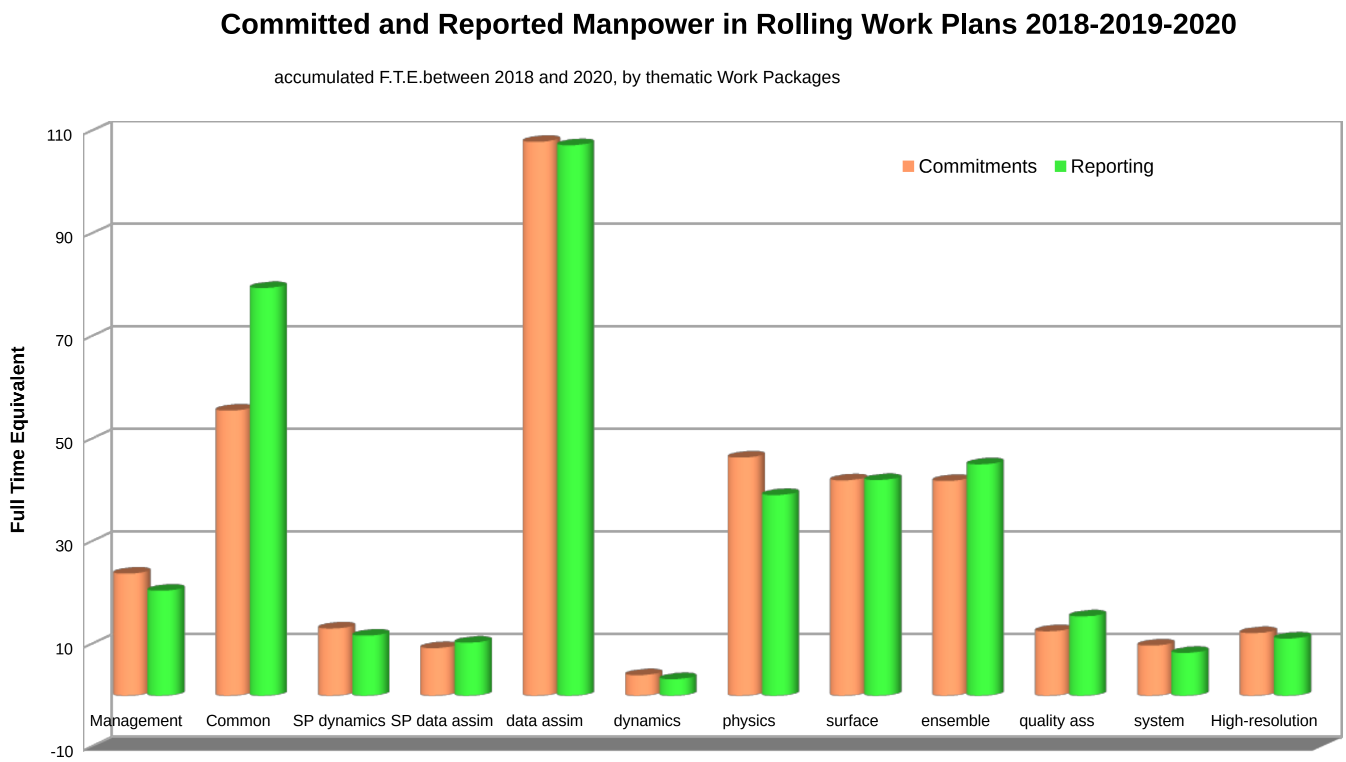

In memory of José Antonio García-Moya

Ernesto Rodríguez, Beatriz Navascués, Jana Sánchez, Javier Calvo, Inger-Lise Frogner and Jeanette Onvlee

It was only two days before of Christmas Eve that we were shocked by the sad news that José Antonio had passed away as a consequence of being hit by a car while he was cycling around the city of Santander, Spain, where he used to spend long stays. He was very well known and respected among the European community working on limited area modelling, a field in which he developed most of his professional career. José Antonio had a degree in Physics and a M.Sc. in Meteorology and Geophysics from the Universidad Complutense in Madrid when he was recruited in 1980 by the Spanish Meteorological Service (INM), the predecessor of the current agency AEMET. He moved to Majorca where he initially served as observer, soon afterwards as forecaster and then as head of forecasting at the INM Balearic Islands Regional Centre. There, he familiarized himself with the vagaries of Mediterranean meteorology, in particular the generation of cyclones so different from the well-studied midlatitude cyclones associated with air masses and frontal systems. His interest for atmospheric modelling brought him back to Madrid where he integrated in the INM NWP unit.

After the incorporation of Spain into the HIRLAM consortium, Jose Antonio's work was decisive for the operational implementation and first tests of the HIRLAM model in the INM high performance computer. His first contributions to model development, as a continuation of his previous interests, were related to improving the description of convective processes. However, his main efforts in the last 20 years were in the field of regional probabilistic forecasts. Jose Antonio assumed the task of leading a small group at AEMET for the development of short range probabilistic forecasts, based on a multi-model multi-boundary approach that afterwards evolved towards a meso-ϒ scale system. When in 2005 HIRLAM and ALADIN signed a collaboration agreement, Jose Antonio also faced the new challenge of contributing to this cooperation (mainly in the area of predictability), and to the implementation of the new HARMONIE modelling system at AEMET. He is very well known in this field both at European scale, where he coordinated the first EUMETNET program for the development of short range ensemble prediction system (SRNWP-EPS), and overseas.

Jose Antonio has been a key person for the continuity and maturity reached by the AEMET NWP team over the years, but he has also contributed significantly to many other AEMET R&D activities which he led for some time. In this respect, he was convinced of the benefits brought by international interaction and scientific cooperation, and he always promoted this in all fields as the way to ensure the provision of the best meteorological services. In particular, he was proud of the achievements in AEMET produced by the collaboration within HIRLAM, and highly appreciative of the excellence of ECMWF, an organisation that he always admired and saw as an example to follow.

In the HIRLAM EPS team he is remembered as a pioneer in LAM EPS in general, and in multi-model LAM EPS in particular. He had a deep understanding of both theory and practical applications, and was always very active and enthusiastic in discussions. Jose Antonio was at almost every HIRLAM EPS working week, and his colleagues remember many nice dinners and excursions, from Mount Teide in the south to Tromsø in the north. Even a few days before his retirement he was still taking an active part in a discussion about the future of ensemble systems.

Apart from his scientific, technical and organizational abilities, Jose Antonio was very much appreciated and respected for his enormous human qualities. All those who have collaborated with him knew his energy, optimism, hard work and determination. Even when tasks represented a great challenge of effort and coordination, his perseverance never ceased until he achieved the objectives he had set. He also demonstrated to be a very good friend to some of his closer collaborators when they needed him. Jose Antonio was a knowledgeable, enthusiastic and inspiring colleague for the LAM

EPS community in Europe, and in HIRLAM in particular. He was a warm and generous colleague you could trust.

After his voluntary retirement in 2018, he diversified his activities in many different fields: sports (mostly cycling), travelling, writing fiction books, following on-line courses on very different topics, activity in social media, and overall enjoying family life. Nevertheless, he still liked to follow up on everything that happened in the European NWP community that he knew so well. Only a few months ago, he said that he had been very lucky in his professional career because he had enjoyed his work so much, but that now, being retired, he was also living a very happy and satisfying life.

We have received plenty of messages coming from many people from different European countries expressing their condolences. Many friends and colleagues have reminded us of their experiences lived with him that underline the different aspects of his rich personality. We will miss Jose Antonio's smile, humour and enthusiasm. We want to record the most meaningful and emotional memories and the admiration that he has left among all of us.

In Tromsø on his birthday during the EPS working week in May 2017. Source: Inger-Lise Frogner.

Jean-François Geleyn and the numerical weather forecasting

Pascal Marquet (Météo-France/CNRM/GMAP)

1 Introduction

There is no need to recall here who Jean-François Geleyn was or how much he influenced and counted for so many people of ALADIN and HIRLAM teams! However, it may be worth mentioning that a special issue of the French journal “La Météorologie” will be published in February 2021, following the symposium held on 6 February 2020 at the International Conference Centre (CIC) in the Météopole at Toulouse in honour and memory of Jean-François Geleyn, 5 years after his death on 8 January 2015 at the age of almost 65.

Jean-François Geleyn in December 2010 at the 15th Aladin Programme Assembly in Prague, which coincided with the 20th anniversary of the launch of the Aladin project and the departure of Jean-François as programme manager.

More information on this day at the CIC can be found on the website http://www.meteo.fr/cic/meetings/2020/JFG/. As for the oral presentations (PDF) they are available on the ALADIN page http://www.umr-cnrm.fr/aladin/spip.php?article349, as well as videos of the presentations and a slide-show describing the testimonies of many people who knew Jean-François.

2 The 13 papers

The whole set of papers of the special issue of the French journal “La Météorologie” may enable those who knew this eminent researcher, manager and professor, but also those who did not, to appreciate the importance of his work, which had a strong impact since the 1970s on the development of many weather forecasting models in France (Émeraude, Peridot, Arpège and Aladin) as well as elsewhere in Europe (ECMWF model in the United Kingdom, other Aladin models in several other European and African countries).

In the first paper, Olivier Moch explains how necessary it was to honour Jean-François. This is the testimony of a student who was at the same time as Jean-François in the prestigious Ecole Polytechnique (still in Paris in 1968). Jean-François was also admitted to the no less famous Ecole Normale Supérieure (Ulm) in Paris, at the age of 18 and two years ahead of most other students. All this already showed Jean-François’ remarkable intellectual abilities, as many of us have witnessed since then.

The paper by Daniel Rousseau, Michel Jarraud and Pascal Marquet describes the first scientific actions by Jean-François. After he joined “la Météorologie Nationale” (which later became Météo-France), the career of Jean-François began with a key internship at the University of Mainz in Germany (1973-75), where he trained in the parameterisation of atmospheric radiation, a subject that has accompanied him until the 2010s. Jean-François returned to Paris in 1975 to the “Dynamic Meteorology Group” (GMD) to work on radiation in all models of “la Météorologie Nationale”. He then joined the ECMWF in July 1976 in Reading, UK, where he remained until December 1982. It should indeed be remembered that Jean-François was one of the actors who determined and developed the first ECMWF models.

The next paper written by Jean Coiffier, Régis Juvanon du Vachat and Jean Pailleux describes the period from the beginning of 1983 to September 1991 when Jean-François returned from the ECMWF to join the “Centre de recherche en météorologie dynamique” (CRMD) in 1983 and, from 1985 onwards, to head this CRMD, in order to work on the development of the Émeraude (global) and Péridot (limited area) models. The birth of the Arpège-IFS (variable mesh) project from 1987 onwards is then presented in the article written by Jean Pailleux, Jean Coiffier, Philippe Courtier and Emmanuel Legrand, with the variable mesh Arpège model being initially intended to replace both Émeraude and Peridot. These two articles show the extent of the actions on which Jean-François has intervened: from the whole set of physical parameterizations to the dynamics, the algorithmic and the coherence of the codes, with a real support to the variational assimilation of the data!

Many people from the national and international communities were present at the symposium on 6 February 2020, coming from the CNRM and other services of Météo-France, Cerfacs, Hirlam, Aladin, ECMWF, etc. (see Fig.2). Among these people, András Horányi and Radmila Brožková wrote a paper describing the birth and development of the Aladin model and cooperation, aspects that were initiated and wanted by Jean-François in the early 1990s and following the fall of the Berlin Wall. This paper shows the very great influence that Jean-François has had on this vast European cooperation formed by the Aladin project.

In 1991, Jean-François created and directed the “Group of modelling and assimilation for forecasting” (Gmap) at the CNRM in Toulouse. The aim was to continue the developments and finalize the implementation of the Arpège operational NWP model. This stage of Jean-François’ career is described in the paper written by François Bouyssel, Marta Janisková, Éric Bazile, Yves Bouteloup and Jean-Marcel Piriou, with a focus on the physical parameterizations and the “simplified physics” part of the data analysis.

The following paper by Pierre Bénard describes the non-hydrostatic aspects that Jean-François first wanted to develop for the dynamic core of the Aladin model, which are now used for the components of many Aladin weather prediction systems (the Arome and Alaro models) and which are currently being tested for the global version of the Arpège model.

Figure 2: The participants in the symposium "A tribute to Jean-François Geleyn" held on 6 February 2020 at the CIC in Toulouse.

After his departure in 2003 from the CNRM and the management of Gmap, Jean-François became fully involved in the management of the Aladin programme, of which he became the programme manager. This part of his career is described in the article written by Piet Termonia and Patricia Pottier, in which his listening and coaching qualities, both scientific and human, are shown. One could only think of Jean-François when the new consortium called Accord was created at the end of November 2020, bringing together now 26 countries on developments related to Aladin, RC-Lace and Hirlam. It is precisely for this action that the European Meteorological Society (EMS) awarded its highest distinction (the silver medal) in 2011 to Jean-François for his "outstanding contribution to the development of scientific cooperation in Europe".

The following three papers deal with three physical parameterisations on which Jean-François worked a lot throughout his career, between 1973 and 2014: radiation (written by Ján Mašek), turbulence (written by Ivan Bašták Ďurán and Pascal Marquet) and convection (written by Jean-Marcel Piriou and Radmila Brožková). These three papers describe not only the evolution of Jean-François' scientific choices over this long period, but also the experiences and sometimes the intimate thoughts of researchers who worked with him.

The last paper written by Steven Caluwaerts, Daan Degrauwe and Piet Termonia describes an aspect of Jean-François' late life of which he was very proud, when he created the "Atmospheric Physics Research Group" within the "Department of Physics and Astronomy" at Ghent University, Belgium, by becoming a visiting professor in 2011. Jean-François had a strong link with Belgium, already because he was born in Cousolre in the very north of France (close to Maubeuge and the boundary between France and Belgium), going so far as to find in 2014 with Piet Termonia a testimony of the origin of the name Geleyn in the town of Kallo, near Antwerp. This was the last period when Jean-François was able to give courses and train many students, in spite of his illness, a real source of satisfaction for him.

3 References

Numéro spécial: "Jean-François Geleyn et la prévision numérique du temps", ***La Météorologie*****, février 2021 (*****A special issue: "Jean-François Geleyn and numerical weather prediction"*****).**

1) Pascal Marquet, Radmila Brožková: *Introduction,* p.19-20.

2) Olivier Moch: "*Oui, il faut honorer Jean-François Geleyn"*, p.21 ("*Yes, we must honour Jean-François Geleyn"*).

3) Daniel Rousseau, Michel Jarraud, Pascal Marquet: *Les débuts de Jean-François Geleyn : Mayence, Paris et son expérience au CEPMMT*, p.23-28 (*Jean-François Geleyn's beginnings: Mainz, Paris and his experience at the ECMWF*).

4) Jean Coiffier, Regis Juvanon du Vachat, Jean Pailleux: *De Émeraude/Péridot à Arpège/Aladin*, p.29-34 (*From Émeraude/ Péridot to Arpège/Aladin*).

5) Jean Pailleux, Jean Coiffier, Philippe Courtier, Emmanuel Legrand: *La naissance du projet Arpège-IFS à Météo-France et au CEPMMT*, p.35-40 (*The birth of the Arpège-IFS project at Météo-France and ECMWF*).

6) András Horányi and Radmila Brožková: *Naissances du modèle et de la coopération Aladin*, p.41-46 (*Births of the Aladin model and cooperation*).

7) François Bouyssel, Marta Janisková, Éric Bazile, Yves Bouteloup, Jean-Marcel Piriou: *L'évolution opérationnelle du modèle Arpège et de ses paramétrisations physiques*, p.47-54 (*The operational evolution of the Arpège model and its physical parameterisations*).

8) Pierre Bénard: *Les aspects non hydrostatiques pour Aladin, Arome et Arpège*, p.55-62 (*Non-hydrostatic aspects for Aladin, Arome and Arpège*).

9) Piet Termonia, Patricia Pottier: *Jean-François Geleyn, fondateur et premier directeur de programme d'Aladin*, p.63-67 (*Jean-François Geleyn, founder and first Programme Manager of Aladin*).

10) Ján Mašek: *Les travaux de Jean-François Geleyn sur la paramétrisation du rayonnement atmosphérique*, p.68-78 (*Jean-François Geleyn's work on the parameterisation of atmospheric radiation*).

11) Ivan Bašták Ďurán et Pascal Marquet: *Les travaux sur la turbulence: les origines, Toucans, Cost-ES0905 et influence de l'entropie*, p.79-86 (*The* works *on turbulence: origins, Toucans, Cost-ES0905 and the influence of entropy*).

12) Jean-Marcel Piriou et Radmila Brožková: *Les travaux de Jean-François Geleyn sur la convection*, p.87-93 (*Jean-François Geleyn's work on convection*).

13) Steven Caluwaerts Daan Degrauwe Piet Termonia: *Jean-François Geleyn, professeur à l'université de Gand*, p.94-96 (*Jean-François Geleyn, professor at Ghent University*).

Assimilation of GPS observations for weather prediction: Case of Morocco

Fatima Zahra Hdidou, University Hassan II of Casablanca, Ben M'sik faculty of science

Supervisor: prof. Soumia Mordane, PhD.

Date of defence: 16/10/2020

Abstract

The aim of this thesis is to exploit the potential of ground-based GPS observations for data assimilation into a high-resolution NWP model. The first part of this PhD work evaluates the accuracy of NRT ZTD of the Moroccan ground-based GPS meteorology network. The accuracy is evaluated first in relation to the IGS final products, and then by comparison to equivalent values derived from radiosonde profiles. The comparison shows good agreement and a seasonal signal with higher values of ZTD in summer. Then the impact of assimilating ZTD observations from the Moroccan GPS meteorology network into the high-resolution operational model AROME-Morocco (2.5 km) is assessed. The objective is to investigate the impact on moisture field and rainy event forecasts in a 3D-Var data assimilation framework. As a first step, a pre-processing of ZTD observations is performed for quality control and bias correction. Then, two parallel experiments, with and without assimilation of GPS ZTD, are performed over one month period. Compared against other observation systems of humidity (radiosonde and surface network), a beneficial improvement is found in the atmospheric moisture short-range forecast in the low and middle troposphere. Regarding the quality of the rainy events forecasting, the objective verification scores against daily rain gauge observations show that the impact is mixed, positive for larger rainfall accumulations and neutral to negative for smaller rainfall accumulations. A specific evaluation for a case study of a rain event highlights an improvement in terms of intensity and location of precipitating areas when GPS ZTD observations are assimilated. Furthermore, to take into account the horizontal variability of water vapour contained in the tropospheric horizontal gradient observations, a new assimilation system for these observations has been developed during this thesis. The influence of these new observations has been evaluated through a single observation experiment. The results showed reasonable specific humidity analysis increments.

Keywords: data assimilation, numerical weather prediction, GPS meteorology, ZTD, tropospheric horizontal gradients, water vapour, precipitation.

Summary

The Moroccan meteorology service (DMN) has acquired a ground-based GPS network intended to meteorological use. The GPS measurements are concentrated in Near Real-Time (NRT) to DMN. They are locally processed by Bernese software 5.2 in order to produce tropospheric parameters, mainly Zenith Total Delay (ZTD) and tropospheric gradients. An additional module is used to derive Integrated Water Vapour (IWV) from ZTD. The main aim of this thesis is to exploit the potential of ground-based GPS observations for data assimilation into a high-resolution Numerical Weather Prediction (NWP) model.

We have first presented the Moroccan GPS meteorology network, as well as the methodology used for the processing of zenith total delays. The direct use of GPS observations within a NWP system is not possible without quality assessment. Therefore, the first objective of this thesis consisted in evaluating the accuracy of zenith delays resulting from data processing of GPS measurements. First, a preliminary consistency check was made regarding to the International Global Navigation Satellite System Service (IGS) final products. The comparison of NRT ZTD with the IGS final product showed a bias of -1 mm with a standard deviation of 6 mm. Then, an inter-comparison was performed with respect to radiosondes. This inter-comparison was mainly made at two contrasting climate GPS stations: CASA (Casablanca) and DAKH (Dakhla) that are representative of semi-dry and hyper-arid

climates respectively. In addition, operational weather radiosonde data were also available at these stations, over a period of almost a year (2016). The results show a good agreement with a bias of -2.82 mm and a standard deviation of 14.01 mm. We have evidenced an overall wet bias in the radiosonde data with respect to GPS. This behaviour is common for Modem M10 Radiosondes used in this thesis. The results revealed also a consistent seasonal evolution of ZTD with higher values recorded in summer. The work presented in this part highlighted the potential of GPS, to quantify water vapour with an accuracy comparable to radiosonde observations. This first part of thesis was published in *Meteorological applications* journal: "Hdidou, F. Z. , Mordane, S. and Sbii, S. 2018. Global positioning systems meteorology over Morocco: accuracy assessment and comparison of zenith tropospheric delay from global positioning systems and radiosondes. Met. Apps. 25, 606–613".

The second objective of this thesis was the investigation of the impact of GPS ZTD observations within the Three-Dimensional VARiational (3D-Var) data assimilation system of the meso-scale model AROME-Morocco (2.5 km of horizontal resolution). Besides the Moroccan network, we further include observations from IGS in order to increase the number of GPS ZTD stations in the domain of interest. To satisfy the hypothesis of unbiased errors required by the 3D-Var assimilation system, a static bias correction was applied. The bias is calculated for each station from one-month average of observed GPS ZTD minus background model equivalent ZTD. The bias found, which is ranging between 0.3 mm and 13 mm, is removed from ZTD observations before their assimilation. To assess the impact of a ZTD observation when it is assimilated into AROME-Morocco model, we have performed a single observation assimilation experiment. As previously shown, we found that the assimilation of GPS ZTD data modifies the moisture field in the low to mid-troposphere with a maximum correction around 900 hPa. Then, two parallel experiments of assimilation were carried out over a period of one month: a reference experiment which includes the usual observations assimilated by AROME-Morocco system (satellite data, radiosondes, etc.) and a second experiment including the same data together with GPS observations. An overall positive impact for the low to mid-level specific humidity of the background (3h forecast) was found by comparison with radiosonde observations. A neutral to positive impact was also revealed on the forecast up to 24 hours of 2 m relative humidity as verified against surface observations.

Objective verification of precipitation accumulation forecasts against rain gauge observations has been examined using Quantitative Precipitation Estimates (QPE) scores computed on the total rainy episodes over 1-month. The results of verification reported a mixed impact, positive for larger rainfall accumulations and neutral to negative for smaller rainfall accumulations. The impact has been also evaluated on the forecast of a heavy event that occurred on 1 March 2018 over the South of the Atlas region. The assimilation of ZTD observations highlighted two major impacts: an increase in the moisture field over the Western part of the domain and a change in dynamics allowing more advection of moist air from the Atlantic Ocean. These factors made it possible to better simulate precipitation that is more in agreement with the reality as reported by radar QPE. These Results have revealed that assimilating GPS ZTD observations is relevant for improving the initial conditions and forecasts of mesoscale models. This part was published in *Tellus* journal: "Hdidou, F.Z.; Mordane, S.; Moll, P.; Mahfouf, J.-F.; Erraji, H.; Dahmane, Z. Impact of the variational assimilation of ground-based GNSS zenith total delay into AROME-Morocco model. Tellus A Dyn. Meteorol. Oceanogr. 2020, 72, 1–13"

The work conducted in this thesis concerns also the development of a system of assimilation for the horizontal gradients in the framework of AROME model. The system development consists of constructing the observation operator allowing the computation of horizontal gradients from the model variables (temperature, humidity and pressure). Moreover, the tangent-linear observation operator and its adjoint are implemented. To evaluate the developed system, a single observation experiment has been performed. The resulting specific humidity analysis increments have a reasonable aspect with the ability to capture the asymmetric atmospheric humidity structure. These results represent a positive contribution to the effort raised by scientific community to exploit the potential of horizontal gradients in NWP.

Assimilation of radar observations for numerical weather prediction

Zahra Sahlaoui, Faculty of Sciences Ben M'Sik, University Hassan II. Casablanca. Morocco

Supervisor: prof. Soumia Mordane, PhD.

Date of defence: 15.10.2020

Abstract

During the last years, Morocco had witnessed several extreme precipitation and flash flood events that caused life losses and material damages. Therefore, good quality precipitation measurement and accurate forecast are highly needed for better risk management. However, it is difficult to characterize the precipitation either in terms of intensity, localisation, frequency or nature. Because of the complexity of the processes involved and the variety of spatial and temporal scales, many issues related to the measurement and the forecast of the precipitation still rise. In this context, the current thesis work has two main objectives: i) to enhance the radar quantitative precipitation estimate and ii) to produce a better quality forecast for heavy precipitation events. Firstly, the quantitative precipitation estimate (QPE) from weather radars is assessed over Morocco. Methods for quality control are proposed and tested. Additionally, a merging algorithm is used to adjust radar QPE with rain gauges data. The adjusted QPE performance is evaluated through different case studies and a positive impact is observed. Secondly, we focus on the precipitation forecast by the numerical weather prediction models AROME. A key component for a reliable precipitation forecast is the assimilation of moisture related observations in order to prepare the model initial conditions. A new approach is proposed for the precipitation assimilation in AROME. Indeed, the precipitation is converted to the humidity profile and then fed to the AROME assimilation system. This method is tested in the case of an extreme precipitation event (> 150 mm in 24 hours). The moisture information provided by the precipitation data allows a substantial improvement of the precipitation forecast.

Keywords: numerical model, data assimilation, weather radar, precipitation measurement and forecast.

Summary

The objective of my thesis is to propose robust and well-tested methods allowing high quality precipitation observation and forecast. Thus, I first focused on investigating the impact of gauge adjustment on the rainfall estimate from the Moroccan C-band weather radar network. The Khouribga city radar was considered as the experimental framework for the proposed data handling algorithm. The radar reflectivity underwent a quality check before deployment in order to retrieve the rainfall amount. The process consisted of clutter identification and correction of the signal attenuation. Thereafter, for several rainy days, the radar reflectivity was converted into rainfall depth over 24 hours. An assessment of the accuracy of the radar rainfall estimate over the study area showed an overall underestimation when compared to the rain gauges (bias = −6.4 mm and RMSE = 8.9 mm). The adjustment method was applied and the validation of the adjusted rainfall versus the rain gauges showed a positive impact expressed by the reduction of the bias and RMSE (bias = −0.96 mm and RMSE = 6.7 mm). The case study conducted on December 16, 2016 revealed substantial improvements in the adjusted quantitative precipitation estimate with reference to the African Rainfall Climatology version 2 (ARC2) precipitation. The enhancement was observed for both precipitation structure and intensity. More details on this work can be found on "**Radar Rainfall Estimation in Morocco: Quality Control and Gauge Adjustment**" published in *Hydrology* MDPI journal.

When it comes to the forecast side, it should be mentioned that, in meteorology, the precipitation forecast at several time ranges is mainly based on numerical weather prediction (NWP) models products. In Morocco, the convective scale NWP model AROME is used to provide the forecast of several meteorological parameters to different users. The initial conditions are of great importance for the NWP model, especially those resulting from data assimilation processes such as multi-dimensional variational methods. Therefore, the impact of initial conditions on the precipitation forecast by AROME model was assessed over two case studies (flash flood on Rabat city in February 23, 2017 and rainy episode over the North-East of Morocco in January 19, 2018). Initial conditions provided by the dynamical adaptation and by the three dimensional variational (3D-Var) data assimilation method were tested. Thus, two model simulations were run for each one of the case studies. The precipitation forecasts were compared to the adjusted QPE from Larache and Debdou radars that were used as the reference. The results showed that the use of initial conditions produced by the 3D-Var assimilation method led to enhanced precipitation forecast in term of both intensity and localisation.

The 3D-Var assimilation method performances depend closely on the digested meteorological observations. Former research works underlined the importance of humidity observations to produce reliable precipitation forecasts. Therefore, the ability of precipitation assimilation was assessed in the AROME model. The proposed assimilation method was based on a two-step approach. First, one-dimensional variational (1D-Var) assimilation was applied on hourly accumulated precipitation ANTILOPE in order to retrieve temperature and specific humidity profiles. These retrieved profiles were then combined in relative humidity profiles before being assimilated by the AROME 3D-Var system. The precipitation forecast was studied for a Mediterranean heavy rain event that took place on November 4, 2017. Three experiments were run for this case study. The results showed that the precipitation assimilation has a positive impact on the moisture analysis, according to moisture sensitive satellite channels assimilated in AROME 3D-Var. Additionally, the forecast of dynamical fields was more favourable for the production of strong convection and heavy precipitation, which led to precipitation forecasts in better agreement with ANTILOPE precipitation. The statistical evaluation against rain gauges showed that the additional rain observations had produced precipitation forecasts with improved skills, something which supports the previous results. This work was published in *Meteorological Applications* journal under the title: "**Improving heavy rainfall forecasts by assimilating surface precipitation in the convective scale model AROME: A case study of the Mediterranean event of November 4, 2017**".

All issues of the joint ALADIN-HIRLAM NL

No.16

this last issue

February 2021

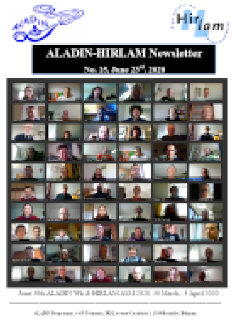

No.15 June 2020

No.14 January 2020

No.13 August 2019

No.12 January 2019

No.11 August 2018

No. 10. January 2018

No. 9. September 2017

[No. 8. January 2017].

[No. 7. September 2016]

[No. 6. February 2016].

[No. 5. August 2016]

[No. 4. February 2015]

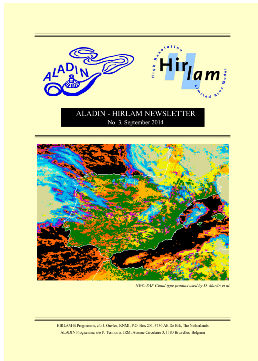

[No. 3. September 2015]

[No. 2. April 2014]

[No. 1. September 2013]